LBL-35768
UC-413

NUCLEAR SCIENCE DIVISION

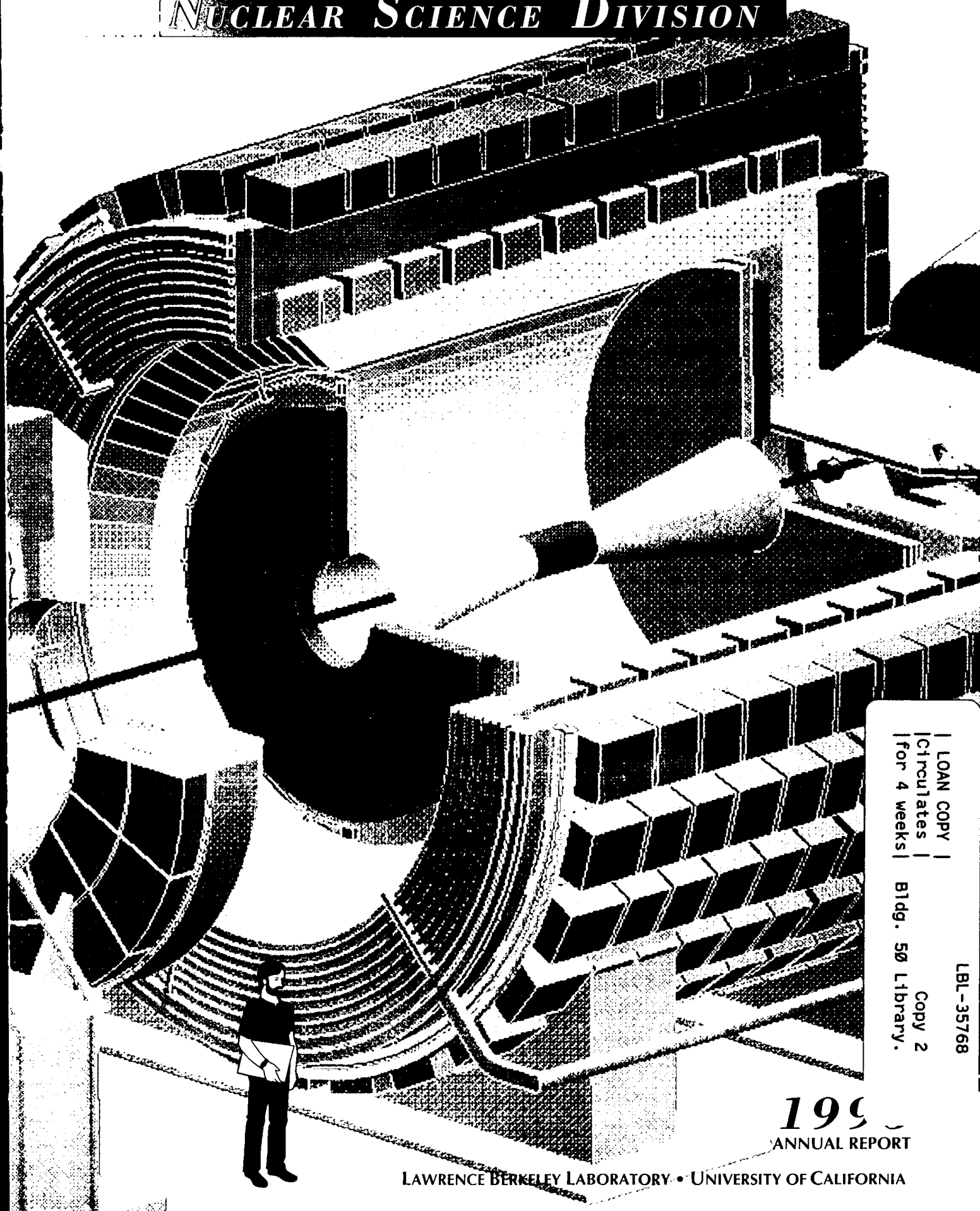

19

ANNUAL REPORT

LAWRENCE BERKELEY LABORATORY • UNIVERSITY OF CALIFORNIA

DISCLAIMER

LBL-35768
UC-413

NUCLEAR SCIENCE DIVISION

1993
ANNUAL REPORT

Division Director
T. J. M. Symons

Division Deputy
Janis M. Dairiki

Editor
W. D. Myers

JUNE 1994

Lawrence Berkeley Laboratory
University of California
Berkeley, CA 94720

This work was supported by the Director, Office of Energy Research, Office of High Energy and Nuclear Physics, Division of Nuclear Physics, and by the Office of Basic Energy Sciences, Division of Nuclear Sciences, of the U.S. Department of Energy under Contract No. DE-AC03-76SF00098.

Table of Contents

Relativistic Nuclear Collisions 119

INTRODUCTION

LAWRENCE BERKELEY LABORATORY • UNIVERSITY OF CALIFORNIA

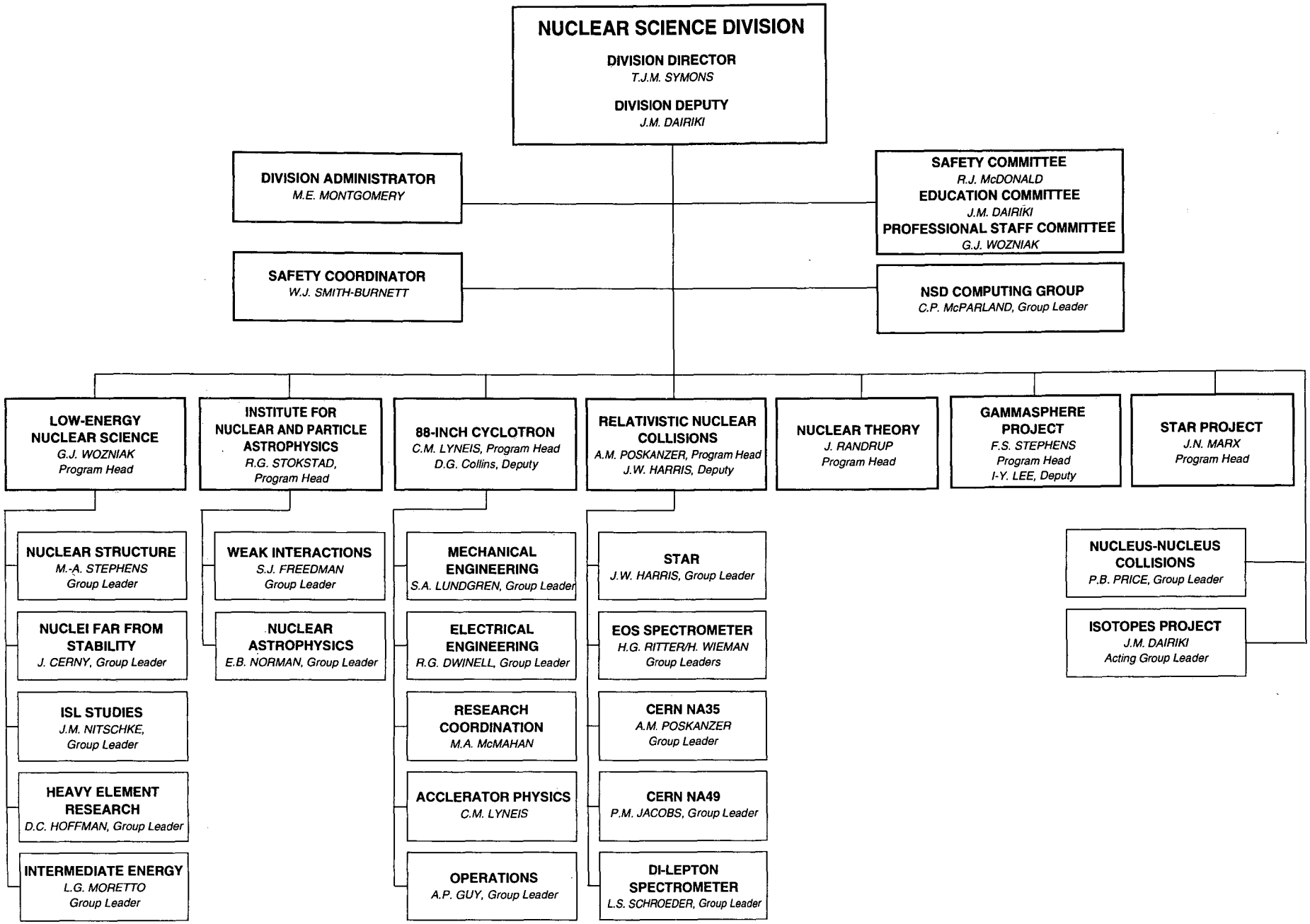

Introduction

This report describes the activities of the Nuclear Science Division for the 1993 calendar year. This was another significant year in the history of the Division with many interesting and important accomplishments.

One of the most exciting developments was the start of experiments using Gammasphere. In March, the program was launched with 30 of the final 110 detectors operating. Although the capability of this system is only a fraction of the final one, it is much more powerful than any of the gamma arrays presently available in the United States. In the first year, 30 experiments were carried out involving 104 users from 31 universities and laboratories. In late 1994 the number of operating detectors will be increased to 50 and the project will be complete in October 1995. Already, many interesting results have been obtained, particularly in the characterization of superdeformed nuclear states.

Another important milestone was the completion of the photomultiplier support frame for the Sudbury Neutrino Observatory. The geodesic structure was assembled at the contractor's facility in Petaluma before being crated for shipment to Canada. A great deal of work remains to be done before the facility detects its first neutrinos; however, with our main technical work nearing completion, the interests of the local group are already turning to physics analysis and the software that must be developed for results to be obtained in a timely way.

In the relativistic heavy-ion program, we were delighted when the Department of Energy formally approved the construction of the STAR detector for RHIC in March 1993. It took many years of patient work from all the members of the STAR collaboration to bring the project to this point. Work on detailed design

and construction of prototypes is now well under way and the project is on a tight schedule for completion when RHIC commences operation in 1999. In the meantime, we are actively involved in analysis of the data taken by the DLS and EOS detectors in the last years of Bevalac operation, and we are also preparing for the NA49 experiment that will run at CERN in 1994.

One final milestone was the formation of the Institute for Nuclear and Particle Astrophysics (INPA). This was noteworthy in several respects, not least because it is jointly operated with the LBL Physics Division and seeks to bring together high-energy and nuclear physicists to advance this field. INPA is off to a strong start with much enthusiasm from the participants.

This is not the easiest time for nuclear physics, with so much discussion taking place of changes in the mission of the national laboratories and movement away from fields such as nuclear science toward areas that address national problems in a more direct way. However, from this local perspective it is hard not to be optimistic. In the past few years we have made a substantial investment in new equipment and instrumentation with unique capabilities. The scientific opportunities of the coming years are truly exceptional.

OVERVIEWS

Nuclear Structure and Reactions Program

G. J. Wozniak

The Nuclear Structure and Reactions Program at LBL addresses important problems in nuclear science. The aim of this program is to understand the nuclear system and to develop new ways of probing basic physical concepts by studying nuclear systems at extremes of angular momentum, isospin, Z & A, and temperature. New instrumentation has played a vital role in these studies and LBL has maintained a leading part in developing and implementing new instruments and techniques.

The 88-Inch Cyclotron is the center of much of this work. The Cyclotron is operated as a national facility and is equipped with two state-of-the-art electron cyclotron resonance (ECR) ion sources capable of producing high-charge-state ions of most elements. Beams of ions from helium to neon are available with energies up to 32.5 MeV/nucleon. For heavier ions, the maximum energy per nucleon decreases with increasing mass, approaching the Coulomb barrier in the light rare-earth region. In addition, intense light-ion beams of isotopes of hydrogen and helium, as well as polarized beams, are available. The high reliability and ease of changing beam species make the 88-Inch Cyclotron ideally suited for nuclear structure studies.

Gammasphere is a National γ-Ray Facility consisting of a 4π array of 110 Compton-suppressed high-purity germanium detectors. Completion of this system is scheduled for October 1995; however, it was recognized several years ago that even a small fraction of the full system would be considerably more powerful than any other array existing at that time. Thus an Early

Implementation phase of operation was planned; it began in April 1993 with 22 detectors. As of the beginning of February 1994, the number of detectors is at 34; 27 runs have been completed that used about 60% of the 88-Inch Cyclotron research time. About 75 users came from 13 U.S. and 10 foreign institutions. At this stage, Gammasphere is comparable in resolving power to Eurogam I and GASP, the other new-generation arrays.

Nuclear Structure at High Spin

The nucleus is a few-body quantal system that leads to unique behaviors generally characterized by an interplay between single-particle and collective properties. The objective of the Nuclear Structure Group is to understand this system and how its behavior is related to other systems, both quantal and classical. Although observations often appear complex, our aim is to express the physics wherever possible in terms of the underlying symmetries, which may (or may not) exist in other systems. We are therefore looking primarily for new types of behavior that may indicate new symmetries in the nucleus. Also very interesting to us is the mechanism by which the known symmetries (quantum numbers) are destroyed through level mixing, when the behavior of the nucleus becomes chaotic. An exciting step in the search for symmetries is the observation of superdeformed (SD) nuclei. They are much better rotors than other nuclei, and this regularity enables us observe smaller deviations that may be linked to new symmetries and/or correlations.

The major part of our work in recent years was devoted to the study of these SD nuclei. We found "identical bands" in SD nuclei of the mass-190 region and developed an interpretation in terms of pseudospin and other remnants of SU(3) symmetry. Such an interpretation is still under discussion and we are trying to find new ways to test it, using the properties of the moments of inertia of terminating bands in normally deformed nuclei. We were the first to observe transitions deexciting SD bands (in the mass-130 region), thereby establishing the spins that are essential for the interpretation of "identical bands." So far the linking transitions have not been observed in any other region where identical bands occur, in spite of numerous attempts. In the last three years, we have discovered 23 SD bands in the three "known" regions. The systematics of the moments of inertia, and the discovery of M1 "cascade" transitions between two SD bands, have enabled us to assign configurations to most of these bands. In addition, from the variation of the moments of inertia of these SD bands with frequency, we have shown that weak pairing correlations must exist in many, if not all, of these SD bands. Recently, we discovered a $\Delta I = 2$ staggering in several SD bands in the mass-190 region and found the second example of this staggering in the mass 150-region. The cause of the stagger is unknown and we are trying to identify the underlying symmetry (probably C_4) and understand the mechanism through which this effect is generated.

Nuclear Structure of Nuclei Far from Stability

The nuclear structure of nuclei far from stability in the region of light proton-rich nuclei and of very heavy nuclei is being investigated at the 88-Inch Cyclotron by two faculty-led groups working in those respective areas. In addition, in support of future radioactive beam facilities, a third group, the IsoSpin Laboratory (ISL) Studies Group, is performing research and development on the production and acceleration of radioactive nuclear beams.

Proton-Rich Nuclei

Studies near the proton drip line can provide excellent tests of the limitations of nuclear models and stimulate improvements. For nuclides beyond the drip line, searches for new ground state (g.s.) proton emitters are of interest to compare reduced widths to nuclear structure theory, as are searches for the quantum mechanically interesting decay mode of g.s. two-proton emission (^{2}He) as predicted by Gol'danskii in 1960. For nuclides near the edge of stability, the large available β-decay energies permit new decay modes (such as β-delayed two-proton emission). Results from β-2p, and the simpler β-p decays, also test both the mass surface and nuclear structure predictions (e.g., large-basis shell-model calculations, Gamow-Teller strength functions). Finally, these nuclei often are important because they are termination points for nucleosynthesis processes.

Recent research has utilized a new low-threshold proton ball, consisting of six triple telescopes—made of ΔE(gas), ΔE(gas), Si(E) detectors—each with a 200-keV proton threshold, in conjunction with a helium-jet transport system. These fusion-evaporation experiments have led to the observation of the β-delayed proton decays of the $T_z = 3/2$, $A = 4n + 1$ nuclei ^{65}Se and ^{73}Sr. These recent data, and earlier results on ^{61}Ge ($T_z = -3/2$), clearly show that independent-particle, mass-recursion-relation models are currently much better than microscopic-macroscopic models in this mass region.

A recent study has observed the lightest known example of g.s. proton decay, ^{105}Sb. It has a proton energy of 478 keV with a proton decay branch estimated as only 1% (β-decay is dominant) that is consistent with emission from a $d_{5/2}$ level. Several prior searches were unable to observe this decay. The β-2p decay of ^{39}Ti has been observed and its deduced mass leads to the prediction of a g.s. 2-proton branch of <1%.

Heavy Nuclei

In the heavy actinides and transactinides, the strong Coulomb force plays an important role. The liquid drop barrier against fission is small and nuclear stability against fission is principally due to shell effects. The study of the nuclear decay properties of the heavy elements allows the determination of nuclear masses and the strength of these shell effects, giving a better understanding of nuclear structure in general and enabling predictions of nuclear stability in other regions, such as the newly discovered shell near neutron number 162. During the past few years, the heavy nuclei group has measured

the half-lives, α-decay energies, α-decay branches, electron-capture (EC) branches, and spontaneous fission (SF) for many actinide and transactinide isotopes.

Spontaneous fission studies are useful in understanding nuclear stability at large deformations. Several interesting effects are currently being studied, including (a) the instability against fission in nuclides near Z = 100 and N = 164, which can fission into shell-stabilized fragments each near Z = 50 and N = 82; (b) the stability against fission near the deformed nuclear shell at Z = 108 and N = 162, and competition with the instability mentioned above; (c) the transition from asymmetric fission mass distributions near ^{252}Cf to the symmetric fission mass distributions at higher Z; and (d) the systematics of the total kinetic energy distributions.

Electron-capture-delayed fission (ECDF) occurs when electron-capture populates high-lying states in the daughter, which then fissions before deexciting to the daughter ground state. ECDF allows the study of fission from relatively low excitation energies in nuclides where SF branches are immeasurably small. In the neutron-deficient actinides, the heavy nuclei group has found ECDF branches whenever the EC Q-value is greater than 4.0 MeV. Recently, they have measured ECDF branches, EC branches, α-decay branches, half-lives, ECDF fragment mass distributions, and ECDF total kinetic energy distributions in ^{234}Am, ^{232}Am, ^{238}Bk, and ^{228}Np.

Until recently, little was known about the chemical properties of elements with Z > 100 because of their very short half-lives. The study of the chemical properties of the elements from Md (Z = 101) through element 106 is of fundamental interest. In recent years, the heavy nuclei group has progressed from measuring the most basic chemical properties (such as the most stable oxidation state in aqueous solution) of elements 103–105 to making detailed comparisons between the chemical properties of these heavy elements and their lighter periodic table homologs. In aqueous-phase chemical separations, the group has measured (a) the ionic radius of Lr^{3+}, (b) the stability of anionic, neutral, and cationic chloride complexes of Rf (element 104), and (c) the formation and stability of halide complexes of Ha (element 105). In the gas-phase, they have measured the volatilities and adsorption enthalpies of chlorides and bromides of both Rf and Ha.

IsoSpin Laboratory Studies (Radioactive Beam R&D)

The first generation of radioactive beam facilities began a new wave in nuclear structure studies of nuclei far from stability. A classic example is the deluge of experimental data and theoretical predictions for the very weakly bound ^{11}Li nucleus. However, the experimental effort has been severely handicapped by the low beam intensity and poor beam quality of the present-generation facilities. A second-generation facility, with its promised large improvements in both beam intensity and beam quality, would greatly facilitate these studies.

In 1989 the group working on this problem outlined a plan to build a National High Intensity Radioactive Nuclear Beam (RNB) Facility that later became known as the IsoSpin Laboratory (ISL). The ISL concept generated wide national and international interest (there are presently over 450 scientists in the ISL USERS group) and led to many conferences, workshops, and symposia. In 1990 a Steering Committee was formed to build a solid scientific case for the ISL, to address technical challenges, and to promote the ISL as the next major nuclear science construction project within DOE. During the intervening years, radioactive beam science has evolved into one of the most stimulating emerging new directions in nuclear physics.

LBL is one of the leading laboratories making the technical and physics case for the ISL. Our physics interest lies (a) in new regions of deformation that can only be reached with radioactive projectiles; (b) in the fusion of neutron-rich targets and/or projectiles to synthesize heavy elements and the formation of neutron-rich isotopes of *known* elements in multi-neutron-transfer reactions with neutron-rich RNBs, in particular, near the N = 162 neutron shell; and (c) in the elucidation of the properties of exotic nuclei near the drip lines. The ISL Studies Group has contributed to several technical developments: a conceptual design for both a 600-MeV cyclotron and a Rapid Cycling Synchrotron; a system to post-accelerate very-low-velocity RNBs with low q/A; a set of computer codes that allows the prediction of accelerated RNB intensities; and a new gas-cooled target system for high beam power (50 kW).

Nuclear Reactions

The absence of fragments between light evaporated particles and fission at low energies defines in a negative way the range and the physics of intermediate mass fragment emission. An increase in excitation energy brings the emission of these fragments to the forefront, until they dominate with their sheer abundance the reaction scene. The group studying these reactions has striven, both theoretically and experimentally, to characterize the physics of this emission process from its onset as binary compound nucleus decay to its full deployment as multifragmentation.

Theoretically, the group has explained complex fragment emission as a generalized fission process controlled by a set of conditional barriers (along a ridge line) constrained to a given mass asymmetry. Experimentally, the group has characterized this process as a legitimate compound nucleus decay channel in statistical competition with the more traditional light particle decay channels. The study of excitation functions for fragments spanning the entire mass asymmetry range allows the extraction of the associated barriers. As the fission barriers in medium-heavy nuclei were instrumental in defining uniquely the liquid drop model parameters, the conditional barriers offer a unique tool to fix the parameters of its more modern descendants like the finite-range models.

At larger excitation energies, the cross-sections for complex fragment emission increase as expected from compound nucleus theory. Multifragment events are trivially predicted as arising from sequential decay. However, for the more

violent collisions, the sheer number of fragments leads one to suspect that a new mechanism of simultaneous multifragmentation may be at work. Speculations on the origin of multifragmentation due to spinodal (volume) instabilities or Rayleigh-like surface instabilities are being intensely investigated theoretically and experimentally. In this research, this group has identified a new class of instabilities, unknown heretofore, which are caused by surface-surface interactions in thin sheets or bubbles of nuclear matter.

Alternatively, the possibility of a global chemical equilibrium has also been put forth. In an attempt to decide experimentally between a dynamical and statistical picture, this group has studied the excitation functions of binary, ternary, quaternary, and quinary events. The relative intensities of these channels as a function of excitation energy indicate quite clearly that they are in statistical competition.

The Institute for Nuclear and Particle Astrophysics

R.G. Stokstad

In November of 1993 James Symons and Robert Cahn (Director of the Physics Division) made the following announcement:

> LBL is home to a diverse program of research in astrophysics, including solar neutrinos, cosmic rays, weak interactions, dark matter, supernovae, cosmic background radiation and theoretical astrophysics. Because astrophysical events, including the very origin of the Universe, are governed by the physics of nuclei and particles, cooperative research in these disciplines is especially appropriate and should be encouraged. In this context, we are announcing the formation of an interdivisional center to be called the Institute for Nuclear and Particle Astrophysics. It is intended for the Institute to bring together experimenters and theorists with common scientific goals and shared techniques that transcend divisional boundaries to create a vital astrophysics community at LBL.

The plan for the Institute (or INPA) has been to bring some six different experimental groups working in astrophysics at LBL together under one roof, both physical and intellectual. Since the announcement, the relocation of the scientists to the Building 50 complex is mostly complete and the intellectual community-building is proceeding apace. From the Nuclear Science Division (NSD) comes the Nuclear Astrophysics Group, led by Eric Norman; Stuart Freedman's Weak Interactions Group; and Henry Crawford's effort in cosmic rays. The Physics Division contributes research on the Cosmic Microwave

Background (George Smoot), the Supernovae Search Team (Saul Perlmutter), Dark Matter Search (Bernard Sadoulet), and the diverse interests of Richard Muller. There is also a relatively new and strong educational program, the Hands-On-Universe (Carl Pennypacker). The interests of a number of theorists in the NSD and Physics theory groups have astrophysical components.

The Institute sponsors a seminar series, the "Astrophysics Journal Club"; further, it has initiated a visitor program, is coordinating proposals for new research activities in this area, and interacts with similar organizations, such as the NSF-sponsored Center for Particle Astrophysics located on the Berkeley campus. A direct result of INPA's formation is that contacts among scientists in the Physics Division and in the Nuclear Science Division have increased substantially.

The Physics Division Annual Report covers the work in dark matter, the supernovae search, and cosmic background radiation. The NSD Nuclear Theory Group's studies of neutron stars, pulsars, and neutrino transport in supernovae explosions are described in the corresponding section of this annual report. The research of the Nuclear Astrophysics, Weak Interactions, and Cosmic Ray Groups is overviewed here.

The Nuclear Science Division's program in nuclear astrophysics and weak interactions pursues fundamental questions in nuclear physics and astrophysics. The contributions to astrophysics made by nuclear physics (the properties and reactions of nuclei, the properties of particles produced in nuclear decay, and the underlying symmetries exhibited by these nuclei and decay processes) are mirrored by the opportunities that astrophysical phenomena provide for increasing our knowledge of fundamental nuclear physics. This relationship is manifest in the solar neutrino problem, studies of neutrino masses, and searches for neutrino oscillations; in the symmetry of time reversal; in the measurement of the parameters of the weak interaction; in searches for dark matter; and in studies of cosmic rays.

The Nuclear Astrophysics Group and the Weak Interactions Group conduct research at LBL and the 88-Inch Cyclotron and at UCB, participate in national and international collaborative experiments, and interact with other groups engaged in experimental and observational research in the interdisciplinary area of nuclear and particle astrophysics. The Cosmic-Ray Group (H. Crawford, et al.) has research efforts in astrophysics that are mentioned in this overview. Graduate and undergraduate students from the University of California play important roles in many of the experimental programs and receive extensive training. Selected highlights of the research conducted by these three groups follow.

Substantial progress was made during the past year in the experimental research conducted at the 88-Inch Cyclotron. The most significant achievement was the trapping of radioactive sodium atoms. Neutral ^{21}Na atoms produced in the ^{24}Mg(p,α) reaction were transported in an atomic beam transversely cooled by laser light and then contained in a magneto-optical trap. An intensity of several thousand atoms was maintained in the trap, providing sufficient

fluorescence to be observed with the naked eye. Improvements in the efficiency with which fast-moving atoms in a beam can be slowed down and then loaded in the trap have been made, with the result that 20% of the atoms in the beam can now be trapped. A study of losses in the trap due to cold (or exoergic) collisions has shown how these losses depend on the population of hyperfine levels in the atomic groundstate. This, and the discovery of a previously unobserved trapping mechanism, point to rapid progress toward a series of fundamental experiments that will exploit this new technique.

A series of irradiations with protons from the 88-Inch Cyclotron (and other accelerators) has been undertaken to study the effect of cosmogenic transmutation on geochemical measurements of double beta-decay rates. Since the ratio of ^{128}Te and ^{130}Te in ancient tellurium ores is affected not only by double beta decay but also by the reactions of energetic cosmic-ray protons on the isotopes in natural tellurium, it is necessary to know the proton-induced reaction rates and correct for this effect. This work has been completed on tellurium; similar measurements have now been made for natural isotopic targets of Se and Zr, whose double-beta decays have also been studied by geochemical techniques. Here it has been shown that in the geochemical measurement of the double-beta decay of ^{96}Zr and ^{82}Se the (p,xn) reactions give a negligible contribution, but in the proposed geochemical measurement of the double-beta decay half-life of ^{80}Se, (p,xn) the yields represent a competing mechanism for the production of ^{80}Kr over geologic periods of time.

The Sudbury Neutrino Observatory, a solar neutrino detector that is also capable of detecting neutrino oscillations, is about to begin underground installation of detector components. The photomultiplier support structure, a major component supplied by LBL, has progressed from the design and fabrication of individual parts to assembly and delivery of subcomponents to Sudbury. In July of 1993 the entire geodesic dome was assembled above ground in Petaluma, California, and provided an occasion for a ceremony to mark the completion of this stage of the project. The steel geodesic dome was delivered to Sudbury in FY93 while the plastic panel assemblies, which house the PMTs, were assembled in LBL's clean-room assembly facility and shipped in April 1994. Additional responsibilities have been assumed for contamination control and contamination reduction in the cavity. The Sudbury group's expertise in low-level radiation counting, and both its local and Oroville counting facilities, are essential for contamination control. All materials used in the construction of the photomultiplier support structure have been analyzed for uranium and thorium contamination and are typically a factor of ten under project requirements. The group effort in preparation for data analysis and in applying Monte Carlo programs for the collaboration continues to expand, with heavy involvement in developing the graphics interface and the on-line detector monitoring programs. A low-energy on-line trigger using neural networks is being pursued. As effort is shifted from engineering matters, the group will concentrate increasingly on the problems of solar neutrino data-collection and analysis.

An improved and more sensitive experimental variation on a classic test of time-reversal invariance—the triple correlation in the beta decay of the neutron—is in preparation at the NIST reactor. The feasibility of this experiment was

recently demonstrated in an in-beam test of the beta detectors and the proton detectors. The Nuclear Science Division is designing and building the beta detectors for this collaboration involving six U.S. institutions. Eventually the apparatus will be moved to the ILL reactor in Grenoble, France, where a higher cold neutron flux will improve the statistical precision by another order of magnitude.

A number of nuclear physics experiments are planned or are being done at LBL and at UCB using long-lived activities that permit off-line counting. These experiments include placing limits on double-beta decay (in Ca, Sn, Nd, Sm, and Gd nuclei), studies of nuclei to be used in gamma-ray astronomy (^{44}Ti) and as cosmo-chronometers (^{54}Mn), and a test of time-reversal invariance in the isospin-hindered beta decay of ^{134}Cs. In the case of ^{44}Ti, the ^{45}Sc(p,2n)^{44}Ti reaction was undertaken to obtain information on the cosmic-ray exposures of meteorites; the half-life of ^{44}Ti is also being measured more accurately to estimate Ti production in supernovae.

The Cabibbo-Kobayashi-Maskawa mixing matrix describes the weak interactions among the quarks and thus contains fundamental parameters of the standard model. One of these, vector coupling constant V_{ud}, can be determined from the ft-values of the superallowed Fermi nuclear beta-decays. The corrections that have to be made to determine V_{ud} become smaller with decreasing charge of the emitting nucleus. The lowest-Z nucleus that has a Fermi decay transition is ^{10}C. A program to measure the branching ratio for the Fermi decay of ^{10}C has been in progress for several years and uses the EN tandem accelerator facility at Western Michigan University. One measurement has been made (yielding a branching ratio in agreement with earlier measurements), but further improvements are planned before making a second measurement.

The matter of the 17-keV neutrino was finally laid to rest this past year with experiments completed by the Freedman and the Norman groups. Substantial progress has been made by the latter group toward understanding the origin of the kink in their earlier experiment on ^{14}C embedded in a Ge detector. They used a planar germanium crystal in which the collection electrode was divided by a circular groove into a "center region" and an outer "guard ring" in order to reject events not fully contained in the center region. Subsequent additional tests, reported here, have now shown that systematic effects related to the active guard ring and to the clustering of carbon inside the detector were the likely causes of the distortion in the spectrum that was attributed to the presence of a massive neutrino.

One proposed form of dark matter is the "stranglet." Such particles have a very small charge-to-mass ratio and contain a large percentage of strange quarks. They might be created in relativistic heavy-ion collisions in which the quark-gluon plasma is also formed, and experimental searches for stranglets are being conducted by the Crawford group using the AGS at Brookhaven National Laboratory. The same research group also studies nuclear fragmentation collisions as a part of their work on the origin and transport of cosmic rays, and they recently joined the Deep Underwater Muon and Neutrino Detector

collaboration. In the latter case, they hope to use the high-energy neutrinos present in cosmic rays to make a tomographic study of the earth's core.

The research groups and personnel in the Nuclear Science Division that participate in the Institute for Nuclear and Particle Astrophysics are as follows:

Nuclear Astrophysics Group

Eric Norman, Yuen-dat Chan, Alejandro García (until December 1993), Iuda Goldman, Ruth-Mary Larimer, Kevin Lesko, Robert Stokstad, Fred Wietfeldt, and Igor Žlimen.

Weak Interactions Group

Stuart Freedman, Chris Bowers, Brian Fujikawa, Laura Lising, Zheng-tian Lu, Justin Mortara, Jürgen Reich, Mary Rowe, Song-quan Shang, and Eric Wasserman.

Cosmic-Ray Group

Henry J. Crawford, Mats Cronqvist, Jack Engelage, Leo Greiner, I. Flores, Chancey Kuo, J. Larsen, J. Romanski, Craig Tull, and L. Wu.

Relativistic Nuclear Collisions Program

A.M. Poskanzer

The Relativistic Nuclear Collisions Program (RNC) is carrying out experiments studying the collision of heavy ions in four energy regimes: (1) the Bevalac, where nuclear matter is compressed sufficiently to study its equation of state; (2) the AGS at Brookhaven National Laboratory (BNL), extending the studies of the Bevalac to an energy range where the maximum pressure from the baryons is likely to occur; (3) the SPS at CERN, where the energy density of the nucleons in the collision of very heavy nuclei may be sufficient to produce a phase transition to a plasma of free quarks and gluons; and (4) RHIC, where the energy density of the produced particles will be sufficiently high that production of the quark-gluon plasma is expected to occur. Understanding the reaction dynamics and the nuclear-matter equation of state is of fundamental interest.

The major efforts at the Bevalac have involved the Dilepton Spectrometer (DLS) and the EOS Time Projection Chamber (TPC). Because of the shutdown of the Bevalac in January 1993, the extensive local activities are now in the analysis stage. The EOS TPC will be moved to the AGS in the next year to continue its studies at higher energies as experiment E895. The various experiments at CERN with LBL participants have finished data-taking with ^{32}S beams and have been consolidated into one experiment, NA49, for the start of the Pb beams program in November 1994. However, the main focus of the future high-energy heavy-ion research program at LBL is the STAR experiment at RHIC, which will begin data-taking in 1999.

Bevalac/AGS Physics

Because dileptons interact relatively weakly with matter, they provide a unique tool for probing the early phase of the hot, condensed system created in central A-A collisions. Theoretical calculations indicate that the yield of dileptons is sensitive to the density and temperature of this early phase of the collision, and thus the dilepton yield could provide information on the nuclear-matter equation of state. These indications formed the basis of the experimental program of the DLS.

Experiments with the first-generation 4π hadronic detectors at the Bevalac—namely, the Plastic Ball and the Streamer Chamber—provided the first insight into the dynamics of nuclear matter at high densities and temperatures through comparison of the experimental data with macroscopic and microscopic model calculations. However, still more precise and systematic data were needed to determine the parameters of the nuclear equation of state. Such high-quality data have now been accumulated by the EOS TPC at the Bevalac. It is expected that the source temperature can be inferred from energy distributions, the pressure reached in the reaction zone from measurements of the collective flow, the entropy from the ratio of protons to composite particles and from pion production, the source radii at freeze-out from the study of the correlations of identical particles, and the amount of stopping from the rapidity distributions. Another important aspect is the study of multifragmentation. E895 will utilize the EOS TPC to extend all these measurements to the higher energies of the AGS.

CERN/RHIC Physics

At CERN, two large acceptance experiments measuring hadrons have been carried out. The main goal of the NA36 TPC experiment was to determine if the trends in strange particle production indicate a signature of the quark gluon plasma, while the NA35 experiment covered a wide region of phase space with both a streamer chamber and a TPC, addressing several experimental topics.

The collisions of the heaviest nuclei at the highest energies (Pb ions at the SPS, Au ions at RHIC) are expected to create systems whose space-time dynamics are qualitatively different from those of the colliding light ions studied up to now. The heavy systems have significantly higher energy densities over longer time scales. The extremely large number of produced hadrons in such collisions (several thousand in a central Au-Au event at RHIC) presents a real technical challenge and a unique opportunity: nontrivial, statistically significant signals can be extracted from single events, a technique known as *event-by-event analysis*. The correlation of extreme values of several observables sensitive to the quark-gluon plasma phase transition in a single event is a powerful tool for selecting ensembles of interesting events for detailed study. An event-by-event measurement of the produced particles provides the opportunity to select events with extreme values of temperature (particle spectrum), flavor (strangeness content), shape of the flow (particle momenta), and size (two-particle correlations). This technique requires a large acceptance detector that can

determine the momentum and identify a large fraction of the particles emitted in the collision.

NA49 is a fixed-target experiment at the SPS designed to study Pb-Pb collisions at 160 GeV/nucleon. Its goal is to simultaneously measure many hadronic signals that are thought to be sensitive to the quark-gluon plasma. To perform event-by-event analysis, it will measure and identify almost all charged particles in the forward half of phase space and will carry out detailed ensemble measurements of all the single-event observables as well as strange particle decays, two-particle correlation functions, and other hadronic observables.

STAR is a collider experiment at RHIC designed to study Au-Au collisions at $\sqrt{s_{nn}}$ = 200 GeV. Its goal is similar to NA49's, to simultaneously measure many hadronic signals. To perform event-by-event analysis, it will measure and identify almost all charged particles over two units of rapidity, centered at midrapidity. At RHIC there will be a high rate of hard processes. Hard-scattered partons (the precursors of high p_t particles and jets) are predicted to be sensitive to the medium through which they propagate and are directly calculable in perturbative quantum chromodynamics. The study of high p_t particles and jets as a function of energy and mass of the colliding system may also be an attractive experimental approach to identify the presence of quark matter, and STAR is being planned with this capability.

Experiments

The Dilepton Spectrometer (DLS)

The DLS collaboration, from early 1987 until the closure of the Bevalac, carried out a systematic study of e^+e^- production as a function of mass and energy. The DLS results, about 30k pairs, represent the world's only e^+e^- data at Bevalac/SIS energies. Important results include: (1) existence of a dielectron signal in both p-p and A-A collisions, (2) observation of contributions from mesonic decays (π^0, η, ρ/ω), bremsstrahlung, and Δ/N^* decays, (3) strong energy dependence of the pd/pp yield ratios signifying the presence of the η-meson, (4) absolute value and shape of the mass spectrum at 5 GeV in p-p and p-d collisions, which shows a need to modify existing N-N model calculations (pp vs. pn contributions, inelasticity), and (5) observation of high mass pairs (>500 MeV) in Ca-Ca collisions, which may be evidence for pionic annihilation. Analysis continues on the high-statistics Ca-Ca studies and evolution of mass and p_t distributions with projectile/target mass.

EOS TPC at the Bevalac

EOS was designed to study heavy-ion reactions over the whole energy range of the Bevalac. The TPC enables the measurement of the production cross-sections for protons, light composite particles, and pions over a large dynamic range. The EOS collaboration performed an extensive series of measurements prior to the shutdown of the Bevalac. Excitation functions of four systems (Ni + Cu, Ni + Au, La + La, and Au + Au) were measured from 250 MeV/nucleon up to the highest

energy. In addition, the systems Au + C, Kr + C, and La + C at 1 GeV/nucleon were measured.

The physics analysis of the data is being performed at LBL and other collaborating institutes. A complete excitation function for the directed flow in the Au + Au system has been measured. The new flow results show a striking scaling behavior that would be expected from nonviscous hydrodynamics. New correlation methods to study the nature of the directed flow have been developed. It can be shown that the flow is generated by particles being focused and having larger mean momenta in the flow direction. Systematic comparison of the data with model calculations are in progress. Preliminary results favor models with momentum-dependent interactions and a soft equation of state. In addition, multifragmentation of the Au + C system at 1 GeV/nucleon has been analyzed as a critical phenomenon. A method to extract critical indices from the data has been developed. Preliminary results show that the critical indices extracted are compatible with the critical indices of the liquid-gas phase transition.

EOS TPC at the AGS (E895)

E895 will carry out a systematic and exclusive measurement of the energy and mass dependence of particle production, correlations, and collective effects in Au + Au collisions at the AGS. In addition, E895 will study the dynamics of dilute nuclear matter and explore the emergence of critical phenomena (liquid-vapor phase transition) by varying the energy deposited into the Au projectile nucleus. E895 will measure the four-momentum of light mass particles, projectile fragments, and antiproton production. The experiment provides a large acceptance and thus many observables can be examined in fine detail at once.

NA36 at the SPS

NA36 was a TPC-based experiment designed to handle high charge multiplicity and high event rates. It measured strangeness production in relativistic heavy-ion collisions using ^{32}S beams at 200 GeV/nucleon. About 6 million events were recorded, mainly with a Pb target. The experiment had very wide acceptance in rapidity and transverse momentum, so that it overlapped the phase space of all other experiments. Neutral strange particles (Λ°, $\bar{\Lambda}^\circ$, K°_S), which decay to pairs of charged particles (protons, antiprotons, pions), were identified by the topology of their decays. Data-taking was completed in 1990.

NA36 recently published data on the multiplicity dependence of strange particle production, showing that the production rate rises for low multiplicity and saturates for high multiplicity. The value of the ratio of $\Xi^+/\bar{\Lambda}^\circ$ seen by NA36 is close to what could be expected from a hadronic gas source.

NA35 at the SPS

NA35 was a large acceptance experiment, having a large-volume Streamer Chamber within a 1.5T magnetic field and a TPC downstream of the magnet. It

was a survey experiment of hadronic signals and has delivered published results on particle spectra, two-particle correlations, strange particle yields, and other observables. LBL produced 6,000 channels of readout electronics for the TPC, significantly expanding its capability. Data-taking was completed in 1992.

Current analysis at LBL concentrates on TPC data on strange particle production, nuclear stopping, and pion interferometry. Preliminary TPC results on K^- production indicate a strangeness enhancement at midrapidity in agreement with previous results backward of midrapidity from the Streamer Chamber. This enhancement is a factor two with respect to an independent superposition of p + p or p + A interactions. Nuclear stopping, defined as the mean rapidity shift of projectile protons from beam rapidity, is estimated using TPC data in the forward direction by subtracting the number of negative hadrons from positive hadrons. For central S + Au collisions the rapidity shift measured indicates a significant amount of stopping (as large as at AGS energies). With the high statistics of the NA35 TPC data, we are investigating the dependence of observed source size on transverse momentum.

NA49 at the SPS

NA49 is a large acceptance experiment based on a set of Time Projection Chambers. Particle identification is performed primarily by the measurement of dE/dx in the relativistic rise regime (leading to TPCs that are 3.6 m deep), supplemented by time-of-flight over a part of phase space. Event characterization for triggering is performed by forward calorimetry.

LBL's responsibility for NA49 hardware is the development and manufacture of electronics for the 160k TPC readout channels. This very large number of channels necessitated new developments in TPC front-end integrated circuitry for cost, engineering, and reliability reasons. Developments of a 16-channel integrated preamplifier/shaper-amplifier and a 16-channel switched-capacitor-array/ADC were recently completed, and both integrated circuits are in production. We are nearing completion of the development of additional electronics components for the front-end electronics and data-acquisition. Lead beams will first be delivered by the SPS in November 1994.

STAR at RHIC

This experiment will consist of a Time Projection Chamber (TPC) and Silicon Vertex Tracker located inside a 5.2-m-diameter solenoidal magnet to provide tracking, momentum analysis, and particle identification of charged particles using the dE/dx technique. The trigger detector systems include a central scintillator barrel around the TPC, vertex position detectors near the beamline just outside the magnet, and calorimeters located in the region of the beam insertion magnets to selectively veto events according to the number of spectators. An electromagnetic calorimeter to trigger on transverse energy and measure jet cross-sections, a time-of-flight system surrounding the TPC for particle identification at higher momenta, and external time projection chambers

outside the magnet to extend the pseudorapidity coverage are anticipated as upgrades.

LBL's Relativistic Nuclear Collisions Program is providing a focus for these RHIC activities. With 40 physicists and engineers from LBL working on this experiment, the STAR collaboration now consists of 259 physicists and engineers from 30 institutions internationally. Within the STAR organization, RNC responsibilities also include primary responsibility for the TPC, TPC electronics, and overall detector integration. RNC also has significant responsibilities within the DAQ and software efforts in STAR. RNC physicists form the core of the software development that is focused on tracking and particle identification by dE/dx in the TPC. STAR will be ready to begin taking data in 1999 when RHIC begins operations.

Development

Microstrip Gas Chambers for TPC Readout

Traditionally, TPCs have been read out with multiwire proportional chambers located over a surface of pads that pick up the induced signal from avalanches on the wires. This technology sets a practical limit on the two-track resolution and the position resolution that can be obtained with a TPC. The new Microstrip Gas Chamber (MSGC) devices can overcome this limit and allow TPCs to be operated in much higher track density environments with improved position resolution. Tests of the MSGCs, which we have constructed with glass substrates, show that these devices are suitable for use in a TPC.

P-Type Silicon Drift Detectors

P-type silicon drift detectors have been designed and fabricated at LBL. Preliminary tests show that the detectors are functioning. Leakage currents and noise are higher than expected; however, potential sources have been identified and solutions are pending. Possible nonuniformities in the drift time can be monitored, and the proper design modifications are presently being incorporated into the design of the next set of detectors.

DLS Collaboration

S. Beedoe[3], M. Bougteb[4], **J. Carroll**[1], T. Hallman[1], L. Heilbron, H.Z. Huang[9], G. Igo[1], P. Kirk[6], G. Krebs, A. Letessier-Selvon[8], L. Madansky[5], F. Manso[4], H.S. Matis, D. Miller[7], J. Miller, C. Naudet, R.J. Porter[2], G. Roche[4], **L. Schroeder**, P.A. Seidl, Z.F. Wang[6], R. Welsh[5], W.K. Wilson, A. Yegneswaran[3].

[1]University of California at Los Angeles, Los Angeles, CA, USA.
[2]University of California at Davis, Davis, CA, USA.
[3]CEBAF, Newport News, VA, USA.
[4]Université de Clermont II, Aubière, France.
[5]The Johns Hopkins University, Baltimore, MD, USA.

[6]Louisiana State University, Baton Rouge, LA, USA.
[7]Northwestern University, Evanston, IL, USA.
[8]Université de Paris, LPNHE, Paris, France.
[9]Purdue University, West Lafayette, IN, USA.

EOS Collaboration

S. Albergo[1], F. Bieser, F.P. Brady[2], Z. Caccia[1], D.A. Cebra[2], A.D. Chacon[6], J. Chance[2], S. Costa[1], J. Elliott[5], M. Gilkes[5], A. Hauger[5], A. Hirsch[5], E. Hjort[5], A. Insolia[1], M. Justice[4], **D. Keane**[4], J. Kintner[2], V. Lindenstruth[3], M. Lisa, U. Lynen[3], H.S. Matis, M. McMahan, C. McParland, W.F.J. Mueller[3], D.L. Olson, M.D. Partlan[2], N. Porile[5], R. Potenza[1], G. Rai, J. Rasmussen, **H.G. Ritter**, J. Romanski[1], J.L. Romero[2], G.V. Russo[1], H. Sann[3], **R. Scharenberg**[5], A. Scott[4], Y. Shao[4], B. Srivastava[5], T.J.M. Symons, M. Tincknell[5], C. Tuvè[1], S. Wang[4], P. Warren[5], **H. Wieman**, K. Wolf[6].

[1]University of Catania, Catania, Italy.
[2]University California at Davis, Davis, CA, USA.
[3]Gesellschaft für Schwerionenforschung (GSI), Darmstadt, Germany.
[4]Kent State University, Kent, OH, USA.
[5]Purdue University, West Lafayette, IN, USA.
[6]Texas A & M University, College Station, TX, USA.

E895 Collaboration

S. Albergo[2], J. Alexander[6], F. Bieser, F.P. Brady[1], Z. Caccia[2], T. Case, D.A. Cebra[1], A.D. Chacon[7], J. Chance[1], S. Costa[2], K. Crowe, W. Gong, L. Heilbronn, A.S. Hirsch[5], E. Hjort[5], G.W. Hoffmann[8], A. Insolia[2], M.L. Justice[3], D. Keane[3], R. Lacey[6], M. Lisa, H. Lui[3], R. McGrath[6], C.P. McParland, J. Miller, C.F. Moore[8], S. Mordechai[8], D.L. Olson, M.D. Partlan[1], G. Peilert[4], N. Porile[5], R. Potenza[2], **G. Rai**, J. Rasmussen, H.G. Ritter, J. Romanski[2], J. Romero[1], C.V. Russo[2], R. Scharenberg[5], A. Scott[3], Y. Shao[3], B. Shrivastava[5], T.J.M. Symons, C. Tuvè[2], S. Wang[3], D. Weerasundara[3], H. Wieman, K.L. Wolf[7], C. Zeitlin.

[1]University of California at Davis, Davis, CA, USA.
[2]INFN, Catania, Italy.
[3]Kent State University, Kent, OH, USA.
[4]Lawrence Livermore National Laboratory, Livermore, CA, USA.
[5]Purdue University, Lafayette, IN, USA.
[6]State University of New York at Stony Brook, Stony Brook, NY, USA.
[7]Texas A & M University, College Station, TX, USA.
[8]University of Texas at Austin, Austin, TX, USA.

NA36 Collaboration

E. Andersen[1], R. Blaes[9], J.M. Brom[9], H.L. Caines[3], M. Cherney[7], B. de la Cruz[6], C. Fernández[8], C. Garabatos[8], J.A. Garzón[8], W. Geist[9], **D.E. Greiner**[2], C.R. Gruhn[2,a], M. Hafidouni[9], A. Hill[3], J. Hrubec[10], P.G. Jones[2], E.G. Judd[2,b],

J.P.M. Kuipers[4], M. Ladrem[9], P. Ladrón de Guevara[6], G. Løvhøiden[1], J. MacNaughton[10], J. Mosquera[8], Z. Natkaniec[5], J.M. Nelson[3], G. Neuhofer[10], C. Perez de los Heros[6], M. Pló[8], P. Porth[10], B. Powell[4], A. Ramil[8], H. Rohringer[10], I. Sakrejda[2], T.F. Thorsteinsen[1], J. Traxler[10], C. Voltolini[9], K. Wozniak[5], A. Yañez[8], and R. Zybert[3].

[1]University of Bergen, Department of Physics, Bergen, Norway.
[2]Lawrence Berkeley Laboratory, University of California, Berkeley, CA, USA.
[3]University of Birmingham, Department of Physics, Birmingham, UK.
[4]European Organization for Nuclear Research (CERN), Genève, Switzerland.
[5]Instytut Fizyki Jadrowej, Krakow, Poland.
[6]CIEMAT, Div. de Física de Partículas, Madrid, Spain.
[7]Creighton University, Department of Physics, Omaha, NE, USA.
[8]Universidad de Santiago, Dpto. Física de Partículas, Santiago de Compostela, Spain.
[9]Centre de Recherches Nucléaires, Université L. Pasteur, Strasbourg, France.
[10]Institut für Hochenergiephysik (HEPHY), Wien, Austria.
[a]Present address: CERN, PPE Division, Genève, Switzerland.
[b]Present address: MIT, Cambridge, MA, USA.

NA35 Collaboration

J. Bächler[4], J. Bartke[3], H. Bialkowska[10], M. Bloomer, R. Bock[4], R. Brockmann[4], P. Buncic[11], S.I. Chase, J. Cramer[13], I. Derado[8], V. Eckardt[8], J. Eschke[5], C. Favuzzi[2], D. Ferenc[11], B. Fleischmann[4], P. Foka[4], M. Fuchs[4], M. Gazdzicki[5], E. Gladysz[3], O. Hansen[5,12], J.W. Harris, W. Heck[5], M. Hoffmann[6], P. Jacobs, S. Kabana[5], K. Kadija[11], A. Karabarbounis[1], R. Keidel[7], J. Kosiec[5], M. Kowalski[8], A. Kühmichel[5], M. Lahanas[5], J.Y. Lee[5], M. LeVine[12], A. Ljubicic, Jr.[11], S. Margetis, R. Morse, E. Nappi[2], G. Odyniec, G. Paic[11], A.D. Panagiotou[1], A. Petridis[1], A. Piper[7], F. Posa[2], A.M. Poskanzer, F. Pühlhofer[7], W. Rauch[8], R. Renfordt[5], W. Retyk[9], D. Röhrich[5], G. Roland[5], H. Rothard[5], K. Runge[6], A. Sandoval[4], J. Schambach, E. Schmidt[5], N. Schmitz[8], E. Schmoetten[6], I. Schneider[5], **P. Seyboth**[8], J. Seyerlein[8], E. Skrzypczak[9], P. Spinelli[2], P. Stefanski[3], R. Stock[5], H. Ströbele[5], T. Trainor[13], G. Vasileiadis[1], M. Vassiliou[1], G. Vesztergombi[8], D. Vranic[11], S. Wenig[5].

[1]Department of Physics, University of Athens, Athens, Greece.
[2]Dipartimento di Fisica, Università di Bari and INFN Bari, Bari, Italy.
[3]Institute of Nuclear Physics, Cracow, Poland.
[4]Gesellschaft für Schwerionenforschung (GSI), Darmstadt, Germany.
[5]Fachbereich Physik der Universität, Frankfurt, Germany.
[6]Fakultät für Physik der Universität, Freiburg, Germany.
[7]Fachbereich Physik der Universität, Marburg, Germany.
[8]Max-Planck-Institut für Physik u. Astrophysik, München, Germany.
[9]Institute for Experimental Physics, University of Warsaw, Warsaw, Poland.
[10]Institute for Nuclear Studies, Warsaw, Poland.
[11]Rudjer Boskovic Institute, Zagreb, Croatia.
[12]Department of Physics, Brookhaven National Laboratory, Upton, NY, USA.
[13]Nuclear Physics Laboratory, University of Washington, Seattle, WA, USA.

NA49 Collaboration

J. Bächler[10], J. Bartke[7], H. Bialkowska[13], F. Bieser, M. Bloomer, R. Bock[10], L. Boroczky[5], P. Brady[3], D. Brinkman[8], R. Brockmann[10], P. Buncic[16], D. Cebra[3], J. Cramer[15], I. Derado[12], W. Dominik[14], J. Dunn[3], V. Eckardt[12], F. Eckhardt[11], J. Eschke[8], D. Ferenc[8], H. Fessler[12], H.G. Fischer[6], P. Foka[10], M. Fuchs[10], V. Gazakanian[4], M. Gazdzicki[8], H.J. Gebauer[13], E. Gladysz[7], J.W. Harris, S. Hegyi[5], M. Hoffmann[9], I. Huang[3], G. Igo[4], P. Jacobs, P.G. Jones, E. Judd, S. Kabana[6], K. Kadija[16], A. Karabarbounis[1], R. Keidel[11], J. Kosiec[14], M. Kowalski[7], A. Kühmichel[6], J.Y. Lee[6], A. Ljubicic, Jr.[16], V. Manske[11], S. Margetis, K. Marks, J.T. Mitchell, R. Morse, J.M. Nelson[2], G. Odyniec, G. Paic[16], A.D. Panagiotou[1], A. Petridis[1], A. Piper[11], A.M. Poskanzer, F. Pühlhofer[11], W. Rauch[12], R. Renfordt[6], W. Retyk[14], H.G. Ritter, D. Röhrich[8], H. Rothard[6], H. Rudolph, K. Runge[9], A. Sandoval[10], J. Schambach, N. Schmitz[12], E. Schmoetten[9], J. Seyboth[12], P. Seyboth[12], J. Seyerlein[12], E. Skrzypczak[14], I. Szenpetery[5], J. Sziklai[5], P. Stefanski[7], **R. Stock**[8], H. Ströbele[8], M. Toy[4], T. Trainor[15], S. Trentalange[4], G. Vasileiadis[1], M. Vassiliou[1], G. Vesztergombi[5], D. Vranic[16], S. Wenig[6], H. Wieman, C. Whitten[4], L. Wood[3], J. Zimanyi[5], X.-Y. Zhu[15], R. Zybert[2].

[1]Department of Physics, University of Athens, Athens, Greece.
[2]School of Physics, University of Birmingham, Birmingham, UK.
[3]University of California at Davis, Davis, CA, USA.
[4]University of California at Los Angeles, Los Angeles, CA, USA.
[5]Central Research Institute of Physics, Budapest, Hungary.
[6]CERN, Genève, Switzerland.
[7]Institute of Nuclear Physics, Cracow, Poland.
[8]Fachbereich Physik der Universität, Frankfurt, Germany.
[9]Fakultät für Physik der Universität, Freiburg, Germany.
[10]Gesellschaft für Schwerionenforschung (GSI), Darmstadt, Germany.
[11]Fachbereich Physik der Universität, Marburg, Germany.
[12]Max-Planck-Institut für Physik u. Astrophysik, München, Germany.
[13]Institute for Nuclear Studies, Warsaw, Poland.
[14]Institute for Experimental Physics, University of Warsaw, Warsaw, Poland.
[15]Nuclear Physics Laboratory, University of Washington, Seattle, WA, USA.
[16]Rudjer Boskovic Institute, Zagreb, Croatia.

STAR ★ Collaboration

W.J. Abraham[13], D.L. Adams[22], N. Added[23], S. Ahmad[22], S.A. Akimenko[20], B.D. Anderson[12], G.T. Anderson[2], R.M. Anjos[23], A. Aprahamian[18], Yu.I. Arestov[20], E.V. Atkin[16], A. Baldwin[12], V.V. Baublis[16], M.E. Beddo[1], N.I. Belikov[20], R. Bellwied[29], V.I. Belousov[20], S. Bennett[29], J. Bercovitz[13], I. Bertram[22], H. Bichsel[28], J. Bielecki[29], F. Bieser[13], N.N. Biswas[18], M.A. Bloomer[13], B.E. Bonner[22], M. Botlo[4], F.P. Brady[6], W.J. Braithwaite[2], L. Braun[13], J.A. Buchanan[22], N. Carlin[23], J.B. Carroll[7], R.J. Caylor[13], D.A. Cebra[6], A.D. Chacon[24], C.S. Chan[17], K.-S. Chan[25], S.I. Chase[13], M.G. Cherney[9], R.K. Choudhury[24], W. Christie[4], B.V. Chujko[20], J.M. Clement[22], M.D. Corcoran[22], T.M. Cormier[29], J.G. Cramer[28], P.B. Cramer[28], H.J. Crawford[5], A.M. Davidenko[20],

J.W. Dawson[1], R. Debbe[4], A.A. Derevschikov[20], P.A. DeYoung[8], W. Dominik[26], L. Dou[29], J.E. Draper[6], I. Duck[22], W.R. Edwards[13], E. Efstathiatis[17], S.E. Eiseman[4], J.M. Engelage[5], S.V. Erin[20], A. Etkin[4], D. Ferenc[10], I. Flores[5], K.J. Foley[4], Z. Fraenkel[30], A. French[29], E. Friedlander[13], D. Fritz[13], U. Garg[18], M. Gazdzicki[10], V. Ghazikhanian[7], G. Glass[25], W. Gong[13], O.A. Grachov[20], J. Grebiezkow[26], D. Greiner[13], L. C. Greiner[5], E. Grimson[14], D.P. Grosnick[1], V.V. Grushin[16], V.J. Guarino[1], W.N. Haberichter[1], R.W. Hackenburg[4], J. Hall[29], T.J. Hallman[7], **J.W. Harris**[13], W.E. Hearn[13], D.A. Hill[1], N. Hill[1], A.S. Hirsch[21], E. Hjort[21], G.W. Hoffmann[25], H. Huang[21], T.J. Humanic[19], G.J. Igo[7], P.M. Jacobs[13], R.C. Jared[13], R. Jayanti[19], P. Jensen[25], P. Jones[13], E. Judd[14], M.L. Justice[12], K. Kadija[3], M. Kaplan[8], P.J. Karol[8], T. Kasprzyk[1], D. Keane[12], V.P. Kenney[18], A.M. Khodinov[16], S.A. Kleinfelder[13], A.S. Konstantinov[20], D.V. Kostin[16], I. Kotov[20], V.N. Kozlov[16], M.A. Kramer[17], V.N. Kuryatkov[16], B. Lasiuk[7], A.N. Lebedev[16], M.J. LeVine[4], Q. Li[29], S.J. Lindenbaum[17], V. Lindenstruth[13], P.J. Lindstrom[13], M. Lisa[13], A. Ljubicic Jr.[3], W.J. Llope[15], R.S. Longacre[4], D.X. Lopiano[1], W.A. Love[4], S. Lubianov[16], L. Madansky[11], S. Margetis[13], J. Marx[13], H.S. Matis[13], Yu.A. Matulenko[20], C.P. McParland[13], T.S. McShane[9], A.P. Meschanin[20], Z. Milosevich[8], N.G. Minaev[20], N.M. Miphtakhov[16], K. Mirk[13], J. Mitchell[13], J.L. Mitchell[6], C.F. Moore[25], S. Mordechai[25], R. Morse[13], J. Murgatroyd[29], G.S. Mutchler[22], A.I. Mysnick[20], J. Nasiatka[1], A.Ju. Nazarov[16], V.N. Nevolin[16], T.L. Noggle[13], S.B. Nurushev[20], G. Odyniec[13], C. Ogilvie[14], D.L. Olson[13], A.St. Oltchak[16], E.M. Onischenko[16], E. Paganis[25], G. Paic[3], A.I. Pavlinov[20], T. Pawlak[26], D.M. Penzin[16], W. Peryt[26], E. Petereit[1], E.D. Platner[4], J. Pluta[26], A.Yu. Polyarush[20], N.T. Porile[21], A.M. Poskanzer[13], D.G. Prindle[28], T.I. Prokofieva[16], C. Pruneau[29], G. Rai[13], J. Rasson[13], R.L. Ray[25], D. Read[25], R.E. Renfordt [10], P.J. Riley[25], H.-G. Ritter[13], J.B. Roberts[22], D. Roehrich[10], A.A. Rollefson[2], J.L. Romero[6], A.I. Ronzhin[20], M. Ruckman[4], H. Rudolph[13], V.L. Rykov[20], I. Sakrejda[9], A.C. Saulys[4], J. Schambach[25], R.P. Scharenberg[21], L.S. Schroeder[13], J.E. Seger[9], V.A. Sergeev[20], D. Seymour[28], A.V. Shalnov[16], J. Sheen[29], K.E. Shestermanov[20], D. Shuman[13], A.B. Simakov[16], L.F. Soloviev[20], H.M. Spinka[1], B.K. Srivastava[21], R. Stock[10], M.N. Strikhanov[16], B. Stringfellow[21], H. Ströbele[10], R.J. Strzelinsky[4], A.T. Sustich[2], T.J.M. Symons[13], Yu.I. Sytsko[16], E.M. Szanto[23], A. Szanto de Toledo[23] , J.-L. Tang[25], S.I. Tarakanov[16], M.L. Tincknell[21], M. Toy[7], T.A. Trainor[28], S. Trentalange[7], O.D. Tsay[20], I. Tserruya[30], C.E. Tull[13], T. Tustonic[3], A.G. Ufimtsev[20], D.G. Underwood[1], A. Vander Molen[15], A.M. Vanyashin[16], A.N. Vasiliev[20], V.N. Vasiliev[16], G. Vilkelis[19], Yu.A. Volkov[16], S.V. Voloshin[16], D. Vranic[3], H.J. Ward[25], J.W. Watson[12], D.D. Weerasundara[12], R.P. Wells[13], R.C. Welsh[11], S. Wenig [10], G.D. Westfall[15], J. Whitfield[8], C.A. Whitten Jr.[7], H. Wieman[13], W.K. Wilson[29], D.C. Wold[2], K.L. Wolf[24], P. Yepes[22], A. Yokosawa[1], W. Zhang[12], K.H. Zhao[17], X.-Z. Zhu[28], Y. Zhu[17], V.E. Zyrin[16].

[1]Argonne National Laboratory, Argonne, IL, USA.
[2]University of Arkansas, Little Rock, AR, USA.
[3]Rudjer Boskovic Institute, Zagreb, Croatia.
[4]Brookhaven National Laboratory, Upton, NY, USA.
[5]University of California at Berkeley, Space Science Laboratory, Berkeley, CA, USA.
[6]University of California at Davis, Davis, CA, USA.
[7]University of California at Los Angeles, Los Angeles, CA, USA.

[8]Carnegie Mellon University, Pittsburgh, PA, USA.
[9]Creighton University, Omaha, NE, USA.
[10]University of Frankfurt, Frankfurt, Germany.
[11]Johns Hopkins University, Baltimore, MD, USA.
[12]Kent State University, Kent, OH, USA.
[13]Lawrence Berkeley Laboratory, Berkeley, CA, USA.
[14]Massachusetts Institute of Technology, Cambridge, MA, USA.
[15]Michigan State University, East Lansing, MI, USA.
[16]Moscow Engineering Physics Institute, Moscow, Russia.
[17]City College of New York, New York, NY, USA.
[18]University of Notre Dame, Notre Dame, IN, USA.
[19]Ohio State University, Columbus, OH, USA.
[20]Institute of High Energy Physics, Protvino, Russia.
[21]Purdue University, West Lafayette, IN, USA.
[22]Rice University, Houston, TX, USA.
[23]Universidade de São Paulo, São Paulo, Brazil.
[24]Texas A & M University, College Station, TX, USA.
[25]University of Texas at Austin, Austin, TX, USA.
[26]Warsaw University, Warsaw, Poland.
[27]Warsaw University of Technology, Warsaw, Poland.
[28]University of Washington, Seattle, WA, USA.
[29]Wayne State University, Detroit, MI, USA.
[30]Weizmann Institute of Science, Rehovot, Israel.

Nuclear Theory Program

J. Randrup

The Nuclear Theory Program at LBL seeks to address important problems at the frontier of nuclear science with the aim of achieving a deeper understanding of the physical nature of quantal many-body systems at and below the hadronic level. Such studies involve developing and applying theories and methods for prediction, analysis, and interpretation of experiments. Current research topics include relativistic nuclear collisions, properties and probes of hot and dense matter, structure of compact stellar objects, and macroscopic static and dynamical nuclear properties (e.g., microscopic simulations, transport theory, and chaos studies).

Ultrarelativistic Nuclear Collisions

In the exploration of the chromodynamic plasma phase of matter, experiments at the RHIC collider at Brookhaven National Laboratory (BNL) (and the proposed LHC at CERN) will involve novel dynamics, in which hard and semihard parton scatterings are expected to dominate the interaction mechanism and, consequently, perturbative Quantum Chromo-Dynamics (pQCD) may be brought to bear on the problem. Our research is motivated by the need to develop a realistic pQCD-based description that incorporates the hard processes. Such an approach will make it possible to address parton production and equilibration, and the associated hard probes of the dense partonic matter. This undertaking requires the solution and incorporation of many formal and fundamental problems. We therefore need to establish a diverse research program with strong components in both formal theory and phenomenological modeling that involves many aspects of high-energy nuclear physics.

Accomplishments and Impact

Since 1990, we have pursued a research program with special emphasis on the role of hard and semihard processes in pp, pA, and AA reactions at collider energies. Detailed systematic comparison of our results with a wide range of data has demonstrated, for the first time, that a quantitative understanding of the interplay between soft and hard QCD interaction can be achieved. Based on the extrapolation to AA collisions, we proposed the study of parton dynamics through jet quenching. We also studied the space-time structure of initial parton production and the parton equilibration. These studies revealed that the main uncertainties are associated with nuclear modifications of the parton distributions and the modeling of soft processes. Two-particle azimuthal correlations with different p_T cutoffs were proposed to constrain the model, thus reducing the uncertainties. Gluon shadowing in heavy nuclei was also investigated by perturbative parton recombination, which will provide theoretical guidance for calculating the parton distributions in nuclei.

The issues of parton equilibration and jet quenching also stimulated research on various problems in field theory. We have begun a systematic study of multiple scatterings and radiation within pQCD. The interference pattern of gluon radiation induced by multiple scatterings has a unique non-Abelian character. Because of the Landau-Pomeranchuk-Migdal effect, the radiative energy loss is highly sensitive to the color screening mass as an infrared cutoff scale. We are investigating whether this extra sensitivity could be exploited as a tool to "measure" that unknown scale in the vicinity of the Quark Gluon Plasma (QGP) transition. Transport properties of a weakly interacting QGP are also studied. Our research has had a significant impact in the relativistic heavy-ion physics community, as reflected in the explosive interest in the high p_T physics that has been emphasized by both the STAR and PHENIX collaborations at RHIC. The Monte-Carlo model *HIJING* (Heavy Ion Jet INteraction Generator) based on our theoretical studies has been made available and is currently used in simulations for RHIC and LHC detectors. Our studies have also led to broad interests in parton equilibration via pQCD. To further stimulate research in this area, a summer workshop, *Pre-equilibrium Parton Dynamics*, was organized at LBL in 1993, attracting about 40 active experts from around the world.

Plans

Our goal is to address all essential features of the fundamental theories to develop a quantitative model for ultrarelativistic nuclear reactions from presently available energies to those at future colliders. In the near future, we plan to carry out systematic calculations of the possible signatures and background contributions for the proposed hard probes of partonic matter. Toward this goal, two workshops are planned for 1994 in association with the CERN theory group. Collaborations with physicists from the Physics Division at LBL are also under way. By attacking the most fundamental problems related to our efforts, we intend to develop a diverse research program in ultrarelativistic heavy-ion physics and related areas, and we should be well positioned for taking advantage of new physics opportunities further into the future.

Intermediate-Energy Reactions/Nuclear Dynamics

When heavy nuclei collide at intermediate and high energies, transient systems are formed that have unusual physical properties, being small quantal many-body systems far from equilibrium. Such processes may thus reveal novel aspects of transport theory, and their study is a requisite for the analysis and interpretation of heavy-ion experiments. This prospect has motivated a continuing series of investigations.

Boltzmann-Langevin Transport Theory

Many macroscopic nuclear properties, both static and dynamic, can be well described on the basis of semiclassical models, in which nucleons moving in a self-consistent effective one-body field experience occasional two-body scatterings subject to Pauli suppression. In general, and especially when instabilities are encountered, it is necessary to incorporate the stochastic character of the elementary scattering processes, thus gaining an ability to treat catastrophic developments. This challenge has provided the focal point for a continuing research effort.

First a Fokker-Planck formulation was given of this nuclear Boltzmann-Langevin problem, allowing instructive analytical studies of the stochastic evolution of the reduced one-nucleon phase-space density, including the relaxation of the correlated fluctuations toward the appropriate quantum-statistical equilibrium and the triggering of catastrophes in nuclear matter. This advance has clarified certain long-standing theoretical issues.

A major remaining task is to explore nuclear multifragmentation processes since they offer the most suitable testing ground for the theory. While the work has also established a well-founded method for simulating the problem numerically, it is still too costly to treat the full theory. Recent efforts have been directed toward deriving suitable approximate treatments, and the confrontation with data has been brought closer to realization. Most recently, we derived simple analytical expressions for the transport coefficients that are expected to be quantitatively useful for multifragmentation scenarios; practical application is in progress, thus bringing the confrontation with data within reach.

These studies have generated considerable interest and activity among both theorists and experimentalists, and an increasing number of meetings are being organized with this topic as the focal point. In addition to the formal contributions to transport theory, the work is also expected to lead to a quantitative means for probing hitherto inaccessible dynamic properties of nuclear systems, such as spontaneous symmetry-breaking and characteristic times of spinodal modes.

Many-Body Simulations

A novel analysis method has been developed that is capable of recognizing quasibound clusters of nucleons in microscopic nuclear simulations, even when the system is still compact. This work has stimulated worldwide interest because of its bearing on the multifragmentation mechanism. The equilibrium properties of antisymmetrized molecular dynamics were also investigated. The level density remains essentially classical, despite the wave mechanics, which poses a key obstacle for a reliable description of nuclear fragmentation processes by microscopic many-body simulations.

A simple and general method was developed for treating the effect of N-body interactions in nuclear collisions, especially for subthreshold particle production.

Statistical Multifragmentation

An extended statistical multifragmentation model was developed and released. It includes a collective expansion and the interfragment Coulomb force. The code is being employed by several experimental groups, and application to recent data on central Au + Au collisions has revealed a significant radial flow.

The development of a transition-state theory for multifragmentation has led to the discovery of a simple, efficient, and exact method for generating statistical samples of particle momenta subject to microcanonical constraints on energy and linear, radial, and/or angular momentum, which was formerly believed to be an intractable problem.

Chaos Studies

The development of a macroscopic theory of nuclear dynamics has continued based on the parallel between a transition from ordered to chaotic nuclear motions and the transition from an elastic to a dissipative collective response of the nucleus. This research has many interdisciplinary ramifications, including mesoscopic solid-state problems, aspects of the acceleration of cosmic rays, theoretical dynamics (the diffusion of energy in chaotic time-dependent systems), and aspects of quantum chaos. The theory of nuclear dynamics is now firmly embedded in the vast current research on chaos, both classical and quantal.

Nuclear Astrophysics

There has been an explosive growth in the discovery of pulsar-related phenomena in the past decade. Binary partners range from planets to low-mass white dwarfs to neutron stars, and period glitches have emerged as a common feature of young pulsars. A unified understanding of these diverse phenomena poses an interesting challenge and some of our research has already suggested possible answers. This topic makes contact with high-energy nuclear physics, the subsaturation phase transition, hypernuclei, and other nuclear physics areas.

A wide range of topics in the category of compact stars has been pursued. For example, a perturbative approach to rotating relativistic stars has been developed, and their gravity wave instabilities and limiting periods have been explored with a wide sample of equations of state. We have also investigated strange quark stars, strange dwarfs, the stability of white dwarfs to growing cores of strange matter accumulated as strangelets, and computed the solution of rotating strange stars with a suspended nuclear crust, and we have found that the fractional change in the moment of inertia of the crust can in fact account for known glitches. Furthermore, we have clarified a long-standing misunderstanding in general relativity concerning the dragging of local inertial frames by rotating stars.

We have derived a model-independent limit on the rotation period of gravitationally bound stars (neutron stars). This has stimulated an experimental search for sub-ms pulsars that break the limit, which would indicate the existence of self-bound compact stars and constitute a fundamental discovery concerning the strong interaction.

It has been found that the free precession of pulsars can account qualitatively for the observed pulse drifting, nulling, and mode switching. We have also shown that precession can mimic planetary companions of neutron stars, a timely finding in view of the current intense reexamination of radio-astronomy timing residuals data.

Perhaps most importantly, we have discovered that hadronic and deconfined quark matter may coexist in a neutron star, if the phase transition is of first order. The two phases are intermixed and may form a Coulomb lattice with a depth-dependent structure extending for several kilometers. Therefore, pulsars are expected to be highly individualistic with regard to a number of observables, including the glitches in their periods.

The effect of neutrino transport on type-II supernovae is being investigated. A new relativistic code including the hydrodynamic flow and the stellar matter is being applied.

Macroscopic Nuclear Properties

In our continuing efforts to develop a systematic macroscopic-microscopic theory of static and dynamic nuclear properties, several milestones have been reached.

Droplet Model

The fine-tuning of the Finite Range Droplet Model of nuclear properties has been completed, resulting in currently the most comprehensive macroscopic-microscopic theory of nuclear binding energies, deformations, fission barriers, α-decay energies, etc., with theoretical predictions for 8,979 nuclei ranging from mass number 16 to 339. These quantities can now be estimated for heavy and superheavy nuclei with a degree of confidence not previously attainable.

Thomas-Fermi Model

We have developed a Thomas-Fermi model of average nuclear properties capable of reproducing the binding energy and density of nuclear matter, the surface and symmetry energies, the surface diffuseness, the optical potential (including its energy and isospin dependence), and other properties. Moreover, fast and accurate numerical techniques have been implemented solving the Thomas-Fermi equations for deformed (fissioning) nuclear shapes. The foundation now exists for a reliable description of the nuclear fluid in a range of applications, especially in astrophysics and multifragmentation.

An extension has been made of the self-consistent Thomas-Fermi model to finite temperatures, so thermostatic nuclear properties can be addressed. This extension has led to liquid-drop-type expansions for the level density and the free energy of hot nuclei embedded in a nucleon vapor.

Nuclear Data Evaluation Program: Isotopes Project

J.M. Dairiki

The Isotopes Project compiles, evaluates, and disseminates nuclear structure and radioactive decay data for basic and applied research. The Isotopes Project serves a broad user community and plays an active role in promoting the science of nuclear data evaluation. Since 1979, the Project has coordinated its activities with both the national and international data networks. In the past year, the Isotopes Project has increased its leadership role in the U.S. Nuclear Data Network (USNDN) and has become the lead center for the development of new electronic dissemination and publication methods for nuclear data.

At the present time, a member of the Isotopes Project, as chairman of the first USNDN Executive Committee, is serving as the Coordinator of the U.S. Nuclear Data Network. The Executive Committee has established several task forces to address important network issues and to help develop a long-range plan for the network. The Isotopes Project is well represented on these task forces.

Data Evaluation

The traditional strong data-evaluation effort of the Isotopes Project continues and has expanded to include pioneering efforts in horizontal data evaluation. The Isotopes Project is responsible for the evaluation of the nuclear properties of nuclei with mass numbers A = 81, 83, 89–93, 167–194, 206, 210–212, 215, 219, 223, and 227 (43 mass chains). This responsibility includes preparing data in computerized form for entry into the Evaluated Nuclear Structure Data File

(ENSDF). The group has accepted temporary responsibility for evaluating mass chains with A = 59, 76, 79, and 80, originally assigned to other centers, and for adapting evaluated data with A = 23–26, 33–44 into the ENSDF format. Six mass-chain evaluations were completed in 1993 and submitted to the National Nuclear Data Center at Brookhaven National Laboratory (BNL) for inclusion in the ENSDF file and for publication in *Nuclear Data Sheets*.

In addition to the mass-chain-oriented evaluations, there is a growing need for properties-oriented (or horizontal) evaluations to provide for changing research needs. For example, there is a clear need for an up-to-date high-spin database in support of research with the new generation of large detector arrays such as Gammasphere and Eurogam. The Isotopes Project initiated efforts to provide this community with the development of a file that includes data for over 3,000 bands from ENSDF and up-to-date superdeformed band data evaluated in collaboration with McMaster University. The Isotopes Project is represented on the USNDN task force assigned to working with the experimental community to recommend a procedure for incorporating the high-spin data and keeping it up to date. With Gammasphere located at LBL, the Isotopes Project expects to direct a part of its evaluation activities toward the high-spin effort, in coordination with other data centers and the research community.

The Isotopes Project is also participating in the USNDN task force charged with determining how best to provide the decay data needed by both basic and applied users. The task force is currently exploring the data needs of different areas of the scientific community, including the growing needs of the radioactive beam community.

Concurrent with evaluation of data, the Isotopes Project develops methods and computer codes for data analysis. The methods include minimization procedures for deducing best values from various sets of data, and the codes include data-verification codes for ensuring correctness and uniformity. The Project has a continuing interest in methods for propagation of the experimental uncertainties reported for nuclear properties.

Table of Isotopes, 8th Edition

Between 1940 and 1978, the Isotopes Project produced seven editions of the *Table of Isotopes*. Each edition provided a comprehensive and critical evaluation of the known nuclear properties deduced from radioactive decay and reaction data. The 8th edition of the *Table of Isotopes* is now being prepared; the book is derived from a file generated from ENSDF. Considerable updating and editing is being carried out to achieve more uniform quality of information and presentation. The book will contain mass-chain decay schemes similar to those in previous editions, tabular summaries of adopted levels, gamma-ray data, combined decay schemes, rotational band drawings, and various appendices. The book is expected to run about 3,000 pages and will be published in two volumes by John Wiley & Sons, Inc., in 1995. In addition to the published version, the book will be available electronically on a CD-ROM.

Database Development

The Isotopes Project is developing electronic access to ENSDF, the Nuclear Structure References (NSR) file, and related files. New electronic publications will provide an alternative to the traditional hard-copy publications. Because the ENSDF format was developed 20 years ago, the file lacks the indexing, organization, and data structures necessary for fast and efficient data retrieval. Therefore, modernization of the database is central to the task of electronic publishing.

The database development has been divided into two stages. The first stage involves completion of most indexing and limited file reorganization. The second stage will involve incorporation of the file into a database management system. In its final form, ENSDF will be provided with an interactive file editor that will free evaluators from specific knowledge of data formats and will also allow many more scientists to use the ENSDF tools and participate in evaluation.

Electronic "Publications"

The group has made considerable progress toward developing an electronic version of the *Table of Isotopes*, to be published on CD-ROM. This medium provides a convenient way for updating the book at regular intervals. The group is working with John Wiley & Sons, Inc., as this development proceeds. Technology is changing rapidly in this area and the recent release of Adobe's ACROBAT software, for example, has opened up tremendous opportunities. A beta version of the CD-ROM will be completed this year and distributed (free) to all interested testers. This version includes bookmarks (interactive indices to the data) and hypertext links between skeleton schemes, tables, and drawings.

A University of Lund–LBL collaboration has implemented the NSR file on IBM/PCs as a complement to the existing on-line system maintained by BNL. Retrieval of information can be done using the PAPYRUS bibliographic database management system, produced by Research Software Design, Inc. The entire database is up to date as of December 1993 and contains about 130,000 references requiring over 50 Mbytes of disk memory; it will be distributed on CD-ROM and is expected to be released in May 1994. This system will be useful in particular for those who do not have on-line computer network access to NSR.

Another new development is the VuENSDF computer program, which provides extensive interactive display capabilities for data in ENSDF format. The program is provided with the complete ENSDF database and supports the selection and display of any ENSDF dataset. Both level scheme drawings and tabular listings are available and multiple windows can be created. The drawings can be scaled and manipulated interactively, and transitions can be shown in groups feeding or deexciting a level, or by establishing coincidence requirements. The VuENSDF code is currently available for beta testing on Macintosh computers and a PC version is under development. Because VuENSDF can display any data file that uses the ENSDF format, it is a useful tool

for both evaluators preparing datasets and researchers analyzing experimental information.

Publications

1. C.M. Baglin, *Nuclear Data Sheets*, **69**, 733 (1993).
2. C.M. Baglin, *Nuclear Data Sheets*, **69**, 267 (1993).
3. C.M. Baglin, *Nuclear Data Sheets*, **70**, 1 (1993).
4. E. Browne, *Nuclear Data Sheets*, **68**, 747 (1993).
5. A.O. Macchiavelli and E. Browne, *Nuclear Data Sheets*, **69**, 903 (1993).
6. H.W. Taylor and B. Singh, "Radioactivity in Paper," *J. Environ. Radioactivity*, **21**, 177 (1993).
7. E. Browne, I. Ahmad, K.E. Gregorich, S.A. Kreek, D.M. Lee, and D.C. Hoffman, "Electron-Capture Decay of ^{231}U," *Nucl. Instr. Meth.*, **339**, 209 (1994).
8. B. Singh and H.W. Taylor, "Half-Lives of Microsecond Isomers in ^{151}Eu and ^{181}W," *Appl. Radiat. Isotopes*, **45**, 374 (1994).

88-Inch Cyclotron Operations

C.M. Lyneis, D.J. Clark, D. Collins,
A. Guy, S.A. Lundgren, M.A. McMahan,
and Z.Q. Xie

The 88-Inch Cyclotron is operated by the Nuclear Science Division as a national facility in support of U.S. Department of Energy programs in basic nuclear science. The central component of this facility is a sector-focused, variable-energy cyclotron fed by two Electron Cyclotron Resonance (ECR) high-charge-state ion sources—the LBL ECR and the Advanced ECR. This versatile combination produces heavy ion beams from helium to neon with energies up to 32 MeV/nucleon. For heavier ions the maximum energy per nucleon decreases with increasing mass. Typical ions and maximum energies (MeV/nucleon) are argon (22), krypton (13), xenon (8), and bismuth (4). Light ions—p, d, ^{3}He, and ^{4}He—are produced up to total energies of 55, 65, 135, and 130 MeV, respectively. Polarized beams at intensities of up to 0.5 microampere are also available. After acceleration in the Cyclotron, the beam can be delivered to any one of 11 experimental stations in 8 caves. Some of these stations are dedicated to a particular experimental group; others are for general-purpose use. Beams directly from the ECR source at up to 10 keV per charge state can be delivered by a transport system on the vault roof to target stations for atomic physics research.

Ions and Energies

The 88-Inch Cyclotron, fed by the two ECR sources, provides a wide range of ions, energies, and intensities in support of the experimental program. By using the low- and high-temperature ovens, most elements can be accelerated. A

flammable gas cabinet was added in FY93 to run beams such as protons and silicon in a safe manner. Figure 1 shows the ions that have been accelerated in the Cyclotron for experiments. A list of beams with maximum energy and typical intensities is given in Table 1 (see end of this Overview). The high efficiency of the ECR source makes it economical to run some of the beams with isotopically enriched material. Common examples are ^{18}O and ^{22}Ne for the heavy-element program and ^{36}S and ^{48}Ca for Gammasphere.

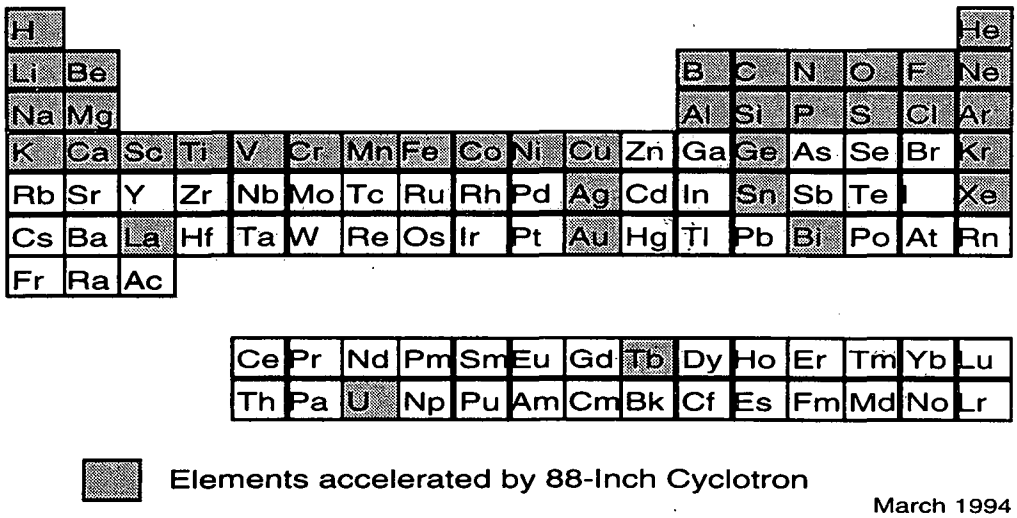

Fig. 1. Beams produced by the LBL ECR source and the 88-Inch Cyclotron.

The beams listed in Table 1 are generally developed as needed by the wide range of experiments proposed by users of the 88-Inch Cyclotron. As the Gammasphere detector continues operation we expect to develop an even wider range of ion species, particularly neutron-rich isotopes, which are used to produce high spin states in compound nuclei. Heavy element radiochemistry experiments require several eμA of beams up to mass 48 at 6–8 MeV/nucleon. Groups studying heavy-ion reaction mechanisms and complex fragmentation of highly excited nuclei use higher energy beams such as nitrogen and oxygen at 32 MeV/nucleon, neon at 25 MeV/nucleon, and nickel, krypton, and tin at 13–20 MeV/nucleon. In addition to the heavy-ion beams used with the Cyclotron, the light-ion beams continue to be frequently used. For example, the project to develop laser trapping of radioactive sodium beams requires 25 MeV proton beams. The study of β-delayed proton emission requires several eμA beams of

^{3}He at 40 to 110 MeV. The nuclear astrophysics group typically uses beams of protons, deuterons, ^{3}He, and ^{4}He at 8–25 MeV/nucleon.

ECR Ion Source Development

The Advanced ECR (AECR) is in regular use for the experimental program, providing beams of greater intensity and higher charge states than are available from the LBL ECR. (The AECR operates at 14 GHz, compared to 6 GHz for the LBL ECR, and incorporates an electron gun to inject cold electrons into the plasma and boost the production of high-charge-state ions.) In the last year, development of the source has greatly improved its short- and long-term stability. Development of the source for the production of beams from solids, with special emphasis on the efficiency of source feed, is continuing.

Accelerator Improvement Projects

An accelerator improvement project to upgrade the heavy-ion performance of the Cyclotron is under way. One upgrade will improve the heavy-ion transmission in the Cyclotron by providing better vacuum. A new cryopanel is being designed and tests with additional cryopumps are in progress. Another upgrade will develop a system to reduce the beam phase width to improve beam timing. Orbit tracking codes are being used to determine how to best accomplish this and tests with internal slit systems are in progress. In FY94, an upgrade of the Cyclotron's personnel radiation safety interlock system was begun.

Accelerator Use

Late in FY93, Cyclotron operation increased from five to seven days/week to accommodate the Early Implementation of Gammasphere. In FY93, 4,320 hours of research time were produced, and in FY94, with full seven-day/week operation, 5,360 research hours are anticipated. Gammasphere is now using approximately 60% of the nuclear science time and is projected to reach a 3,000 hour per year operating level in FY94. Table 2 (see end of this Overview) summarizes the time distribution and research statistics. The Accelerator Operation Summary shows that Cyclotron reliability was very high, with less than 2% of the operating time being lost to unscheduled maintenance. The "Other Research" category under "Experiment Summary" consists mainly of testing electronic integrated circuits in partnership with the aerospace industry by using Cyclotron beams to simulate space radiation.

User Support

Our users fall into two classes: (1) scientific users whose experimental proposals are reviewed by a Program Advisory Committee (PAC) and who are awarded time based on the scientific merits of these proposals, and (2) industrial users who purchase beam time for their own proprietary use.

Written proposals for experiments in nuclear science are evaluated by the PAC on the basis of the science proposed. Current members are R. Janssens (ANL), R.W. Hoff (LLNL), J. Waddington (McMaster), N. Koeller (Rutgers), R.L. McGrath (SUNY), and L. Sobotka (Washington University). The current membership of the Users' Executive Committee is J.M. Alexander (SUNY), J.A. Becker (LLNL), K.E. Gregorich (LBL), W.D. Loveland (Oregon State University, chairman), and H.R. Weller (Duke University).

The 88-Inch Cyclotron Research Group (88Users) provides information, assistance, and coordination to outside users of the 88-Inch Cyclotron. It is the main contact between the Cyclotron operations staff and outside users, as well as between the users and the rest of LBL. As such, 88Users is responsible for the development and maintenance of experimental facilities at the Cyclotron and for making these facilities attractive to a diverse group of users from around the country and, in some cases, around the world.

88Users coordinates the PAC, which meets three times a year to review proposals for beam time. It supports both the 88-Inch Users' Association and the Gammasphere Users' Association and their Executive Committees by (1) holding annual Users' meetings at the fall meeting of the Division of Nuclear Physics of the American Physical Society, (2) sponsoring periodic telephone conferences of the Executive Committee to carry user concerns to the Cyclotron management, and (3) publishing a semimonthly newsletter distributed to all Users. 88Users also maintains the NSD Equipment Pool.

A computer support effort is aimed at developing and maintaining general hardware and software for experimental data acquisition, on-line diagnostics, and general data-analysis capabilities at the 88-Inch Cyclotron. A DEC Alpha computer is in place for the general computational needs of the occupants of Building 88. The Q-bus-based DEC 3200/Starburst acquisition systems, used now by all but the Gammasphere experiments, are systematically being replaced because of their age and maintenance costs. For the smaller experiments, the replacement (a DEC 3100 workstation coupled to a list processor) has been demonstrated to work and is being used regularly by the heavy element group. Hardware is being obtained to replace two other acquisition systems with this configuration. The future needs of the larger experiments are presently being evaluated.

User Statistics

Research at the Cyclotron is conducted by scientists from many institutions in addition to those from LBL and the University of California at Berkeley. During FY93, the Cyclotron was used by 190 scientists from 34 institutions. These users included 59 scientists from 16 institutions coming to use Gammasphere. (The first six months of FY94 has brought 95 scientists from 29 institutions to use Gammasphere.) The Cyclotron also plays an important role in the education and training of young scientists at the undergraduate, graduate, and postdoctoral stages of their careers. In FY93, 32 graduate students performed all or part of their thesis experiments using the 88-Inch Cyclotron.

Gammasphere

The upgrades to the 4c beamline, cave, and counting area were finished in FY93, and Gammasphere is presently running with 32 detectors in place. The vacuum upgrades to the beamline plus the addition of new quadrupoles have doubled the transmission from the cyclotron to the target to reach a value of ≈45%.

A major effort this year involved using the first auxiliary detector in conjunction with Gammasphere; namely, the Washington University microball, a 96-element CsI detector for particle identification. This detector was used for three experiments in March 1994. In order to run the microball with Gammasphere, a UNIX-based data-acquisition system, based on the Michigan State University 4π detector acquisition system, was implemented.

Applied Research

The 88-Inch Cyclotron is a major source of heavy-ion beams for Single-Event Effect (SEE) testing of solid-state components for the U.S. space program. Because of the ability to run "cocktails" of beams, enabling switches from one ion to another in a matter of minutes, it is possible to quickly establish the energy deposition level at which a SEE will occur. The availability of proton beams, used for studying radiation effects on charge-coupled devices, has further increased the demand for use of the Cyclotron.

The Aerospace Corporation, in cooperation with 88-Inch Operations, is presently installing a specially instrumented scattering chamber on a dedicated beamline. When completed, the 88-Inch will be able to support a state-of-the-art user-friendly facility for industrial and government users on a cost-recovery basis. Work is in progress to develop diagnostics (dosimetry, energy, beam purity) for smaller companies that do not have the resources to provide their own diagnostics.

In FY93, a small Biomed program was transferred to the Cyclotron from the Bevalac. High-energy protons, helium, and nitrogen are used to study the effect of radiation on cells. The use of segmented ion chambers allow the tuning of a large-diameter (10-cm [4-inch]) uniform beam onto the samples. This large-diameter light-ion beam has also been used for some Single-Event Upset (SEU) studies.

Safety

We continue to devote significant effort to improving the safety and conduct of operations at the Cyclotron. The Cyclotron is being brought into compliance with the new Radcon manual. EH&S Division staff are involved early in the scheduling cycle to flag and alleviate potential safety problems before they happen.

Publications

1. D.J. Clark, "A 600 MeV Cyclotron for Radioactive Beam Production," *Proceedings of the 1993 Particle Accelerator Conference*, Washington, D.C., May 1993.
2. C.M. Lyneis, "Concluding Remarks for the 11th ECR Ion Source Workshop," *Proceedings of the 11th International Workshop on Electron Cyclotron Resonance Ion Sources*, Groningen, Netherlands, May 1993, p. 335.
3. M.A. McMahan, *The 88-Inch Cyclotron*, PUB-740, Lawrence Berkeley Laboratory, February 1994.
4. M.A. McMahan, D.J. Clark, A. Guy, C.M. Lyneis, G.J. Wozniak, and Z.Q. Xie, "Fast Energy and Ion Changes Using a Cyclotron with ECR Source," Presented at the American Physical Society Division of Nuclear Physics Fall Meeting, Asilomar, California, October 1993.
5. M.A. McMahan and C.M. Lyneis, "Single Event Upset Testing at the 88" Cyclotron at Lawrence Berkeley Laboratory," Presented at the 9th Symposium on Single Event Effects, Manhattan Beach, California, April 1994.
6. A. Young, K. Bertsche, D. Clark, K. Halbach, W. Kunkel, K.N. Leung, C.Y. Li, R. Schlueter, M. Stuart, R. Wells and J.X. Yu, "Development of a Compact Permanent Magnet Cyclotron for Accelerator Mass Spectrometry," *Proceedings of the 1993 Particle Accelerator Conference*, Washington, D. C., May 1993.
7. Z.Q. Xie and C.M. Lyneis, "Recent Developments on ECR Sources at LBL," *Proceedings of the 11th International Workshop on Electron Cyclotron Resonance Ion Sources*, Groningen, Netherlands, May 1993, p. 106.

Table 1. 88-Inch Cyclotron beam list.

Ion[a]	High Energy[b] (MeV/u)	Typical Current @ High Energy (eμA)	Typical Current @≈5-6 MeV/u (eμA)
p	55	6	20
p (pol.)	50	0.4	0.7
d	32	0.7	20
d (pol.)	32	0.2	0.7
^{3}He	45	10	10
^{4}He	32	2	8
^{7}Li	23	0.4	2
^{9}Be	25	0.15	0.05
^{11}B	26	0.05	0.05
^{12}C	32	0.01	12
^{14}N	32	0.03	5
^{16}O	32	2	6
^{19}F	29	0.9	0.35
^{20}Ne (22)	32	0.25	4
^{23}Na	29	0.07	0.07
^{24}Mg (25,26)	32	0.7	3
^{27}Al	30	0.07	4.5
^{28}Si (29,30)	32	2.2	2
^{31}P	30	0.25	0.5
^{32}S (34)	32	0.32	4
^{35}Cl (37)	30	0.01	0.5
^{40}Ar	23	0.04[c]	1
^{39}K	24	1.0	1.8
^{40}Ca	23	0.13	2.5
^{45}Sc	22	0.023	0.22
^{48}Ti	21.5	0.5	0.5
^{51}V	20	0.6	0.6
^{52}Cr	20	0.6	0.6
^{55}Mn	20	0.3	-
^{56}Fe (54)	20	0.5	0.5
^{59}Co	19	0.006	0.01
^{58}Ni	19	0.3	0.1
^{63}Cu (65)	18.5	0.4	0.4
^{84}Kr (78,82,86)	14	0.1	0.3

Table 1 (continued).

Ion[a]	High Energy[b] (MeV/u)	Typical Current @ High Energy (eμA)	Typical Current @≈5-6 MeV/u (eμA)
^{107}Ag	11	0.007	0.007
^{120}Sn (118)	9	0.002	-
^{132}Xe (129,131,136)	8	0.013[c]	0.013[c]
^{139}La	8	0.002	0.03
^{159}Tb	7	0.006	0.006
^{209}Bi	5	0.001	0.0001
^{238}U	4	0.001	0.01

Notes for Table 1:

[a]Most abundant isotope is listed. Other isotopes run from natural feed are shown in parentheses. Their intensities are proportional to the isotopic abundance, and their high-energy values proportional to $1/A^2$.
[b]For M>60, the high energy corresponds to 1 pnA of beam from the AECR.
[c]AECR measurement; other quoted currents are for ECR beams. AECR gives roughly 5x the ECR beam intensity for all but the heaviest, (M>80) highest energy ions.

The following ions have been run at the 88-Inch Cyclotron using isotopically enriched source material (the intensity is proportional to enrichment factor and currents for the same element in the table):

$$^{13}C,\ ^{15}N,\ ^{18}O,\ ^{21,22}Ne,\ ^{33,34,36}S,\ ^{36}Ar,\ ^{44,48}Ca,\ ^{70}Ge,\ ^{78,86}Kr,\ ^{136}Xe\ .$$

All intensities given are from actual Cyclotron runs, thus they may not reflect the true limits of the facility for a given ion. Intensities are measured at the exit of the Cyclotron. Transmission varies according to the beamline optics, collimation, and energy resolution requirements and is typically on the order of 15–20% for Gammasphere, 4a, and 4b lines, and 40% elsewhere. Low-intensity, high-charge-state ions can be tuned using an analog beam of the same q/M. Cocktails are available of ions of similar q/M. Beam energies down to 0.3 MeV/u are available.

Table 2. FY93 88-Inch Cyclotron operating statistics.

Accelerator Operation Summary	
Research	4,320 hours
Tuning	475
Machine Studies	136
Unscheduled Shutdowns	81
Scheduled Shutdowns	3,748
Electrical Energy Consumption (GWH)	7.0
Experiment Summary	
Beam Utilization for Research	
Nuclear Research	3,622 hours
Biology and Medicine	30
Other Research	668
Total	4,320
Number of Nuclear Science Experiments	50
Number of Scientists	146
Number of Students	32
Institutions Represented	
Universities	10
Other DOE National Laboratories	3
Other	12
Applied Research	
Number of Scientists and Engineers	44
Institutions and Companies	9
Percentage of Beam Time	
In-House Staff	54
Universities	5
DOE National Laboratories	21
Foreign Institutions/Universities	4
Applied	16
Total	100

GROUP LISTS

Group Lists

Following are the lists of people in the Nuclear Science Division groups. At the end of each list are the long-term visitors with their home institutions in parentheses.

Administrative Staff
K. Balder-Froid
A.K. Calloway
J.M. Dairiki, Assistant Director
G. Goodman
R.E. Hodges
J.B. Lofdahl
M.K. Loo
M.E. Montgomery
B.E. Phillips
T.S. Pouncey
W.J. Smith-Burnett
M.B. Star
C.J. Sterling
J.C. Sterling
T.J.M. Symons, Director
J.M. Tarzian
For Glenn T. Seaborg, Associate Director at Large:
N.B. Lockhart
S.L. Whyte
D. Yan

Isotopes Project
C.M. Baglin
E. Browne-Moreno
S-Y. F. Chu
Janis M. Dairiki
R.B. Firestone
V.A. Shirley
B. Singh
J.H. Zipkin
J.Z. James (UCB)

Software Group
R.A. Belshe
S. Jacobson
C.P. McParland
W.H. Rathbun
E.B. Yee

OASIS
J.M. Nitschke
M.A. Stoyer
T. Sikkeland (University of Trondheim)

Theory
M. Asakawa
J. Cernohorsky
N.K. Glendenning
M. Harlander
H. Heiselberg
C. Jarzynski
W.D. Myers
J. Randrup
W.J. Swiatecki
R. Vogt
X. Wang
J.P. Helgesson (Lund University)

Exotic Nuclei: RAMA
J. Cerny
J.C. Batchelder*
D.M. Moltz
T.J. Ognibene*
M. Rowe*
R.J. Tighe

High-Spin Studies
S.J. Asztalos*
B.W. Cederwall
M.A. Deleplanque-Stephens
R.M. Diamond
P. Fallon
I.Y. Lee
A.O. Macchiavelli
F.S. Stephens
J.E. Draper (UC Davis)
C. Duyar* (UC Davis)
E. Rubel* (UC Davis)

*Graduate student. **Undergraduate student. **Group leaders in bold face.**

Special Projects
H. E. Conzett
B. G. Harvey
H.H. Heckman
J.O. Rasmussen

Nuclear Astrophysics and Fundamental Symmetries
Y.D. Chan
A. García
R.M. Larimer
K.T. Lesko
R.J. McDonald
M.C. Moebus
E.B. Norman
R.G. Stokstad
F.E. Wietfeldt*
I. Žlimen
I.D. Goldman (Universidade de São Paulo)

Weak Interactions
C.J. Bowers*
S.J. Freedman
B.K. Fujikawa
L. Lising*
Z. Lu*
J. Mortara*
A-T. Nguyen**
J. Reich*
M. Rowe*
S. Shang
E. Wasserman
K. Yasamura**

Heavy Element Nuclear and Radiochemistry
N.J. Forinash**
A. Ghiorso
K.E. Gregorich
N.J. Hannink*
D.C. Hoffman
C.D. Kacher*
M.R. Lane*
D.M. Lee
M.F. Mohar
G.T. Seaborg
E. R. Sylwester*
J. Yang**
H.L. Hall (LLNL)
B.A. Kadkhodayan (LLNL)
W.D. Loveland (Oregon State)
Y. Watanabe (Fuji Electric Corp., Ltd.)

88-Inch Cyclotron Operations
D.J. Clark
R.C. Coates
D.E. Deutscher
A.P. Guy
R.M. Larimer
C.M. Lyneis
S.A. Meaney
M.A. Norris
V.L. Saling
C.R. Siero
Z.Q. Xie
A. Katz (RAFAEL)

Intermediate Energy
K.A. Hanold*
K. Jing*
L.W. Phair
L.G. Moretto
W. Skulski
K. Tso*
A.C. Veeck*
G.J. Wozniak

Cosmic Rays
M. Cronqvist
C. Kuo*
L. Wu
S. Costa (Catania)
H.J. Crawford (UCSSL)
J.M. Engelage (UCSSL)
I. Flores (UCSSL)
L.C. Greiner (UCSSL)
J. Romanski (Catania)
C.E. Tull (LSU)

Crystal Barrel
D. Armstrong
R.R. Bossingham
T.A. Case
K. Crowe
M. Lakata*

Plastic Track Detectors
Y.D. He
D.M. Lowder
P.B. Price
A.A. Richards*
D. Snowden-Ifft

Secondary Radioactive Beams
K. Matsuta

Subthreshold Kaons and Antiprotons
J. Drewery
S.N. Kaplan
V. Perez-Mendez

Relativistic Nuclear Collisions
F.S. Bieser
M.A. Bloomer
S. Chase*
W.B. Christie
E.M. Friedlander
W. Gong
D.E. Greiner
J.W. Harris
P.M. Jacobs
P.G. Jones
E. Judd
V. Lindenstruth
P.J. Lindstrom
M. Lisa
S. Margetis
J.N. Marx
H.S. Matis
J.T. Mitchell
R.J. Morse
C.J. Naudet
G. Odyniec
D.L. Olson
A.M. Poskanzer
G. Rai
H-G. Ritter
H. Rudolph
I. Sakrejda
J.J. Schambach
L.S. Schroeder
A. Sobel**
N.W. Wang
H.H. Wieman
W.K. Wilson
J.D. Wolf
M. Belt** (Creighton)
J. Carroll (UCLA)
D.A. Cebra (UC Davis)
E. Chan* (UT Austin)
N. Chan** (SF State)
J. Chance* (UC Davis)
A. D. Chacon (Texas A&M)
S. Costa (Catania)
R. Dass* (UT Austin)
Z. Fraenkel (Weizmann)
T.J. Hallman (UCLA)
E.C. Hjort (Purdue)
E. Holtmann** (UC Berkeley)
M.L. Justice (Kent State)
M. Kirk** (Santa Clara)
D. Lewak** (SF State)
J. Moelis** (UC Berkeley)
T. Munsat** (No. Carolina)
S. Paganis* (UT Austin)
M. Partlan* (UC Davis)
R.J. Porter* (UC Davis)
W. Retyk** (Warsaw)
G.R. Roche (Clermont II)
Y. Shao* (Kent State)
A. Tang* (UT Austin)
M. Toy* (UCLA)
S. Whitten** (Nebraska)

NUCLEAR STRUCTURE AND REACTIONS

High-K bands in the ^{166}Yb region*

*J.R.B. Oliveira††, S. Frauendorf†, M.A. Deleplanque, B. Cederwall, R.M. Diamond, A.O. Macchiavelli, F.S. Stephens, J. Burde‡, J.E. Draper§, C.Duyar§, E. Rubel§, J.A. Becker**, E.A. Henry**, M.J. Brinkman**, A. Kuhnert**, M.A. Stoyer**, T.F. Wang*

The high-spin states of $^{166\text{-}168}$Yb nuclei were populated in the reaction ^{124}Sn(^{48}Ca,xn) at 210, 220 and 225 MeV and the γ-ray deexcitation of these nuclei was observed at the 88-Inch Cyclotron with HERA, an array of 20 Compton-suppressed Ge detectors with a 40-element central ball. About 420, 570, and 166 million events (~80% high-fold (>11) doubles and 20% triples) were recorded.

Using high-multiplicity and high-total-energy cuts, weakly populated high-K bands have been observed in these nuclei (see Fig.1). In ^{167}Yb, this band, previously assigned to the ν[505]11/2 configuration, has been extended and the B(M1)/B(E2) ratio observed is in agreement with this assignment. The properties of the bands observed for the first time in ^{166}Yb and ^{168}Yb have led to rather unusual tentative configuration assignments, i.e. π[7⁻]xν[AB] and π[7⁻]xν[AE] respectively. (A and B are the first and second positive parity quasiparticle excitations (from the $i_{13/2}$ subshell) and E is the first negative parity quasiparticle excitation (from [523]5/2 and [521]1/2 parentage)). The "Tilted Axis Cranking"[1] model predicts lower excitation energies for such bands than would be expected from traditional models, and is able to reproduce the large B(M1)/B(E2) ratios observed.

Footnotes and References

*Submitted to Phys. Rev. C

† † University of Sao Paulo, Brazil

† Inst. of Nucl. Phys. Rossendorf, Germany

‡Racah Inst. of Phys. Jerusalem, Israel

§UC Davis, Davis, CA

**LLNL

1. S. Frauendorf, Nucl. Phys. A557 (1993) 259c.

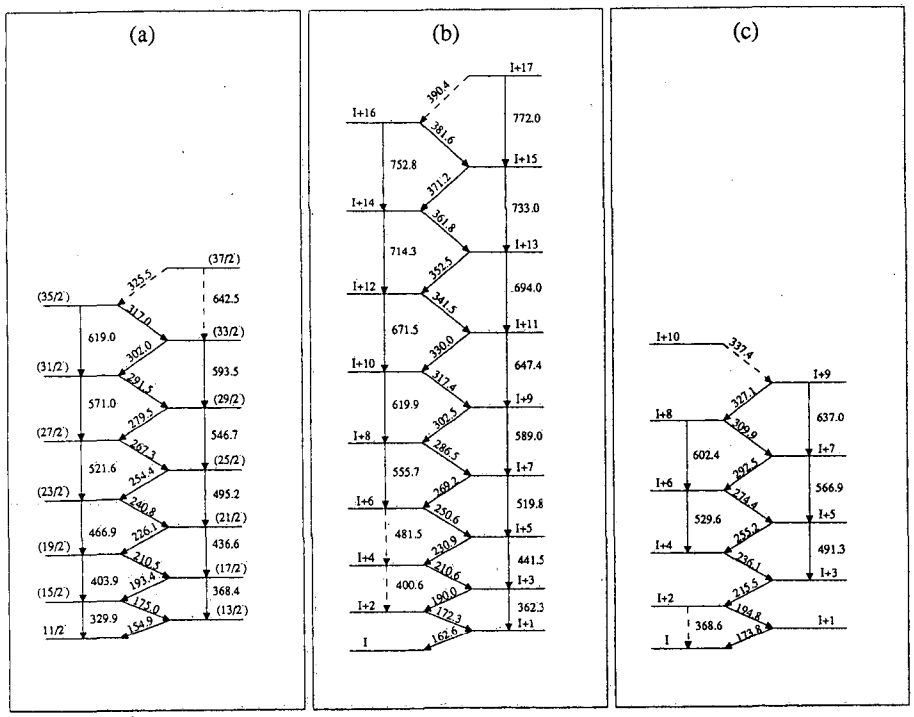

Fig. 1. Level scheme for the ΔI=1 bands in (a) ^{167}Yb, (b) ^{166}Yb, and (c) ^{168}Yb.

Pair Excitations and a Proton Band-Crossing in Superdeformed ^{150}Gd*

P. Fallon[1], C.W. Beausang[2], S. Clarke[2], P.J. Twin[2], F.A. Beck[3], Th. Byrski[3], D. Curien[3], P.J. Dagnall[2], G. deFrance[3], G. Duchêne[3], P.D. Forsyth[2], B. Haas[3], M.J. Joyce[2], A.O. Macchiavelli[1], E.S. Paul[2], J.F. Sharpey-Schafer[2], J. Simpson[4] and J.P. Vivien[3].

and

S. Åberg[5] and W. Nazarewicz[6,7]

High spin states in ^{150}Gd were populated by the reaction ^{26}Mg $+^{130}$Te at a beam energy of 149 MeV. The Eurogam spectrometer was used to record the coincident γ-ray energies. An unsuppressed Ge fold $\geq$7 was required before accepting an event and the resulting event rate was $\sim 5\times10^3$ events per second. A total of $\sim 1\times10^9$ suppressed coincidence events with Ge fold $\geq$3 were obtained.

Five SD bands, assigned to ^{150}Gd, have been observed in this data set. Four of the SD bands have been reported previously[1,2,3,4], the fifth is the subject of this report. The new band in ^{150}Gd (band 5) has an intensity of $\sim$40% relative to the yrast SD band (band 1). Above E_γ=1 MeV the transition energy spacing for band 5 is regular ($\Delta E_\gamma \approx 49$ keV) and thus its dynamical moment of inertia, $\Im^{(2)} \equiv 4\hbar^2/\Delta E_\gamma$, is constant as a function of rotational frequency ($\hbar\omega \equiv E_\gamma/2$) and similar to that of the yrast SD band (band 1) in ^{152}Dy. Since the $\Im^{(2)}$ moment of inertia is sensitive to the occupation of specific high-N intruder states, band 5 in ^{150}Gd is assigned the same intruder configuration ($\pi 6^4 \nu 7^2$) as ^{152}Dy band 1. In addition, at high spins, the transition energies in band 5 are similar to those in ^{152}Dy band 1. The most likely excitation, involving two N=6 protons, can be associated with the two-particle two-hole (2p-2h) proton excitation from the $[301]\frac{1}{2}$ level to the $[651]\frac{3}{2}$ intruder level and thus, at least at high spins, the configuration of band 5 is considered to be two proton holes in the ^{152}Dy yrast SD core.

However it is the differences, rather than the similarities between ^{150}Gd band 5 and ^{152}Dy band 1 which are most interesting. At $E_\gamma\sim$1 MeV the transition energy spacing becomes irregular, in addition the peaks at $\sim$997 and $\sim$996 keV are broader than the neighboring SD transition peaks. The extra intensity carried by these transitions is consistent with them being SD doublets. Based on this information we suggest that ^{150}Gd band 5 is undergoing a backbend in this region. Band 5 is seen to decay through the proposed backbending region.

It is intruiging to note that the spectrum gated by band 5 contains peaks which have the same energy as the low spin transitions observed in ^{150}Gd band 1. These band 1 transitions show an increase in intensity (as a function of decreasing spin) which is consistent with the decay of band 5. Thus this data may also includes evidence for the decay of an excited SD band to the yrast SD band.

[1] Lawrence Berkeley Laboratory.
[2] University of Liverpool.
[3] Centre de Recherches Nucléaires.
[4] SERC Daresbury Laboratory.
[5] Lund Institute of Technology.
[6] Oak Ridge National Laboratory.
[7] University of Tennessee.

Footnotes and References

*Submitted to Phys. Rev. Lett.

[1] P.Fallon *et al.*, Phys. Lett. **218B**, 137 (1989); Phys. Lett. **257B**, 269 (1991).
[2] T.Byrski *et al.*, Phys. Rev. Lett. **64**, 1650 (1990).
[3] W.Nazarewicz, P.J.Twin, P.Fallon and J.D.Garrett, Phys. Rev. Lett. **64**, 1654 (1990).
[4] C.W.Beausang *et al.*, Phys. Rev. Lett. **71**, 1800 (1993).

Superdeformation in ^{195}Pb

L.P. Farris, E.A. Henry,* J.A. Becker,* M.J. Brinkman,* B. Cederwall,†*
J.A. Cizewski,‡ M. A. Deleplanque,† R.M. Diamond,† J.E. Draper,§ C. Duyar,§ P. Fallon,†
J.R. Hughes, W.H. Kelly,** I.Y. Lee,† A.O. Machiavelli,† E.C. Rubel,§ F.S. Stephens,†*
M.A. Stoyer, D.T. Vo***

Superdeformed bands have been identified in ^{195}Pb, the first odd-A Pb nucleus where such states have been found. ^{195}Pb was populated in the ^{174}Yb(^{26}Mg,5n) reaction with a beam energy of 133 MeV provided by the LBL 88-inch Cyclotron. The target consisted of three stacked 500μg foils of ^{174}Yb. Data were obtained with the Early Implementation of Gammasphere with 29 detectors. More than 4×10^8 events were collected with a coincidence requirement of three or more Compton-suppressed gamma rays. Two pairs of signature partner superdeformed bands, four bands in all, were discovered. These have been labeled bands 1, 2, 3a and 3b.

The properties of the ^{195}Pb bands are expected to be similar to those of the superdeformed bands in its isotones, ^{194}Tl and ^{193}Hg, because of the superdeformed shell gaps at Z=80 and 82. However, bands 1 and 2 of ^{195}Pb have an approximately constant dynamic moment of inertia (Figure 1). The only other nucleus in this mass region with superdeformed bands displaying this property is ^{192}Tl [1] in which blocking of high-j intruder orbitals by odd proton and neutron quasiparticles was invoked as an explanation. In the case of ^{195}Pb, this mechanism would require proton excitations across the Z=82 superdeformed shell gap, whereas, based on relative intensities and other properties, the bands with flat $\mathcal{J}^2$s are most likely the yrast band and its signature partner, a quasineutron excitation.

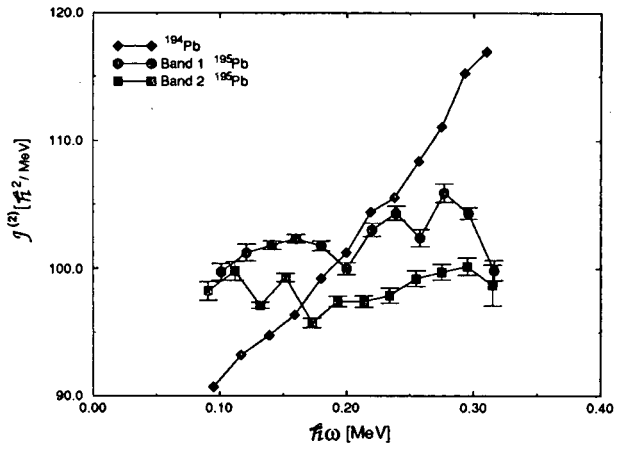

Figure 1: Dynamic moments of inertia for SD bands 1 and 2 of ^{195}Pb, with the SD band for ^{194}Pb[2] for comparison.

Footnotes and References

*Lawrence Livermore National Laboratory.
†Lawrence Berkeley Laboratory.
‡Rutgers University.
§UC Davis.
**Iowa State University.

[1] Y. Liang et al., Phys. Rev. C,R2136 (1992).

Footnotes and References

[2] M.J. Brinkman, et al., Z. Phys. A336, 115 (1990).

New Features of Superdeformed Bands in ^{194}Hg*

B. Cederwall,[1] *R.V.F. Janssens,*[2] *M.J. Brinkman,*[3] *I. Y. Lee,*[1] *I. Ahmad,*[2] *J.A. Becker,*[3] *M.P. Carpenter,*[2] *B. Crowell,*[2] *M.A. Deleplanque,*[1] *R.M. Diamond,*[1] *J. E. Draper,*[4] *C. Duyar,*[4] *P. Fallon,*[1] *L.P. Farris,*[3] *E.A. Henry,*[3] *R.G. Henry,*[2] *J.R. Hughes,*[3] *T.L. Khoo,*[2] *T. Lauritsen,*[2] *A.O. Macchiavelli,*[1] *E. Rubel,*[4] *F.S. Stephens,*[1] *M.A. Stoyer,*[3] *W. Satula,*[5], *I. Wiedenhoever,*[6], *R. Wyss*[7]

A striking difference between the superdeformed (SD) nuclei near A = 190 and those in other regions of the nuclear chart is the behavior of the dynamic moment of inertia $\Im^{(2)}$ with the rotational frequency $\hbar\omega$. While the $\Im^{(2)}$ patterns of the SD bands near A = 130 and A = 150 show pronounced variations, the majority of the SD bands near A = 190 display the same large, smooth increase of $\Im^{(2)}$ with $\hbar\omega$ in the frequency range $0.15 \leq \hbar\omega \leq 0.40$ MeV. Current understanding of this rise of $\Im^{(2)}$ within mean field theories[1] invokes the gradual alignment of quasiparticles occupying high-N intruder orbitals (originating from the $i_{13/2}$ proton and $j_{15/2}$ neutron shells) in the presence of pair correlations. It is a direct consequence of these interpretations that, after the quasiparticle alignments have taken place, $\Im^{(2)}$ will exhibit a downturn with increasing $\hbar\omega$ toward the rigid-body value. Before the present work, no downturn in $\Im^{(2)}$ for the SD bands in the A $\approx$ 190 mass region has been observed (see e.g. [2]), raising some doubt as to our understanding of pair correlations and alignment effects at these large deformations.

Excited states in ^{194}Hg were populated with the reaction ^{150}Nd(^{48}Ca,4n)^{194}Hg at a beam energy of 206 MeV. The γ rays emitted in the reaction were detected with the Gammasphere detector array [3]. In this particular experiment, 32 large Compton-suppressed germanium detectors were used. In the present work, the three SD bands of ^{194}Hg observed earlier[4] have been extended to higher rotational frequencies, and the first experimental evidence for the expected downturn in $\Im^{(2)}$ was obtained.

The appearance of a regular staggering pattern in a SD band in ^{149}Gd [5] may be interpreted as possible evidence for a new symmetry term in the Hamiltonian which is invariant under a rotation by $\frac{\pi}{2}$.

The increased resolving power obtained from high-fold coincidence data allowed us to determine the SD transition energies in ^{194}Hg with greater accuracy than in previous work and evidence for a staggering of the γ-ray energies, similar to that observed for the SD band in ^{149}Gd, is observed in all three SD bands.

(1)Lawrence Berkeley Laboratory, Berkeley, California 94720, USA
(2)Argonne National Laboratory, Argonne, Illinois 60439, USA
(3)Lawrence Livermore National Laboratory, Livermore, California 94550, USA
(4) Physics Dept., University of California, Davis, California 95616, USA
(5)Institute of Theoretical Physics, University of Warsaw, PL-00681 Warsaw, Poland
(6)Universität zu Köln, IKP, D-5000 Köln, Germany
(7)Manne Siegbahn Institute of Physics, S-104 05 Stockholm, Sweden and Royal Inst. of Technology, Physics Dept., S-100 44 Stockholm, Sweden

Footnotes and References

*Accepted for publication in Phys. Rev. Lett.

[1]D. Ye *et al.*, Phys. Rev. **C41**, R13 (1990), M. A. Riley *et al.*, Nucl. Phys. **A512**, 178 (1990)
[2]T. Lauritsen *et al.*, Phys. Lett. **B279**, 239 (1992)
[3]I.Y. Lee, Nucl. Phys. **A520**, 641c (1990)

Footnotes and References

[4]M. A. Riley *et al.*, Nucl. Phys. **A512**, 178 (1990), C. W. Beausang *et al.*, Z. Phys. **A335**, 325 (1990)
[5]S. Flibotte *et al.*, Phys. Rev. Lett. **71**, 4299 (1993)

Lifetime measurement in excited and yrast superdeformed bands in ^{194}Hg

J.R. Hughes, I. Ahmad,† J.A. Becker,* M.J. Brinkman,* M.P. Carpenter,† B. Cederwall, M.A. Deleplanque, R.M. Diamond, J.E. Draper,‡ C. Duyar,‡ P. Fallon, S. Harnfenist, E.A. Henry,* R.G. Henry,† R.V.F. Janssens,† T.L. Khoo,† T. Lauritsen,† I.Y. Lee, E. Rubel,‡ F.S. Stephens, and M.A. Stoyer.*§*

Superdeformed (SD) bands in the $A \sim 194$ region are associated with a second minimum in the potential energy surface at large deformation. To probe the behaviour of the second minimum with respect to quasiparticle excitations, we have measured level lifetimes in the yrast and an excited SD band in ^{194}Hg[1]. using the Early Implementation of GAMMASPHERE.

Excited states in ^{194}Hg were populated with the ^{150}Nd(^{48}Ca, $4n$) reaction at a beam energy of 205 MeV. The target consisted of 1.7 mg/cm^2 ^{150}Nd evaporated onto a 20 mg/cm^2 Au backing. In-beam γ-rays were detected with 25 Ge detectors, five each at angles of 163°, 148°, 143°, 32° and 17° with respect to the beam direction. Approximately 4×10^8 expanded three-fold events were recorded.

The fractional Doppler-shift $F(\tau)$ obtained in band 2 (excited) are very similar to those in band 1 (yrast). The difference, $\Delta F(\tau)$, is 4(5)%, and is independent of systematic errors and model assumptions. The $\Delta F(\tau)$ is sensitive to differences in the side-feeding lifetimes and the relative Q_t in the two bands. Assuming similar side-feeding lifetimes into the two bands, the $\Delta F(\tau)$ values imply that band 2 has a slightly larger Q_t than that of band 1 [$\Delta Q_t = 0.7(9)\ e$b].

Level lifetimes were extracted from γ-ray lineshapes using the code DSAMFT_OR [2]. For each transition the in-band lifetime, along with that of the side-feeding, has been determined using a χ^2 minimization technique. The individual quadrupole moments for both bands are plotted against E_γ in Fig. 1. The average in-band Q_t observed for band 1 is $Q_t = 17.2(20)\ e$ b, whereas for band 2 the average is $Q_t = 17.6(30)\ e$ b. These values are consistent with those obtained from the centroid-shift analysis, and imply a quadrupole deformation $\beta_2 \sim 0.5$.

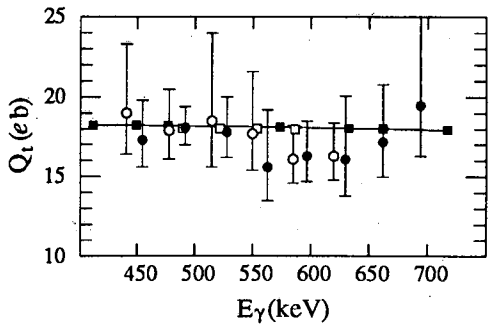

Figure 1: Experimental transition quadrupole moment, Q_t, as a function of γ-ray energy for band 1 (•) and band 2 (○). Theoretical values calculated with the CHF Method including pairing for band 1 (■), and band 2 (□).

This work was supported in part by U.S. Department of Energy, under Contract No. W-7405-ENG-48 (LLNL), and No. DE-AC03-76SF00098 (LBL), and in part by the U.S. Department of Energy, Nuclear Physics Division under Contract No. W-31-109-ENG-38 (ANL).

Footnotes and References

*Lawrence Livermore National Laboratory.
†Argonne National Laboratory.
‡UC Davis.
§Present address LBL

[1] J.R. Hughes *et al.*, Phys. Rev. Lett. **72**, 824 (1993)
[2] DSAMFT_OR, original code by J.C. Bacelar, modified by J. Gascon and by J.C. Wells; J.C. Wells private communication.

Observation of excited superdeformed band in ^{194}Pb

J.R. Hughes, J.A. Becker,* L. A. Bernstein,† M.J. Brinkman,* B. Cederwall, J. A. Cizewski,† M.A. Deleplanque, R.M. Diamond, J.E. Draper,‡ C. Duyar,‡ P. Fallon, E.A. Henry,* R.W. Hoff,* W.H. Kelly,§ I.Y. Lee, A.O. Machiavelli, E. Rubel,‡ F.S. Stephens, M.A. Stoyer,***and D.T. Vo.§*

Observation of excited superdeformed (SD) bands is of particular importance for understanding the structure in the second well. Questions regarding the single-particle spectrum near the SD Fermi surface, the effects of pairing (blocking), deformation changes, and the phenomenon of identical bands (IB) can all be addressed by the characterization of excited SD bands. The new generation γ-ray arrays provide the increased sensitivity and resolving power needed to observe weaker bands than previously possible. The increased dimensionality of the data, while providing increased resolving power presents a huge space in which to search for SD bands. For this purpose, an algorithm designed to find the most promising candidates for SD band members has been implemented. We have identified an excited superdeformed band in ^{194}Pb with the aid of a three-dimensional search algorithm (see Fig.1a). The band is interpreted as a high-K neutron excitation. There is good evidence for the expected signature partner band (see Fig.1b), although its identification is tentative due to the proximity of the yrast SD transitions. The excited band is very weak, representing only $\sim 5\%$ intensity relative to the yrast SD band. This is the weakest SD band observed to date in the $A \sim 194$ region, consistent with expectations from the calculated single-particle spectrum. *This work was supported in part by U.S. DOE, under Contract No. W7405-ENG-48 (LLNL), and No. DE-AC03-76SF00098 (LBL), the Research Corporation (ISU) and in part by the NSF (Rutgers).

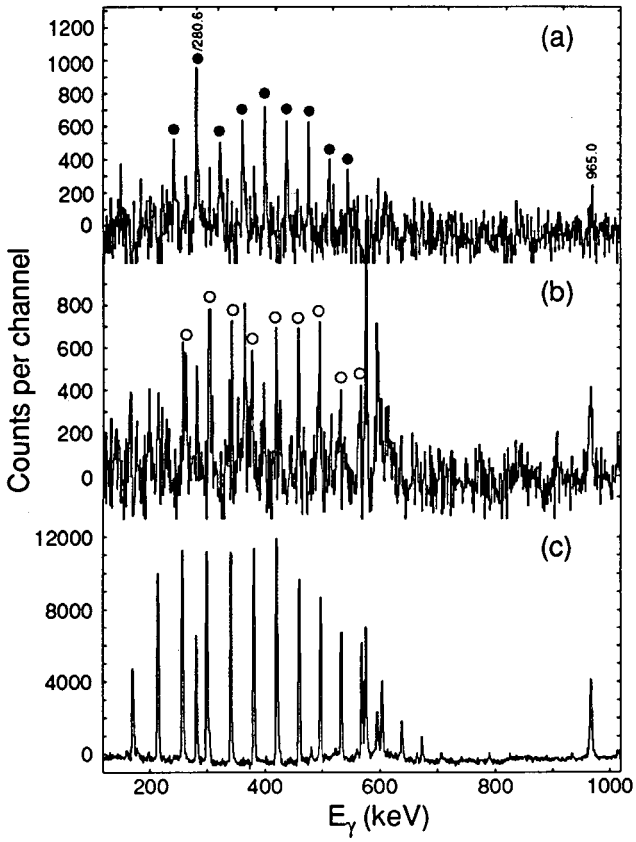

Figure 1: Background-subtracted coincidence spectra for the new bands (a) band 2a, (b) band 2b, and the yrast band (c) band 1. Band members are denoted by • (band 2a), and by ○ (band 2b). Low-lying yrast transitions are labeled by energy in keV. The spectra for bands 2a, and 1, were obtained by summing all combinations of double double gates set on the 240–545 keV, and 213–532-keV transitions, respectively. The spectrum for band 2b was obtained by a similar summation (261–528 keV), with a normalized fraction of band 1 subtracted.

Footnotes and References

*Lawrence Livermore National Laboratory.
†Rutgers.
‡UC Davis.
§Iowa State.
**Present address LBL

Discrete Decay from the Superdeformed Band in $^{194}Pb^{*}$

M.J. Brinkman, J.A. Becker, E.A. Henry, L.P. Farris, J.R. Hughes, M.A. Stoyer–Lawrence Livermore National Laboratory B. Cederwall, M.A. Deleplanque, R.M. Diamond, P. Fallon, I.Y. Lee, A.O. Macchiavelli, F.S. Stephens–Lawrence Berkeley Laboratory L.A. Bernstein, J.A. Cizewski, H.Q. Jin, W. Younes–Rutgers University J.E. Draper, C. Duyar, E. Rubel–U.C. Davis W.H. Kelly, D.T. Vo–Iowa State University

Within the past five years the neutron–deficient Au, Hg, Tl, and Pb nuclei near A ~ 190 have been shown to support a broad region of superdeformation. Despite worldwide experimental activity, a number of the most fundamental quantities remain unknown—in particular, the excitation energy, well depth, and barrier width of the second minimum and the spins and parities of the superdeformed bands are not directly measured. The observation of discrete decay from the superdeformed band to the states at more moderate deformation may provide direct experimental data on these open questions. Recently a series of experiments on ^{194}Pb were conducted on the Early Implementation of GAMMASPHERE, in an attempt to observe discrete transitions connecting the superdeformed levels to the low–lying yrast states. The $^{174}Yb(^{25}Mg,5n)^{194}Pb^{*}$ reaction was used to populate the known superdeformed band in this nucleus. Over three experiments a total of 1.9 billion unfolded three–fold events were collected. Early analysis of these data has uncovered a discrete transition at ~2.75 MeV that is in coincidence with both the superdeformed band and a select number of low–lying yrast transitions in this nucleus (see the figure below). This transition populates the 6_1^+ state. The simplest interpretation of this decay implies that for the SD band, $E_x(6/8) \geq 4.89$ MeV.

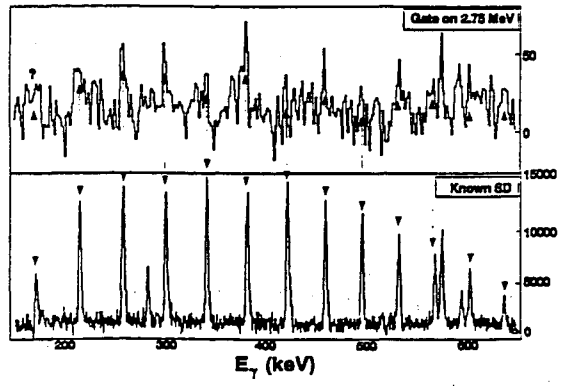

Figure: Top–A gate set at ~2.75 MeV with a resolution of 2 keV/channel. Bottom–The known superdeformed band from double–gated triples with a resolution of 0.5 keV/channel. The arrows denote the energies of the known superdeformed transitions with energies ≤ 650 keV.

* This work was supported in part by the U.S. Department of Energy under contracts W–7405–ENG–48 (LLNL) and DE–AC03–76SF00098 (LBL), and in part by the National Science Foundation (Rutgers).

Gamma-Ray Studies of the Spontaneous Fission of ^{242}Pu and ^{252}Cf Using Gammasphere

M.A. Stoyer, J.O. Rasmussen, S.Y. Chu, K.E. Gregorich, I.Y. Lee, M.F. Mohar, K. Moody, R. Lougheed,* S.G. Prussin,† S. Asztalos,† R. Aryaeinejad,‡ J. Cole,‡ Y.X. Dardenne,‡ M. Drigert,‡ J. Hamilton,§ Q.H. Lu,§ W.C. Ma,§ and A.V. Ramayya§*

Spontaneous fission gamma-rays of ^{242}Pu and ^{252}Cf have been studied at Gammasphere. Preliminary analysis of the ^{242}Pu data has concentrated on extracting relative intensities of ground rotational transitions as a function of number of neutrons emitted. "Cold fission", or zero-neutron fission,[1] is observed in a number of fissioning systems (see for example Fig. 1). The Xe-Zr fissioning pair was one of the first systems studied. The relative intensities of the $6^+ \rightarrow 4^+$ (stars) and $4^+ \rightarrow 2^+$ (triangles) transitions for the ^{138}Xe partners ($^{104-98}$Zr) are shown in Fig. 1. Some isotopic series show a trend of decreasing fragment average spin with increasing numbers of neutrons emitted, contrary to the initial expectations of a simple quantal model based on neck thickness expected at scission.

Preliminary results from ^{252}Cf gamma-ray counting in April 1994 using 36 Ge detectors in Early Implementation of Gammasphere are shown in Fig. 2. This run was coupled with additional neutron detectors and 1 X-ray detector. The spectrum shown in Fig. 2 is from the x-ray detector. The neutron detectors will help in distinguishing prompt fission γ-rays from γ-rays following β-decay of fission products.

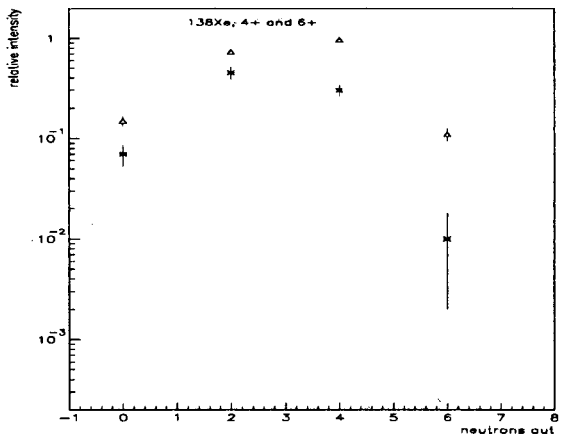

Fig. 1. Relative intensities vs. neutrons emitted for ^{138}Xe. The triangles represents the relative intensity from the $4^+ \rightarrow 2^+$ transitions, while the $*$ represents the $6^+ \rightarrow 4^+$ transitions in the ^{104,102,100,98}Zr isotopes.

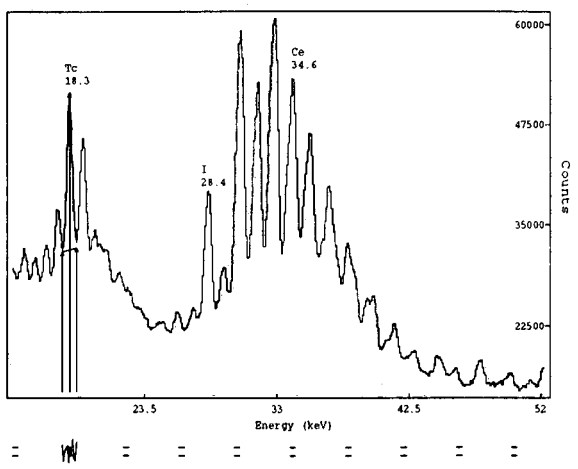

Fig. 2. X-ray spectrum of ^{252}Cf fission (approximately $\frac{1}{3}$ of the data collected). All peaks were assigned to an element; however, only three are labelled.

Footnotes and References

*LLNL, Livermore, CA 94550
†UCB, Berkeley, CA 94720
‡INEL, Idaho Falls, ID 83415
§Vanderbilt Univ., Nashville, TN 37235

[1] J. Trochon, G. Simon, and C. Signarbieux, **Proc. of 50 Years with Nuclear Fission** (Illinois: American Nuclear Society) (1989) 313, and F. Gönnenwein and B. Börsig, **Proc. of 50 Years with Nuclear Fission** (Illinois: American Nuclear Society) (1989) 515.

Spectroscopy of ^{238,239}Pu Studied by Quasielastic Reactions*

M. Devlin,[†] *D. Cline,*[†] *K. G. Helmer,*[†] *R. Ibbotson,*[†] *and C. Y. Wu,*[†]
P.A. Butler,[‡] *A. J. Cresswell,*[‡] *and G. D. Jones,*[‡]
M. A. Stoyer,[§]
and J. O. Rasmussen

The selective population mechanism of heavy-ion transfer reactions has been used to attempt to directly populate the (0^+, $T_{\frac{1}{2}}$ = 0.5 ns, E_x = 2.4 MeV) fission isomer of ^{238}Pu, and thereby investigate the mixing between the collective normal-deformed states and the superdeformed second-minimum states. The inelastic excitation and one-neutron-transfer reactions ^{239}Pu(^{117}Sn,^{117,118}Sn)^{239,238}Pu at a beam energy of 630 MeV were studied, simultaneously supplying data on the deexcitation γ rays from high-spin states in these plutonium isotopes. The ground state Q-value for the one-neutron transfer reaction is 3.7 MeV. From previous studies of reactions of this type, the population of states typically is confined to a Q window of approximately 2−4 MeV excitation above the yrast line, with angular momentum up to about 30$\hbar$.[1] The fission isomer results are in final stages of analysis. The gamma-ray transitions in the ground-state bands of ^{239}Pu and ^{238}Pu up to spins 26^+ and $\frac{51}{2}^+$, respectively, were observed (see Fig. 1). Another band in ^{239}Pu was observed, and is tentatively identified as the high-spin continuation of the 0^- octupole excitation built an the $\frac{1}{2}^+$ ground band in ^{239}Pu. The measured gamma ray multiplicity and total energy provided data on the population of entrance states in both ^{238}Pu and ^{239}Pu. The one-neutron-transfer cross section, as determined by the yield of the $6^+ \rightarrow 4^+$ transition in ^{238}Pu, was measured to be 65 ± 25 mb. This transition yield is estimated to represent between 80% and 90 % of the total one neutron-transfer cross section.

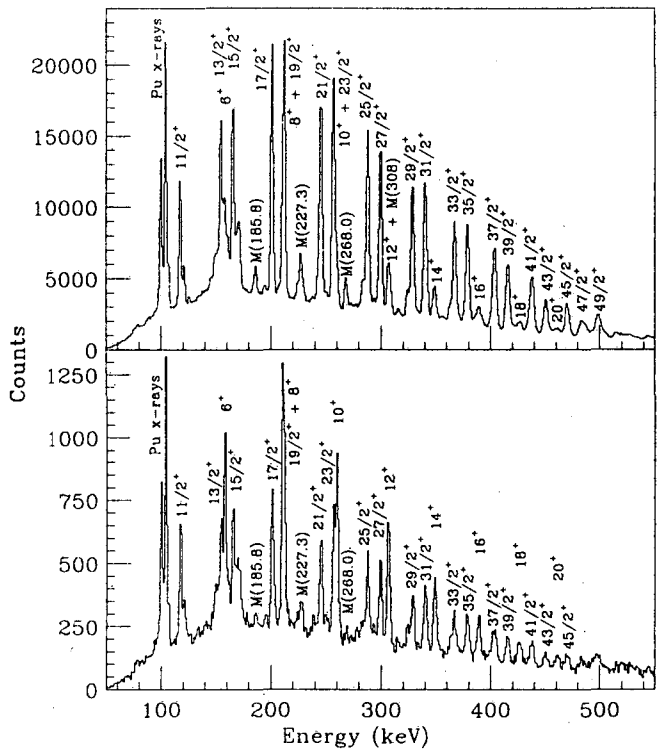

FIG. 1. Top: Total coincident γ-ray spectrum, with the ground band $\Delta J = 2$ transitions labeled by their initial spin. The half-integer transitions are ground band ^{239}Pu, integer ones are ^{238}Pu, and "side-band" lines are labeled by M's. Bottom: High H-K gated γ spectrum, showing the enhancement of the transfer lines relative to the inelastic lines (see text).

Footnotes and References

*Published in Phys. Rev. **C47** (1993) 2178.

[†]Nuclear Structure Research Laboratory, University of Rochester, Rochester, New York 14627

[‡]Oliver Lodge Laboratory, University of Liverpool, Liverpool L69 9BX, United Kingdom

[§]Lawrence Livermore National Laboratory, Livermore, California 94550

[1]C.Y. Wu, et al., **Phys. Lett. B188** (1987) 25.

Observation of Strong Isospin Mixing in ^{23}Al Beta-Delayed Proton Emission From Its Astrophysically Interesting Isobaric Analog State in ^{23}Mg

R. J. Tighe, J. C. Batchelder, D. M. Moltz, T. J. Ognibene, M. W. Rowe, and Joseph Cerny

We have observed the beta-delayed proton emission of ^{23}Al, proceeding via its Isobaric Analog State (IAS) in ^{23}Mg (E^*=7.795 MeV, $J^\pi=5/2^+$, T=3/2). Beta-delayed proton emission from ^{23}Al was first observed in 1972 [1] using standard Si-Si particle identification telescopes. A proton group with a center-of-mass energy (Ecm) of 870±30 keV was assigned to emission from an excited state in ^{23}Mg 665 keV above the IAS. A low-energy proton threshold of ~700 keV (lab) excluded any attempt to observe decay from the IAS.

The ^{23}Na(p,γ)^{23}Mg has been of considerable recent interest with regard to the "hot" Ne-Na cycle [2]. Specifically, reaction rates for determining ^{22}Na abundances are important, as the decay of ^{22}Na($T_{1/2}$=2.6 y) provides an attractive mechanism for producing the ^{22}Ne isotopic anomalies (NeE), which have been observed in meteoritic inclusions.

We utilized a helium-jet system to collect and transport reaction products produced in the p+^{24}Mg reaction. The 40 MeV pulsed proton beams from the 88-Inch Cyclotron with intensities up to ~2 μA were incident on ~1 mg/cm^2 enriched targets. Radioactivity was deposited in the center of our low-energy proton detector ball. This detector consists of four gas-ΔE, gas-ΔE, Si-E triple telescopes, each subtending a solid angle of 4% of 4π and capable of detecting protons with energies down to ~200 keV.

Fig. 1 gives an example of the proton spectrum measured with one of these telescopes. Three strong lines are clearly evident, and a partial ^{23}Al decay scheme is inset in the figure which indicates their assignments. The proton line corresponding to decay from the IAS in ^{23}Mg is clearly seen at ~210 keV. This represents the lowest-energy identified proton group measured to date. Furthermore, this is the first case (and perhaps the only possible case) whereby a member of the A=4n+3, Tz=-3/2 series has been observed to emit delayed protons via its IAS.

Using the measured cross section for the 838 keV group [1], a predicted total production cross section for ^{23}Al of 108 μb, and a calculated log(ft) for ^{23}Al beta decay to its IAS in ^{23}Mg of 3.28 [3], a proton branching ratio from the IAS of ~2-3% can be determined. Proton emission from the IAS is isospin forbidden, and can therefore only proceed due to isospin mixing with nearby states. Compared to full basis 1s-0d shell model calculations which include isospin mixing, our measured proton decay branch is ~5-10 times larger than predicted [3].

Utilizing a value of Γ_γ = 3.0 eV for the IAS, a resonance strength of 30 meV is determined for the ^{23}Na(p,γ)^{23}Mg reaction at E_{cm} = 218 keV. This will have significant implications with regard to the stellar reaction rates and the relevant temperatures whereby NeE abundances can be explained. For example, this resonance will dominate the ^{23}Na(p,γ) reaction at stellar temperatures [2].

[1] R. A. Gough *et al.*, Phys. Rev. Lett. 28, 510 (1972).

[2] S. Seuthe *et al.*, Nucl. Phys. A514, 471 (1990).

[3] B. A. Brown, *private communication.*

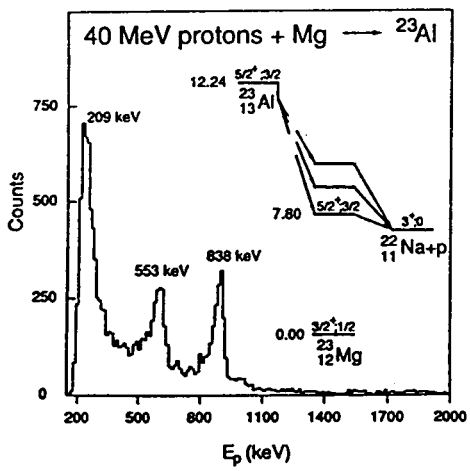

Fig. 1. The proton spectrum from a p+^{24}Mg bombardment at 40 MeV.

Observation of Beta-Delayed Proton Emission From ^{24}Al

J. C. Batchelder, R. J. Tighe, D. M. Moltz, T. J. Ognibene, M. W. Rowe, and Joseph Cerny

Beta-delayed particle studies have provided a wide variety of spectroscopic information. A general trend in this research has been to study nuclei further and further from beta stability. However, beta-delayed particle precursors with relatively small particle branches are known to exist close to the stability line for light nuclei.

We have recently investigated low-energy beta-delayed protons emitted from the A=4n+3, T_z=-3/2 nucleus ^{23}Al. In the course of a 40 MeV proton bombardment of a ^{24}Mg target, an apparent continuum of proton events was observed between ~300-1100 keV. The only potential delayed proton emitters produced in this reaction are ^{20}Na, ^{23}Al, and ^{24}Al, with thresholds of 25.0 MeV, 30.8 MeV, and 15.3 MeV (lab energies), respectively. To unambiguously determine the origin of this proton continuum, we proceeded to perform bombardments of ^{24}Mg targets with proton beams at energies of 28.5 MeV and 20.0 MeV.

We utilized a helium-jet system to collect and transport reaction products to the center of our low-energy proton detector ball. This detector consists of an array of four gas-ΔE, gas-ΔE, Si-E triple telescopes, each subtending a solid angle of ~4% of 4π and capable of detecting protons with energies down to ~200 keV. To eliminate neutron induced background events and allow for half-life determinations, the proton beam (~1 μA) from the 88-Inch Cyclotron was pulsed and the counting electronics were enabled only during the beam-off periods.

The proton spectrum from the sum of three telescopes resulting from a 4.7 mC bombardment at 28.5 MeV is shown in Fig. 1. A proton continuum from ~30-1100 keV is evident. This bombarding energy precludes the production of ^{23}Al. A 13 mC bombardment at 20.0 MeV was also performed. This energy is below the ^{20}Na production threshold. Again a proton continuum was observed from ~300-1100 keV. Therefore, the observed proton continuum can unambiguously be assigned to ^{24}Al. Although the ^{24}Al production cross section is reduced at this lower energy, the elimination of the strong delayed alpha groups from ^{20}Na allowed for a comparison of the half-lives of the known ^{24}Al delayed alpha groups [1] and the proton continuum. Good agreement was found. It was also possible to use the known absolute decay branch for the 1.982 MeV ^{24}Al alpha line [1] to determine an absolute beta-delayed proton decay branch from ^{24}Al of $(1.2\pm0.3)\times10^{-5}$.

The high density of excited states in the beta daughter (^{24}Mg) which are open to proton emission, results in the nondiscrete nature of the observed proton spectrum. Following the beta decay of ^{24}Al to excited states in ^{24}Mg, proton emission begins to compete with alpha decay at ~12.0 MeV excitation in ^{24}Mg. Simple penetrability calculations predict (ℓ=2) proton decay will compete with (ℓ=4) alpha decay only after ~12.6 MeV in excitation energy of ^{24}Mg is reached. This discrepancy could readily be due to the fact that alpha-particle preformation factors and other nuclear structure effects are neglected in these calculations.

[1] J. Honkanen *et al.*, Phys. Scr. **19**, 239 (1979); Phys. Scr. 34, 608 (1986).

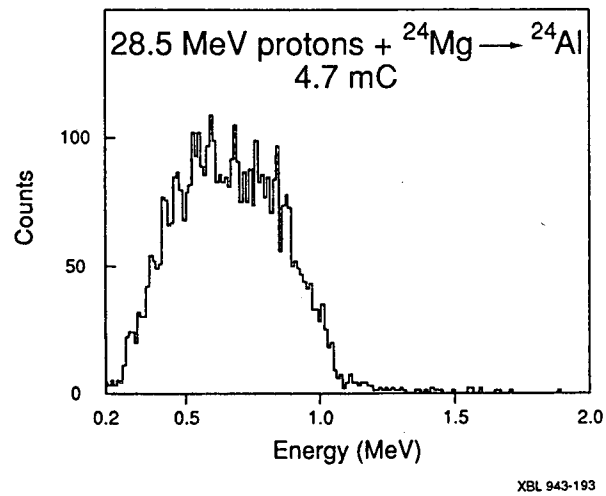

Fig. 1. The proton spectrum from the p+^{24}Mg bombardment at 28.5 MeV.

Evidence for the Ground-State Proton Decay of ^{105}Sb

R. J. Tighe, D. M. Moltz, J. C. Batchelder, T. J. Ognibene, M. W. Rowe, and Joseph Cerny

Proton emission from the nuclear ground state is not only expected to determine the limit of stability for proton-rich nuclei, but also yields information on nuclear masses and structure very far from beta stability. Ground-state (gs) proton decay has thus far been observed in two regions of the nuclear chart; near the N=82 closed neutron shell and just above the expected doubly-magic nucleus ^{100}Sn (Z=N=50). Prior to our work on proton emission from ^{105}Sb (Z=51), eight cases of ground-state proton emission had been reported; six of these in the region of the nuclear chart near N=82.

Ground-state proton decay from ^{109}I (Z=53) and ^{113}Cs (Z=55) was first observed by a group at Munich [1]. There have been unsuccessful searches for gs proton emission from ^{105}Sb at Munich [2] and with both SHIP and the on-line mass separator at GSI [3]. In each case, low-energy proton thresholds of ~500 keV were reported. Our observation of the proton decay of ^{105}Sb represents the lightest observed case of gs proton emission. The measured energy and yield of this proton peak give a stringent test of mass models and provide valuable spectroscopic information near the long sought doubly-magic ^{100}Sn.

We have utilized a helium-jet system to collect and transport reaction products made in the ^{58}Ni+^{50}Cr$_2$O$_3$ compound nuclear reaction (E_{lab} = 220, 260 MeV) to the center of our low-energy proton detector ball. This detector consists of an array of four gas-ΔE, gas-ΔE, Si-E triple telescopes, each subtending a solid angle of ~4% of 4π and capable of detecting protons with energies down to ~200 keV.

Figure 1 shows the summed proton spectrum from three independent bombardments (a total of 20.3 mC of ^{58}Ni^{13+} beam from the 88-Inch Cyclotron incident on a ~1 μg/cm^2 ^{50}Cr$_2$O$_3$ target). Two low-energy proton groups are apparent in this spectrum. We have assigned the group at 478±15 keV to the gs proton decay of ^{105}Sb produced in the p2n exit channel. The group at ~390 keV has been assigned to the beta-delayed proton decay of ^{25}Si produced via complex rearrangement reactions on the Al stopping foils used to slow down the reaction products. A separate ^{16}O+^{nat}Ni bombardment was performed to account for possible reactions on the oxygen component of the target. No proton group was observed in the region near ~480 keV resulting from the O+Ni cross bombardment.

If we use the observed yield of the 478 keV group and assume a production cross section of ~50 μb [2] for the p2n channel, the resulting proton branching ratio is ~1%. If we assume emission from a $d_{5/2}$ state (*i.e.*, an ℓ=2 proton decay), our penetrability calculations combined with a predicted ß-decay half-life of 500 ms result in a spectroscopic factor consistent with unity. (A $g_{7/2}$ assignment can be ruled out due to proton half-life considerations.) This is in contrast to the relatively small spectroscopic factors determined for ^{109}I and ^{113}Cs [2] (0.09 and 0.03, respectively). Of the various mass model predictions [4], that of Wapstra, *et al.* (E_p = 456 keV) most closely agrees with our measured proton decay energy.

[1] T. Faestermann *et al.*, Phys. Lett. **137B**, 23 (1984).

[2] A. Gillitzer *et al.*, Z. Phys. A 326, 107 (1987).

[3] S. Hofmann *et al.*, AMCO-7, Darmstadt, p 184 (1984); I. S. Grant *et al.*, ibid, p 170.

[4] P. E. Haustein (ed), 1986-87 At. Mass Pred., At. Data Nucl. Data Tables 39, 185 (1988).

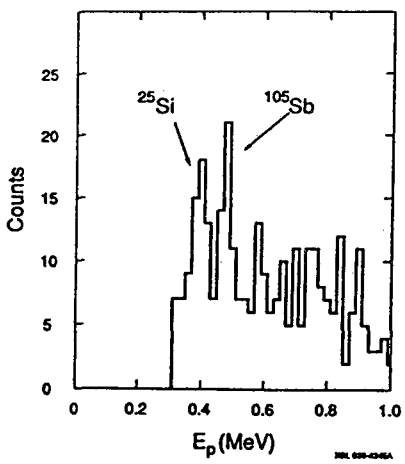

Fig. 1. The summed proton spectrum from our ^{58}Ni+^{50}Cr$_2$O$_3$ bombardments.

Report on the RAMA Upgrade

T. J. Ognibene, D. M. Moltz, M. W. Rowe, R. J. Tighe and Joseph Cerny

As one approaches the proton drip line, the experimental investigation of nuclei becomes increasingly difficult due to the shorter half-lives and diminishing production cross sections. There are two methods available to us in which to mitigate these difficulties. One is to employ mass separation to select out the nucleus of interest and the other is to use a fast He-jet transport technique to a detector system to look for a unique decay signature such as beta-delayed proton emission.

Previously, the use of RAMA[1] (Recoil Atom Mass Analyzer) had been hampered by a relatively long transport time between the target and ionizer which had prevented the study of nuclei with half lives less than 150 ms. The current RAMA upgrade remedies this problem by moving the ion source region closer to the production chamber. Additionally, the upgrade takes full advantage of both the aforementioned techniques to study short lived proton rich nuclei.

As shown in the figure below, the RAMA system starts at the He-jet target chamber 2 where energetic radioactive nuclear recoils are thermalized and transported via KCl aerosols suspended in helium through a short capillary to the RAMA ion source. The recoils are then ionized, accelerated, mass separated and deposited on a thin foil in the center of our low energy proton detector ball[2,3] at the Shielded Detector Station.[4]

The original optics calculation suggested parallel beam optics from the mirror to the first electrostatic quadrupole triplet. At that point, the optics solution through the rest of the system would be similar to that used previously. However, off-line tests proved that the beam envelope was larger than that calculated and that the divergence was non-zero, resulting in unacceptable transport losses. This problem was solved by installing two Einzel lenses and changing the optics to waist-to-waist transport.

At this time, the upgrade is completed and we are currently performing on-line tests with radioactive beams. We expect to begin production experiments in summer 1994.

1. D. M. Moltz, *et al.*, NIM 172, 507 (1980).
2. D. M. Moltz, *et al.*, NIM A (in press).
3. R. J. Tighe, *et al.*, PRC-Rapid Com. (in press).
4. F. B. Blönnigen, *et al.*, NIM B26, 328 (1987).

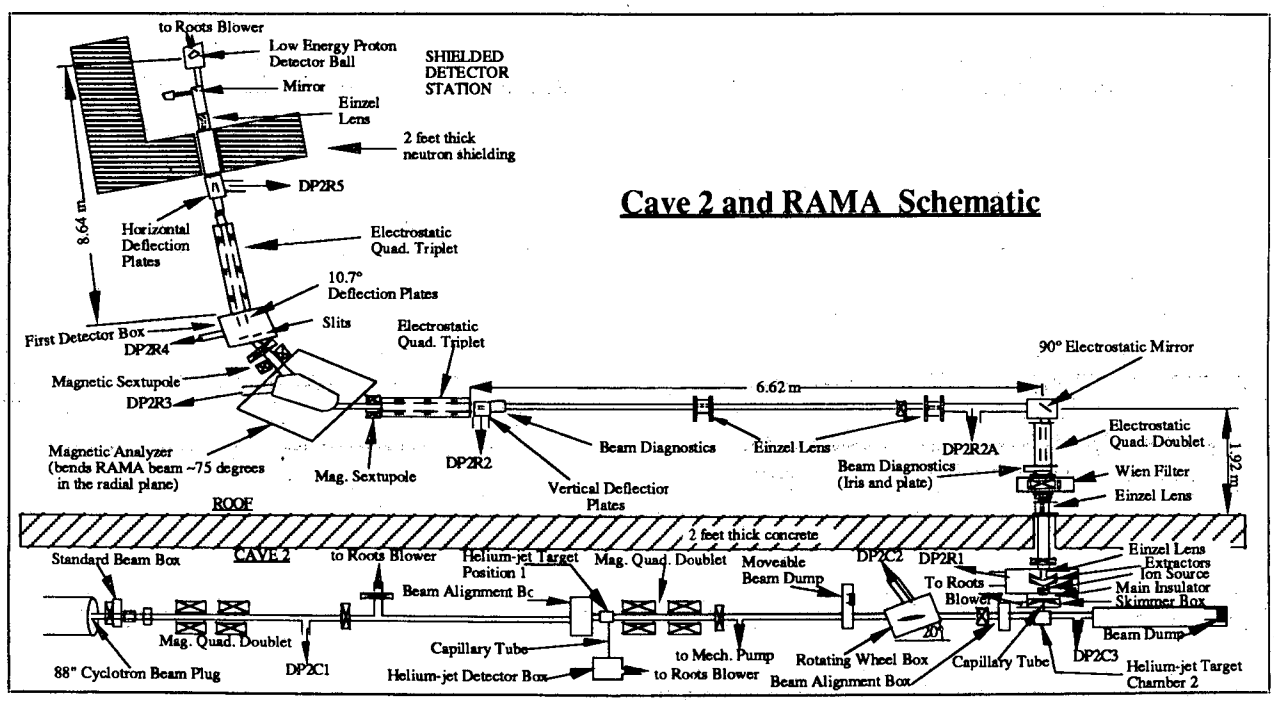

Determination of $NpO_2^+ \cdot UO_2^{2+}$ Cation-cation Complex Equilibrium Constant using LIPAS *

N.J. Hannink, D.C. Hoffman, and R.J. Silva†

Cation-cation complexes are the result of the specific interaction between two cations to form a complex; this type of complex has been observed to occur between an actinyl(V) cation and another cation. The first actinyl(V)-cation complex [1] discovered, $NpO_2^+ \cdot UO_2^{2+}$, was reported in 1961. Neptunyl(V) is the most widely studied of the actinyl(V) cations. Equilibrium constants(K_{eq}) have been reported for five neptunyl(V)-cation complexes and at least fourteen other complexes are known. Plutonyl(V) is the only actinyl(V) that does not have a K_{eq} reported for a cation-cation complex. All measurements of K_{eq} were obtained using absorption spectroscopy or Raman spectroscopy, sometimes in combination with potentiometric, kinetic, or electron paramagnetic resonance studies.

Actinyl(V)-cation complexes are difficult to study since they have a small K_{eq}, involve radioactive species, and typically have small molar absorptivities for at least one of the species involved. Laser Induced PhotoAcoustic Spectroscopy(LIPAS) is a very sensitive spectroscopic technique that is used to overcome the difficulties imposed by a small K_{eq} and small molar absorptivities. The remote apparatus described in last years annual report [2] was used for the present experiments.

The $NpO_2^+ \cdot UO_2^{2+}$ cation-cation complex has been well studied in the past, four studies include a K_{eq} (See table 1). In order to verify the LIPAS method, we remeasured this K_{eq}. A value of 2.4±0.2 M^{-1} at an ionic strength of 6 M ($NaClO_4$) was obtained. Our result is consistent with previously reported values. Figure 1 shows the measured LIPAS spectra which were used to calculate the K_{eq}.

Constant (M^{-1})	Ionic Strength (M)	Ref.
0.69±0.013	3.0	1
3.7±0.1	7	3
2.5±0.5	6.26	4
2.25±0.03	6.0	5

Table 1. Reported K_{eq} for the $NpO_2^+ \cdot UO_2^{2+}$ complex and the ionic strength used in the measurements.

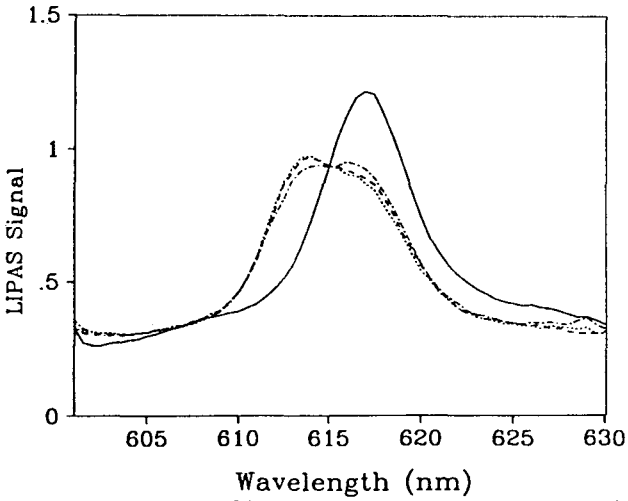

Figure 1. $NpO_2^+ \cdot UO_2^{2+}$ spectra. All spectra have NpO_2^+ concentration of 2.48×10^{-4} M. UO_2^{2+} concentrations are: solid line, 0 M; dash-dot line, 0.1455 M; dashed line, 0.1617 M; and dotted line, 0.1779 M.

Footnotes and References

*Work partially supported by The Glenn T. Seaborg Institute for Transactinium Science.

†Nuclear Chemistry Division Lawrence Livermore National Laboratory, Livermore CA 94550

[1] J.C. Sullivan, J.C. Hindman, and A.J. Zielen, *J. Amer. Chem. Soc.* **83**, 3373 (1961).

[2] Nuclear Science Division 1992 Annual Report, page 50.

[3] C. Madic, B. Guillaume, J.C. Morisseau, and J.P. Moulin, *J. Inorg. Nucl. Chem.* **41**, 1027 (1979).

[4] B. Guillaume, G.M. Begun, and R.L. Hahn, *Inorg. Chem.* **21**(3), 1159 (1982).

[5] B.E. Stout, G.R. Choppin, F. Nectoux, and M. Pages, *Radiochimica Acta* **61**, 65 (1993).

Ha Separation Chemistry: A. Batch Experiments With MnO_2 Powder

C.D. Kacher, A. Bilewicz, and D.C. Hoffman*

The technique of surface sorption allows us to observe the behavior of rutherfordium and hahnium in a new chemical environment. Previous studies examined sorption on cobalt (II) ferrocyanide surfaces[1]. The current study examines the chemical behavior of the homologs of hahnium as well as other tracers using surfaces coated with a variety of surfaces.

In this study, batch experiments were performed with manganese dioxide (MnO_2) powder using various concentrations of HCl. Each batch sample contained 20 uL of tracer, 10ml of various concentrations of HCl, and 100 mg of Sb_2O_5 powder. 1 ml of solution was taken from each sample before the powder was added and counted in a Ge(Li) drifted detector. The samples were then shaken in an ultrasonic bath for 3 hours. After shaking, 1 ml of solution was taken from each sample and counted to see how much activity had remained in solution. The before and after count values were then used to calculated a distribution coefficient. Favorable conditions were identified for sorbing various radiotracers into powder so that sorption on MnO_2 coated surfaces could be studied. The sorption behavior of various cations including the hahnium homologs Nb and Ta was observed. Only low concentrations of HCl were studied because MnO_2 coatings on surfaces are not resistant to HCl concentrations above 3 M. Trivalent cation sorption behavior was also studied to establish conditions which would inhibit trivalent actinide sorption. Trivalent actinides are formed along with hahnium during on-line experiments at the cyclotron. Their activity interferes with detecting hahnium activity.

The radiotracers studied were trivalent Eu-152, tetravalent Zr-95, and pentavalent Np-237, Pa-233, Ta-182, and Nb-95. The tracers sorb onto the $(MnO_2)(H^+)$ surface by way of cation exchange with H^+.

Figure 1 shows the tracer sorption distribution coefficients vs. HCl concentration from 0.5 M to 1.5 M. Kd values greater than 10000 and less than 10 are not meaningful and should be interpreted as nearly complete or minimal adsorption, respectively. Trivalent Eu-152 adsorption decreased with increasing HCl concentration. The separation between the pentavalent cations and trivalent Eu was excellent especially at 0.5 M HCl. Interestingly, Np-237 adsorption remained low.

Footnotes and References

1. C.D. Kacher et al., LBL-33333 Nuclear Science Division 1992 Annual Report, p 52.

*Institute of Nuclear Chem., Warsaw, Poland

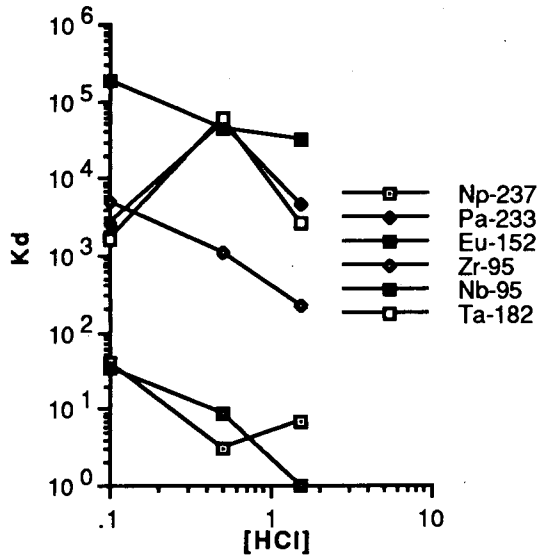

Fig. 1. Distribution coefficients (K_d's) of various radiotracers obtained from batch experiments performed at several HCl concentrations. The Kd of Eu-152, a 3+ cation, is small; hence, these surfaces may be used to study hahnium.

Ha Separation Chemistry: B. Surface Sorption With Sb_2O_5

C.D. Kacher, A. Bilewicz, and D.C. Hoffman*

A series of sorption experiments with Sb_2O_5 surfaces were performed using various concentrations of HCl with and without $CaCl_2$ to identify favorable conditions for sorbing hahnium by observing the sorption behavior of various pentavalent cations, including the hahnium homologs Nb and Ta. Trivalent cation sorption behavior was also studied to establish conditions which would inhibit their sorption.

The radiotracers studied were trivalent Eu-152, tetravalent Zr-95, and pentavalent Np-237, Pa-233, Ta-182, and Nb-95. The tracers sorb onto the $MnO_2{}^-H^+$ surface by cation exchange with H^+.

Batch experiments were performed with Sb_2O_5 powder and HCl (fig. 1). Np pentavalent cations formed positively charged univalent complexes such as NpO_2^+ in the solution studied, and a plot of log Kd vs. log [HCl] gave a straight line indicating ion exchange. The slope of -1 indicates that Np is sorbing as NpO_2^+. The slope of -3 for Eu-152 indicates that Eu is sorbing as the +3 bare ion. A possible sorption reaction for pentavalent neptunium in our system is: $NpO_2^+ + (Sb_2O_5)(H^+) \leftrightarrow Sb_2O_5(NpO_2^+) + H^+$. Likewise, the sorption reaction for Eu(III) was $Eu^{3+} + 3(Sb_2O_5)(H^+) \leftrightarrow (Sb_2O_5)_3(Eu^{3+}) + 3H^+$. These reactions assume Cl^- does not influence the slope. This assumption is not entirely correct and further studies should be done to consider chloride effects on tracer sorption. $CaCl_2$ was used in subsequent surface sorption experiments. It is believed to occupy surface sites and compete successfully for sorption with tracers that ion exchange slowly, especially trivalent cations.

Tracer sorption between 0.5 and 5 M HCl with 1 M $CaCl_2$ for 140 second equilibrations was studied (fig 2). All tracers were pentavalent except for Zr(IV) and Eu(III). Eu sorption was low throughout the range of HCl studied. Straight lines were not achieved, possibly because of competition with Ca^{2+} for surface sites. Further, sorption depends on the kinetics of the species being sorbed and reestablishment of solution equilibrium. The kinetics may change with changing HCl concentration.

*Institute of Nuclear Chem., Warsaw, Poland

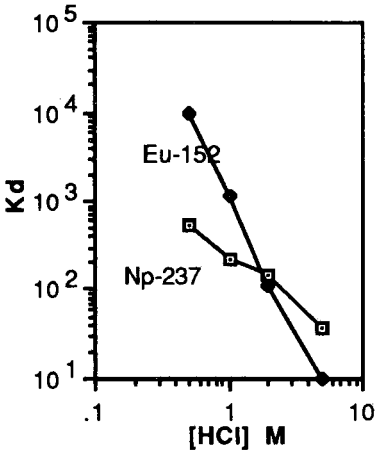

Fig. 1. Distribution coefficients (K_d's) of Eu-152 and Np-237 from batch sorption studies vs. HCl concentrations.

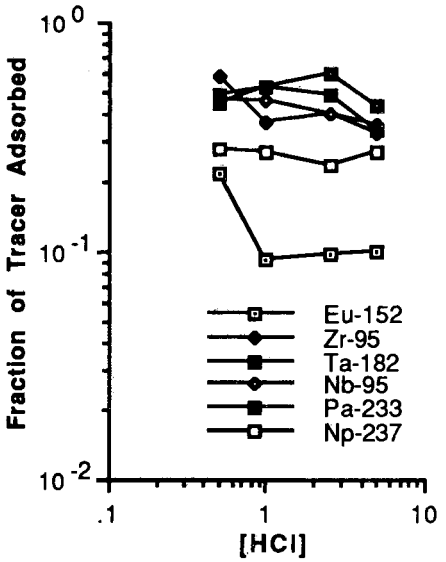

Fig. 2. Sorption of various radiotracers from a surface sorption study vs. a range of HCl concentrations with 1M $CaCl_2$.

On-Line Isothermal Gas Chemistry Experiments with Bromides of Rf (Element 104)

E. Sylwester, K.E. Gregorich, B. Kadkhodayan, C.D. Kacher, M.R. Lane, D.M. Lee, M.F. Mohar, M.P. Neu, and D.C. Hoffman

The Heavy Element Volatility Instrument[1] (HEVI) was used to investigate the volatility of rutherfordium tetrabromide ($RfBr_4$). HEVI is an on-line isothermal gas chromatography system which separates short-lived volatile halides according to their volatility. 76-s ^{261}Rf was produced in fusion reactions of 94-MeV ^{18}O + ^{248}Cm at the LBL 88-Inch Cyclotron. Reaction products, transported by a He/MoO_3 gas jet, were continuously collected on a quartz wool plug kept at 900°C inside a quartz chromatography column. $RfBr_4$ was formed by adding 100 ml/min HBr gas. The volatile $RfBr_4$ molecules were carried to the isothermal section of the column by the He flow, where gas-phase chromatography was performed. Here, the retention time of $RfBr_4$ was measured (using the half-life of 76-s ^{261}Rf as a clock) as a function of the temperature of the isothermal section of the column. The $RfBr_4$ molecules which survived the retention time in the column were then transported by a second gas-jet to the MG rotating wheel[2] counting system. At the MG, products were collected on thin polypropylene foils (40 $\mu g/cm^2$) which were stepped through 6 pairs of detectors for the measurement of α- and SF-decay. Rf was detected by observation of the 8.2-8.4-MeV α-particles from the decay of ^{261}Rf and its 26-s daughter, ^{257}No. A decay curve analysis of the α-peak at 8.15-8.38 MeV resulted in a ^{261}Rf half-life of 74^{+8}_{-6} s.

Fig. 1 shows the relative chemical yield of $RfBr_4$ as a function of the isothermal temperature in the chromatography column. This shows that the $RfBr_4$ becomes volatile between 150° and 200° centigrade.

A Monte Carlo simulation[3] was used to model the processes within the column. A comparison of the simulation with the yield curve in Fig.1 has been used to determine the adsorption enthalpy of $RfBr_4$ to be -89±5 kJ/mol. This is very similar to the adsorption enthalpy of -91 kJ/mol measured[4] for $ZrBr_4$. Also, comparison with previous experiments[4] in which the adsorption enthalpy of $RfCl_4$ was found to be -79±5 kJ/mol shows $RfBr_4$ to be less volatile than $RfCl_4$.

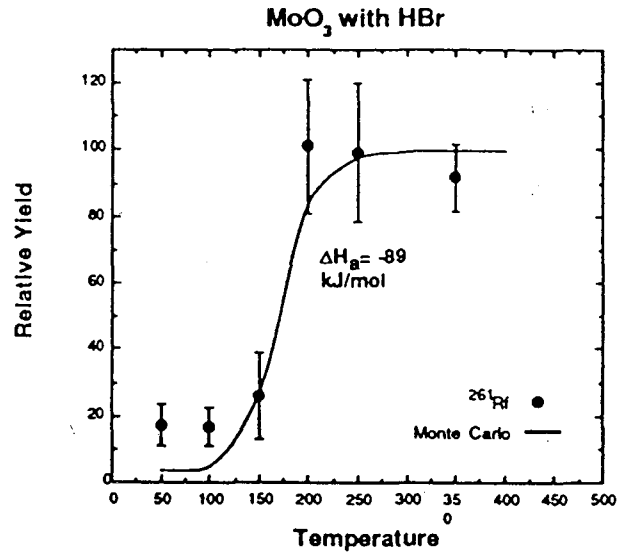

Fig. 1. Relative yield curve for $^{261}RfBr_4$ with a He/MoO_3 gas-jet and HBr used as the brominating agent.

References

1.B. Kadkhodayan et al., *Nucl. Instr. Meth.* A317, 254 (1992)

2. D.C. Hoffman et al., *Phys. Rev. C* 41, 631 (1990)

3. A. Türler et al., LBL-31855, Annual Report (1991).

4. B. Kadkhodayan et al., Annual Report (1992).

Production of New 2.1-sec SF Activity of ^{262}Rf

D. C. Hoffman, D. M. Lee, K. E. Gregorich, M. F. Mohar, M. R. Lane, N. J. Hannink, C. D. Kacher, M. P. Neu, E. R. Sylwester, M. Hsu, and J. C. Yang

A Dubna-Livermore group recently reported[1] the production of an unusually long (15-30 sec) alpha-decaying isotope in the ^{248}Cm(^{22}Ne, 4n) reaction. Based on separations using their gas-filled separator and the measurement of 6 alpha decays correlated with a 1-sec spontaneous fission (SF) activity, they assigned the alphas to ^{266}106 decaying to a previously unknown 1-sec SF activity of ^{262}Rf. These unusually long half-lives for even-even isotopes were attributed to the influence of a deformed shell at 162 neutrons. In order to check the assignment of the 1-sec SF, we produced ^{244}Pu via the (^{22}Ne, 4n) reaction at the LBL 88-Inch Cyclotron. We found a previously unreported 2.1-sec SF activity with a cross section of about 0.5 nb using 114.4-MeV ^{22}Ne ions. We measured its fission properties with our MG rotating wheel system. Based on the decrease in cross section at 119 and 123 MeV, we attribute the activity to ^{262}Rf. It may be the same as the 1-sec SF activity reported to be the daughter of ^{266}Sg; however, our statistics are much better.

The measured total kinetic-energy (TKE) and mass distributions are shown in Figs. 1 and 2. The TKE of 214.8 MeV is not unusually high as is the case for $^{258,\ 259}$Fm. Although the mass distribution has a narrow, symmetric region, it also appears to have "wings", consistent with its placement as a transition nucleus. A possible problem with the assignment is that a 50-msec SF activity was previously assigned[2] to ^{262}Rf based on cross bombardments and excitation functions. It may be that these two activities are K-isomers associated with the presence of a high spin quasiparticle state of the type discussed by Baran and Lojewski[3].

References

1. R. W. Lougheed et al., Actinides-93 Internatl. Conf., Sept.19-24, 1994, Santa Fe, New Mexico,
2. L. P. Somerville et al., Phys. Rev. C 31, 1801 (1985).
3. A. Baran and Z. Lojewski, Nucl. Phys. A 475, 327 (1987).

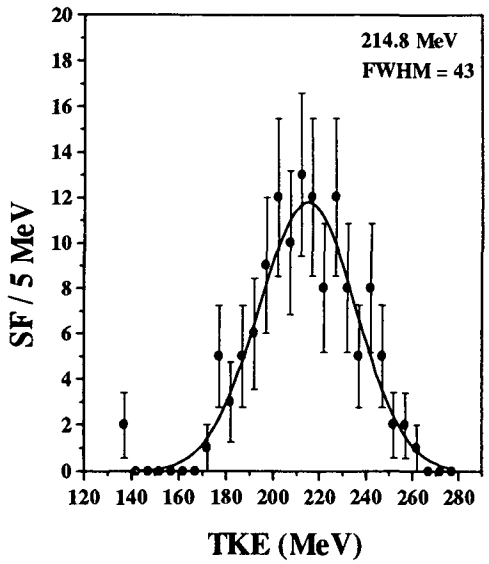

Fig. 1. Mass-Yield Distribution for ^{262}Rf.

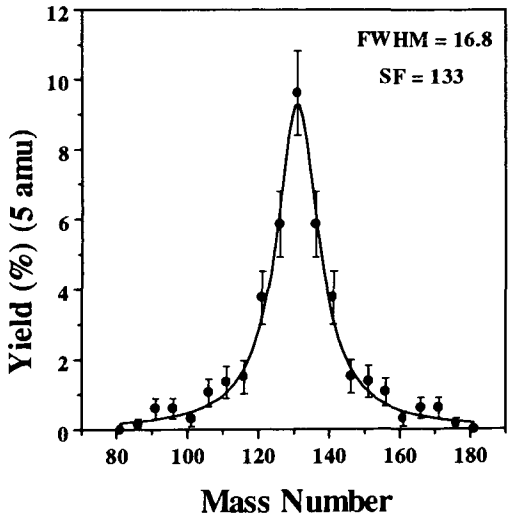

Fig. 2. TKE Distribution for ^{262}Rf.

The N=162 Shell in ^{262}Rf

K.E. Gregorich, D.C. Hoffman, D.M. Lee, M.F. Mohar, M.R. Lane, N.J. Hannink, C.D. Kacher, M.P. Neu, E.R. Sylwester, M. Hsu, J.C. Yang

A 2.1-s spontaneous fission (SF) activity[1] has been observed in ^{22}Ne + ^{244}Pu bombardments at the 88-Inch Cyclotron. The excitation function for this 2.1-s SF activity peaks near E_{lab} (^{22}Ne) = 114 MeV, with a maximum cross section of 0.5 nb. The production cross section is slightly lower at E_{lab} = 110 MeV and 119 MeV, and much lower at E_{lab} = 125 MeV. The shape and magnitude of the excitation function are consistent with those expected for the ^{244}Pu(^{22}Ne,4n) reaction, and therefore this activity has been tentatively assigned to the decay of ^{262}Rf. This is presumably the same activity seen by the Dubna-Livermore collaboration[2] as the daughter of ^{266}Sg. In earlier studies[3] a SF activity with a half-life near 50 ms, was also assigned to the decay of ^{262}Rf.

Baran and Lojewski[4], have predicted fission from K-isomeric states in the heavy elements. They predict that in almost all cases, partial half-lives for fission from K-isomeric states should be longer than for the ground states. However, in ^{256}Fm, the only case where fission from a K-isomer in the first well of the fission barrier has been measured[5], the partial fission half-life for the K-isomer is 10^{-7} of the ground sate SF half-life. If we assign the 2.1-s SF activity to decay of the ^{262}Rf ground state and the 50-ms SF to decay of a K-isomeric state, the partial half-lives for SF- and α-decay have implications for the extent and magnitude of the predicted deformed nuclear shell[6] centered at N=162 and Z=108.

In the absence of the N=162 shell, the ground-state partial SF half-life for ^{262}Rf is expected to continue the trend observed for the lighter e-e Rf nuclides, resulting in a half-life of tens of milliseconds. The 2.1-s half-life observed is a strong indication of enhanced stability for this N=158 nuclide, providing experimental evidence for the predicted N=162 shell.

Alpha-decay of ^{262}Rf should be followed closely in time by the SF decay of 1.2-ms ^{258}No, providing an unambiguous signature for this decay mode. During the studies of the 2.1-s SF activity[1], we searched for ^{262}Rf α-decay by looking for time correlated α-SF events with E_α = 7.5-9.0 MeV. To date, we have measured approximately 160 of the 2.1-s SF events and without observing any α-SF correlations. Considering detection efficiencies in the MG rotating wheel system, we can place an upper limit of 1% on the α-decay branch in ^{262}Rf, resulting in a lower limit of 200s for the partial half-life for α-decay.

Using an extrapolation of experimental masses[7] which do not take into account the N=162 shell, the ^{262}Rf Q_α of 8.6 MeV results in a predicted partial α-decay half life[8] of 10s. This partial half-life for α-decay would result in an α-decay branch of 20% which is inconsistent with our 1% upper limit. However, when Sobiczewski considers the N=162 shell, an expected E_α of 8.1 MeV is obtained. The resulting 150-s partial half-life for α-decay gives an expected I_α of 1.3% which is consistent with our present upper limit of 1%. The small α-decay branch observed in these experiments is therefore another indication of the existence of strong shell effects, consistent with those predicted near N=162 and Z=108.

References

1. D.C. Hoffman et al., see preceding report.
2. R.W. Lougheed et al., Actinides-93 Internatl. Conf., Sept. 19-24, 1994, Santa Fe, New Mexico.
3. Sommerville et al., Phys. Rev. C31, 1801 (1981).
4. A. Baran, Z. Lojewski, Nucl. Phys. A475, 327 (1987).
5. H.L. Hall et al., Phys. Rev. C 39, 1866 (1989).
6. A. Sobiczewski, Actinides-93 Internatl. Conf., Sept. 19-24, 1994, Santa Fe, New Mexico.
7. Private Communication, Audi et al., (1993).
8. Y. Hatsukawa et al,. Phys Rev. C 42, 674 (1990).

Evidence for the Discovery of ^{263}Rf

K.E. Gregorich, C.D. Kacher, M.F. Mohar, D.M. Lee, M.R. Lane, E. R. Sylwester, D.C. Hoffman, M. Schädel, W. Brüchle,* J.V. Kratz,† Rolf Günther**

In previous attempts[1,2] to identify ^{263}Rf, the ^{248}Cm(^{18}O,3n) reaction was used to produce this new isotope. A chemical separation based on the extraction of Rf^{4+} into thenoyltrifluoroacetone (TTA) was used to separate the Rf atoms from actinides, allowing a search for the α- and spontaneous fission (SF)-decay of ^{263}Rf. In these experiments a total of 7 SF events were observed which were interpreted as preliminary evidence for the production of ^{263}Rf with a SF half-life near 500-s and a production cross section of 140 pb.

A second attempt to identify ^{263}Rf was made during our German-Swiss collaboration at the LBL 88-Inch Cyclotron to study the chemical and nuclear properties of Rf and Ha in the fall of 1993. The ^{249}Bk(^{18}O,4n) reaction was used to produce[3] ^{263}Ha. Chemical separations were carried out to study the decay properties of ^{263}Ha and search for evidence of ^{263}Rf which could be produced by electron-capture (EC) in ^{263}Ha. Activities from the ^{18}O + ^{249}Bk reaction were transported by a gas-jet to the Automated Rapid Chemistry Apparatus[4] (ARCA) where computer controlled separations were repeatedly performed, on a one-minute time scale, producing Rf and Ha samples for α- and SF-pulse height analysis. The separation involved eluting Ha from cation exchange columns in 0.05M α-hydroxyisobutyrate (α-HIB) and Rf fractions from a slightly higher concentration of α-HIB. All these fractions had an extremely high degree of purity from actinides, allowing a search for SF decay at detection rates as low as one event per hour.

We observed a total of 22 fissions over the course of 155 experiments. Approximately 8.8 of these were attributed to ^{256}Fm decay, leaving 13.2 SFs due to the decay of ^{263}Rf. These ^{263}Rf fissions had a half-life of 600 seconds, close to the 500 second fission half-life observed from a previous study[1].

Once the 6-nb ^{263}Ha production cross section[3] is considered, these 13.2 SF events correspond to a ^{263}Ha EC branch of ~8%. The resulting effective ^{263}Rf production rate is about a factor of 4 larger than that expected or observed[1] in either the ^{248}Cm(^{22}Ne,α3n) or ^{248}Cm(^{18}O,3n) reactions.

Alpha half-life predictions of ^{263}Rf were made using mass models from Satpathy[5] and Möller[6]. If the alpha energy of ^{263}Rf is between 7.74 and 8.0 MeV, we would expect a 30% alpha branch based on the two events we observed at 7.9 MeV and an alpha half-life between 800 and 8000 seconds. If the alpha energy of ^{263}Rf is between 7.65 and 7.74 MeV, then any alphas from ^{263}Rf would be masked by alphas from ^{214}Po. If the alpha energy is less than 7.65 MeV, then the predicted alpha half-life for ^{263}Rf would be greater than 10,000 sec, and thus too long to be observed.

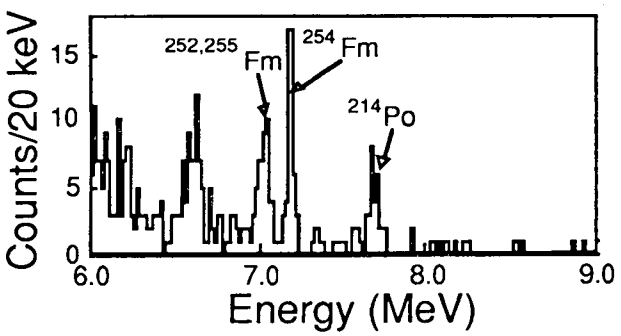

Fig.1 Summed α-particle spectrum from 155 ^{263}Rf separations.

Footnotes and References

* Gesellschaft für Schwerionenforschung, Germany.

† Universität Mainz, Germany.

1. K.R. Czerwinski, et al., LBL Nucl. Sci. Div. 1991 Ann. Rept., LBL-31855 p.54 (1992)

2. K.R. Czerwinski, Ph.D. Thesis, LBL-32233, (1992).

3. J.V. Kratz, et al., Phys. Rev. C 45, 1064) (1992).

4. M. Schädel, et al, GSI Preprint, GSI-89-38, (1989).

5. P. Möller, J.R. Nix, Atom. Data Nucl. Data Tables, 39, 241 (1988).

6. L. Satpathy, R.C. Nayak, Atom. Data Nucl. Data Tables, 39, 241 (1988).

Continued Search for ^{263}Rf

C.D. Kacher, K. E. Gregorich, M.R. Lane, E.R. Sylwester, N.J. Hannink, M.P. Neu, B.A. Kadkhodayan, S.A. Kreek, M.F. Mohar, D.M. Lee, and D.C. Hoffman

The recent discovery[1] of long-lived neutron-rich isotopes of element 106 and its implications about a deformed shell[2] at N=162, have sparked new interest in decay studies of neutron-rich transactinide isotopes. The discovery of a longer-lived isotope of Rf would greatly facilitate our studies of the chemical properties of Rf. We have performed a search for a new neutron-rich isotope of element 104, ^{263}Rf. We used the ^{248}Cm (^{22}Ne, α3n) reaction with a beam energy of 116 MeV on target and estimated a potential cross section of 120 pb using the JORPL[3] tables. Folding in the gas jet yield, chemical yield, and detector efficiencies, the detection rate for a cross section of 120 pb would be 0.56 events per hour.

Presently, the longest-lived known isotope of Rf is 78-s ^{261}Rf. Because of lower Q values for α and EC decay, the partial half-lives of ^{263}Rf are expected to be longer than for the lighter isotopes of Rf. The predicted EC half-life is 1.5h (Q_{EC} = 1.33, log (ft) = 6.0), and the predicted α half-life is several hours (Q_α = 7.82). If the SF hindrance factor associated with the 159th neutron in Rf is between 10^3 and 10^5, we expect the overall half-life to be dominated by SF decay and lie between 20s and 2000s.

Based on the above ^{263}Rf half-life estimates for fission and alpha decay, two procedures were designed to a) look for the possibility of short-lived Rf-263 fissions and b) to look for long-lived Rf-263 fissions and both short- and long-lived Rf-263 alphas. Rf^{4+} was chemically separated from lower valent species by extraction into 0.5 M thenoyltrifluoroacetone (TTA) from 0.05 M HCl.

To search for short lived Rf-263 fissions, the activity was collected for ten minutes, picked up with 10 uL of 0.05 M HCl, mixed and centrifuged with 0.5 M TTA. Then the organic phase was removed, evaporated on a glass cover slip, and counted with a PIPS detector for fissions and alphas.

To search for long-lived ^{263}Rf fissions and both short and long lived ^{263}Rf alphas, a special collection procedure was used. The activity was collected for five minutes, picked up with 10 uL of 0.05 M HCl, mixed with 0.5 M TTA and centrifuged. The organic phases from the separations performed on the 5-minute collections were combined over a one hour period. An equal volume of 12M HCl was added to this organic phase to back extract $^{259}No^{2+}$, the daughter of $^{263}Rf^{4+}$. The aqueous layer was removed, evaporated on a glass cover slip, and alpha counted. Detection of ^{259}No alphas would imply ^{263}Rf production.

The organic phase was saved and new organic phases from subsequent exports were added to the original organic sample. The procedure was repeated two more times, and, after the back extraction with 12 M HCl, the organic phase was evaporated on a glass cover slip and counted for long-lived Rf-263 fissions and alphas. This complete 3-hour procedure was repeated six times.

We saw no evidence for alphas from ^{259}No or ^{263}Rf. Our sensitivity for detection of fissions was hampered by the relatively large amounts of ^{256}Fm also produced in the ^{22}Ne + ^{248}Cm reaction. We detected 16 fissions, about the number expected for ^{256}Fm calculated from its known cross section[4]. Hence none of the observed fissions could be attributed to ^{263}Rf. We estimate we could have detected an equal number of fissions from ^{263}Rf if present. Based on a ^{263}Rf half-life of 1000 sec, we would have been sensitive down to a 125 pb cross section, close to the predicted cross section.

References

1. R. Lougheed et al., Proc. Actinides '93, Santa Fe, NM, 1993.

2. A. Sobiczewski, Proc. Actinides '93, Santa Fe, NM 1993.

3. J. Alonso, Gmelin Handbuch der Anorganischen Chemie, 7b, 28 (1974).

4. D. Lee, et al, Phys. Rev. C, 25, 1, 289 (1982).

First Confirmation of the Discovery of Element 106

K.E. Gregorich, M.R. Lane, M.F. Mohar, D.M. Lee, C.D. Kacher, E. R. Sylwester, D.C. Hoffman

^{263}Sg ($t_{1/2}$=0.9s)[1] was produced at the Lawrence Berkeley Laboratory 88-Inch Cyclotron by the ^{249}Cf(^{18}O,4n)^{263}106 reaction with a 350 particle-nanoAmpere beam of 95-MeV $^{18}O^{5+}$ ions. The reaction products recoiling out of the target were transported to the MG rotating wheel system by a He/KCl gas-jet. These products were deposited on thin polypropylene foils around the periphery of an 80-position wheel. The wheel was stepped to position the foils with newly collected reaction products sequentially between six pairs of α- and SF-detectors. ^{263}Sg was identified by measuring its α-decay (E_α = 9.06 MeV) followed closely in time by the α-decay of the 3.4-s daughter[2], ^{259}Rf (E_α ~ 8.8 MeV). For this experiment, a special parent-daughter stepping mode was used to minimize random α-α correlations. Details can be found in Ref. 3.

The experiment was run for 60 hours. The spectrum of all α-particle events recorded during daughter search intervals is shown in Figure 1. Nine events were recorded the energy range expected for ^{259}Rf. Table 1 lists the detectors, lifetimes, and α-decay energies of the nine ^{259}Rf events, along with the ^{263}Sg parent events which preceded them. A statistical analysis of the data is given in Ref. 3.

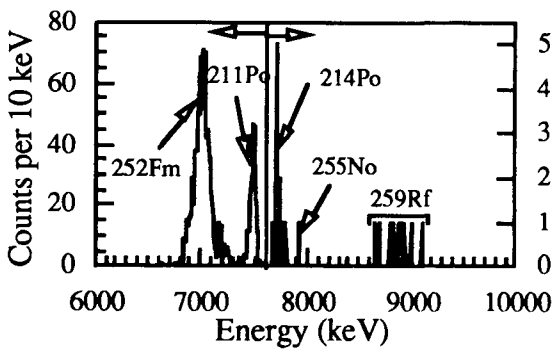

Figure 1: Decay of ^{263}106 and its daughter activities

Using these events, the half-life of ^{263}106 was determined to be $1.1^{+2.8}_{-0.6}$s. The distribution of parent energies fits well with a single α-group at 9.04±0.06MeV, and the production cross section is calculated to be 0.3 nb. All this is consistent with the data reported by Ghiorso et al.[1] in their 1974 discovery experiment. In addition, the half-life and α-decay energy observed for the ^{259}Rf agree with previously published values[2]. This work constitutes the first confirmation of the discovery of element 106.

Detectors	Parent		Daughter	
Parent/ Daughter	Lifetime (s)	E_α (MeV)	Lifetime (s)	E_α (MeV)
-----/3-bot			0.717	8.70
1 bot/1-bot	0.283	8.99	0.717	8.66
1 bot/1-top	0.283	9.09	2.850	8.99
3 bot/3-top	1.117	9.00	1.933	8.93
3 bot/3-top	1.183	9.05	0.267	8.80
3 bot/3-top	0.783	9.08	5.467	8.87
1 bot/1-top	0.200	8.95	10.883	8.90
5 bot/5-top	1.733	8.90	0.517	8.83
-----/5-top			4.633	9.10

Table 1: Daughter mode ^{259}Rf events and ^{263}106 events which initiated the daughter mode.

References

1. A. Ghiorso et al., *Phys. Rev. Lett.* 33, 1490 (1974).
2. J.K. Tuli, R.R. Kinsey, and M.J. Martin, *Nucl. Data Sheets* 59, 618 (1990).
3. K.E. Gregorich et al., *Phys Rev. Lett.* 72, 1423 (1994).

Evidence for the Synthesis of Element 110 by the $^{59}Co + ^{209}Bi$ Reaction

A. Ghiorso, D.Lee, L.P. Somerville, W. Loveland, J.M. Nitschke, W. Ghiorso, G. T. Seaborg, P. Wilmarth, R. Leres, A. Wydler, M. Nurmia, K. Gregorich, R. Gaylord, T. Hamilton, N. Hannink, D.C. Hoffman, C. Jarzynski, C. Kacher, B. Kadkhodayan, S. Kreek, M.Lane, A. Lyon, M.A. McMahan, M. Neu, T. Sikkeland, W.J. Swiatecki, A. Turler, J. T. Walton, and S. Yashita.

We have found what we believe to be credible evidence for the synthesis of element 110 using the $^{209}Bi(^{59}Co,n)^{267}110$ reaction. This experiment, the final one at the SuperHILAC, was performed in 1991 utilizing the SASSY2 gas-filled magnetic separator. The integrated beam fluence of $1.5x10^{18}$ ions was delivered over a period of 41 days.

One unique event, involving multiple correlated signals, was seen at a projectile energy of 300 MeV; the characteristics of this event are shown in Fig. 1. A recoil atom with the correct values of Bρ, dE/dx, and E was implanted in focal plane detector #28. Four microseconds after implantation, an 11.6-MeV α-particle was observed in detector #28 and 6.0s later a 2.2 MeV α-particle was observed in the same detector. Finally, an 8.31-MeV α-particle was found at the same implantation site 19s after the arrival of the recoil. All of these alphas were detected during the beam-on time (30% duty cycle). The gross background during the beam pulse for the run in which this event occurred was only 1 c/s.

We postulate that the 4-μs 11.6-MeV alpha particle comes from $^{267}110$ and that its daughter ^{263}Hs, was not observed due to the dead time of the ADC following the first decay (For technical reasons our Transient Recorder was not available for this experiment). At this point, we believe that, instead of decaying by alpha emission, the element-106 granddaughter ^{259}Sg, decayed by electron-capture (significant EC branches are observed for the other N=153 nuclei: ^{252}Es, ^{253}Fm, ^{254}Md, ^{255}No, ^{256}Lr, ^{257}Rf, and ^{258}Ha). The resultant unknown-^{259}Ha, in turn would alpha decay to ^{255}Lr with a half-life assumed to be a second or two. In this scenario the 2.2-MeV particle would come from the escape alpha of ^{259}Ha and the 8.31-MeV particle would be the full energy alpha from the 22-s ^{255}Lr. The decay of this nuclide would lead to unobservable daughters in this experiment.

Using the data from all of the runs, we calculate that the probability of a chance correlation between the initial implantation and the 11.6-MeV α-particle is less than 10^{-7}. Because that alpha follows so soon after the 34-MeV recoil we have used a double-pulser technique to measure the small correction in pulse height (about 8%) that takes place because of our electronic circuitry. Although there are some weak points in our scenario, we are compelled to the belief that the association of this single event with the formation of an isotope of element 110 is the simplest explanation for our observations. Plans are under way to attempt to confirm our work with a new separator at the 88-inch Cyclotron.

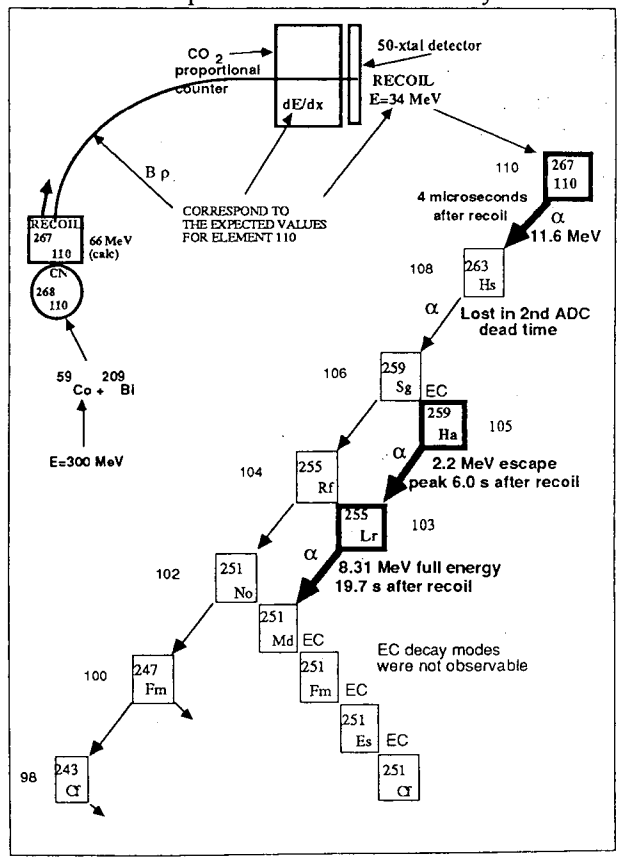

Fig. 1. Proposed Scenario for the Element-110 Event The highlighted boxes indicate the observed sections of the postulated alpha decay chain.

Prompt Neutron Emission Functions for Spontaneous Fission

D. M. Lee, D. C. Hoffman, B. D. Wilkins *

Very little detailed experimental information exists for prompt neutron emission from spontaneous fission (SF) of heavy isotopes of fermium (Z=100) and still higher Z elements. Such data are needed to make corrections for neutron emission in order to derive pre-neutron emission total kinetic-energy and mass-yield distributions from kinetic-energy measurements of coincident fission fragments. Although much detailed information is available for SF of ^{252}Cf, it is not readily applicable to SF of the heaviest isotopes. A realistic correction for neutron emission from the individual fragments should be based on the excitation energy (E^*) and deformation of the fragments. A simple model is constructed based on the Scission Point Model (SPM) of Wilkins et al. [1] in which there is repeating structure of the fragment shells as a function of nucleon number in the deformation space. The deformation energies are divided into the following three regions for ^{252}Cf with limits which conform to the repeatable structure seen in the SPM.

Region	Deformation
A	$0.0 \leq \beta \leq 0.35$
B	$0.35 < \beta < 0.80$
C	$0.80 \leq \beta \leq 1.0$

The results of the calculation of E* (energy available for neutron and photon emission) for all combinations of two fission fragments with deformations in regions A, B, and C as a function of heavy fragment mass are shown in Fig 1. A comparison of the calculated and experimental prompt neutron emission functions for SF of ^{252}Cf is shown in Fig. 2.

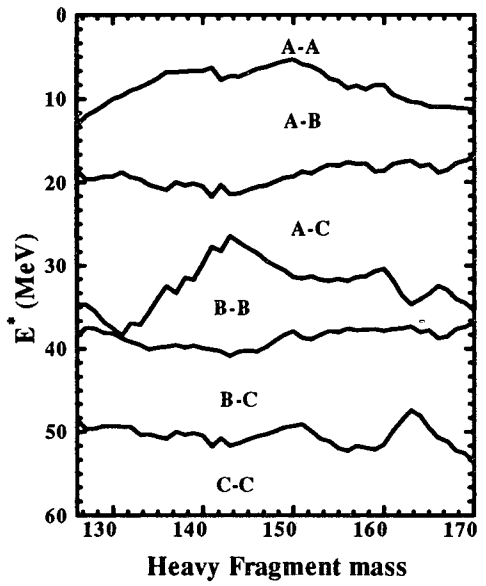

Fig. 1. Deformation regions vs. heavy fragment mass and E^*.

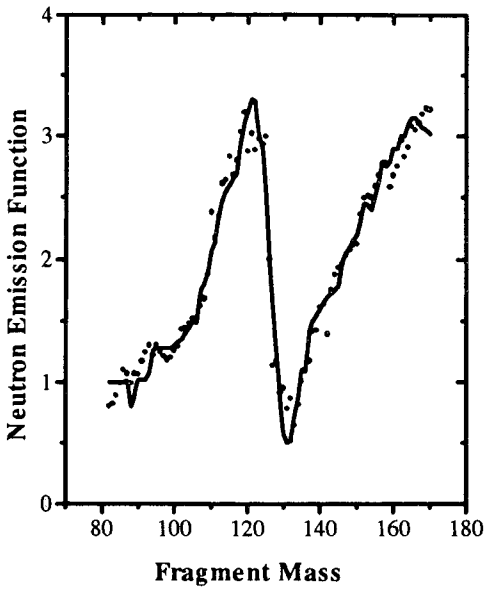

Fig. 2. Comparison of calculated (circles) and experimental (line) neutron emission for ^{252}Cf.

Footnotes and References

* Environmental Assessment and Information Sciences Division, Argonne National Laboratory, Argonne, IL.

1. B. D. Wilkins et al. Phys. Rev. C 14, 1832 (1976).

Gas-Jet Transport Tests : Improving The Yields

K.E. Gregorich, C.D. Kacher, E.R. Sylwester, M.F. Mohar, and D.C. Hoffman

Heavy element research is dependent on transporting heavy element activities from the target system to a collection site where their chemical and/or nuclear properties can be studied. Typically, product nuclei, recoiling out of a thin target, become attached to KCl aerosols in He gas at a pressure near 1 atmosphere. The He gas and aerosols are then pumped through a capillary and collected at the far end. A laminar flow profile within the capillary tube creates Bernoulli forces felt by the aerosol-sized particles, focusing them near the center of the capillary. This focusing effect on the activity-bearing aerosol particles results in few collisions with the capillary wall, and very efficient transport. Inconsistent gas-jet yields during recent experiments have prompted studies to understand and improve gas-jet transport efficiencies. Two sets of experiments were performed. The first was to optimize the recoil chamber parameters, and the second was to optimize the KCl aerosol formation for efficient transport of activities.

In the first set of experiments, 3-minute ^{211}Fr was produced in the ^{197}Au(^{18}O,4n) reaction at the 88-inch cyclotron. The gas-jet transport yield was measured by detecting the ^{211}Fr α-decay with our MG rotating wheel system. The gas jet efficiency was measured while varying: 1) capillary diameter, 2) recoil chamber diameter and 3) position of capillary out of recoil chamber.

Gas-jet efficiencies were measured using Teflon capillaries with inner diameters of 0.8 mm, 1.4 mm, and 1.6 mm. The 1.4-mm diameter capillary gave the best yield, and 0.8-mm, the worst yield.

Recoil chamber inserts which limited the gas-jet sweep volume were constructed with 0.75-, 1.00-, and 1.25-inch inside diameters. Each had four positions into which the capillary could fit (1.5, 2.0, 2.5, and 3.0 cm downstream of the target). The gas-jet efficiency was found to be independent of these parameters, except a decrease in yield was measured using the smallest recoil chamber with small capillary-to-target distances.

The aim of the second set of experiments was to determine optimum conditions to produce KCl aerosols for efficient transport of the activities. KCl aerosols are produced by subliming KCl from the solid in a furnace and allowing the KCl vapor to condense into aerosol-sized particles. This He/KCl-aerosol mixture was then passed over a ^{225}Ac ($t_{1/2}$=10d) source. The α-decay of ^{225}Ac resulted in ^{221}Fr daughter atoms recoiling from the source. A bias voltage of ~50V/cm was used to help move the ^{221}Fr recoils away from the source. These recoils became attached to the aerosol particles and were then transported to a collection site at the far end of the capillary. By measuring the yield of 5-minute ^{221}Fr atoms at the collection site, the gas-jet efficiency was determined.

A four-zone tube furnace was used to find the temperature profile resulting in the highest transport efficiency. We found high transport efficiencies when the solid KCl was maintained at 640°C and there was a sharp drop in the temperature profile after this 640° section. The sublimation temperature of 640°C resulted in about 0.1 μg of KCl aerosols per second. This KCl thickness was determined by measuring the energy loss of alpha-particles upon passing through the KCl deposit. The sharp drop in the temperature profile produces a highly super-saturated KCl vapor which then condenses into relatively large aerosol particles.

A List Processor-Based Data Acquisition System

W.H. Rathbun, K.E. Gregorich, M.F. Mohar

A new data acquisition system has been developed by interfacing a commercially available SCSI/CAMAC Crate Controller and a list processor with the *Chaos* data acquisition and analysis software. This provides a powerful yet compact data acquisition system that can be used in a wide variety of experiments.

Although individual CAMAC operations are slow when conducted using the SCSI protocol, block-mode transfers become quite fast when the basic SCSI protocol overhead is amortized over several thousand words. This suggested the use of a list processor to perform CAMAC reads and buffer data for block-mode transfers.

The list processor (HyTec LP1341) performs a user-supplied list of CAMAC commands and buffers incoming data in a 256k x 24-bit data memory before transfer to the host workstation via the industry-standard SCSI bus through the CAMAC crate controller (Jorway 73A-1). It performs commands at a rate approaching the CAMAC dataway limit, resulting in data acquisition rates of 1 word (24 bits) per 1.5 μsec (2MB/sec). In effect, data acquisition rates are limited by ADC conversion times. The list processor can be read-out asynchronously while acquiring new data. Execution of instruction lists by the LP1341 can be initiated by up to seven individual prioritized triggers, and/or it can be LAM-initiated. The *Chaos* software supplies simple defaults for quick-and-easy data acquisition.

The Heavy Element Nuclear and Radiochemistry Group has successfully used this data acquisition system for recent experiments. The hardware and software development has progressed to the point where it can be easily adapted to other experimenters' data acquisition needs.

Mass Asymmetric Fission Barriers for Compound Nuclei ^{90,94}Mo

K. Jing[a], A. Veeck, I. Lhenry[b], N. Colonna[c], K. Tso, K. Hanold, W. Skulski, Q. Sui[a], G. J. Wozniak, and L. G. Moretto

Earlier measurements of the mass asymmetric fission (conditional) barriers for compound nuclei ^{75}Br and $^{110-112}$In agreed very well with the prediction of the Rotating Finite Range Model (RFRM)[1,2]. Upon closer inspection, this agreement seems to be somewhat accidental. When corrections are made for ground state shell effects on the conditional barriers, the RFRM tends to underestimate the conditional barriers by 3 MeV.

In this work, the excitation functions for complex fragment emission from the compound nuclei ^{90,94}Mo, with n/p ratios 1.14 and 1.24 respectively, have been measured and the conditional barriers extracted. These barriers, together with the barriers for ^{98}Mo (n/p=1.33) measured in another experiment, will provide a stringent test on the n/p dependence of the conditional barriers, and allow an improvement in the determination of surface energy and suface asymmetry constants in the nuclear mass formula.

Compound nuclei ^{90,94}Mo were produced in the reverse kinematics reactions ^{78,82}Kr + ^{12}C at several beam energies ranging from 6.0 to 12.2 MeV/u. The experiment was carried out at 88-Inch Cyclotron. Complex fragments from the reactions were detected with two position-sensitive quad gas-silicon telescopes placed on either side of the beam. At each bombarding energy, the angular distribution for fragments from Z=5 to 25 were measured over a large center-of-mass angular range. For each fragment the isotropic component of the angular distributions is integrated to give the cross section associated with compound nucleus decay. At each beam energy the charge distributions were constructed. In addition, the excitation functions for fragments with certain Z values were constructed by combining the data from all the bombarding energies.

The conditional barriers (see Fig.1) for ^{90,94}Mo have been extracted by fitting the excitation functions with a transition state formalism. The extracted barriers are 3.5 MeV higher on average than the calculations of the RFRM, both in the case of ^{90}Mo and ^{94}Mo. The isospin dependence of the conditional barriers are clearly observed. The barriers for ^{94}Mo are about 3 MeV higher than for ^{90}Mo, which shows a stronger n/p dependence than the RFRM predicts. Odd-even effects are visible for light fragments where one can clearly resolve the fragment Z.

The results of this measurment are consistant with our previous measurments for ^{75}Br and $^{110-112}$In. These results indicate that the RFRM systematically underestimates the mass asymmetric fission barriers for nuclei in the mass range of 75-112.

Footnotes

[a] Institute of Atomic Energy, Beijing, China
[b] IPN, Orsay, France; [c] INFN, Bari, Italy

[1] D. Delis et al., Nucl. Phys. A534, 403 (1991)
[2] M. McMahan et al., Phys. Rev. Lett., 54, 1995(1985)

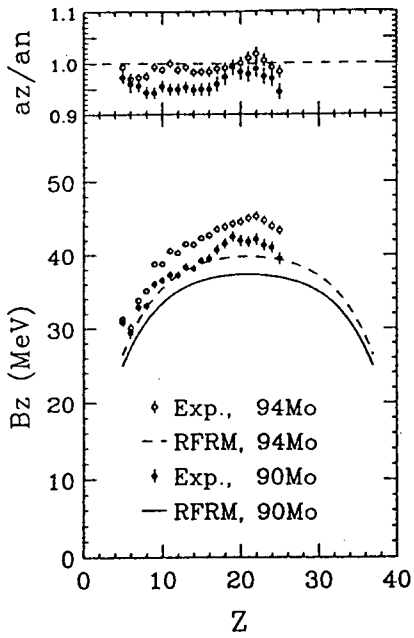

Fig. 1. Mass asymmetric fission barriers Bz and the ratio of the level-density parameters az/an for ^{90,94}Mo as a function of fragment Z. The symbols are barriers extracted from experimentally measured excitation functions. The lines are the RFRM calculations. Note that the data are corrected for the shell effects of the ground state.

Mass Asymmetric Fission Barriers for the Neutron Rich Compound Nucleus ^{98}Mo

A. Veeck, K. Jing[a], K. Hanold, N. Colonna[b], D. Delis, K. Tso, W. Skulski, G.J. Wozniak, and L.G. Moretto

Earlier work by this group studied the mass asymmetric conditional fission barriers for the nucleus ^{75}Br, and found that the Rotating Finite Range Model (RFRM) accurately predicts these barriers. To test the model for heavier systems, charge distributions and excitation functions for the compound nucleus ^{98}Mo, representing a neutron-rich (n/p=1.33) compound nucleus, were measured and used to extract the experimental barriers for each emitted fragment Z-value. In addition to evaluating the accuracy of the RFRM barriers, the conditional fission barriers can be used to improve the determination of the surface energy (a_S) and surface asymmetry (k_S) constants in the nuclear mass formula, and to fine-tune simulated sequential decay calculations.

To create the excited compound nucleus ^{98}Mo, a carbon target was bombarded with a beam of ^{86}Kr at several energies ranging from 7.3 MeV/A to 13.2 MeV/A. The 88-inch Cyclotron with its new Advanced ECR (AECR) source provided steady beams of high charge state ions for this study. Eight telescopes, each consisting of a gas ΔE detector followed by a position sensitive silicon detector, measured the energy, atomic number, and spatial location of fragments resulting from the decay of the compound nucleus.

The extracted experimental barriers, shown in Fig. 1, are approximately 7 MeV higher than the barriers predicted by the RFRM, and approximately 5 MeV lower than the barriers predicted by the simpler Rotating Liquid Drop Model (RLDM). The difference between the RFRM and experiment may be due to shell structure effects at the saddle configuration of the fissioning nucleus. We are currently pursuing this explanation.

Footnotes

[a] Institute of Atomic Energy, Beijing, China

[b] INFN, Bari, Italy

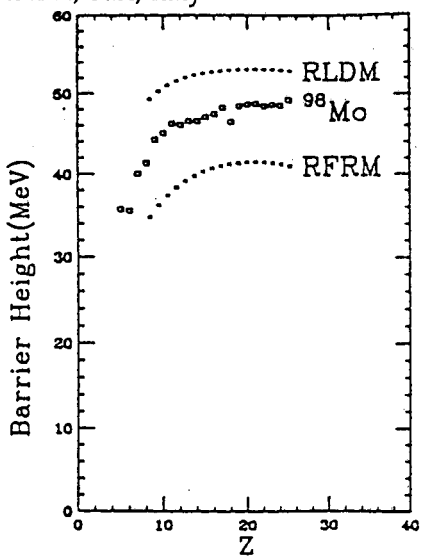

Figure 1. Experimental fission barriers measured for each fragment emitted by the compound nucleus ^{98}Mo, along with the predictions of the RFRM and RLDM. The fissioning system is below the Businaro-Gallone point, displaying a maximum for symmetric fission.

Investigation of High Purity Carbon Foils

A. Veeck, K. Jing[a], Q. Sui[a], G.J. Wozniak, and L.G. Moretto

As presented in this annual report, our group has an ongoing investigation of complex fragment emission from various compound nuclear systems. Due to the very low cross sections of the nuclear reactions used in our investigation, target foils, especially carbon foils, of very high purity are mandatory. Some earlier experimental data from fission barrier measurements indicated a sizable quantity of impurity in the carbon foils we were using; therefore, a study of the type, amount, and source of impurites in carbon foils was undertaken in order to find a cleaner foil.

Rutherford Backscattering Spectrometry (RBS) and Secondary Ionization Mass Spectrometry (SIMS) were used to study two foils manufactured by different methods. Foil A was manufactured by vacuum evaporation, a technique in which spectrographically pure graphite is evaporated onto a substrate coated with a parting agent. Foil B was manufactured by chemical vapor deposition, a technique in which spectrographically pure graphite is evaporated onto a bed of molten metal, then allowed to cool and roll off the metal surface. Fig. 1, the RBS spectra of both foils, shows that Foil B contains much less impurity than Foil A; this is undoubtedly due to the fact that in chemical vapor deposition no impurities are introduced by a parting agent. Indeed, both RBS and SIMS indicate that the impurity in Foil A comes from the parting agent and is localized on the surface of the foil. Although the majority of the parting agent can be rinsed from the surface of the foil, a trace amount remains. Since very pure starting material is used, these data indicate that the technique used to manufacture a foil is the largest source of contamination. Foils prepared by vacuum evaporation show sizable levels of nitrogen, oxygen, and sodium, whereas foils prepared by chemical vapor deposition are substantially purer.

Footnotes

[a] Institute of Atomic Energy, Beijing, China

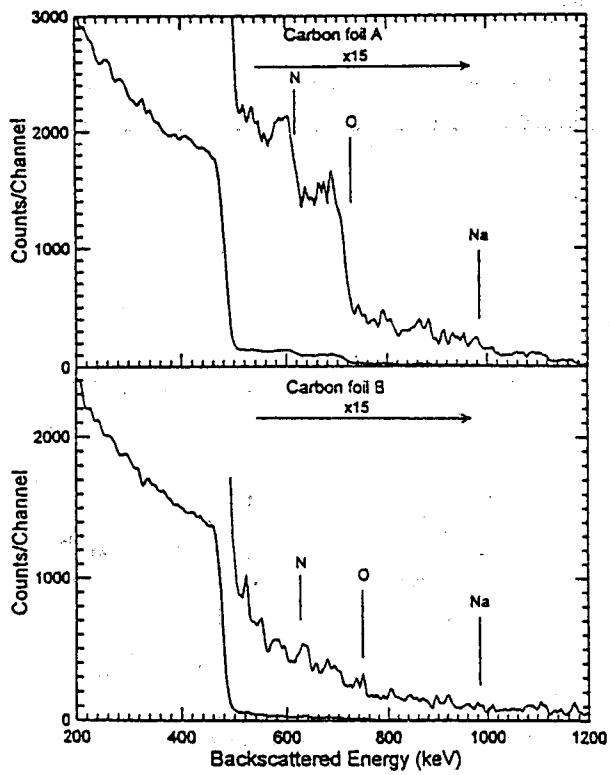

Figure 1. RBS spectra of Foil A and Foil B; Foil A contains much larger quantities of nitrogen, oxygen, and sodium, introduced by the parting agent.

Sequential Time Scales and Branching Ratios in Multifragmentation

L.G. Moretto, K. Jing, L. Phair, K. Tso, G.J. Wozniak

This work addresses the issue of sequential vs simultaneous emission in multifragmentation. The fragment Coulomb interaction measured in recent work appears to be weak at low excitation energy and strong at high excitation energy. This has been interpreted as a transition from ordinary "sequential" multifragmentation to "true" simultaneous multifragmentation[1]. However, the time scales associated with **sequential** emission can be short, and more importantly, undergo a dramatic contraction with excitation energy, in agreement with observation. The sequential time-scales and their contraction with excitation energy can be directly related to the excitation functions for binary, ternary, quaternary, etc., decays.

In statistical decay the partial decay width associated with a given channel can be written as $\Gamma = \hbar\omega_0 e^{-B/T}$ where ω_0 is a frequency characteristic of the specific channel, B is the barrier associated with the channel and T is the temperature. The corresponding time is given by $\tau = \tau_0 e^{B/T}$. The characteristic dependence of the binary decay time on exciation energy can be nicely illustrated by the linear plot of $\frac{\tau}{\tau_0}$ vs $E^{-1/2}$ shown in figure 1.

We have shown elsewhere[2] that if $p = e^{-B/T} \ll 1$ the n-fragment sequential emission probability $P(n)$ is proportional to $e^{-nB/T}$. If this condition is not satisfied, namely if the probability p is rather large, one expects an approximately binomial distribution $P(n,m) = \frac{m!}{n!(m-n)!}p^n(1-p)^{m-n}$. The introduction of the additional parameter m is quite helpful, since it allows one to fix the mean fragment multiplicity $< N_{IMF} >= mp$. Assuming, for the moment, that m depends weakly on excitation energy one obtains for the n-fragment sequential emission probabilities the excitation energy dependence shown in figure 2. The uncanny resemblance of these theoretical curves with those seen in some yet unpublished work, suggests the following analysis: 1) at each "excitation energy", determine m from $< N_{IMF} >$. 2) Use this value of m to calculate p for the binomial distribution

$$\frac{1}{p} = \frac{P(n)}{P(n+1)}\frac{m-n}{n+1} + 1 = \frac{\tau}{\tau_0}. \qquad (1)$$

using the experimental values of $P(n)$ and $P(n+1)$.

If the present approach is correct, all the excitation functions like those in figure 2 should collapse into the single straight line of figure 1. A redundant determination of p at each excitation energy is then obtained for the different ratios $\frac{P(n)}{P(n+1)}$. Preliminary analysis of a large body of data shows that this approach works astonishingly well. This validates the use of the binomial distribution. The linear dependence of $\frac{\tau}{\tau_0}$ vs $E^{-1/2}$ underscores both the sequential statistical nature of the probabilities and the expected tendency of the sequential time scales toward the characteristic channel time.

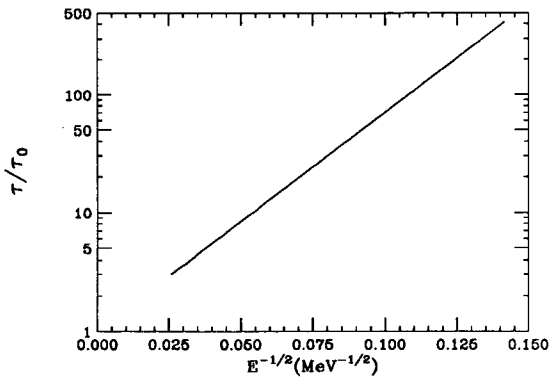

Figure 1: Contraction of sequential time-scale as a function $E^{-1/2}$ for B=11MeV, A=150, $a = \frac{A}{10MeV}$.

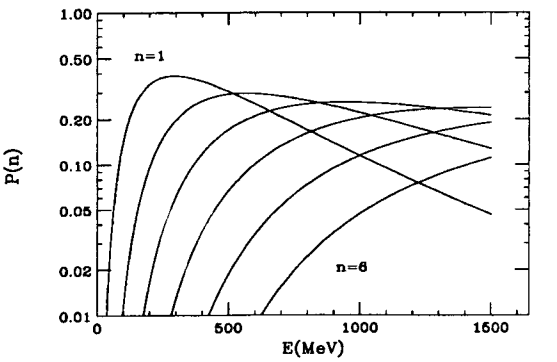

Figure 2: The n-fold probability (calculated using p from figure 1 and m=12) as a function of E.

Footnotes and References

1. M. Abouffirassi et al., preprint LPCC 94-01, Lab. de Physique Corpusculaire.
2. L.G. Moretto et al., Phys. Rev. Lett. **71**, 3935 (1993).

Sequential Multifragmentation in 40 & 60 MeV/n ^{129}Xe + ^{197}Au Reactions

K. Tso, L. Phair, W. Skulski, N. Colonna, G. J. Wozniak, L. G. Moretto, D. R. Bowman**, M. Chartier+, C. K. Gelbke+, W. C. Hsi+, M. A. Lisa+, W. G. Lynch+, G. F. Peaslee+, C. Schwarz+, and M. B. Tsang+*

Multifragmentation in intermediate energy heavy-ion reactions, in particular the issue of sequentiality versus simultaneity, are currently under intense study. Statistical theory predicts that if the multifragmentation is a sequence of binary events, the n-fold probability should follow approximately the binomial distribution:

$$P(n,m) = \frac{m!}{n!(m-n)!} p^n (1-p)^{m-n}$$

The parameter m can be interpretated as the number of chances for the system to emit an inert fragment with fixed binary decay probability p, whereas $p=e^{-B/T}$ is related to its corresponding lifetime by $\tau=\tau_o/p$. Both m and p can be extracted from experimental values of the mean, <n> and width, σ_n^2 using the binomial relationships:

$$\langle n\rangle = mp \quad \text{and} \quad \sigma_n^2 = \langle n\rangle (1-p).$$

To verify the above simple theoretical predictions, we have performed this analysis on ^{129}Xe + ^{197}Au reactions at 40 & 60 MeV/n. The reaction products were detected with a combination of the MSU Miniball and LBL array, which covered most of 4π. We use the transversal energy of the event, $E_t=\Sigma\epsilon_i\sin^2\vartheta_i$ as a measure for the "excitation energy". ϵ_i is the kinetic energy of each fragment and ϑ_i is angle between the fragment and the beam direction. In figure 1, we plot the multiplicity distribution for intermediate mass fragments ($3\leq Z\leq 25$) as a function of $E_t^{-1/2}$ for the 60MeV/n data. The lines, calculated assuming a binomial distribution with p and m extracted experimentally, agree remarkably well with the data. This means that the process is indeed sequential and the n-fold probability P_n can be reduced to the elementary binary decay probability p. Furthermore, ln(1/p) is found to be linear with $E_t^{-1/2}$ as shown in figure 2. This linearity is strong evidence for the thermal nature of the binary decay at all excitation energies. We can also extract 1/p "differentially" using the ratios P_n/P_{n+1} from the same multiplicity distribution in figure 1, and they collapse tightly onto the straight line shown in figure 2. The same analysis was performed for the 40MeV/n data, and a similar result was obtained. These quantitative agreements between the calculations and the data are stunning, and leave little doubt regarding the "sequential" and "thermal" nature of multifragmentation.

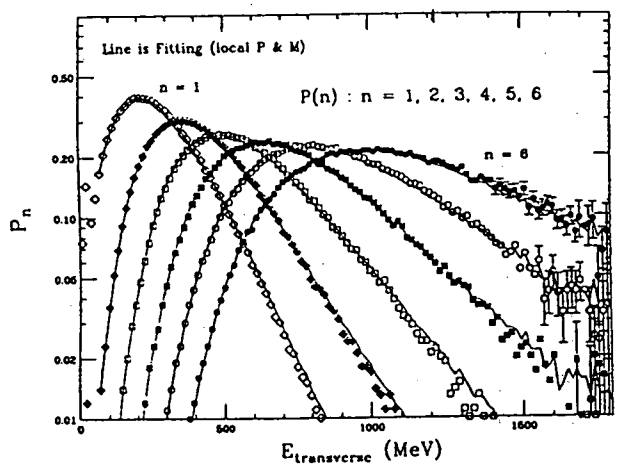

Figure 1: The n-fold probability for intermediate mass fragments ($3\leq Z\leq 25$) as a function of the transersal energy. The lines are probabilities calculated using values of m and p extracted from the Xe + Au at 60MeV/n data.

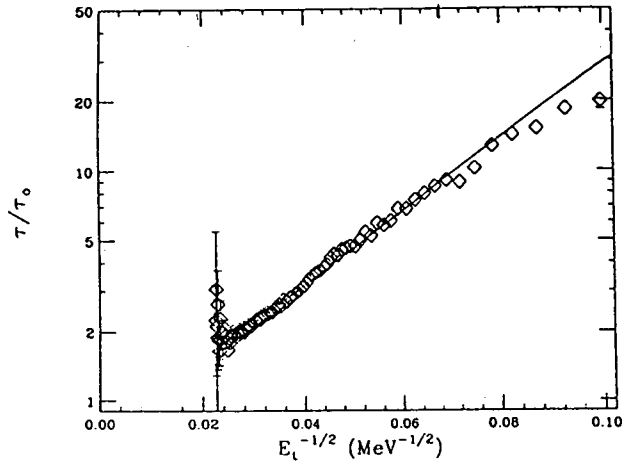

Figure 2: 1/p or τ/τ_o as a function of $E_t^{-1/2}$ for Xe + Au at 60 MeV/n. The line is a linear fit to ln(1/p).

Footnotes and References

*INFN, Bari, Italy

+NSCL, Michigan State University.

**Chalk River Labs, Canada

Time–scale for Sequential Multifragmentation in 40 & 60 MeV/n $^{129}Xe + ^{197}Au$ Reactions

K. Tso, L. Phair, W. Skulski, N. Colonna, G. J. Wozniak, L. G. Moretto, D. R. Bowman**, M. Chartier+, C. K. Gelbke+, W. C. Hsi+, M. A. Lisa+, W. G. Lynch+, G. F. Peaslee+, C. Schwarz+, and M. B. Tsang+*

In an earlier contribution we show that multifragmentation, observed in $^{129}Xe + ^{197}Au$ reactions at 40 & 60 MeV/n, is a sequence of thermal binary events. This analysis has shown that the probability P_n of observing n fragments ($Z_{threshold} \leqq Z \leqq 25$) can be reduced to the elementary probability $p=e^{-B/T}$ for binary decay. Moreover, the corresponding decay lifetime τ/τ_o for sequential emission is equal to 1/p. This means that the slope of ln(1/p) or ln(τ/τ_o) versus temperature T will give us information about the magnitude of the barrier B, and the rate of time contraction with increasing T. In this analysis, we use the transversal energy of the event, E_t as a measure for the "excitation energy", and hence $T \propto E_t^{-1/2}$.

One may wonder why a single binary barrier suffices, since different mass asymmetries with many different barriers may be present. Let us consider a barrier distribution as a function of mass asymmetry x of the form $B = B_o + ax^n$, where B_o is the lowest barrier in the range considered. Then,

$$p = \int e^{-B_o/T} e^{-ax^n/T} dx \cong (\frac{T}{a})^{1/n} e^{-B_o/T} \qquad (1)$$

Thus the elementary probability p is dominated by $e^{-B_o/T}$ with a small pre-exponential modification. In figure 1, we plot ln(1/p) or ln(τ/τ_o) versus $E_t^{-1/2}$ for the fragment distributions with different values of $Z_{threshold}$ (2 to 9). The linearity of all these plots is stunning, and leaves little doubt regarding the "thermal" nature of p. Furthermore, the slope which is proportional to the barrier B_o, increases with $Z_{threshold}$ suggesting that the binary decay is truly dominated by the lightest fragment ($Z_{threshold}$) with the lowest barrier B_o.

Equation 1 shows that the decay probability p and hence the decay lifetime τ/τ_o is dramatically affected by changes in T for a fixed barrier B_o. Indeed, for all barriers considered in figure 1, their decay lifetime decreases as T increases until it almost approaches the characteristic time constant of that channel τ_o, whereby the temperature becomes comparable with the barrier, and the decay probability approaches unity. We conclude that this observed time contraction is consistent with the energy dependence of sequential decay, rather than a transition from sequential to simultaneous multifragmentation.

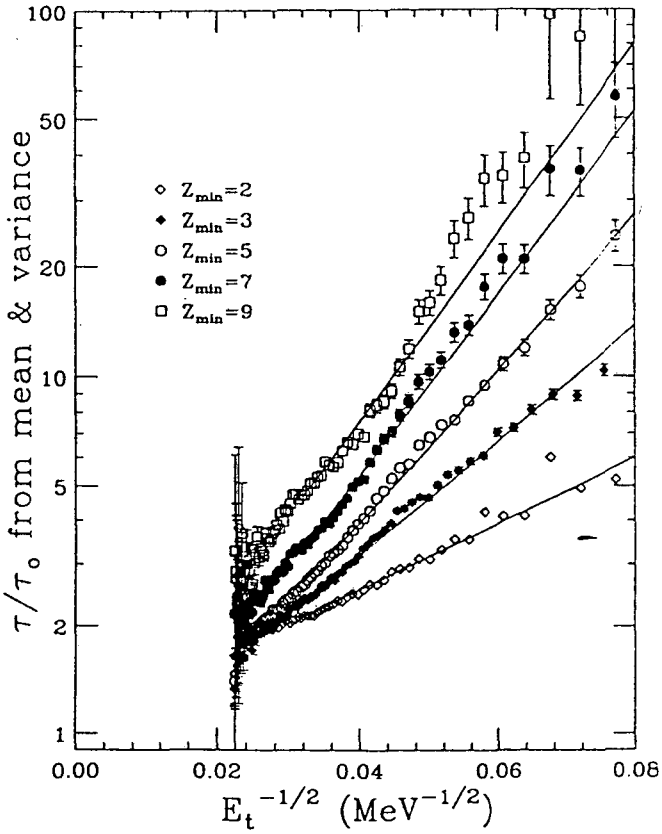

Figure 1: The reciprocal of the binary decay probability 1/p or the ratio τ/τ_o (calculated from the mean and variance of fragment distributions) as a function of $E_t^{-1/2}$ for the reaction $^{129}Xe + ^{197}Au$ at E/A=60 MeV.

Footnotes and References

*INFN, Bari, Italy
+NSCL, Michigan State University.
**Chalk River Labs, Canada

Clock Frequencies and their Mass Dependence in Multifragmentation

L. G. Moretto, K. Tso, L. Phair, W. Skulski, N. Colonna, G. J. Wozniak, D. R. Bowman**, M. Chartier+, C. K. Gelbke+, W. C. Hsi+, M. A. Lisa+, W. G. Lynch+, G. F. Peaslee+, C. Schwarz+, and M.B. Tsang+*

In other contributions to this annual report, we have shown that the n-fragment emission probability P_n can be derived from the n-fold application of the elementary binary probability p according to the binomial distribution:

$$P(n,m) = \frac{m!}{n!(m-n)!} p^n (1-p)^{m-n}$$

The elementary probability p has been shown to have a thermal dependence on excitation energy:

$$p = \frac{\Gamma}{\hbar\omega_o} = e^{-B/T} = \frac{\tau_o}{\tau}$$

where Γ is the binary decay width and ω_0 is the characteristic channel frequency and τ_0 the corresponding period.

Analysis of the data provides us not only with the probability p at each energy, but also with the binomial parameter *m*. This parameter gives the number of "tries" successful plus unsuccessful that the system has available in order to emit a fragment. Therefore the product $\tau_0 m$ should correspond to the overall time available to the system for fragment emission. In fig. (1) the value of m is plotted as a function of energy for various lower thresholds on the fragment atomic number Z for the reaction ^{129}Xe + ^{197}Au at 60MeV/n. We observe a strong dependence of m on this lower threshold, with m decreasing dramatically with increasing Z. Two explanations for this effect come to mind. The first is that the clock period is constant and that the overall emission times decreases markedly with increasing Z. The second is that the overall time for multifragmentation is constant and the clock period increases with the mass of the fragment. Of course this second explanation would be much more satisfactory. If we plot the product mZ as in fig. (2) we observe that the Z dependence is completely eliminated with the notable exceptions of Z=1 and Z=2. We disregard for the moment these exceptions attributing them to the fact that a greater time window may indeed be available for the evaporational cooling than for multifragmentation.

For the remaining fragments one is led to surmise that $\tau_0(M)$ is proportional to the mass M of the fragment. It is interesting to notice that for a particle of mass M contained in a square well of diameter d, the period is $\tau = M4d^2/nh$.

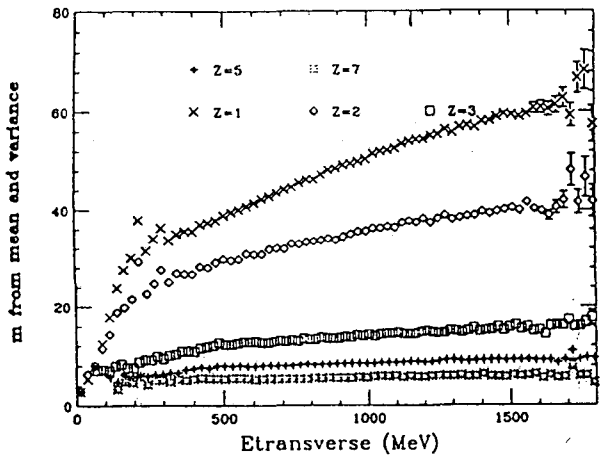

Figure 1: The extracted values of $m=<n^2>/(<n>-\sigma^2_n)$ as a function of the transverse energy E_t for the reaction ^{129}Xe + ^{197}Au at 60MeV/n.

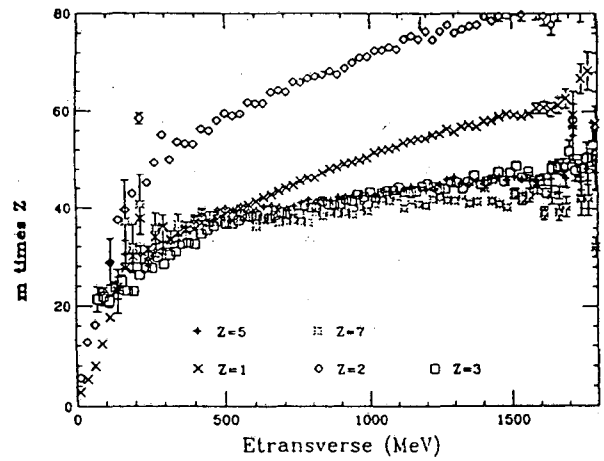

Figure 2: The product of mZ as a function of the transverse energy E_t for the reaction ^{129}Xe + ^{197}Au at 60MeV/n.

Footnotes and References

*INFN, Bari, Italy
+NSCL, Michigan State University.
**Chalk River Labs, Canada

Spin Polarization of Beta-Emitting Fragment ^{23}Mg in ^{24}Mg + Au, Cu and Al Collisions at 91 *A* MeV*

K. Matsuta, S. Fukuda,† T. Izumikawa,† M. Tanigaki,† M. Fukuda,† M. Nakazato,† M. Mihara,† T. Onishi,† T. Yamaguchi,† T. Miyake,† M. Sasaki,† A. Harada,† T. Ohtsubo,† Y. Nojiri,† T. Minamisono,† K. Yoshida,†† A. Ozawa,†† T. Kobayashi,†† I. Tanihata,†† J.R. Alonso, G.F. Krebs, and T.J.M. Symons

The Osaka-LBL collaboration has been studying reaction mechanism of the projectile fragmentation process through measurements of the spin polarization of various projectile fragments. In the present experiment, spin polarization of the beta-emitting fragment ^{23}Mg(I^{π}=3/2^{+}, $T_{1/2}$=11.3 s) produced through the projectile fragmentation process was observed at the RIKEN ring cyclotron. The ^{23}Mg nuclei were produced through the projectile fragmentation of ^{24}Mg on Au, Cu and Al targets at 91±9 *A* MeV. The ^{23}Mg fragments emerging from the target to a certain deflection angle were selected by a slit and separated out from various products and momentum analyzed using the RIPS (RIKEN Projectile Fragment Separator). The polarization of the ^{23}Mg nuclei was measured by means of asymmetric beta-ray emission.

The polarization of ^{23}Mg was measured with respect to target nuclide, fragment momentum and deflection angle. Fig. 1. shows momentum dependence of the polarization with three kinds of targets at a deflection angle of 2°. The general trends of the momentum dependence were found same as the previous studies[1,2]. That is, the polarization is an increasing function of fragment momentum for the heavy Au target, a decreasing function for the light Al target and a parabolic function for the intermediate Cu target. These general trends of the polarization are well reproduced by a simple fragmentation model based on the participant-spectator picture of the collision and the orbital deflection by the combined Coulomb-nuclear potential. However, there still be puzzles in the detail of the polarization behavior, especially in the lower momentum region.

Footnotes and References

† Osaka Univ., Toyonaka, Osaka 560, Japan
†† RIKEN, Wako, Saitama 351-01, Japan

* To be presented at the 5th Int. Conf. on Nucleus Nucleus Collisions

1 K. Asahi et al., Phys. Lett. **B251** (1990)488 and K. Matsuta et al., Phys. Lett. **B281** (1992) 214.

2. K. Matsuta et al., Hyperfine Interactions **78**(1993)127 and M. Ishihara, Nucl. Phys. **A538** (1992) 309c.

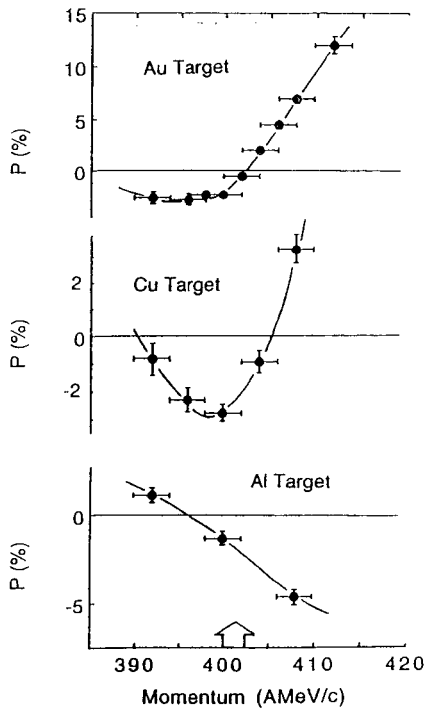

Fig. 1. Polarization of ^{23}Mg.
The arrow indicates the momentum corresponding to the beam velocity.

Cross Sections of Multi-Nucleon Transfer Reactions in 9.4 *A* MeV ^{24}Mg + Ta System

K. Matsuta, S. Fukuda,† T. Izumikawa,† M. Tanigaki,† M. Fukuda,† M. Mihara,† M. Nakazato,† T. Onishi,† T. Yamaguchi,† T. Ohtsubo,† Y. Nojiri,† T. Minamisono,† J.R. Alonso, G.F. Krebs, and T.J.M. Symons

Production cross sections of various reaction products in the 9.4 *A* MeV ^{24}Mg + Ta reactions have been measured as a step towards the measurement of the quadrupole moment of ^{23}Mg.

A 3 μm thick Ta target (5.0 mg/cm^2) was bombarded with a 9.7 *A* MeV ^{24}Mg primary beam extracted from the 88-inch Cyclotron. Energy loss of the beam in the target was about 0.6 *A* MeV. Various reaction products emerging from the target to a laboratory angle Θ_{lab} = 30° were selected and detected by a set of Si detectors (50μm thick and 1000μm thick) placed 6.5 cm away from the target. A 3 mm diameter collimator was installed in front of the detector.

In order to identify atomic number Z and mass number *A* of the product nuclei, the *PI* was calculated as $PI=(E+\Delta E)^{\gamma}-E^{\gamma}$ from the energy loss and the energy (ΔE, $E+\Delta E$) detected by the detectors, where γ was taken to be 1.675 for the best result. Production yields were reduced by integrating energy distributions of the fragments.

Cross sections for 42 different reaction products were obtained as shown in Fig. 1. As shown in the figure, cross sections are exponentially decreasing with decreasing ground state *Q* values (Q_{gg}) in general as was reported on lighter projectile at the same energy region by Artukh et al.[1]. The exponential dependence of the cross section is regarded as the partial statistical equilibrium at a grazing collision. However, cross sections for several neutron rich nuclei such as ^{26,27,28}Mg, ^{24,25}Na, ^{20}O, are much less productive than the systematics. Cross sections of ^{23}Ne and ^{21}F are also moderately deviated from the exponential dependence. These nuclei with less productivity mostly lay on the neutron excess side of the projectile(^{24}Mg), otherwise have the same neutron number with the projectile. Similar tendency was also reported by Artukh et al.[2] for heavier projectile. This clear deviation from the exponential dependence suggests that the reaction mechanism for the pick-up reactions is different from that for the stripping reactions in the present energy. Mismatching of momenta of the transferred nucleons may play a role in the phenomenon.

Footnotes and References

† Osaka Univ., Toyonaka, Osaka 560, Japan

1 A.G. Artukh et al., Phys. Lett. **33B** (1970) 407, and Nucl. Phys. **A168** (1971) 321.

2. A.G. Artukh et al., Nucl. Phys. **A211** (1973) 299.

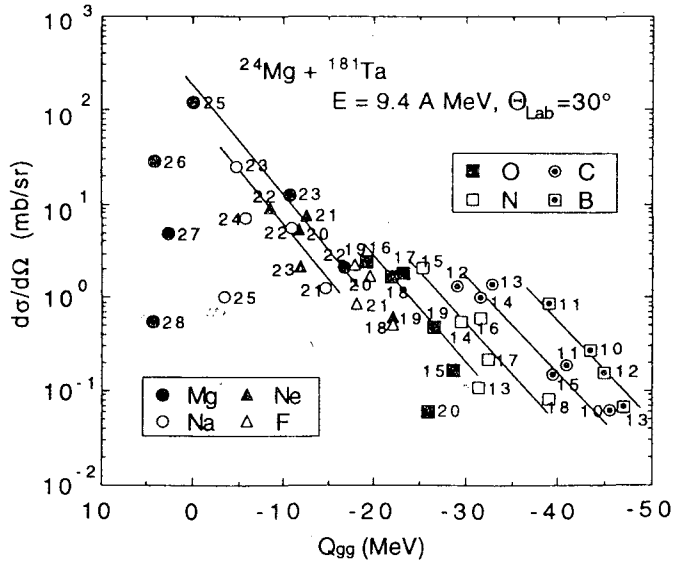

Fig. 1. Production cross sections of reaction products from ^{24}Mg + ^{181}Ta reactions.

Mass numbers are shown beside the individual symbols.

Effect of the Extra Electrons on ECR plasma Potential and Source Performance*

Z.Q. Xie and C.M. Lyneis

The mean plasma potential was measured on the LBL Advanced Electron Cyclotron Resonance (AECR) ion source for a variety of conditions at the 88-Inch Cyclotron. The mean potentials for plasmas of oxygen, argon and argon+oxygen in the AECR have been determined positive and are on the order of tens of volts for microwave power to 600 W and normal operating gas flow. Electrons injected into the plasma by an electron gun or from an aluminum oxide wall coating with a very high secondary electron emission reduce the plasma potential as does gas mixing. Figure 1 shows the oxygen plasma potentials measured with aluminum oxide coating in comparison to the plasma potentials measured without a coating. A lower plasma potential in the AECR source coincides with enhanced production of high charge state ions indicating longer ion confinement times. That is, the effect of the extra electrons from external or internal electron sources is to lower the average plasma potential and increase the $n_e\tau_i$ of the ECR plasma.

Electron injection can eliminate the need for gas mixing or reduce it to a lower level so the source can operate at lower neutral pressures. A reduction of the neutral pressure reduces charge exchange between ions and neutrals and enhances the production of high charge state ions.

An aluminum oxide coating results in the lowest plasma potential among electron injection, wall coatings and gas mixing, and the best source performance. The results with an aluminum oxide coating also show that gas mixing is not necessary for the production of high charge state ions at least for noble gases up to xenon at the intensities achieved by gas mixing. The enhancement in the production of high charge state heavy ions is up to a factor of three to four with an aluminum oxide coating and a biased probe, compared with electrons injected by an electron gun. With an aluminum oxide coating and a biased probe, the AECR has produced 18.5 eμA of Ne^{9+}, 161 eμA of Ar^{11+}, 2.5 eμA of Ar^{16+}, 100 eμA of Kr^{17+}, 0.6 eμA of Kr^{28+}, 68 eμA of Xe^{25+}, 1.5 eμA of Xe^{31+} without gas mixing and 20 eμA of Bi^{29+}, 0.75 eμA of Bi^{38+} with a low level of oxygen support gas.

Footnotes and References

*Condensed from a paper submitted to Rev. Sci. Instrum., 1994.

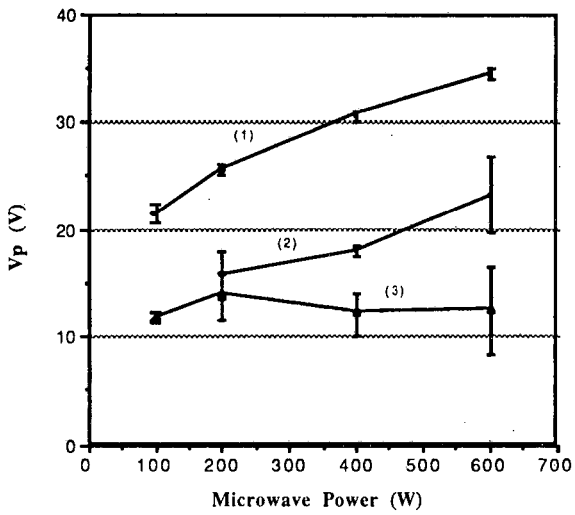

Figure 1. Plasma potentials of oxygen at the same gas flow (pressure P = 1.6×10^{-6} Torr) and various microwave power for three cases. Curve (1) indicates the potential without electron injection and coating. In the case of curve (2), 17 mA electrons with 200 eV energy are injected into the plasma and reduce the plasma potential. An aluminum oxide coating results in the lowest plasma potential as indicated by curve (3).

The IsoSpin Laboratory

J.Michael Nitschke

Since its inception in 1989 the plan for the IsoSpin Laboratory (ISL) has advanced both scientifically and technically, mainly due to the activities of the ISL Steering committee, Working Groups, and a Users community that now numbers almost 500. The Third International Conference on Radioactive Nuclear Beams was held at MSU[1]. Several European laboratories are very active in RNB research, especially GANIL, Grenoble, Louvain, RAL, and ISOLDE. ISL Working Groups now exist for Nuclear Structure, Astrophysics, and Target/Ion Sources. A North American Collaboration for Radioactive Ion Source Tests (NACRIST), with LBL as one of its members, is preparing to test a Ta target with 800MeV, 100μA protons at RAL, England to evaluate whether ISOLDE RNB intensities can be scaled with proton-beam current. Additional tests will be carried out at TRIUMF, Canada. In October 1992 a Workshop on Post-Accelerator Issues at the ISL was held in Berkeley[2]. It concentrated on the technical aspects of constructing a high-intensity, broad-mass-range-, second generation RNB facility, and addressed specifically issues related to target/ion sources, mass separation, and secondary accelerators. Some of the key findings of the workshop are incorporated in the revised ISL concept shown in the figure below, notably BRAMA and the low-β post-accelerator section.

Work at LBL on high-power targets, RNB production, the BRAMA concept, and radiological issues is covered in separate contributions.

References

1. *Proc. Third Intl. Conf. on Radioactive Nuclear Beams,* D.J. Morrissey ed., MSU, Michigan, 1993 (Edition Frontieres, Gif-sur-Yvette, 1993).
2. *Proc. Workshop on Post-Accelerator Issues at the ISL,* Oct. 1993, Berkeley , CA, S. Chattopadhyay and J.M. Nitschke eds., to be published.

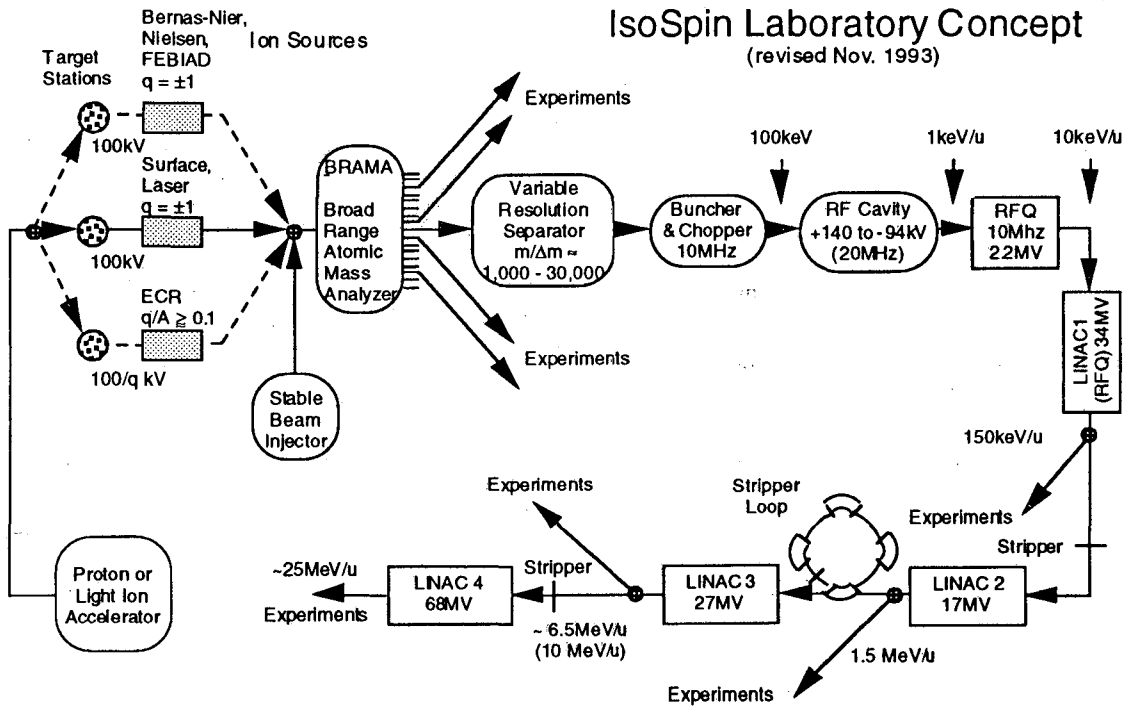

High Power Targets for the ISL

J.Michael Nitschke

A key component of the ISL is the target/ion source combination. The main requirements for the targets are: high temperature operation for a variety of solid and liquid target materials; uniform temperature distribution despite the non-uniform power distribution caused by the primary beam; high diffusivity for the desired radioactive beam element, short hold-up times; chemical selectivity; heating capability for operation with low primary-beam currents; cooling capability to prevent melting of solid targets and target containers at high beam power levels (≲40kW); mechanical/material stability in high radiation fields; remote handling capability; and reliable, low cost manufacturing (spent targets cannot be repaired!).

Only in rare cases will it be possible to combine all of these requirements in a single target. Since it was felt that the target cooling and the temperature distributions were the most urgent problems a high-power target test stand was constructed that allows tests up to 50kW substituting 10keV electrons for the proton beam. Because of the short range of the electrons the test targets have to be made hollow as shown below with the electron emitting cathode wire strung along the axis. Different methods of cooling have been investigated. Water cooling is very efficient, however, the cooling power can not be varied easily, the water will become radioactive, and it may pose a safety risk considering its closeness to a highly radioactive liquid metal target operating at ≲2,000C. The present efforts focus therefore on He gas as cooling medium as shown schematically below. By customizing the size of the cooling channels and slots non-uniform power distributions in the target can be compensated. The target temperature can be adjusted continuously by varying the gas flow; and heating the incoming He gas allows the target temperature to be maintained even at low (or zero) beam power levels. Eventually, the target will be coupled to a multi-cusp ion source, optimized for high temperatures and low hold-up times. If desired these sources can be operates for charge states q>1 and for negative ions.

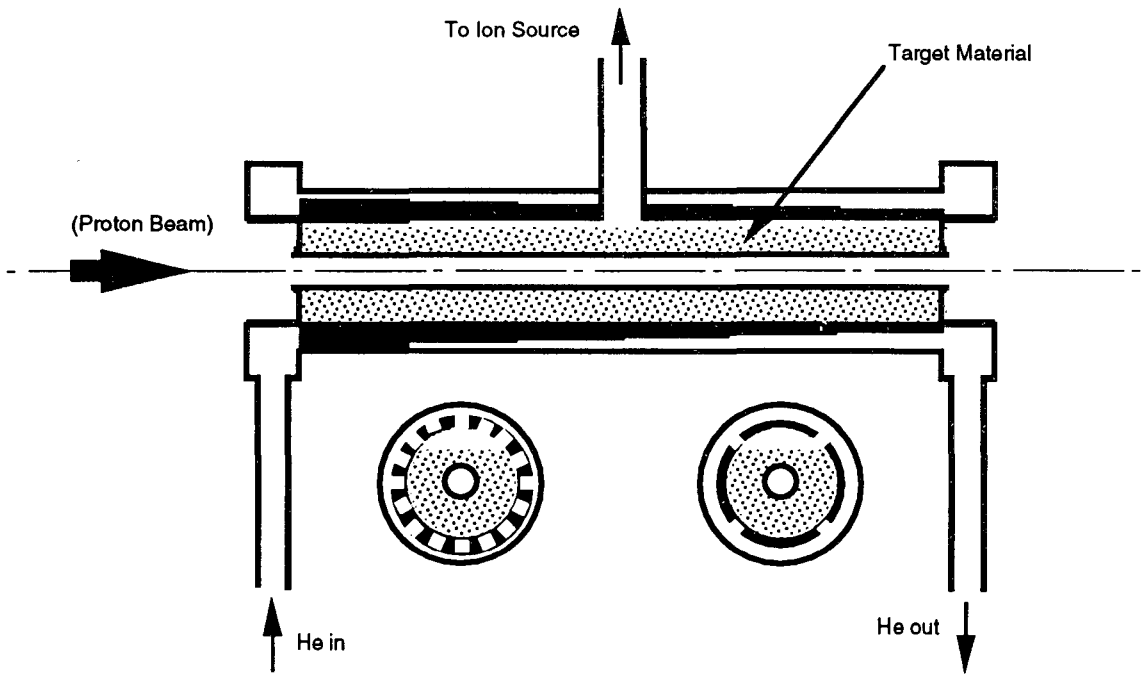

BRAMA, a Broad Range Atomic Mass Analyzer for the ISL

J.Michael Nitschke

An alternative to conventional on-line isotope separators for use in radioactive nuclear beam (RNB) facilities is proposed[1]. It consists of an analyzer with a static magnetic field that is capable of separating a wide mixture of (radioactive) ions into mass bins ranging from 6 to 240u. If incorporated into the ISL, this Broad Range Atomic Mass Analyzer (BRAMA) would make several low-energy RNBs available for experiments *simultaneously*, in addition to the beam that is being delivered to the post-accelerator. A preliminary ion-optical geometry is shown in Fig. 1. After separation into mass bins the desired masses are selected by *mechanically* moving electrostatic deflectors along the focal plane and guiding the radioactive beams to individual experiments using electrostatic optics. Besides running several experiments in parallel this concept has several other advantages: some light RNBs will be available almost all of the time since they are made in most spallation reactions independent of the target; contamination of the separator is avoided since all ions leave the vacuum chamber; many radioactive targets and isotopes of bio-medical interest can be collected for a long time; if ions of only one polarity are desired BRAMA can operate with permanent magnets; and ion source parameters can be controlled by monitoring a suitable support-gas- or mass marker isotope.

Reference

1. Nitschke, J.M., *Proceedings of the Workshop on Post Accelerator Issues at the IsoSpin Laboratory,* October 27-29, 1993, Berkeley CA.

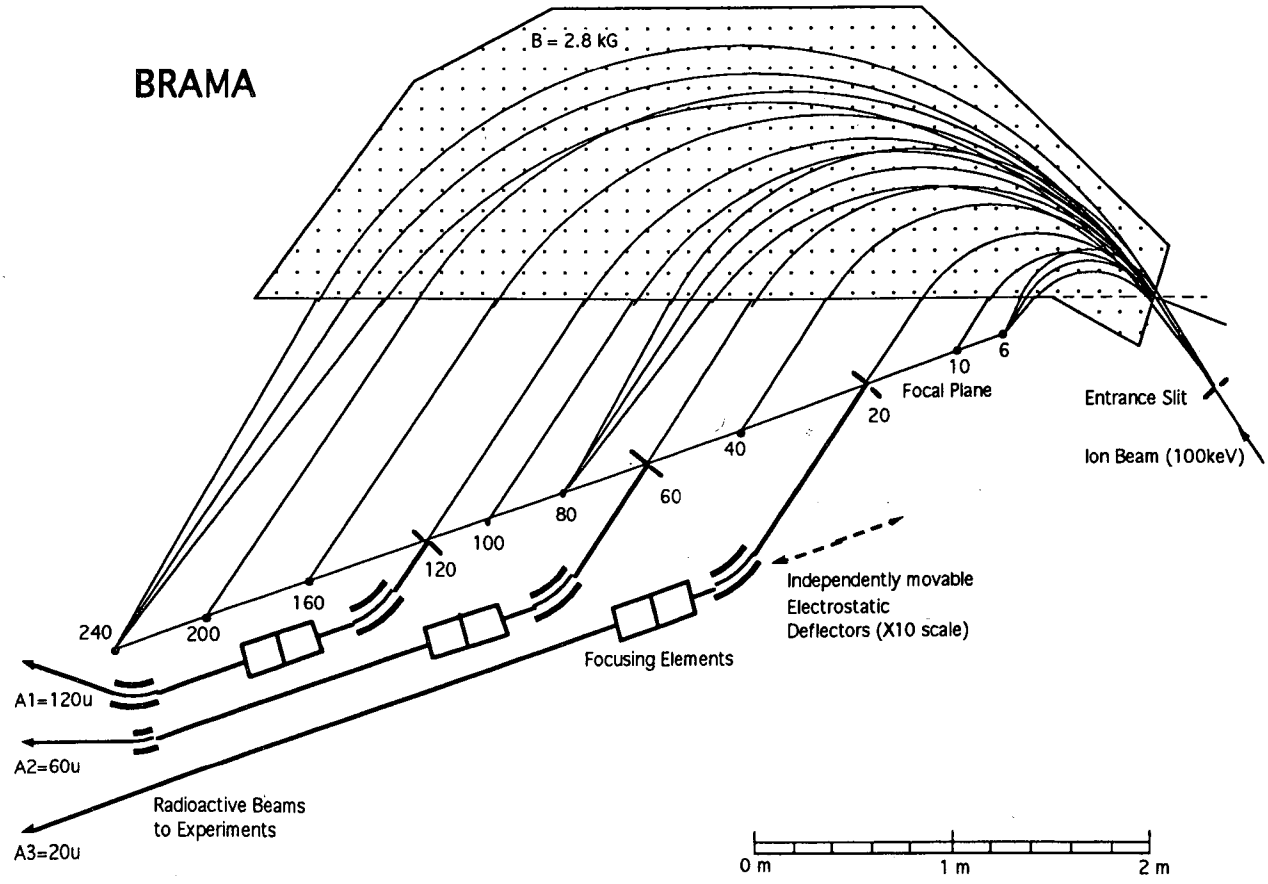

Fig.1 The BRAMA Concept

Code System for Calculating Radioactive Beam Intensities

M.A. Stoyer, R.J. Donahue, and J.M. Nitschke

The prediction of product nuclei for various targets at the IsoSpin Laboratory (ISL) is extremely important for several reasons. Because of low beam intensities, the vast majority of experiments at the ISL will be beam intensity limited. Hence, it is important to estimate the beam intensities acheivable at ISL in order to determine the time required for an experiment. Additionally, safety concerns related not only to residual dose rates due to activation and buildup of products in various parts of the machine, but also to the categorization of the facility itself are important. A system for predicting radioactive beam intensities for the ISL is under development. To determine product yields, LAHET Monte Carlo calculations[1] or TSAO predictions[2] can be used.

The Silberberg and Tsao predictions used in the ISL whitepaper[3] are based on a compilation of experimental data combined with semi-empirical extrapolations in regions where data were not available and do not include radioactive decay losses, secondary reactions, and feeding from radioactive decays. To properly predict isotopic yields, several computer programs have been developed. A block diagram denoting these programs is shown in Fig. 1. Dashed lines indicate missing programs or missing connections between programs. The LAHET Monte Carlo program transports neutrons down to 20 MeV. The MCNP program handles the transport of neutrons below 20 MeV and gives neutron fluxes (Φ). The TSAO program gives predicted yields based on experimental data and extrapolation ("Semi-empirical"). "High" mass yields are the residual mass distributions given by LAHET which don't include contributions from neutrons with energies lower than 20 MeV. "Complete" mass yields (including all neutrons) are currently not available. The program DKCHAINMKR extracts nuclear data from a database (half-life, $t_{\frac{1}{2}}$; decay mode; branching ratios; etc.) and constructs decay chains, including alpha decay (α), electron capture (ϵ), and beta-decay (β^-). The final program, GROWTHDK, calculates the growth and decay of each isotope not only during proton beam irradiation of the target, but also during "cooling" times and gives calculated yields as a function of time.

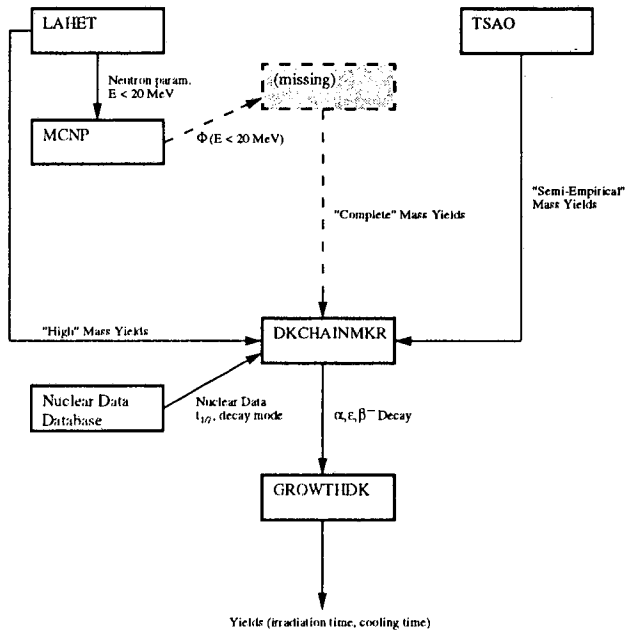

Fig. 1. Block diagram of programs for calculation of isotopic yields. A brief description of the programs and meaning of the symbols is given in the text.

Footnotes and References

[1] R.E. Prael and H. Lichtenstein, LANL Rep. LA-UR-89-3014, Sep. 1989.

[2] R. Silberberg and C.H. Tsao, The Astrophysical Journal Supplement Series **58** (1985) 873.

[3] *The IsoSpin Laboratory: Research Opportunities with Radioactive Nuclear Beams*, LALP-91-51 (1991).

IsoSpin Laboratory Target Studies

M.A. Stoyer, R.J. Donahue, and J.M. Nitschke

The primary proton beam for the IsoSpin Laboratory (ISL) will deposit about 2/3rds of the 600 – 1000 MeV beam energy nonuniformly into a high-Z target of $\sim$ 1 mole/cm^2 thickness. ISL target temperature profiles must be kept uniform along the complete length of the target to prevent cold pockets where target product elements might condense thus preventing release from the target to the ion-source. Targets will be heated or cooled to achieve uniform temperature profiles.

A comparison of various energy deposition profiles as calculated with LAHET[1] and FLUKA[2] for a 100% enriched ^{235}UC target is shown in Fig. 1. The agreement between the calculations is extremely good for all radial intervals and the total energy deposition agrees within 1.2%. Comparisons of experimental data[3] with LAHET predictions[4] generally show good agreement for lead and bismuth targets with larger discrepencies for the low-Z targets, in particular the beryllium target.

Another important factor in target design for the ISL is the yield of product nuclei. The possibility of utilizing neutrons produced in the spallation and fast fission of the primary proton beam interaction with the target for inducing additional fissions, and thus enhancing the yields of certain fission product nuclei, is tantalizing. The target neutron fluence (n/cm^2/p) as a function of energy for a bare and moderated/reflected ^{235}UC target is shown in Fig. 2. The additional n-flux at energies from eV to 1 MeV could potentially enhance fission in the target.

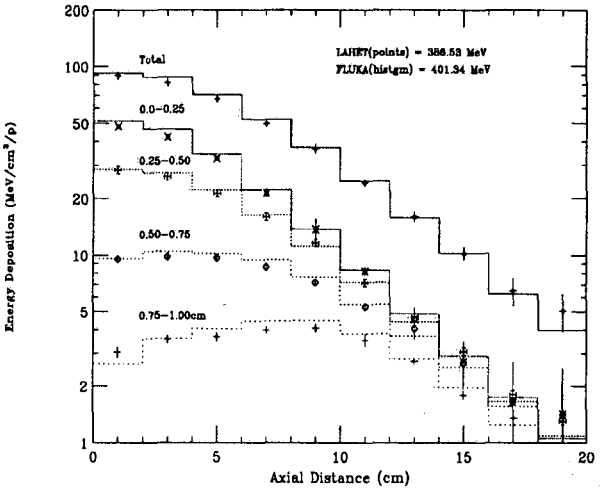

Fig. 1. A comparison between LAHET and FLUKA of energy deposition (MeV/cm^3/p) as a function of axial distance for 600 MeV protons incident on a 20 cm long ^{235}UC target for various radial bins.

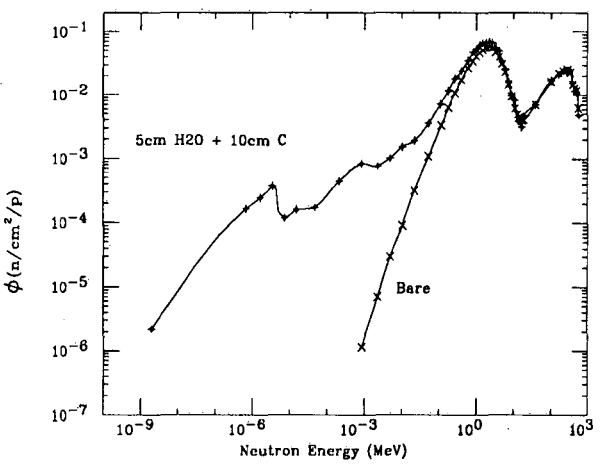

Fig. 2. A FLUKA comparison of target neutron fluence as a function of energy between a bare ^{235}UC target and a H_2O moderated/ graphite reflected target design for 600 MeV protons impinging on a 20 cm long target.

Footnotes and References

[1] R.E. Prael and H. Lichtenstein, Los Alamos National Laboratory Report LA-UR-89-3014, Sep. (1989).

[2] A. Fassò, et al., presented at the Workshop on Simulating Accelerator Radiation Environments, January 11-15 (1993), Sante Fe, NM.

[3] V.I. Belyakov-Bodin, et al., **NIM A295** (1990) 140 and **NIM A314** (1992) 508.

[4] C.A. Beard, et al., Los Alamos National Laboratory Report LA-UR-93-514 (1993).

Radiation Shielding Analyses for the IsoSpin Laboratory

R. J. Donahue, G. C. Moeller, J. M. Nitschke, and M. A. Stoyer

The IsoSpin Laboratory (ISL) being investigated at LBL would require primary proton beam intensities of 100-200 μA with beam energies between 500 and 1000 MeV. Such high proton beam currents, combined with ever-increasing radiation safety standards, requires special techniques to solve radiation transport problems through massive shields. Current analyses entail the coupling of such Monte Carlo codes as FLUKA[1] and LAHET[2] with the discrete ordinates analytical code TWODANT[3]. Since TWODANT only transports neutrons and photons, the coupling must occur at such a depth that secondary proton interactions are minimized while maintaining acceptable statistics. The neutron spectra for various concrete thicknesses are shown[4] in Figure 1. LAHET is used for transport up to 2 m, while TWODANT is used beyond 2 m. After 2-3 meters of concrete (5-6 interaction lengths) an equilibrium spectrum shape develops where only the highest energy neutrons are slowed and all other neutrons are in relative equilibrium. The neutron dose equivalents for various concrete thicknesses are shown in Figure 2. Results such as these can be used to highly refine the required shielding for high intensity proton machines such as the proposed IsoSpin Laboratory.

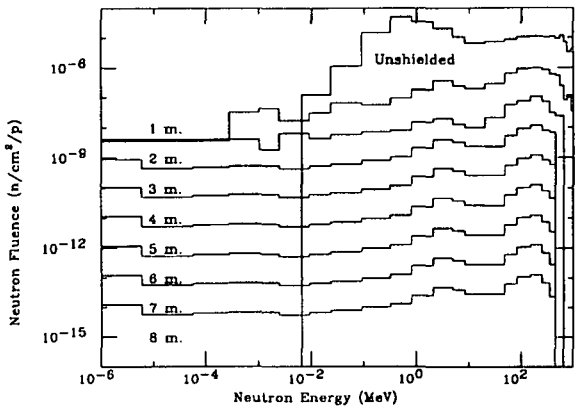

Figure 1: Neutron fluence vs. neutron energy at 0° at various concrete thicknesses for 1 GeV protons on a thick Ta target. LAHET/ONEDANT coupling occurs at 2 meters of concrete. Neutron fluence has been normalized by the log of the energy bin width. The distance from target to shield is 1 m.

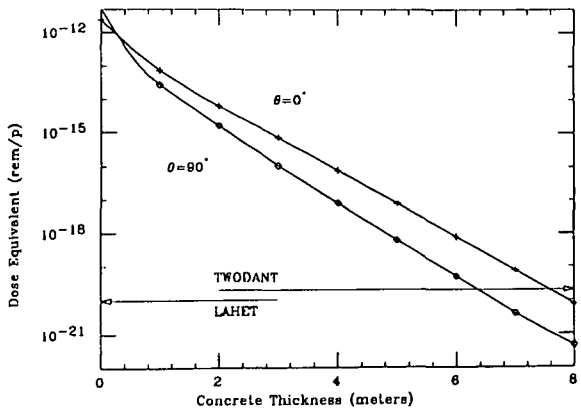

Figure 2: Neutron dose equivalent vs. concrete thickness at 0° and 90° for 1 GeV protons on a thick Ta target. The distance from target to shield is 1 m.

References

[1] A. Fassò, *et al.*, presented at the Workshop on Simulating Accelerator Radiation Environments, January 11-15 (1993) Santa Fe, NM.

[2] R. E. Prael and H. Lichtenstein, Los Alamos National Laboratory Report LA-UR-89-3014, September (1989).

[3] R. D. O'Dell *et al.*, Los Alamos National Laboratory Report LA-9184-M, December (1989).

[4] R. J. Donahue, *et al.*, presented at the Specialists Meeting on Shielding Aspects of Accelerators, Targets & Irradiation Facilities, April 28-29 (1994) Arlington, TX.

Production of ^{114}Ba in ^{58}Ni + ^{58}Ni Reactions and Detection of Its Cluster Radioactivity*

*P. B. Price, A. J. Westphal, R. Bonetti†, A. Guglielmetti†, Z. Janas‡, H. Keller‡, R. Kirchner‡, O. Klepper‡, A. Piechaczek‡, E. Roeckl‡, K. Schmidt‡, J. Szerypo§, B. Blank***

Cluster radioactivity is the spontaneous tunneling decay of a heavy nucleus into a cluster such as ^{14}C, ^{20}O, ^{23}F, ^{24}Ne, ^{28}Mg, or ^{32}Si and a heavy daughter. Until now all 20 examples have involved a heavy daughter near ^{208}Pb. Halflife data for even-even parents define a family of Geiger-Nuttall lines for each type of cluster. Decays of odd-A parents are usually hindered due to poor overlap of single-particle wave functions for parent and daughter. Both fission models and cluster models with preformation factor can be adjusted to fit halflife data for heavy daughters near ^{208}Pb.

The present work addressed the question, "Does cluster radioactivity also occur near doubly magic ^{100}Sn?" The most favorable case is calculated to be $^{114}\mathrm{Ba} \rightarrow {}^{12}\mathrm{C} + {}^{102}\mathrm{Sn}$, with an estimated $Q \sim 20$ MeV. The masses and decay modes of ^{114}Ba, ^{115}Ba, ^{116}Ba, and ^{118}Ba are unknown up until now.

The GSI On-Line Mass Separator was used to (a) search for ^{12}C cluster emission; (b) search for α emission; and (c) measure α and β branching ratios. Fluorination at the target allowed us to separate ^{114}Cs from ^{114}Ba.

We used barium phosphate glass plates to identify etched tracks of $\sim$ 17 MeV ^{12}C ions. From microscopic measurement of diameter and depth, and comparison with tracks from a 17 MeV ^{12}C ion beam, we determined charge, energy, and zenith angle. In a run that yielded $\sim 10^5$ atoms of ^{114}Ba, we found three tracks identified as ^{12}C from decay of ^{114}Ba, based on their energy, charge, and direction. This gives a branching ratio of $\sim 3 \times 10^{-5}$ relative to all decays. Our result is compatible with a recent lower limit set by Tretyakova *et al.* at Dubna. We saw no α-decay, which allowed us to set a stringent upper limit of 10^{-3} on the branching ratio of α decay relative to total decay.

The major result is that cluster radioactivity is found for nuclei decaying into a region of doubly magic ^{100}Sn. In the case of ^{114}Ba decay, the branching ratio for ^{12}C emission relative to α emission, $\mathrm{B}(^{12}\mathrm{C}/\alpha) > 0.03$, is at least seven orders of magnitude greater than the $^{14}\mathrm{C}/\alpha$ branching ratio for nuclei decaying into the doubly magic ^{208}Pb region.

Further analysis of data from the run is in progress. It is expected that halflives for β decay of four light Ba isotopes will be obtained.

---

*Progress Report.

†University of Milan.
‡GSI, Darmstadt.
§Catholic University, Leuven, Belgium.
**CEN Bordeaux-Gradignan, France.

NUCLEAR AND PARTICLE ASTROPHYSICS

Sudbury Neutrino Observatory, Photomultiplier Tube Support Structure

Kevin T. Lesko, David Beck†, Yuen-Dat Chan, Alejandro García, Yoichi Kajiyama†, Gary Koehler†, Eric Norman, Peter Purgalis†, Alan Smith*, Robert Stokstad, Igor Žlimen and the Sudbury Neutrino Observatory Collaboration*

The Sudbury Neutrino Observatory (SNO) detector is a large heavy water Čerenkov detector designed to detect neutrinos in the 1000 ton D_2O target. The detector has sensitivity to the total neutrino flux, ν_x, independent of family (x= e, μ, τ) and to the ν_e flux, separately, by measuring the elastic scattering, charged and neutral current signals. The detector is located in a mine two kilometers below ground near Sudbury, Ontario Canada. The mine is an active nickel mine operated by INCO, Ltd. The D_2O is contained in a thin-wall acrylic sphere, six meters radius, which is itself suspended in a 11 meter radius cavity filled with ~7800 tons of ultrapure water.

The design of the detector components was completed this year and the elements of the support structure manufactured, tested, assembled and delivered to Sudbury for installation. Excavation of the cavity was completed last year and it is being prepared for the final installation of the detector. Most of the underground services have been installed. Prototyping of the acrylic vessel and the bonding process is progressing.

Lawrence Berkeley Laboratory designed and supplied the Photomultiplier Tube Support Structure, which will position and secure the ~10000 PMTs used to detect the Čerenkov light generated by neutrino interactions in the D_2O. The experimental constraints on the design require an extremely low radioactivity contamination of detector components, submersion in ultrapure water for a period of at least ten years, restricted maintenance opportunities, and installation in an active nickel mine while simultaneously maintaining clean-room conditions.

The PMT Support Structure load bearing structure is based on a three-frequency icosahedron geodesic structure, 8.9 m radius. The structure is constructed of 270 stainless steel struts joined in 92 hubs. All elements of the geodesic structure have been tested for low level radioactivity and are below 15 ppb level established for the detector, typically the levels were less than 5 ppb. All low level radioactivity measurements were performed at LBL's Low Level Counting facilities, either at the LBL site or at the Oroville Dam facility.

The support structure underwent a complete trial assembly prior to shipping to Canada. Panel installation was prototyped at LBL using our full-scale model and procedures for installation of the detector were drafted.

The panel assemblies that house the light concentrators and the PMTs were assembled at LBL's clean room assembly facility and shipped to Sudbury, where the PMTs and concentrators will be installed. The components shipped to Canada were packaged to preserve their cleanliness. All fasteners and the plastic elements that make up the panels were tested for cleanliness and low level radioactivity. Again, all components were lower than the 15 ppb level for [U, Th] contamination. These measurements encompassed both the raw materials and the completed components.

All welded components were independently inspected for weld quality and contamination.

LBL continues to supply guidance to and perform R&D for the SNO collaboration on control of contamination. LBL works with the installation contractors and the other detector component suppliers to assure that the low levels of contamination control will be met during the installation of the detector during the next two years.

Footnotes and References

† Engineering Division, Lawrence Berkeley Laboratory.

* Retired.

A Space-Time Pattern Recognization Network for Analyzing Čerenkov Vertices

Y. Chan, D.W. Dong, and the LBL SNO Group*

A three layer feed forward neural network has been developed to analysis Čerenkov radiation patterns obtained by large underground water Čerenkov detectors such as the Sudbury Neutrino Observatory. A typical experimental event comprises a series of phototube-hits at known spatial locations with measured relative firing times. One can therefore formulate the event reconstruction problem as a generalized visual pattern recognition process, including both the space and time dimensions.

The phototubes are divided into P overlapping groups (each containing M phototubes) according to their spatially locations on the detector surface. Each phototube group is connected to a cluster of N neurons in the first layer, where N is a network parameter representing the number of necessary "eigen-features" that can describe the data patterns accurately. The time degree of freedom is included by dividing the event time window into T overlaping bins (see Figure). Within each time bin, the same spatial construction is repeated. Thus the total number of neurons in the first layer is [P $\times$ N] $\times$ T and forms the important preprocessing stage of the network. An individual neuron unit belonging to a cluster and time bin is sensitive to a specific feature of the pattern (such as verticality, horizontal, diagonality, etc., up to N features) through its non-adaptive weights. These weights are uniquely determined by properties of the events making up the training set and are obtained by the statistical principle component analysis (PCA) method. A statistically averaged spatial correlation matrix C is constructed from the training set such that a single element C_{ij} of this M *times* M matrix represents the statistical correlation strength between phototubes i and j within the receptive field of a neuron. This C matrix is then diagonalized and N(<M) of its eigenvectors corresponding to the largest eigenvalues are used as connection weights for the input layer. It has been shown that for a normally distributed data set in the presence of white noise, the eigenvectors with larger eigenvalues carry relatively more information and less noise about the data, and vice versa.

The second and third layer connections are obtained by adaptive supervised training with the back error propagation (BEP) method.

The network has been tested in several situations including its ability to identify whether an event vertex is located inside or outside a given volume of interest inside the detector. After training, we found the network correctly located events 87 percent of the time for a data sample of 10,000 events. This is slightly lower than a comparable conventional χ^2-fitting procedure without any time cuts. However, when artificial random noise tubes are added to an event, the network outperforms the same χ^2-fitter. The performance of the network can also be improved by incorporating much finer time bins into the architecture.

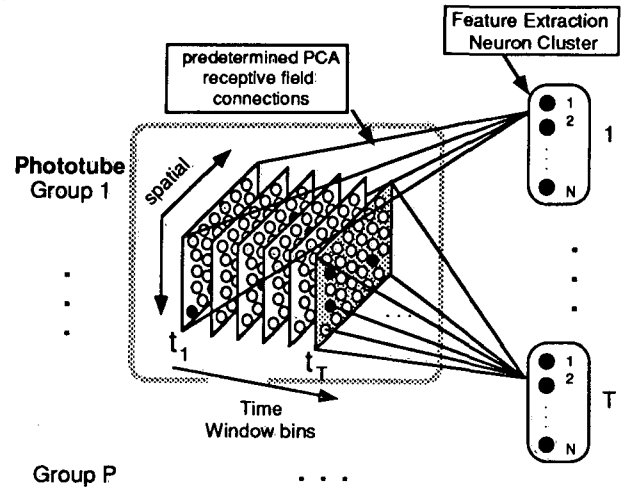

Footnotes and References

*Neural Computing Laboratory, Rockefeller University, Box 272, 1270 Avenue, New York, NY 10021-6399

An Integrated Data Analysis/Acquistion Software Environment for the Sudbury Neutrino Observatory

Y. Chan and the LBL SNO Group

The SNO data analysis and physics Monte Carlo software packages are based on the standard CERNLIB environment where until recently FORTRAN has been the default language. On the other hand, the on-line data acquisition (DAQ) and general detector control packages for SNO are written in other languages (such as C^{++}) that support object-oriented class implementations. Consequently, even though several major software components (such as single event display, event reconstruction/manipulation, histogramming, fitter representation etc.) are common to both tasks, they appear quite different to an user.

Effort has been made to unify and coordinate the software development (such as user interface, display graphics, etc.) in all SNO computing platforms so that an experimenter can perform both the data acquistion and subsequent data analysis task in a very similar if not identical environment, to reduce the learning period needed to use the software, as well as minimizing possible confusion and errors caused simply by platform changing.

A two tier approach has been adopted: (i) due to the already demonstrated value of the CERN software library to the SNO project, the Monte Carlo and data analysis packages will remain within the scope of the CERN distribution, using the latest implementation of the high level CERN tools in areas such as user interface (KUIP/Motif) and graphics, and (ii) identify cross platform language wrappers to integrate the C^{++}-based data acquistion and the FORTRAN77-based data analysis/Monte Carlo software together. Prototypes to incorporate the DAQ class libraries via xm^{++} and CFORTRAN wrappers to the CERN KUIP/Motif scope have been developed.

The upper portion of the following figure shows a CERN KUIP/Motif implementation of the SNO Monte Carlo user interface, which starts at one level down from the main KUIP hierarchy. The lower part shows a single event display screen using CERN graphical tools, together with zoom- and pan-slider control, convenience toolbars and buttons enhancements. Similar to the DAQ approach, event manipulation is done by mouse dragging, rather than the more traditional command driven style in a CERN environment.

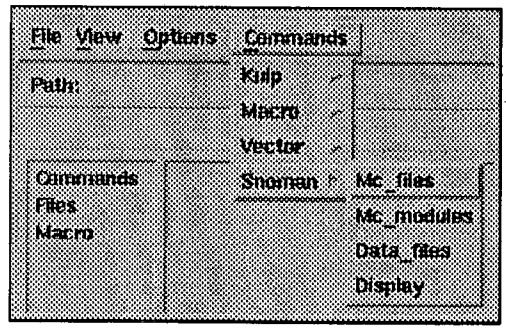

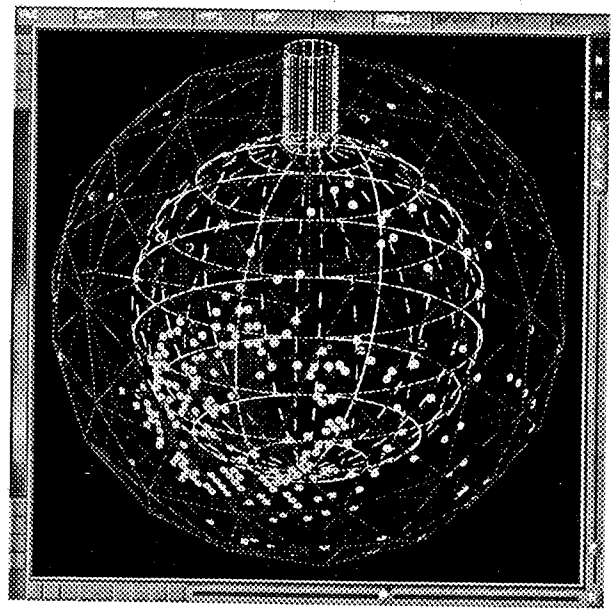

(p,xn) Yields of ^{80,82}Br and ^{96}Nb and the Double - β Decays of ^{80,82}Se and ^{96}Zr

I. Žlimen†, Y.D. Chan, A. García, I.D. Goldman‡, R.M. Larimer, K.T. Lesko, E.B. Norman, and F.E. Wietfeldt

The double-β decays of ^{82}Se and ^{96}Zr have been studied via geochemical techniques[1,2]. A new geochemical experiment is planned to determine the double-β decay half-life of ^{80}Se[3]. In such studies, one determines the excess abundance of the double-β decay daughter isotope in an ancient sample of the parent element. However, cosmic-ray muon- and/or proton-induced reactions on the parent element can produce radioactive species which β decay to the same isotopes that are produced by double-β decay. Thus, one must subtract this cosmic-ray contribution from the measured abundance before the double-β decay half-life can be determined. Since the (p,xn) yields relevant to this aspect of geochemical double-β decay experiments have not been measured previously, we have undertaken a study of these yields.

Irradiations were done at 88"Cyclotron, and the induced target activity was followed in several time-bin intervals for identification by energy and half-life. We have measured thick-target yields of ^{80,82}Br and ^{96}Nb from proton irradiations of natural Se and Zr targets at energies of 15, 30 and 45 MeV. Their contribution to the total number of double-β decay daughter atoms (^{80,82}Kr and ^{96}Mo) in the parent sample is shown in the Table I.

The yields are expressed in number of double-β decay daughter atoms made from the parent sample of natural isotopic composition of abundances per 10^4 incident protons.

The measured yields show that in the geochemical measurement of the double-β decay half-life of ^{96}Zr and ^{82}Se the (p,xn) reactions give a negligible contribution, due to the relatively short half-lives of ^{96}Zr and ^{82}Se. But, in the proposed geochemical measurement of the double-β decay half-life of ^{80}Se, (p,xn) yields represent competing mechanism of production of ^{80}Kr atoms over a geological period of time.

Table I: **(p,xn) Thick Target Yields**

E_p [MeV]	^{80}Kr	^{82}Kr [per 10^4 protons]	^{96}Mo
15	8.0±0.5	1.1±0.1	0.17±0.02
30	12.2±0.6	1.3±0.1	0.22±0.03
45	12.9±0.7	1.2±0.1	0.22±0.06

†On leave from R. Bošković Institute, Zagreb, Croatia
‡ On leave from Univ. de Sao Paulo, Sao Paulo, Brasil

Footnotes and References

[1]T. Kirsten and H.W. Muller, Earth & Planet Sci. Lett. **6**, 271 (1969)
[2]A. Kawashima et al., Phys. Rev. C **47**, R2452 (1993)
[3]T. Bernatowicz, private communication

Cross sections for the ^{45}Sc(p,2n)^{44}Ti reaction and the half-life of ^{44}Ti

I. Žlimen†, Y.D. Chan, M.T.F. Da Cruz‡, R. Ejnisman‡, A. García, I.D. Goldman‡, R.M. Larimer, K.T. Lesko, E.B. Norman, and F.E. Wietfeldt

The long-lived radioisotope ^{44}Ti is of astrophysical interest for several reasons. It is expected to be one of the major sources of nuclear gamma-ray lines from young supernova remnants. It can also be produced in meteorites through cosmic-ray interactions and can be used to obtain information on the cosmic-ray exposures of such meteorites. It is also a significant component of the cosmic radiation. One of the important ^{44}Ti production mechanisms is the ^{45}Sc(p,2n) reaction. There is only one report[1] in the literature for this reaction.

We have studied the excitation function for the ^{45}Sc(p,2n)^{44}Ti reaction from 16 to 22 MeV at the University of Sao Paulo and from 20 to 45 MeV at the 88-Inch Cyclotron at LBL. Scandium targets were irradiated, allowed to cool, and than gamma counted off line. The measured yields of the 68-, 78-, and 1157 keV gamma rays emitted by the decay of ^{44}Ti were then used to determine the ^{44}Ti production cross sections. The results are shown in Figure 1.

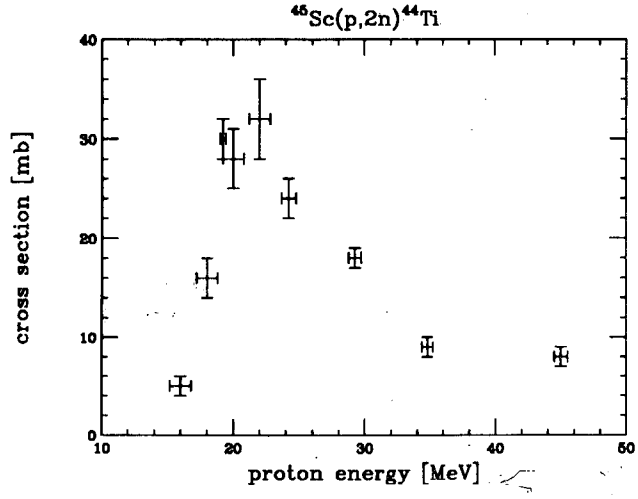

Fig. 1

In a separate experiment we are attempting to measure the half-life of ^{44}Ti by following it's gamma ray activity over one year period. The measured values for the half-life of ^{44}Ti range from 46 to 66 years[2]. A more accurate half life of ^{44}Ti is of particular interest in the supernova observations. Knowing both the half-life and the time elapsed after the supernova explosion, one can calculate the initial amount of ^{44}Ti produced.

In our half-life measurement we are following the decrease of activity in the mixed sources of ^{44}Ti, ^{22}Na, ^{137}Cs and ^{241}Am. The ratios of characteristic gamma lines of these isotopes, together with known half-lives of ^{22}Na, ^{137}Cs and ^{241}Am should allow precise determination of the ^{44}Ti half life. We are expecting to have the result at the end of 1994.

† On leave from R. Bošković Institute, Zagreb, Croatia

‡ On leave from Univ. de Sao Paulo, Sao Paulo, Brasil

Footnotes and References

[1] T. McGee et al., Nucl. Phys. **A150**, 11 (1970)

[2] D.E. Alburger and G. Harbottle, Phys. Rev. **C41**, 2320 (1990)

Further Studies of a ^{14}C-Doped Germanium Detector

F.E. Wietfeldt, E.B. Norman, Y.D. Chan, M.T.F. da Cruz, A. García, E.E. Haller, W.L. Hansen, M.M. Hindi, R.-M. Larimer, K.T. Lesko, P.N. Luke, R.G. Stokstad, B. Sur†, and I. Žlimen*

We have continued studies of our germanium detector doped with ^{14}C. In 1991 we reported a distortion in the beta spectrum of ^{14}C that could be explained by the emission of a 17 keV mass neutrino in approximately 1% of the decays.[1] The final data set contained 392 days of data (about 6.8×10^8 total events) collected in LBL's Low Background Counting Facility on a PC-based data acquisition system. We fit the spectrum in the region 100–160 keV to the theoretical shape and found a best fit of 16.6 ± 0.6 keV for the heavy neutrino mass and 1.25 ± 0.25% for the mixing with 5σ statistical significance.

The detector consists of a 1.28-cm-thick planar germanium crystal grown with a concentration of 6×10^{12} cm^{-3} of 10% enriched ^{14}C. It is segmented at the anode by a 1-mm-wide groove into a central detector and a guard ring. The guard ring was used in anticoincidence to veto events near the edge where charge collection could be incomplete. The guard ring veto threshold was set quite high (20 keV) to prevent vetos on the tiny bipolar image pulses that occur in 100% coincidence with true event signals.

Further tests using an event-mode data acquistion system and collimated γ-ray sources revealed that for events underneath the 1-mm-wide groove (about 14% of the central detector volume) the ionization charge was split between the center and guard ring anodes. This effect was not anticipated in the original experiment. Furthermore, we found evidence that the carbon is concentrated in clusters of 10^{10}–10^{11} atoms. These clusters cause complicated structure in the energy spectrum of the charge-division coincidences.

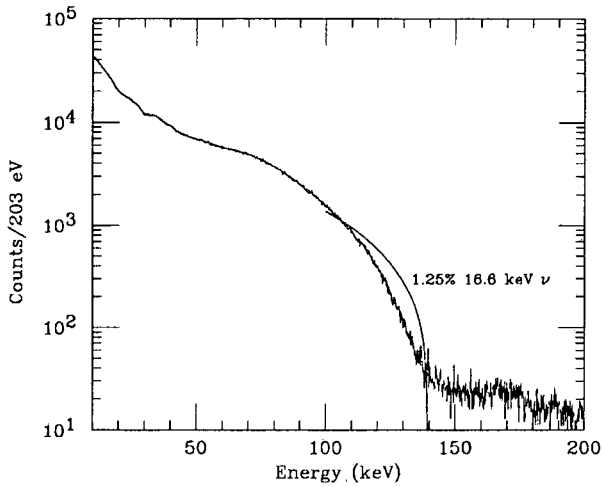

Figure 1. Energy spectrum in the central detector of charge-divided events where the guard ring collected < 20 keV of equivalent charge. The solid line shows the original massive neutrino signal.

Beta decay events under the groove in which the guard ring collected less than 20 keV of equivalent charge were below the veto threshold. These events represented a contamination that was superimposed on the "good" center region beta decay spectrum. Figure 1 shows a recent spectrum of the charge-divided events where the guard ring energy was less than 20 keV. It looks roughly like a beta spectrum, with an "endpoint" about 17 keV below the ^{14}C endpoint, and an amplitude comparable to the 1.25% 17 keV neutrino signal. The shape however is somewhat different. We have some evidence that the shape of this effect has changed over time, due to variations in the electric field under the groove brought about by chemical treatment of the crystal. Analysis of recent data with the guard ring veto threshold lowered to 5 keV shows no preference for a 17 keV neutrino in the fit.

Footnotes and References

*Physics Department, Tennessee Technological University, Cookeville, TN 38505

†AECL Research, Chalk River Laboratories, Chalk River, Ontario K0J 1J0, Canada

[1] B. Sur *et al.*, Phys. Rev. Lett. **66**, 2447 (1991).

Low-background Counting Facilities

A.R. Smith, R.J. McDonald, D.L. Hurley, and E.B. Norman

The LBL Low Background Counting Facilities are now operated by the Nuclear Science Division. These facilities have more than a 30 year history with the laboratory, most recently under the Engineering Division, and most well-known for the double-beta-decay experiment at the Oroville site. The present staff of the Facilities include Al Smith as facility director emeritus, Dick McDonald as a staff scientist, Donna Hurley as a technician at Oroville, and Eric Norman as group leader.

The Berkeley site was established in 1963 and consists of a 3m by 7m room surrounded by 1.6m of concrete shielding. The aggregate in this special concrete consists of serpentine gravel which is low in Uranium, Thorium, and Potassium. This barrier was made to shield against neutrons and natural gamma radiation as well as some cosmic rays. Also, the low-activity concrete emits little radon, and a HEPA filtered air system constantly purges the room.

Detectors at this site include a 20 cm diameter by 10 cm thick NaI detector and two 30% P-type Ge spectrometers. These detectors are shielded by 10 cm of Pb and one of the 30% Ge detectors has an external active cosmic ray suppresser.

The resulting effective shields reduce the background to the point where internal activity in the detectors and cosmic-rays are the dominant source of background. Besides the three detectors operated by the facility, "guest" detectors involved in experiments requiring low-background environments often reside at the facility.

In order to further reduce background for the LBL-UCSB ^{76}Ge double-beta-decay experiment, a site was established in the powerhouse of the Oroville Dam, under 180 m of rock cover. This site now has a 115% N-type Ge spectrometer. This system operates at about a factor of 10 less background than the Berkeley site.

The main projects presently at the facility involve screening of detector-construction materials for SNO and the UCB Dark Matter Search, counting parts from the Long Duration Exposure Facility (LDEF) satellite. Sensitivities of 50 parts-per-trillion (ppt) for Uranium and daughters, 200 ppt for Th and daughters, and 100 parts-per-billion for K are realized at the Oroville site. Sensitivities at Berkeley are about ten times less. In the near future, projects to do Instrumental Neutron Activation Analysis on semiconductor grade Si and counting of some parts returned from the Hubble Space Telescope will be added.

Measurement of the Branching Ratio for the Fermi Decay of ^{10}C

B.K. Fujikawa and S.J. Freedman

The $|V_{ud}|$ term from the Cabibbo-Kobayashi-Maskawa (CKM) quark mixing matrix can be determined precisely from the *ft*-values of the superallowed Fermi nuclear β-decays. The value of $|V_{ud}|$ is very interesting since it is a fundamental parameter in the Standard Model and knowledge of its precise value can be used to test for physics beyond the Standard Model. It is necessary for radiative and isospin mixing corrections have to be made to the raw *ft*-values in order to extract $|V_{ud}|$. Although there is general agreement with respect to the radiative corrections, there is much controversy with the isospin mixing correction since calculations made by different groups do not agree[1]. The magnitude of both the radiative and isospin mixing corrections increase with higher nuclear charge Z. Therefore it is important to measure *ft* from nuclei with low Z. The nucleus with the lowest Z for which there is a Fermi decay transition is ^{10}C.

We have been working for several years on a precision measurement of the branching ratio $^{10}C(0^+, gs) \rightarrow {}^{10}B(0^+, 1.74\,MeV) + e^+ + \nu$. The *ft*-value for the Fermi decay of ^{10}C. is determined from this branching ratio, the ^{10}C. half-life, and ^{10}C β endpoint energy. All ^{10}C decays produce a 0.718 MeV γ-ray. Decays to the $^{10}B(0^+, 1.74\,MeV)$ state produce an additional 1.022 MeV γ-ray. Therefore the branching ratio is simply equal to the relative intensity ratio I(1.022 MeV) / I(0.718 MeV).

This experiment is being done at the Western Michigan University EN tandem accelerator facility which provides a 7.8MeV proton beam to make ^{10}C through the $^{10}B(p, n)^{10}C$ reaction. The γ-rays from ^{10}C decay are detected with two germanium detectors. The relative efficiencies of these detectors are calibrated with the γ cascade that results from the $^{10}B(p, p')^{10*}B$ reaction. The energy of the scattered proton, which is measured with a silicon surface barrier detector is used to tagged excitations to the $^{10}B(0^+, 1.74\,MeV)$ state which decays to the ground state by emitting exactly one 1.022MeV γ-ray and one 0.718MeV γ-ray. Details of this experiment apparatus is described elsewhere[2].

Footnotes and References

1. F.C.. Barker, *et al., Nucl. Phys.* **A540**, 501(1992).
2. M.A. Kroupa, *et al.., Nucl. Inst. Meth.* **A310**, 649, (1991).

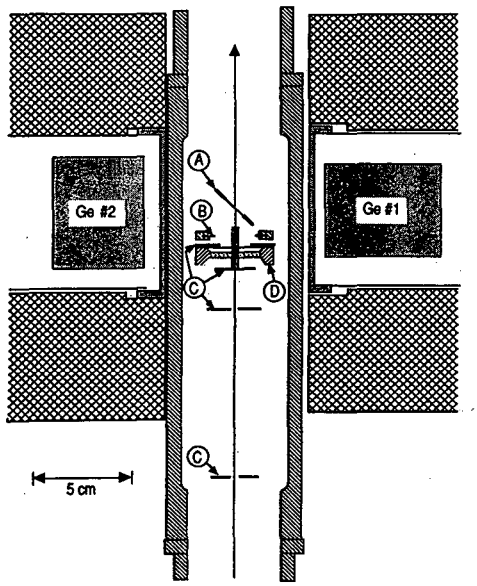

Fig. 1. Setup of the experiment to measure branching ration of the Fermi decay of ^{10}C. A, the target; B, the camera iris; C, collimators; D, the silicon detector.

The status of this experiment is as follows. Analysis of early data have been completed and published[2]. This data obtained a branching ratio of $(1.465 \pm 0.009) \times 10^{-2}$ which is in agreement with measurements made by other experiments. Analysis of recent data has also been completed. Althought we obtained a branching ratio with a statistical precision of ~0.2%, this data was judged unreliable due to inconsistencies in the calibration data. We are currently preparing for another measurement of the branching ratio which will incorporate more germanium detectors and other major improvements.

Time Reversal Invariance in Polarized Neutron Decay*

S. J. Freedman[1], B. K. Fujikawa[1], E. G. Wasserman[1], L. Lising[2], T. J. Bowles[3], S. Elliott[3], M. Fowler[3], J. S. Nico[3], R. G. H. Robertson[3], J. F. Wilkerson[3], K. Coulter[4], T. E. Chupp[4], S. Hwang[4], M. Dewey[5], D. Gilliam[5], G. L. Greene[5], J. Richardson[5], A. Thompson[5], W. M. Snow[5], and A. Garcia[6]

Resolution of the long-standing question of the origins of CP-violation has been hindered by our failure to observe CP-violation outside of the neutral kaon system. In relativistic field theories, invariance under CPT (simultaneous inversion under parity, charge conjugation, and time reversal) is required on very general grounds, so CP-violation implies simultaneous time reversal invariance violation (TRIV). Thus studies of TRIV provide another avenue for investigating CP-violation.

TRIV could be manifested in the beta decay of free polarized neutrons as a non-zero triple correlation, D, among the neutron polarization, and the electron and proton momenta. In the Standard Model TRIV effects in the neutron are vanishingly small. Due to the fortuitous smallness of T-conserving final state effects in neutron decay, the observation of D above the level of 10^{-5} would be a clear indication of physics beyond the Standard Model. Many extensions to the Standard Model contain additional T-violating parameters that contribute to D in lowest order. Improving the current limit would constrain these extensions.

Advancements in detector and neutron polarization technology since the last neutron triple correlation experiments were performed have motivated a group of physicists (the EMIT collaboration) to undertake a new search for TRIV in neutron decay. In addition, a new detector geometry will be used to greatly enhance sensitivity to D. The full detector consists of an octagonal arrangement of four beta and four proton detector panels about a longitudinally polarized cold (~2 meV) neutron beam.

Recently, a proof-of-principle test run using prototype detectors was performed at the NIST Cold Neutron Research Facility (CNRF). Of particular importance was the demonstration of an electrostatic focusing/accelerating array backed by PIN diode detectors. This assembly was used to detecting the low energy (<750eV) recoil protons. With the success of the test run, construction of the full detector system has begun.

The LBL group is responsible for the design, fabrication, and characterization of the scintillator panels that will be used to detect the betas from the neutron decays. The design of the detectors has been completed and tests of prototype detectors are underway. The final fabrication and characterization are expected to be completed this year. In addition, the collaboration will use LBL as the integration point for the full detector system.

After assembly, the detector system will be moved to the CNRF where the first data will be taken in 1995. We expect to achieve a sensitivity to D of 3×10^{-4}, about an order of magnitude better than the previous neutron experiments. In the future, we plan to move the apparatus to the ILL in Grenoble, France where the higher cold neutron flux will allow further improvement to a statistical uncertainty of 2×10^{-5}, the level at which the T-conserving final state effects become significant.

Footnotes and References

* The EMIT collaboration

[1] Lawrence Berkeley Laboratory, Berkeley CA 94720

[2] University of California, Berkeley CA 94720

[3] Los Alamos National Laboratory, Los Alamos, NM 87545

[4] University of Michigan, Ann Arbor, MI 48109

[5] National Institute of Standards and Technology, Gaithersburg, MD 20899

[6] University of Notre Dame, Notre Dame, IN 46556

Evidence Against a 17 keV Neutrino From ^{35}S Beta Decay*

J. L. Mortara, I. Ahmad†, K. P. Coulter†, S. J. Freedman, B. K. Fujikawa, J. P. Greene†, J. P. Schiffer†, W. H. Trzaska†, A. R. Zeuli†

We have searched for the effect of a 17 keV/c^2 mass neutrino in the beta decay of ^{35}S with an apparatus incorporating a high-resolution solid state detector and a super conducting solenoid (fig. 1). The experimental mixing probability $\sin^2\theta$ = -0.0004 ± 0.0008 (stat.) ± 0.0008 (syst.), is consistent with zero, in disagreement with several previous experiments. Our sensitivity to neutrino mass is verified by measurements with a mixed source of ^{35}S and ^{14}C which artificially produces a distortion in the beta spectrum similar to that expected from a massive neutrino.

In 1985 J. J. Simpson interpreted a distortion in his measurement of a tritium beta decay spectrum as evidence for a "17 keV neutrino" [1]. Such a distortion was noted in recent years in the decays of ^{35}S, ^{63}Ni, and ^{14}C [2,3]. Paradoxically, all such distortions were observed with solid state detector systems.

In our measurement we also incorporated a solid-state detector. The principle advantage of this experiment was the use of a super conducting solenoidal field. This transport field allowed for an accurate measurement of the detector response function and an elimination of possible secondary scattering within the apparatus.

When no distortion consistent with the 17 keV neutrino was detected (^{35}S data shown in fig. 2, top), a sensitivity test was devised. We added a known distortion at the level of 1% into the ^{35}S beta spectrum and attempted to detect it. A drop of ^{14}C-doped valine (Q≈156 keV) was deposited on a carbon foil and then a much stronger ^{35}S source was deposited over it. This new spectrum was subjected to an identical analysis and a distortion consistent with 1.4 ± 0.1% ^{14}C was discovered (fig. 2, bottom). This is consistent with the measured value of 1.34% inferred from measuring the total decay rate of the ^{14}C alone.

We are continuing our investigation of this spurious effect by analyzing data from the decays of ^{14}C and ^{63}Ni.

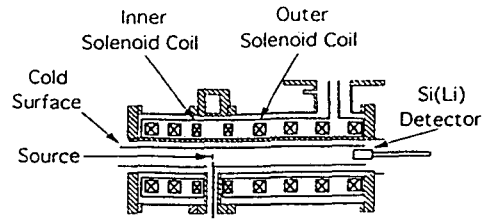

Fig. 1. Cross-section of solenoid.

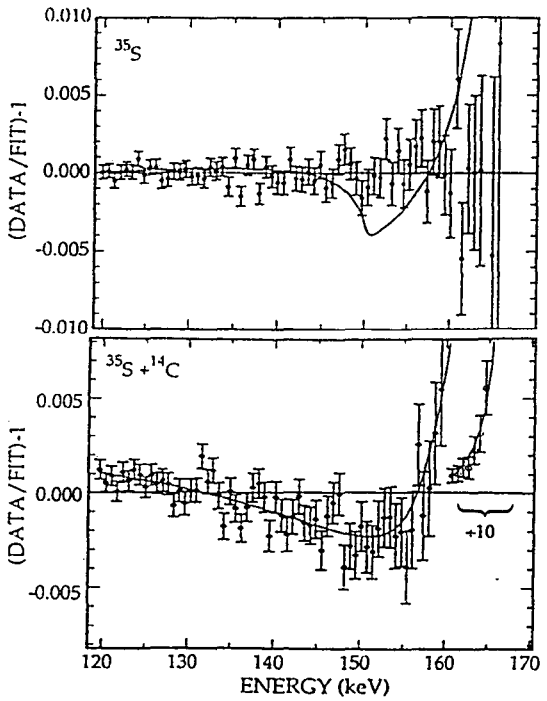

Fig. 2. Top. Residuals from ^{35}S data, solid curve denotes expected deviation for 0.85% 17 keV neutrino. Bottom. Residuals from mixed source, solid curve denotes expected deviation from ^{14}C admixture.

Footnotes and References

*Condensed from PRL 70, 394 (1993).

† ANL, Argonne, IL 60439.

1. J.J. Simpson, Phys. Rev. Lett. 54, 1891 (1985).
2. A. Hime, D. Phil Thesis, Oxford(1991).
3. B. Sur *et al*, Phys. Rev. Lett. 66, 2444 (1991).

An Efficient Method for Loading a Magneto-Optical Trap from a Slowed Atomic Beam

Z-T Lu, S. J. Freedman and, S -Q. Shang

Rapidly developing techniques for trapping neutral atoms are being exploited in several areas of research. Up to now applications have involved stable atoms but learning to trap radioactive isotopes would be useful in particle and nuclear physics for expediting precision measurements of weak interaction parameters. A major experimental challenge is the limited number of a short-lived isotope, which has to be produced on-line. Developing efficient methods for loading magneto-optical traps is essential for advancing this area of research.

We have developed an efficient method for loading magneto-optical traps (MOT) with atoms slowed from an atomic beam. In experiment with sodium atoms, this technique enabled us to capture about 20% of the thermal atoms crossing the trap. The methods described here has proven useful in experiments with rare short-lived radioactive atoms[1].

In order to get a continuous slow atomic beam, we use the Zeeman tuned slowdown technique, which has important advantages for experiments involving rare atoms. A counter propagating laser beam tuned just below the resonance frequency decelerates the atomic beam as it passes along the axis of a spatially varying solenoidal magnetic field. The magnetic field induces a position dependent Zeeman shift which compensates for the changing Doppler shift as the atoms slow down. Since the slowdown process is a sensitive function of laser intensity and detuning, significant improvement is needed for loading the slowed atoms into a MOT. We have added a set of critical extraction coils which are located at the end of the solenoid. The typical field inside the extraction coil is 15 mT. With the currents properly adjusted, atoms are rapidly decelerated from 120 m/sec to rest at the center of the MOT over a path of less than 5 cm. The rapid, final deceleration mitigates against divergence losses from transverse velocity components.

In the experiment, an effusive sodium beam is produced from an oven at 200 ^{o}C, 1.5 from the MOT. The atomic beam is directed along the axis of the gradient solenoid, providing a monotonically decreasing field along its 1.1 m length. A pair of 10-cm diameter coils generate a predominantly quadrapole field center about 15 cm downstream of the solenoid, which provides a field gradient 2 mT/cm for the MOT. The extraction coil is placed between the solenoid and the MOT.

We use a calibrated CCD camera to measure the density of the thermal atomic beam. The fluorescence from the trapped atoms is recorded by a calibrated PIN photodiode which gives the number of the trapped atoms. The loading and decay times were determined by observing the fluorescence as an atomic beam shutter was opened and closed. From these measurements, we determine the absolute loading efficiency, defined as the fraction of thermal atoms crossing the trap region which are captured. With eight measurement at different atomic beam flux, we have obtained an average efficiency of 20%. This shows a 20 times of improvement in loading efficiency comparing with previous record.

Footnotes and References

[1] Z-T. Lu et al., to be published in Phys. Rev. Lett.

Comparison of the Cold-Collision Losses for Laser-Trapped Sodium in Different Ground State Hyperfine Sublevels

S -Q. Shang, Z-T Lu, and S. J. Freedman

The recent developments in neutral atom laser cooling and trapping has provided unique opportunities for studying exoergic collisions. Such a cold collision contributes large effect for the losses of a magneto-optical trap because it is sensitive to the long range atom-atom force and the atom-atom interaction time is comparable to the radiative decay time. Beyond the inherent interest of the new aspects of collision dynamics, a deep understanding is important for achieving high atomic density and realizing the potential physics applications of neutral atom traps.

We have studied the cold collision loss-rate constants for sodium atoms trapped in each of its two ground state hyperfine sublevels which are split by 1772 MHz. To our knowledge, this is the first time such a comparison has been accomplished. Dramatic differences show up at low laser intensity where hyperfine-changing collisions are important. Compared to cesium or rubidium. sodium hyperfine-changing collisions are more difficult to observe because they are effective at a much lower fraction of the saturation laser intensity. In deed we were able to see the effect because of a newly developed highly efficient trap loading scheme. For a trap containing sodium, in the F = 2 ground state, the cold-collision losses are dominated by hyperfine-changing collisions when the total laser intensity is below 4 mW/cm^2. Our experiment confirms that there are no hyperfine-changing collisions for a F = 1 trap.

Figure 1 shows our result of the two body collision-rate constant (β) between trapped sodium atoms. For atoms trapped in the F = 2 ground state, β increased with laser intensity above 4 mW/cm^2. This is the expected behavior for collisions between atoms in the ground state and atoms in the excited state. Below 4 mW/cm^2 hyperfine-changing collisions are effective and the loss rate increases rapidly. In a hyperfine changing collision, two atoms in the F = 2 state undergo an exoergic spin exchange leaving one atom in the F = 1 ground state. The conversion of hyperfine energy into kinetic energy increases each atoms velocity by 6 m/s, allowing both to escape. For sodium atoms, hyperfine changing collision should dominate at total intensity (six beams) below 3 mW/cm^2, corresponding to only about 3% of the saturation intensity for a single beam. Because of the low laser intensity it is difficulty to observe hyperfine changing collision effect in Na relative to cesium and rubidium. For the F = 1 trap, hyperfine changing collisions are absent, and β, the cold collision rate constant increased with laser intensity.

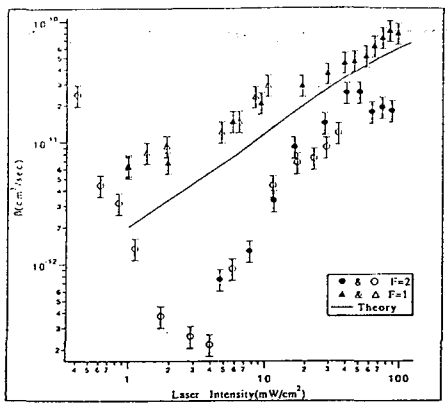

Figure 1. The cold-collision loss rate constant β as a function of trapping laser intensity. The laser frequency is detuned - 10 MHz from the F = 2 to F' = 3 transition for F = 2 trap, and - 21 MHz from the F = 1 to F' = 1 transition for the F = 1 trap. The repumping sideband is 1712 MHz in each case. The solid curve is a theoretical prediction. The 20% error bars reflect the systematic uncertainty in the measurements. Solid and open points indicate from separate runs of the experiment.

Laser Trapping of Radioactive Atoms*

Z-T. Lu† , C. Bowers † , S. J. Freedman† , B. K. Fujikawa† , J. L. Mortara† , S-Q. Shang† , E. Wasserman† , K. Coulter‡ , and L. Young‡

During this fiscal year, we succeeded in trapping of the 22.5-sec half-life ^{21}Na isotope. From a weak thermal atomic beam of ^{21}Na produced on-line at the LBL 88" Cyclotron, we loaded about 4 x 10^3 atoms at a time into a magneto-optical trap (MOT), using a Zeeman-tuning slowdown technique. Our method can be easily adapted to other rare isotopes. A series of experiments exploiting high precision measurements in the low energy weak interactions, such as beta-asymmetry parameter, electron-neutrino correlation coefficient, atomic parity mixing and time reversal invariance, becomes feasible based on the success of our new techniques for trapping and manipulating radioactive atoms. The first experiment is a measurement of the β-asymmetry parameter in the mirror β-decay of ^{21}Na. This measurement can provide an interesting test of the V-A structure of the weak interaction.

The ^{21}Na nuclei are produced with the ^{24}Mg(p, α)^{21}Na reaction with a 25 MeV proton beam. The beam is stopped inside of an atomic beam oven which is loaded with magnesium shavings. The ^{21}Na atoms diffuse from target at 500 ^{o}C with an average dwell time about 40 sec. This gives a total ^{21}Na beam flux about 1 x 10^7 sec^{-1}.

A dye laser pumped by an Ar^+ laser is used in this experiment. Two polarization preserving optical fibers carry laser light to the experimental area near the end of the cyclotron beam line, which provided light for cooling and trapping. Since the divergence of ^{21}Na beam is large, an orthogonal pair of counter propagating laser beams cool the transverse momentum spread near the oven orifice. Following this, a 1.2 m long solenoid with taped windings provides a B-field which decreases from 110 mT to 15 mT along the atomic beam path. ^{21}Na atoms with a velocity below 850 m/s is slowed by a beam of circularly polarized light. To maximize the trap loading efficiency a set of critical "extraction coils" are located at the end of the solenoid. The magnetic field for the MOT provides a gradient about 2 mT/cm. Three pairs of counter propagating laser beams provide light for trapping. The presence of trapped ^{21}Na atoms is verified by observing the optical fluorescence emitted from the trap with a charged coupled device (CCD) camera. Figure 1 shows the variation in the trap fluorescence as the transverse cooling laser beams are turned on and off. The fluorescence is approximately 16 times brighter when the transverse cooling beams are on. The mean lifetime of the trap is 6.3 sec after correcting for the ^{21}Na radioactive decay.

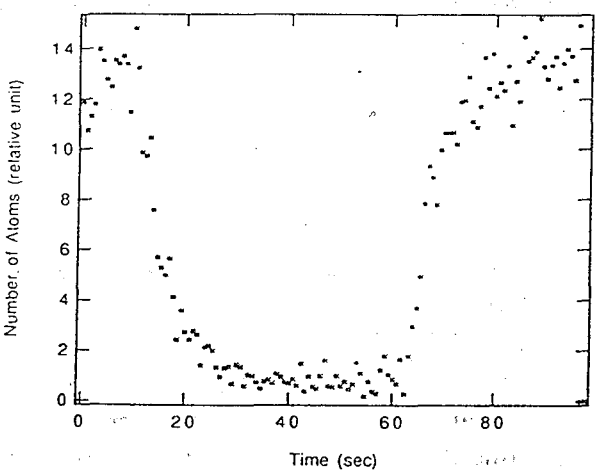

Figure 1. Time spectrum of the fluorescence from trapped ^{21}Na atoms as the transverse cooling beams are turned off and on.

Footnotes and References

*To be published in Phys. Rev. Lett.

† Lawrence Berkeley Laboratory, Berkeley CA 94720

‡ Argonne National Laboratory, Argonne IL 60439

Measurement of Astrophysically Significant Nuclear Cross Sections*

S. Albergo[8], Z.Caccia[8], C.-X. Chen[3], S. Costa[8] H.J. Crawford[4], M.Cronqvist[2], J. Engelage[4], P. Ferrando[7], I. Flores[2], R.Fonte[8], L. Greiner[4], T.G. Guzik[3], A.Insolia[8], F.C. Jones[1], C.N. Knott[5], S. Ko[4], C. Kuo[4], P.J. Lindstrom[2], J. Mazotta[4], J.W. Mitchell[1], R. Potenza[8], J.Romanski[8], A. Soutoul[7], O. Testard[7], C.E. Tull[3], C. Tuve[8], C.J. Waddington[5], W.R. Webber[6], J.P. Wefel[3], X.Zhang[3]

1. Interactions in Hydrogen of Relativistic Ne to Ni projectiles: Total Charge Changing Cross Sections, C.Chen for Transport Collaboration, Phys.Rev.C. (in press, June 1994).

ABSTRACT: One of the fundamental goals of Cosmic Ray Astrophysics is to relate the measurements of the charge and isotope spectra of cosmic rays to the original emissions at the galactic cosmic ray sources (GCRS). Accomplishing this goal will provide important information regarding the mechanism(s) responsible for accelerating the cosmic ray nuclei to high energy, the mixture of material from exotic astrophysical sites making up the GCRS matter, the nucleosynthesis of heavy matter at such sites, and the evolution of matter in the galaxy. Key to this task is a working knowledge of the nuclear fragmentation process capable of predicting the outcome in collisions between primary nuclei emitted from the GCRS and the gas or dust of the ISM. Currently the ability to determine the GCRS composition in many instances is limited by the accuracy of the nuclear fragmentation models or empirical fits and not by the GCR measurements themselves. In turn these theoretical models, are limited by the accuracy of experimentally measured cross sections, on which the models are based.

A critical next step to achieving a better understanding of the GCR source population, acceleration, and propagation is the accurate measuring of cross sections for expected primary GCR nuclei on targets of the most abundant ISM nuclei. The Transport collaboration's specific scientific objectives include providing measurements of critical fragmentation cross sections, studying the mechanisms and energy dependence of these heavy ion collisions, and investigating cross section systematics which might then assist in improving the theoretical predictions of unmeasured cross sections.

The program was performed at Heavy Ion Superconducting Spectrometer at Lawrence Berkeley Laboratory and included measurement of the interaction cross sections and the single particle inclusive isotope production cross sections for a variety of astrophysically important heavy ion beams from Ne to Ni at energies from 393 MeV/nucleon to 910 MeV/nucleon incident on a liquid hydrogen target. The group has finished the analysis of the charge changing and elemental cross sections for all of the measured beams and has two papers currently in press. Attention is now focused on completing the isotopic cross sections and investigating the resultant nuclear systematics. These results should produce significant astrophysics information as well, specifically GCR source abundances for isotopes from C to Fe, confinement times from cosmic clocks like ^{7}Be, and insight into propagation and re-acceleration.

Footnotes and References

[1]NASA/Goddard Space Flight Center, Greenbelt, MD
[2]Lawrence Berkeley Laboratory, Berkeley, CA
[3]Louisiana State University, Baton Rouge, LA
[4]Univ. of California - SSL , Berkeley, CA
[5]University of Minnesota, Minneapolis, MN
[6]University of New Mexico, Las Cruces, NM
[7]Service d'Astrophysique, C.E.N. Saclay, Cedex, France
[8]Universita di Catania and INFN, Catania; Italy

Radial Earth Density Profile by Neutrino Mapping

C. Kuo[1], H. Crawford[2], R. Jeanloz[1], B. Romanowicz[1], G. Shapiro[3], M.L. Stevenson[3]

1. Radial Earth Density Profile by Neutrino Mapping

C. Kuo[1], H. Crawford[2], R. Jeanloz[1], B. Romanowicz[1], G. Shapiro[3], M.L. Stevenson[3]

(To be published, 1994)

ABSTRACT: The recent discovery of a number of very high-energy extra-galactic gamma-ray sources by EGRET on the Compton Gamma Ray Observatory, and the current installation of several prototype neutrino detector arrays (AMANDA, DUMAND, NeSTOR, Lake Baikal Neutrino Telescope) in the Earth, has led us to reexamine the case for measuring the density profile of the Earth using neutrinos. Determining the profile via neutrino absorption would complement the seismological methods now employed to determine the Earth's radial density distribution. High-energy astrophysical gamma-ray sources are believed to emit neutrinos of intensities comparable to or larger than the γ-ray intensities. By measuring the attenuation of the extraterrestrial neutrino flux as it passes through the Earth, essentially a comparison of tangential to diametrical event rates, constraints on the radial density distribution of the planet can be obtained. We investigate the neutrino source and detector characteristics required to measure geophysically interesting features inside the Earth, specifically discussing the possibilities for the prototype neutrino detector arrays being deployed in 1994 and 1995.

Footnotes and References

[1]Geophysics Department
[2]Space Sciences Laboratory
[3]Physics Department
University of California
Berkeley, California, 94720

Constraints on Massive Unstable Dark Matter from Ultrahigh-Energy γ-Ray Flux*

Y. D. He

We ruled out regions in parameter space of the mass, lifetime, and branching ratio for radiative decay of massive unstable dark matter particles based on upper limits to the ultrahigh-energy cosmic diffuse γ-ray spectrum. The lifetime of massive unstable particles is shown to be no shorter than $\sim 10^{17}$ sec if they exist at a density equal to the cosmological critical density. The branching ratio for radiative decay of such massive unstable particles is less than 10^{-11} at mass of 1 GeV and 10^{-2} at 10^5 GeV.

*Abstract of a paper in *Nuovo Cimento A* **107** (1994) 453.

Quark Compositeness, New Physics, and Ultrahigh-Energy Cosmic-Ray Double-Core γ-Family Events*

Z. Cao† *L. K. Ding*† *Q. Q. Zhu*† *and Y. D. He*

We find a significant excess of ultrahigh-energy cosmic-ray events at large transverse momenta with respect to the prediction by standard perturbative QCD at $E_{lab} \sim 10^4 - 10^5$ TeV, an energy regime beyond the reach of existing colliders but within the range of future hadron colliders. Such a large deviation cannot be accounted for by a compositeness model of quarks with a characteristic energy scale $\Lambda_c > 1.4$ TeV allowed by current collider experiments, pointing towards new physics.

*Abstract of a paper in *Phys. Rev. Lett.* **72** (1994) 1794.

†Institute of High Energy Physics, Academia Sinica, Beijing 100039, PRC.

RELATIVISTIC NUCLEAR COLLISIONS

Study of Dilepton Production from Nucleon-Nucleon Collisions

Howard Matis for the DLS Collaboration

The DLS collaboration has finished its analysis of *pp* and *pd* data taken at 4.9 GeV. This study was done to measure the fundamental nucleon-nucleon contributions to dilepton production. It was widely believed that the major contribution was due to the simple elastic brehmsstrahlung. In this "soft-photon approximation", the yield from *pn* collisions is much greater than from *pp* collisions because the dipole contribution cancels in *pp*. Consequently, dilepton production from *pd* collisions should be significantly greater than *pp* collisions.

Fig. 1 displays our measured pair cross section[1] as a function of invariant mass. At this energy, the ratio of pair production from *pd* to *pp* is about two, implying that the *pp* production mechanisms are roughly equal to the *pn* production processes. In order to resolve this discrepancy, Haglin and Gale made a more detailed calculation[2] of *pp* and *pn* elastic bremsstrahlung. Their results, shown in Fig. 1, demonstrate that the *pp* cross section is actually larger in the DLS than *pn* and both are several orders of magnitude smaller than the data.

In the lower graph in Fig. 1, they show that the sum of the inelastic channels for bremsstrahlung is a significant contribution to dilepton production at low mass. Also shown in that figure is the contributions for η Dalitz Decay and $\pi\pi$ annihilation. The addition of those processes approximately describe our data, except for a deficiency around 0.5 GeV.

In conclusion, the DLS nucleon-nucleon data show that a more complete bremsstrahlung calculation is necessary to explain the measured cross sections. In addition to inelastic bremsstrahlung there are several other production mechanisms which contribute to dilepton production at 4.9 GeV.

Footnotes and References

1. H.Z. Huang *et al.*, Phys. Rev. **C49**, 314(1994).

2. K. Haglin and C. Gale, .McGill/93-9, TPI-MINN-93/18-T.

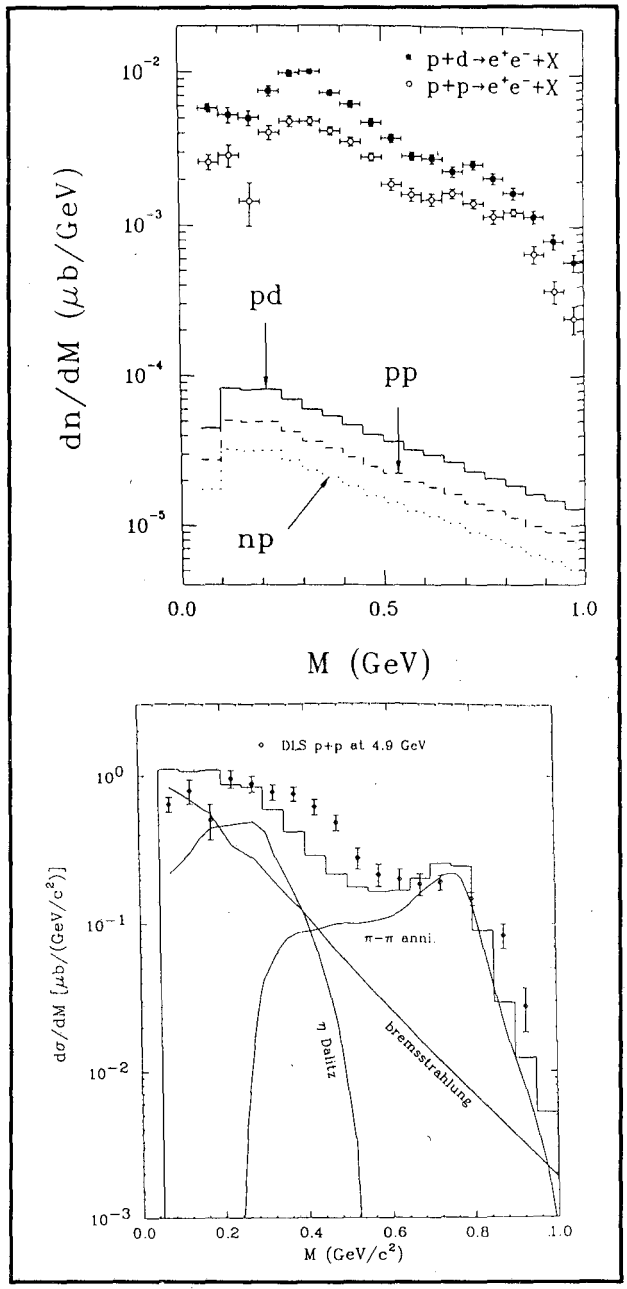

Fig. 1. (Top) Mass distribution for *pp* and *pd* DLS data. A calculation, by Haglin and Gale, of elastic bremsstrahlung is superimposed on the figure. (Bottom) Contributions to *pp* dilepton production.

Measurements of Dielectron Production in A+A Collisions at 1.05 GeV/nucleon Beam Kinetic Energy

R. J. Porter for the DLS Collaboration

Dielectrons produced in A+A collisions have the potential to elucidate features of the interaction dynamics in the heavy ion collision. Unlike hadronic probes, electron-positron pairs produced during the early hot-dense phases of the collision suffer little rescattering with the hadronic medium. Some current estimates of the sources for dielectrons produced in the 1-2 GeV/nucleon collision energy range suggest that mechanisms such as Δ and η Dalitz decays and $\pi^+\pi^-$ annihilation dominate the pair yield [1][2]. Comparisons between the dielectron mass spectra from A+A systems to those from previous DLS measurements in p+p and p+d collisions [3] may probe the hadronic interactions within the collision medium.

The first measurements of dielectron production in A+A collisions in the Bevalac energy range were performed by the Dilepton Spectrometer (DLS) collaboration in a series of experiments from 1987 to 1989 [4] [5]. Although, the pair yields from these experimental runs were limited to a few hundred pairs per system, the data sets established the capability for performing such measurements and prompted theoretical investigations of the dielectron mass spectra. However, detailed interpretations of potential effects from the collision medium on the dielectron signal are hampered by the low statistics in these original pair yields. Therefor, the DLS collaboration devoted long running periods to measuring dielectron pairs in A+A systems with the goal of significantly improving the statistical precision. The analysis of the data from the final DLS experimental runs is nearing completion and the current pair estimates from these data sets are shown in Table 1.

The dielectron data listed for the Ca+Ca system represent an order of magnitude increase in the pair yield over the previous DLS data. The factor of three improvement in the pair statistics enhances the prospects for understanding the contents of the pair mass spectrum. In addition to the production cross section, the dielectron pairs in the new data sets are associated with a measure of the event multiplicity [5]. The multiplicity information allows for comparison of the characteristics between pairs produced in peripheral collisions to those from more central interactions.

To further augment the understanding of the Ca+Ca data, measurements were performed in He+Ca and d+Ca systems at 1.05 GeV/nucleon. The pairs produced from these systems can be used to explore and account for the effects of Fermi momentum in the colliding nuclei in interactions which should not achieve the level of compression as central Ca+Ca collisions. Also a measurement of the A_pA_t dependence in the dielectron cross section is gained with the C+C data obtained as an intermediate mass system.

System	E/A (GeV)	True Pairs	Date
Ca+Ca	1.05	3117±124	Sep 92
He+Ca	1.05	1148±44	Jan 93
d+Ca	1.05	1250±42	Jan 93
C+C	1.05	2168±70	Jan 93

Table 1. True pair summary table for dielectron measurements in A+A systems.

References

[1] G.Wolf et al., *Nuclear Phys.* **A545**, (1992)

[2] V.D. Toneev et al., *GSI Preprint* GSI-92-05, (1992)

[3] W.K.Wilson et al., *Phys. Lett. B* **316**, 245 (1993)

[4] G. Roche et al., *Phys. Rev. Lett.* **61**, 1069 (1988)

[5] S. Beedoe et al., *Phys. Rev. C* **47(6)**, 2840 (1993)

Orthogonal Components of Sideward Flow in the EOS Time Projection Chamber

Y. Shao, D. Keane and the EOS Collaboration

This report describes a sideward flow analysis of data from the EOS TPC that supplements the information provided by $\langle p^x \rangle$ observables, as reported elsewhere in this volume. $\langle p^x(y) \rangle$ characterizes the average collective component of sideward momentum for a fragment at rapidity y, regardless of its azimuth φ relative to the collision reaction plane, and both rotations of fragment azimuths relative to an uncorrelated distribution (which we associate with the azimuthal component of sideward flow) and alterations to the length of $\mathbf{p}^\perp$ vectors relative to an uncorrelated distribution (which we associate with the radial component of sideward flow) contribute to $\langle p^x \rangle$. This alternative analysis provides independent measurements of these two components and allows inferences to be drawn concerning the pattern of sideward flow as a function of φ.

The azimuthal pair correlation function [1] makes use of the variable ψ, the smaller angle between the transverse momenta of two fragments, and is defined as

$$C(\psi) = \frac{P_{cor}(\psi)}{P_{uncor}(\psi)}, \qquad (1)$$

where $P_{cor}(\psi)$ is the ψ distribution for observed pairs, *i.e.*, pairs in which both fragments belong to the same event, and $P_{uncor}(\psi)$ is the ψ distribution for pairs from mixed events, *i.e.*, events generated by randomly selecting M tracks, each from a different observed event with multiplicity M. To characterize the radial component of sideward flow, we introduce a new quantity called the radial pair variance function:

$$\sigma^2(\psi) = \langle p^2_{sum}(\psi) \rangle - \langle p_{sum}(\psi) \rangle^2, \qquad (2)$$

where $p_{sum} = p_i^\perp/A_i + p_j^\perp/A_j$ is the sum of the $\mathbf{p}^\perp$ magnitudes per nucleon for the pair.

[1] S. Wang *et al.* Phys. Rev. C 44, 1091 (1991).

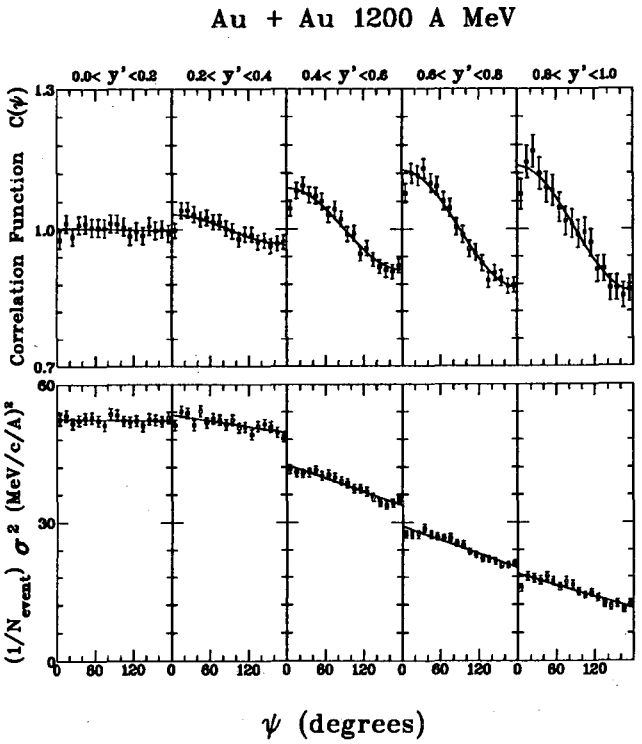

Figure 1. Azimuthal pair correlation functions and radial pair variance functions in five rapidity intervals spanning mid-rapidity to projectile rapidity, for Au + Au at 1.2A GeV.

Fig. 1 shows azimuthal pair correlation functions $C(\psi)$ and radial pair variance functions $\sigma^2(\psi)$ in five rapidity intervals spanning mid-rapidity to projectile rapidity, for Au + Au at 1.2A GeV. The solid curves in the $C(\psi)$ panels represent least-squares fits using the function $1 + 0.5\lambda^2 \cos\psi$, and the $\sigma^2(\psi)$ data in the lower panels are fitted using a straight line. The simplest interpretation [2] that is consistent with these measurements is one where the magnitude and direction of the collective component of sideward momentum is independent of φ.

[2] Y. Shao, Ph.D. dissertation, Kent State U. (1994); Y. Shao *et al.*, to be published.

Preliminary Results of Collective Flow from Au + Au

M. Partlan and the EOS Collaboration

Collective flow is believed to be a signature of fluid-like behavior in heavy ion collisions. This type of collective phenomena has been observed by several experiments. One of the goals of the EOS TPC is to extend the study of the development of collective flow as a function of fragment mass to higher beam energies. For our preliminary study we have focused on the Au + Au excitation function at energies of 0.25, 0.4, 0.6, 0.8, 1.0, 1.15 A GeV.

Figure 1 shows the mean transverse momentum per nucleon in the reaction plane as a function of normalized rapidity for three different energies. The data include all light fragments from semi-central events. A measure of the flow is obtained by simply calculating the slope at mid-rapidity of the 'S' shaped curve.[1] Here the error bars are statistical only.

Figure 2 (bottom) shows the flow values as a function of beam energy extracted from the EOS data along with the flow values measured by the Plastic Ball group.[2] The data are in reasonable agreement over most of the energy range. The discrepancies at higher energies may be explained by the fact that the Plastic Ball data are not corrected for detector bias effects which were most important for the high energy data.

The data may be cast in a scale invariant way by dividing the flow values by the beam momentum per nucleon in the CM frame.[3] These scaled flow values are shown in Fig. 2 (top). Models based on "ideal" hydrodynamics predict that the scaled flow is independent of beam energy.[4]

Footnotes and References

1 P. Danielewicz and G. Odyniec, Phys. Lett. B157, 146 (1985)

2 H. H. Gutbrod, A. M. Poskanzer, and H. G. Ritter, Rep. Prog. Physics 52, 2267 (1989)

3 A. Bonasera and L. P. Csernai., Phys. Rev Lett. 59, 630 (1987)

4 N. L. Balazs, B, Schurmann, K. Dietrich and L. P. Csernai., Nuclear Phy A424, 605 (1984)

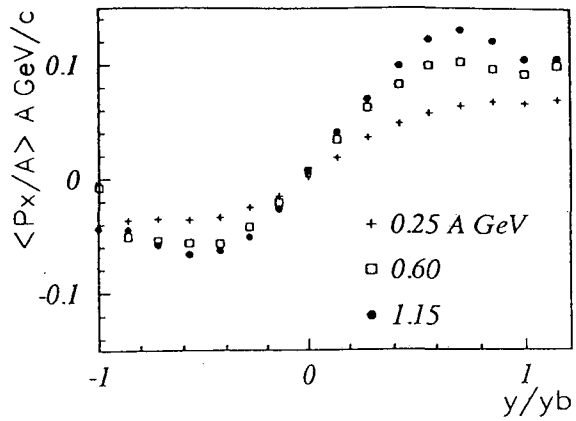

Fig. 1. Mean transverse momentum per nucleon vs. normalized rapidity for mid multiplicity events for three different energies of the Au+Au systems

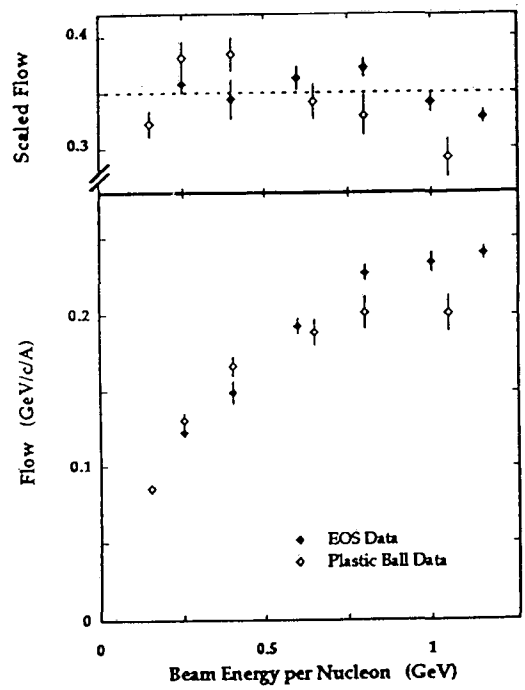

Fig. 2. (Top) Flow values scaled by the beam momentum per nucleon in the CM frame[4]. (Bottom) Flow values as a function of beam energy extracted from the EOS data.

Collective Radial Flow in Au+Au Collisions

M.A. Lisa and the EOS Collaboration

Collective motion may play an important role in the decay of highly excited nuclear matter created in heavy ion collisions. Directed flow effects account for only a small fraction of the energy available in the center-of-momentum frame, whereas entropy studies lead one to expect a much larger portion of the total energy to be contained in collective motion*. Recent studies suggest a large radially-directed flow in central heavy ion collisions†. We have begun a systematic search for this effect, with Au+Au data taken with the EOS TPC.

Good particle identification capabilities and excellent midrapidity coverage, with no low-p_t cut-off, allow the extraction of quality energy spectra for particles emitted at 90° in the center-of-mass. These are shown in Fig. 1, for the reaction Au+Au, E=1.0 A·GeValong with fits to the spectra with a form for a source with temperature T and radial expansion velocity β#:

$$\frac{d^3N}{dEd^2\Omega} \approx p \cdot e^{-\gamma E/T}\left\{\frac{\sinh\alpha}{\alpha}\cdot(\gamma E + T) - T\cdot\cosh\alpha\right\}$$

where E and p are the total energy and momentum of the particle, $\gamma=(1-\beta^2)^{-1/2}$, and $\alpha = \gamma\beta p/T$. Allowing for finite expansion velocity improves the fit, returning χ^2/ν a factor of 4 smaller than the zero-flow (thermal) fit.

Extracted temperatures and flow velocities for light fragments emitted from central Au+Au collisions at bombarding energies in the range E=0.25-1.15 A·GeV are shown in Fig. 2. The flow and temperature increase with bombarding energy, while the fits suggest that the relative amount of energy in thermal and collective modes remains relatively constant at about 1:1.

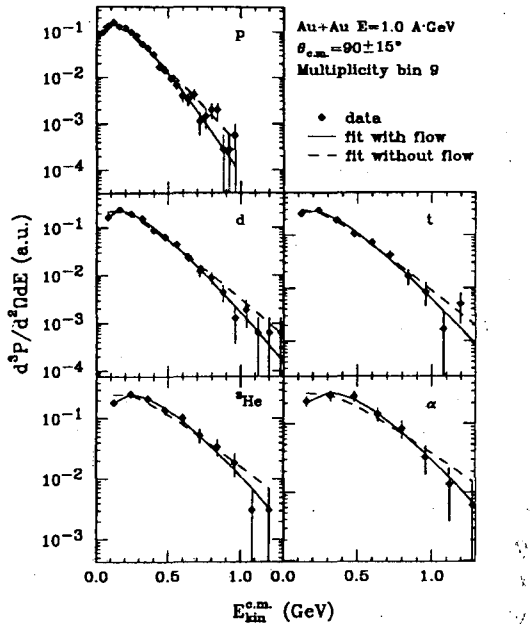

Fig. 1. Energy spectra for light fragments emitted from central Au+Au collisions at E=1.0 A·GeV. Solid and dashed curves indicate fits with and without radial flow.

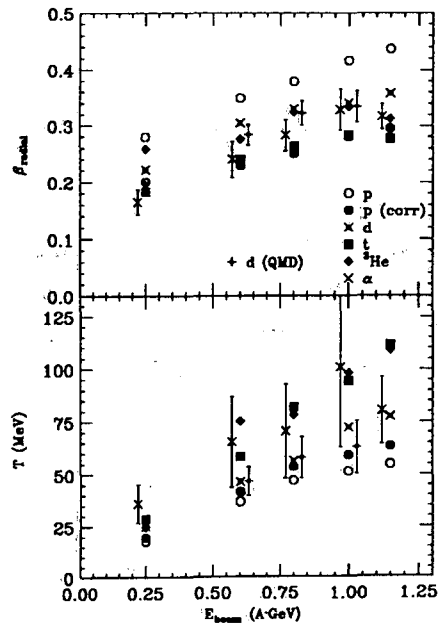

Fig. 2. Flow velocity and temperature parameters as a function of beam energy.

Footnotes and References

* See, e.g. H.H. Gutbrot, A.M. Poskanzer, and H.G. Ritter, Rep. Prog. Phys. 52, 1217 (1989)

† S.C. Jeong *et al.*, GSI Preprint 93-38 (1993)

P.J. Siemens and J.O. Rasmussen, Phys. Rev. Lett. 42, 880 (1979)

dE/dx Resolution and Particle Identification in the EOS Time Projection Chamber

A. Scott and the EOS Collaboration

In the EOS time projection chamber, particles are identified by measuring their curvature in a magnetic field and their energy loss dE/dx. This report focuses on the factors that influence the EOS TPC's dE/dx resolution.

Based on the observed resolution from other detectors similar to the EOS TPC, we expect the resolution for a track with N usable samples to follow the equation[1]

$$\frac{\sigma_{\frac{dE}{dx}}}{\langle\frac{dE}{dx}\rangle} = (0.50)N^{-0.46}(PD)^{-0.32} \qquad (1)$$

where P is the pressure in atmospheres and D is the length in cm of each dE/dx sample. For each track, 30% of the usable samples having the largest ionization are discarded. In the EOS TPC we have $P = 1$, $D = 1.2$ which results in an expected resolution function represented by the dashed line in figure 1. The open data points represent the measured resolution corrected for systematic effects that can be analyzed using the reconstructed momenta and $\langle dE/dx\rangle$. For example, this includes unexpected dependences of dE/dx — for a given velocity and charge — on the dip angle, λ, and fragment multiplicity. These corrections do not include systematic effects which require knowledge of where along the trajectory of the track the usable dE/dx samples were located. The solid points in figure 1 represent the measured resolution after the latter was taken into account. The good agreement with equation 1 confirms that all significant systematic effects have been corrected.

Figure 2 shows a "loading" effect whereby $\langle dE/dx\rangle$ is distorted for a track whose ionization is collected just after that of a strongly ionizing projectile spectator. This graph selects tracks within a limited geometrical region and plots R, $R = \langle\frac{dE}{dx}\rangle_{observed}/\langle\frac{dE}{dx}\rangle_{expected}$, versus track multiplicity. It shows that dE/dx is systematically lowered for tracks just above $\lambda = 0°$ where positive λ corresponds to *upward* sloping tracks.

The EOS TPC has excellent particle identification for the isotopes of hydrogen and helium and can accurately identify charges up to $Z = 7$. Fragments having $Z = 8 - 12$ are discernable but poorly resolved.

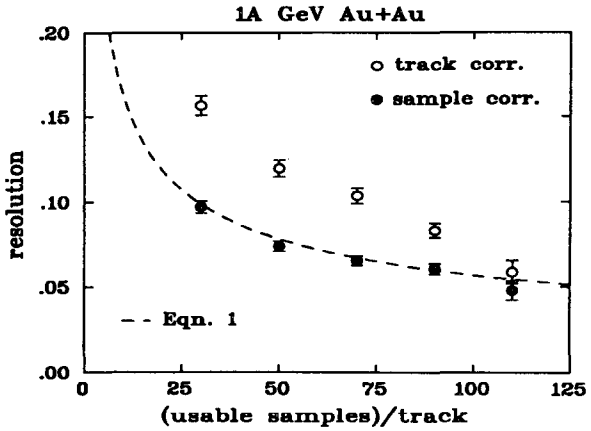

Figure 1: Resolution as a function of the number of dE/dx samples per track.

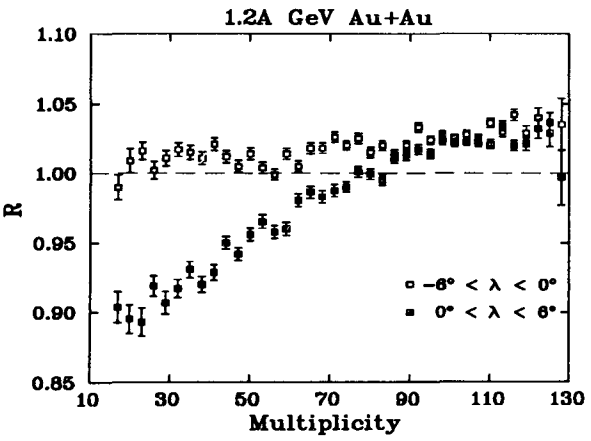

Figure 2: Normalized dE/dx as a function of the charged particle multiplicity.

[1] W.W.M. Allison and J.H. Cobb, Ann. Rev. Nucl. Part. Sci. **30**, 253 (1980). The coefficient 0.5 was determined using the average observed resolution from the detectors: MARKII, CLEO, TOPAZ, DELPHI, PEP TPC, ALEPH, OPAL.

Particle Correlations with the EOS TPC

Eric Hjort and the EOS Collaboration

Because of their sensitivity to quantum statistics and final-state interactions, two-particle correlation functions at small relative momenta contain information about the space-time characteristics of the emitting system, emission temperatures and sequential decay processes. We have completed a preliminary correlations analysis of the EOS data and developed an understanding of the performance of the EOS TPC in terms of momentum resolution and two-track resolution.

Correlation studies require that the two-track resolution of the TPC be well understood. To eliminate double counting of any segmented tracks, and to provide a means by which to measure the separation between the tracks, we require all tracks to exit the TPC. The two-track separation is then defined to be the distance between the endpoints of two tracks, and we find that a minimum track separation of 2.5 cm is required to resolve the individual tracks. However, to achieve a two-track efficiency of 100% it is necessary to require a 5 cm separation. In the analysis we therefore require a minimum two-track separation of 5 cm for both the real pairs and for the background pairs formed by event mixing.

Figure 1 shows the measured d-α correlation function for the reaction Au(Au,dα)X at E/A = 250 MeV. The peak at q≈42 MeV/c is related to the 2.186 MeV excited state in ^{6}Li. The width of this intrinsically narrow peak is determined by the momentum resolution of the TPC. Monte Carlo simulations show that the measured width is consistent with a momentum resolution of $1.0\% < \Delta P/P < 1.4\%$ for the deuteron ($P \approx 1.2$GeV/c) and $\Delta P/P < 1.0\%$ for the alpha ($P \approx 2.4$GeV/c).

Figure 2 shows a two-proton correlation function for the reaction La(La,pp)X at E/A=800 MeV. The peak at q≈20 MeV/c is due to the attractive S-wave interaction between the two protons. Proton correlations with other systems in the EOS data set show the expected source-size sensitivity.

In summary, the momentum resolution and the two-track resolution of the EOS TPC are sufficient to do two-particle correlations. This work is being extended to study velocity correlations of intermediate mass fragments.

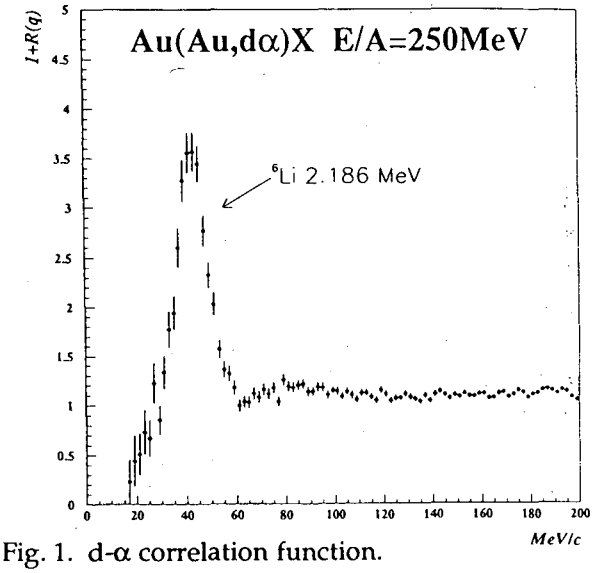

Fig. 1. d-α correlation function.

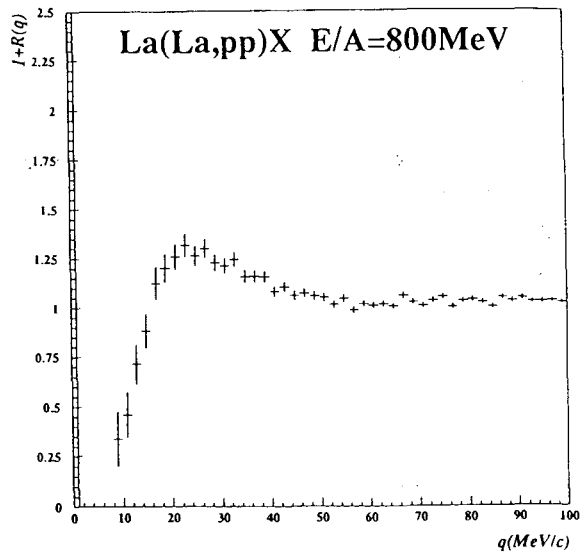

Fig. 2. 2-proton correlation function.

Pion Studies using the EOS TPC at BEVALAC

A. D. Chacon, J. C. Kintner, and the EOS collaboration

Pions are a unique probe of nuclear collisions in that they are not present in the nuclei before the collision, and yet can be detected with a reasonable rate. Studying pion production provides information on the underlying processes in the nuclear collision. Several high statistics data sets were taken with the EOS TPC at the LBL BEVALAC, and these are being analyzed to study the features of pion production at BEVALAC energies.

Figure 1 is a plot of the invariant cross section (in arbitrary units) as a function of the energy in the center of mass for negative pions produced in Ni + Cu collisions at 1.9 A Gev. The fitted slope parameter (E_0 = 109 MeV) is consistent with prior measurements at similar energies, for similar systems.[1]

Figure 2 shows the azimuthal distribution of charged pions relative to the reaction plane,[2] for mid-rapidity pions ($0 < Y_{cm} < 0.4$). The figure includes pions of both charges from Ni + Cu collisions at 1.9 A GeV. The solid line which overlays the histogram is a fit to:

$$N = P_1 + P_2 cos\phi + P_3 cos2\phi$$

The P_2 term is sensitive to emission within the reaction plane, and the P_3 term is a measure of the out-of-plane emission, or "squeeze-out," which has been seen for π^o's in Au + Au.[3] For this fit, $P_1 = 1980$, $P_2 = -39$, and $P_3 = -40$.

Further analysis will increase the statistics available, improve the accuracy of these measurements, and provide a determination the pion source size from pion-pion interferometry.

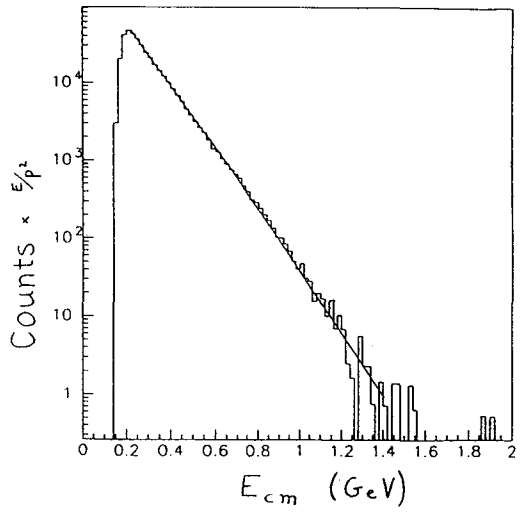

Figure 1: Pion invariant cross section vs Energy in the center of momentum frame.

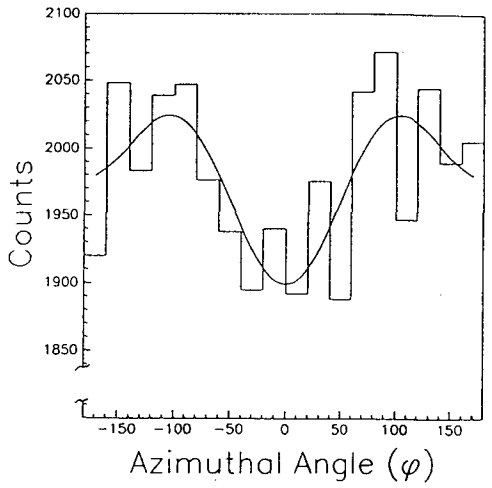

Figure 2: Pion production as a function of the angle from the reaction plane.

Footnotes and References

[1] S. Nagamiya and M. Gyulassy, "High Energy Nuclear Collisions" in *Advances in Nuclear Physics* Editors: J. Negele and E. Vogt, Plenum Publishing Co. (1884).

[2] P. Danielewicz and G. Odyniec, Phys. Lett. **157B**, 146 (1985).

[3] L. Venema *et al*, Phys. Rev. Lett. **71**, 835 (1993).

CERN Experiment NA-36

D. E. Greiner, P. Jones, E Judd and I. Sakrejda

This year the emphasis has been on the multiplicity dependence of strange particle production and the production rates of multiply-strange particles. The data for 200 GeV/c S + Pb has shown that the production of strangeness one particles increases with the negative multiplicity of the event. This effect is unexpected from a strict overlap picture of ion-ion interactions. Study of the details of the increase may allow understanding of the reaction mechanism(s). Comparisons with models and data are shown in Figure 1. One conclusion is possible: Re-interactions appear to be required to show the trend of the data as can be seen be the rough agreement with models utilizing such effects (Venus and RQMD).

The multiply strange particle production compared to the singly strange is also sensitive to the reaction mechanism. For instance, the ratio of $\bar{\Xi}^+/\bar{\Lambda}$ is believed to be large if the production mechanism is dominated by production of Quark-Gluon Plasma. We see this ratio enhanced by a factor of two over that seen in p + p reactions. See Figure 2 for a comparison of various ratios. This value is not high enough to postulate plasma production and can be explained by reactions dominated by hadronic gas production. For more detailed information see;

E. Andersen et al., Phys. Lett. B316 (1993) 603. and LBL-35239 (accepted by Physics Letters)

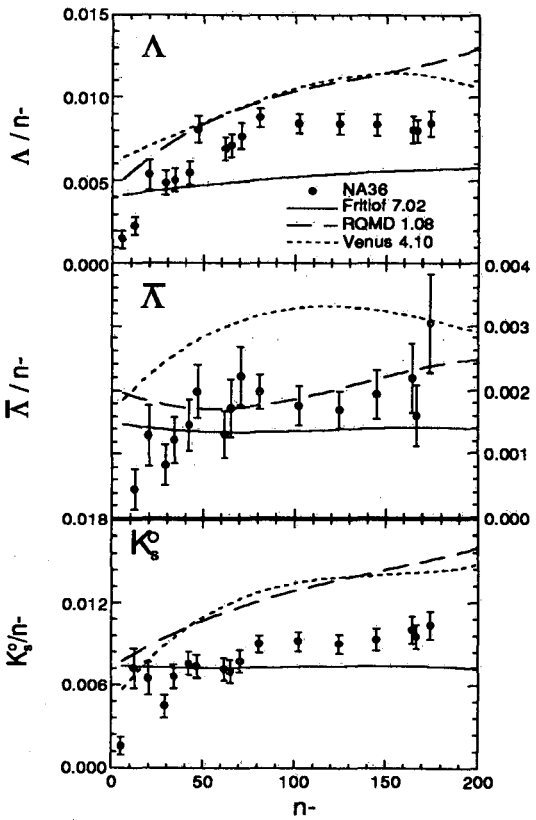

Fig 1. Multiplicity dependence for Λ, $\bar{\Lambda}$ and K^o production.

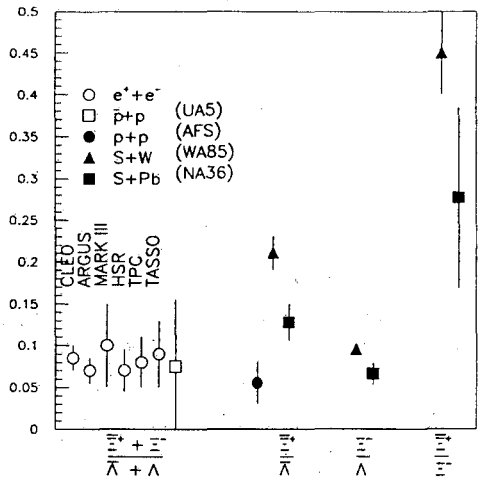

Figure 2. A summary of the world data on various particle ratios involving Λ, $\bar{\Lambda}$, Ξ^- and $\bar{\Xi}^+$.

Centrality Dependence of Negative Hadron Distributions in 200 GeV/A S+Au Collisions

J. T. Mitchell and the NA35 Collaboration

Negatively charged hadrons with rapidities greater than 4 have been measured with the NA35 Time Projection Chamber (TPC). A minimum bias trigger was implemented to record events in which an interaction has occurred. These events were separated into five centrality regions by examining the energy deposited into a calorimeter covering angles less than 0.3 degrees about the beam axis. The more peripheral the collision, the more energy, E_{veto}, will be deposited into the calorimeter.

After determining that the event vertex originated within the target, the negative hadron transverse mass ($m_t=(p_t^2+m_0^2)^{1/2}$) distributions are obtained as a function of rapidity. The rapidity is calculated assuming the pion mass. The distributions are corrected for the detector geometrical acceptance, for the two-track resolution of the TPC, and for the kaon and electron contamination as estimated by the model VENUS 4.02. The resulting spectra are fit to the function:

$$f(m_t) = A \exp(-m_t/T);$$

where T is referred to as the inverse slope parameter. Figure 1 shows T as a function of rapidity for the five E_{veto} regions, showing that T decreases as the rapidity increases. The inverse slope parameters, sometimes referred to as a temperature, do not vary significantly as the collision centrality varies.

The rapidity distributions, dN/dy, are obtained by integrating the fitted curves over the entire transverse mass range. The resulting distribution is shown in Figure 2 for the five E_{veto} regions. As expected, the number of negative hadrons produced in 200 GeV/A S+Au collisions decreases as the collisions becomes more peripheral in nature, reflecting the reduced number of nucleon-nucleon interactions as the target-projectile overlap volume decreases.

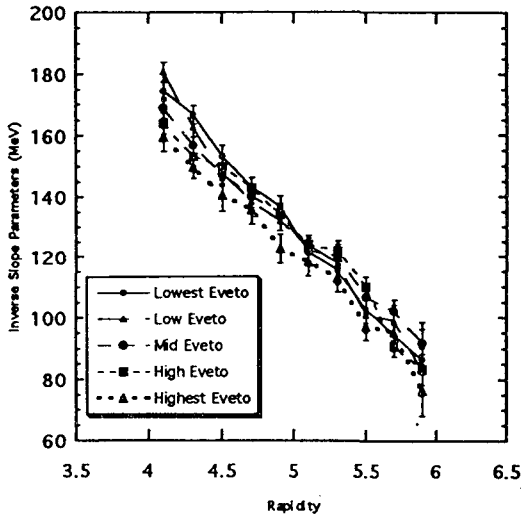

Fig. 1. Inverse slope parameters for negative hadrons as a function of rapidity. The centrality regions are Lowest: $0.4<E_{veto}<1.72$ TeV, Low: $1.72<E_{veto}<3.04$ TeV, Mid: $3.04<E_{veto}<4.36$ TeV, High: $4.36<E_{veto}<5.68$ TeV, Highest: $5.68<E_{veto}<7.0$ TeV.

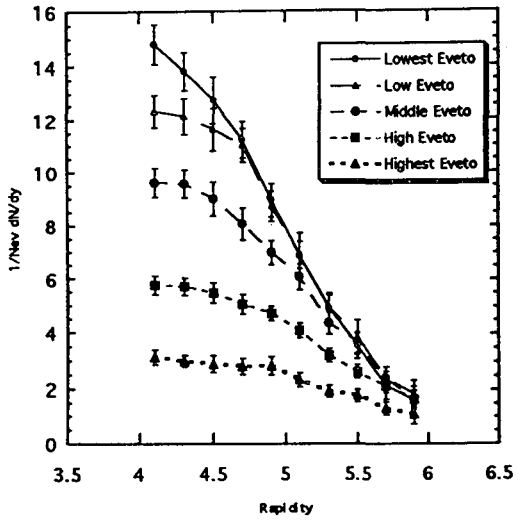

Fig. 2. Rapidity distributions for negative hadrons. Shown are the TPC 200 GeV/A S+Au data for the five E_{veto} regions.

Stopping in Central 200 GeV/A S+Au Collisions.

J. T. Mitchell and the NA35 Collaboration

Positively and negatively charged hadrons have been measured with the NA35 Time Projection Chamber (TPC). The TPC was positioned with the beam passing through its center in order to measure protons with rapidity greater than 3.5. The central event trigger selects the upper 6% of the interaction cross section by examining the amount of energy deposited into a calorimeter covering angles less than 0.3 degrees about the beam axis.

Representative "proton" spectra are obtained by subtracting negative hadron transverse mass ($m_t=(p_t^2+m_0^2)^{1/2}$) distributions from positive hadron distributions as a function of rapidity. The rapidity is calculated assuming the proton mass. The distributions are corrected for the detector geometrical acceptance, for the two-track resolution of the TPC, and for the kaon and electron contamination as estimated by the model VENUS 4.02. The resulting spectra are fit to the function:

$$f(m_t) = A \exp(-m_t/T);$$

where T is referred to as the inverse slope parameter. The extracted "proton" inverse slope parameters are plotted as a function of rapidity in Figure 1, showing a significant decrease as the rapidity increases. VENUS predicts a similar trend.

The rapidity distributions, dN/dy, are obtained by integrating the fitted curves over the entire transverse mass range. The resulting distribution is shown in Figure 2. Again, VENUS agrees well with the data.

An informative observable to quantify the "proton" rapidity distribution in terms of stopping is the mean rapidity shift of the projectile protons, $\langle\Delta y_p\rangle$, from their original beam rapidity. The larger this value, the more the system has stopped. Extrapolating the "proton" dN/dy distribution in Figure 1 until its integral equals the original 16 protons gives $\langle\Delta y_p\rangle=1.98\pm0.05$. This large value is suggestive of a high degree of stopping in these collisions. For more information, refer to the reference[1].

Footnotes and References

[1] J. T. Mitchell, et. al., Nucl. Phys. A566 (1994) 415c.

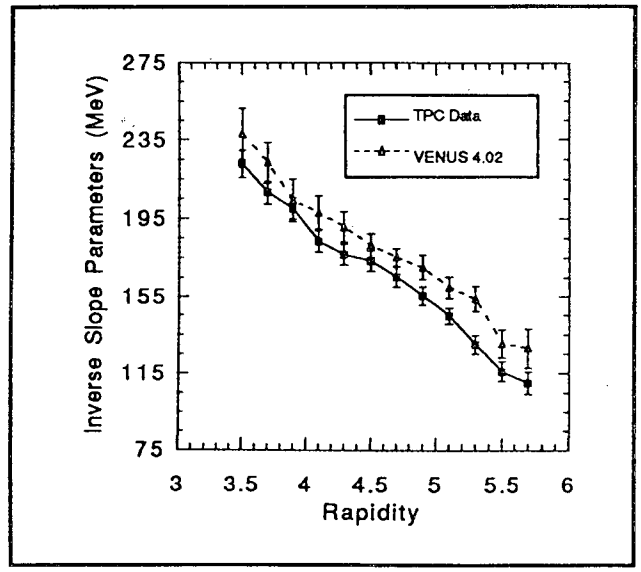

Fig. 1. Inverse slope parameters for positive minus negative hadrons as a function of rapidity.

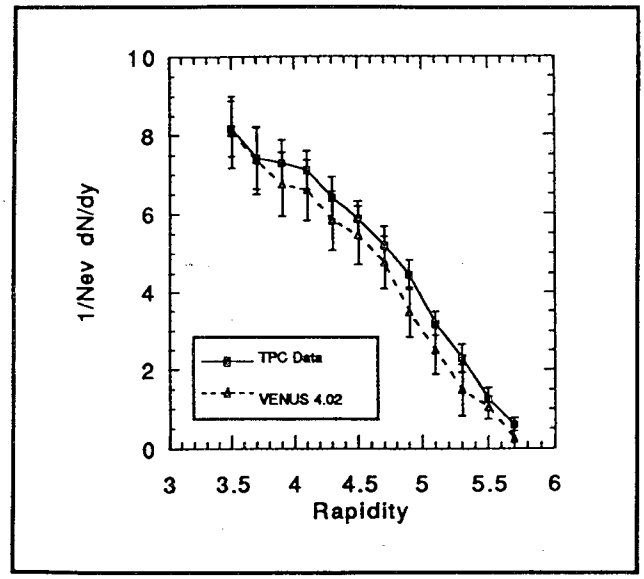

Fig. 2. Rapidity distribution for "protons". Shown are the TPC 200 GeV/A S+Au data and VENUS 4.02 predictions.

Transverse Momentum Dependence of Bose-Einstein Correlations at 200 GeV/nucleon

Richard J. Morse and The NA35 Collaboration

During the Spring 1992 running period at CERN, the NA35 TPC was used in order to collect a central collision data set of E/A=200 GeV S + A reactions. Negative hadrons falling between rapidities 3.6 and 4.6 and p_Ts of 0.1 and 0.6 GeV/c were subjected to a two-particle correlation analysis in order to deduce the p_T evolution of the transverse and longitudinal dimensions of the source of pion production in search of signatures of collective expansion.

In terms of the evolution of R_{long} with p_T, for all three systems we see a distinct and significant trend in which R_{long} decreases with p_T. This evolution of R_{long} with p_T is consistent with predictions of a scaling hydrodynamic expansion description of the particle production process[1].

More interesting is the observed evolution of the so-called sideward component of the correlation function; this is presented in Fig. 2. Note that as the target mass increases and the statistics improve, the significance of the decrease of R_{tside} with p_T increases. This type of behaviour is not unknown in relativistic heavy ion collisions and has been predicted as indicative of a system undergoing collective transverse expansion[2].

In order to try and understand these data in the context of a picture at the opposite extreme from a thermal model, we have adopted the microscopic phase space approach RQMD[3] in combination with a Wigner function formalism[4]. The result of these calculations is presented along with the data in Fig. 1 and Fig. 2. Note that the calculations do a reasonable job of reproducing the evolution of R_{long} with p_T. However the RQMD model, with no a priori transverse expansion mechanism and collectivity only at the level of reinteraction of secondaries and constituent quarks with the medium, essentially fails to reproduce the weak decrease of R_{tside} with p_T.

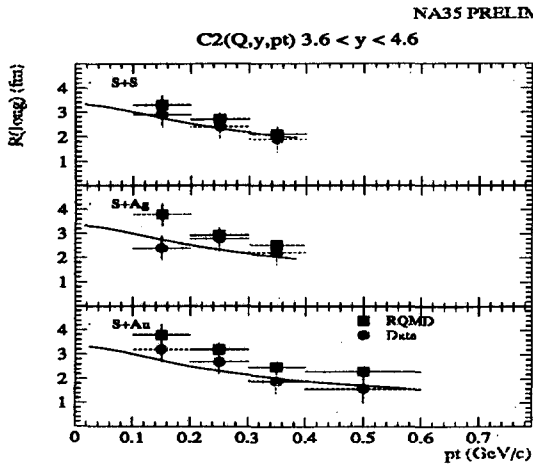

Fig. 1: This figure shows the dependence of the longitudinal source radius (in Fermi) pair transverse momentum.

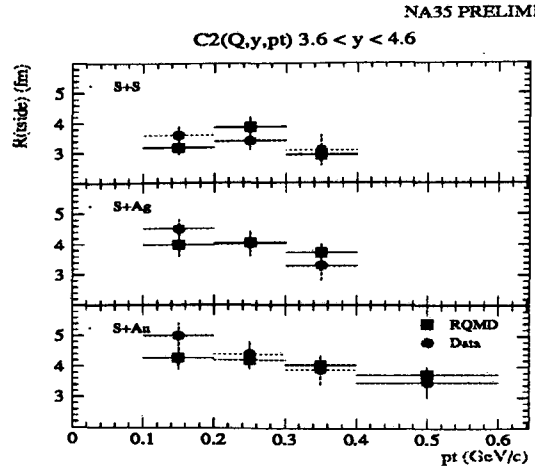

Fig. 2: This figure shows the dependence of the transverse source radius (in Fermi) pair transverse momentum.

Footnotes and References

[1] B. Lörstad and Yu.M. Sinyukov, Phys. Lett. **B256**, 159 (1991).

[2] S. Pratt, Phys. Rev. **D33**, 1314 (1986).

[3] H. Sorge, H. Stöcker, and W. Greiner, Nucl. Phys. **A498**, 567 (1989).

[4] S. Pratt, T. Csörgő, and J. Zimányi, Phys. Rev. **C42**, 2646 (1990).

K^- production in central S + Ag collisions at 200 GeV/nucleon.

S. Margetis, P. Jacobs and the NA35 Collaboration

Charged kaon decays were detected in the NA35 experiment's Time Projection Chamber (TPC) through their characteristic one prong decay. The acceptance of the TPC is complimentary to that of the Streamer Chamber (SC) and covered 1.5 units of rapidity starting around mid-rapidity. Background contamination was suppressed by applying cuts in the observed decay angle.

Central S+Nucleus collisions were selected according to the energy deposited in the veto calorimeter ($\theta < 0.3°$). About 30000 events were processed and about 2500 K^- candidates were reconstructed. K^+ reconstruction is underway. The reconstruction efficiency was calculated by generating raw data from Monte Carlo events processed with the GEANT simulation package of NA35, which were then analysed the same way as the data.

Figure 1 shows the p_T distribution of K^- data in the rapidity interval $2.5 < y < 3.5$ together with a fit to the function:

$$(1) \qquad dN/dp_T = C \cdot p_T \cdot exp(-m_T/\mathrm{T})$$

where the factor C was normalized to the observed number of particles in the measured p_T interval. The slope parameter T was found to be 184±13 MeV. Integrating the normalized function (1) over all p_T values resulted in the number of particles in the corresponding rapidity interval.

Figure 2 shows the rapidity distribution of K^- as measured in both, the SC (filled points)[1] and the TPC (open points). We observe that both distributions (S+Ag and S+S) peak around the *c.m.* rapidity which is 2.7 for S+Ag and 3.0 for S+S. This suggests 'central' production for the K^- particles which, unlike the K^+, do not have any 'associated production' channel available. We also observe that the two distributions show a similar trend beyond rapidity $y = 3$, which suggests a target independent production of this species in the projectile fragmentation region. A more detailed discussion of the strangeness data measured in NA35 can be found in [1].

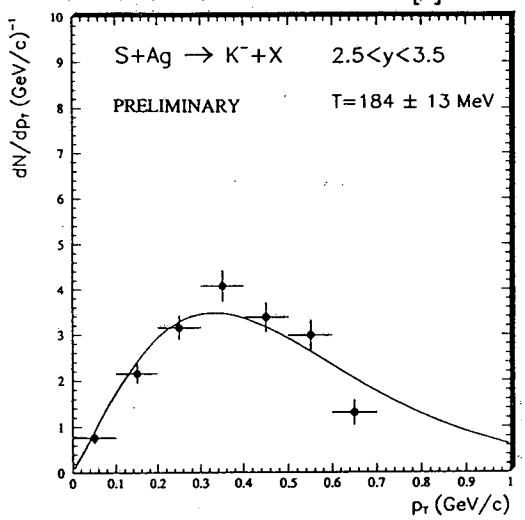

Figure 1. The p_T distribution of K^- in S+Ag central collisions.

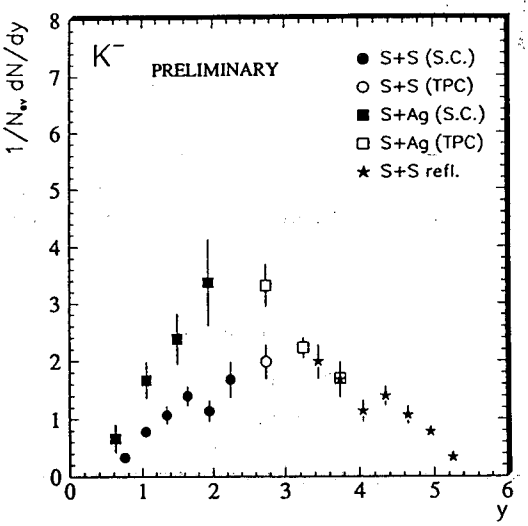

Figure 2. The rapidity distribution of K^- in S+Ag central collisions as measured in the SC and the TPC.

Footnotes and References

[1] T. Alber et. al., submitted to Z. Phys. C

GNA49: A GEANT Simulation Package for the NA49 Experiment

P. Jacobs and the NA49 Collaboration

GNA49 is a general Monte Carlo simulation package for the NA49 experiment, based on the GEANT simulation program written at CERN. GNA49 is intended to be used for a variety of purposes: experimental design, simple physics investigations (e.g. acceptances), simulation of detector response for development of tracking algorithms, and detailed, realistic calculations for physics analysis including all known backgrounds. It incorporates a detailed model of the geometry and materials of the NA49 experiment, comprising the sensitive detectors, a detailed magnetic field map for accurate tracking, and all significant material (such as magnet iron) that may contribute to the signals in the detectors. A mechanism has been introduced to permit accurate tracking of low energy electrons within the TPCs (down to a few KeV), which may both distort charge clusters significantly and deposit considerable charge in the TPCs. All major physical processes that may occur in the setup are modelled in detail by GEANT.

GNA49 utilizes the Zebra interface to event generators and the namelist input mechanism for geometry definition developed for the STAR GEANT. In order to reduce the volume of the output of simulated data, a mechanism has been introduced that suppresses recording of (uninteresting) intermediate tracks generated in electromagnetic and hadronic showers that do not generate hits in the sensitive detectors. Following the development for STAR, input events from the event generator are broken up into "chunks" of manageable size which are written out as separate events. This is necessary because of the enormous multiplicity generated in the central collisions of very heavy ions that will be studied by NA49.

A general analysis shell, called GNA49_ANA, has been written to reassemble the "chunked" subevents output by GNA49 into a complete event and present it in structures for further physics analysis. The track, vertex and hit structures originated in GNA49_ANA have been adopted as the Monte Carlo analysis structures used generally by NA49.

GNA49 and GNA49_ANA are currently being used to develop tracking algorithms for the Main and Vertex TPCs, to design the Time of Flight array, and to investigate the physics capabilities of NA49.

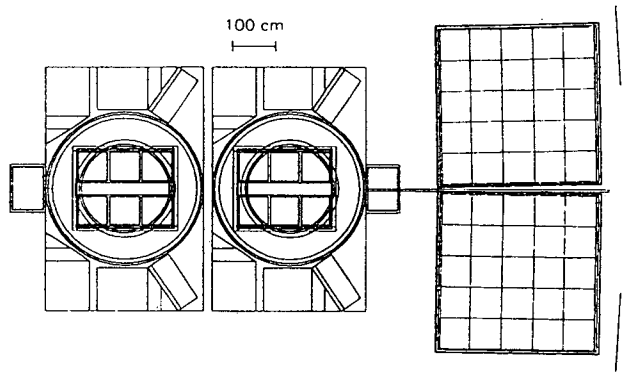

Fig. 1: GNA49 layout of NA49

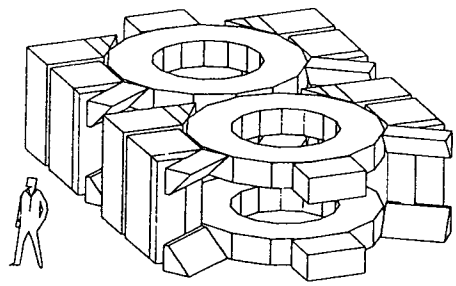

Fig. 2: GNA49 model of magnet coils and iron

Simulations of the NA49 Main TPC Environment

Milton Toy, Peter Jacobs, and the NA49 Collaboration

Central lead-lead collisions will create high multiplicities in the NA49 experiment, particularly in the Main TPC (MTPC) where there will be a substantial amount of charge deposited into the chamber volume. A track may not be accurately reconstructed if some of its charge clusters merge with those from neighboring tracks, due to the large uncertainty in the positions of the hits contained within the clusters. In addition, these clusters can not be used as part of a dE/dx measurement.

The NA49 Monte-Carlo simulator, GNA49, was run using FRITIOF-generated central Pb-Pb events at 160 GeV/A to produce space point hits based on the crossing of tracks with the pad rows. For a typical event, there were 950 tracks accepted into the MTPC, of which 660 were from the primary vertex. The creation and detection of charge clusters was handled by an external fast simulator which took a hit as the center of a cluster and parameterized the variance of the measured charge distribution by a pad response function based on a formulation developed by PEP4 and ALEPH[1]. This function takes into account several factors that determine the cluster size, such as diffusion and geometrical effects due to the crossing angle of the track relative to the pads and sense wires. The amount of ionization contained in a cluster was directly related to the energy loss given for the hit by GNA49, which averaged 1.4 keV/cm for a fill gas of $NeCO_2$.

Figure (1) shows the number of clusters per centimeter per padrow in the MTPC summed over the drift direction, as well as the number of merged clusters and clusters due to background processes such as hadronic showering in the magnet iron and support structures. While these background tracks produce on average 26% of the hits in the MTPC, their contribution to the number of merged hits is not significant compared to the case of two close primary tracks which create doubly ionizing track segments. The number of merged clusters is greatest in the pad rows adjacent to the beam, where up to 25% of the hits are merged.

Figure (2) shows a plot of the distance between all hits and merged hits. Clusters with a large width or low charge density may merge even when separated by several centimeters, but the majority of merged hits are within one centimeter. Based on the distance where two hits have at least a 50% chance of merging, the two track resolution is 8.5±0.5 mm.

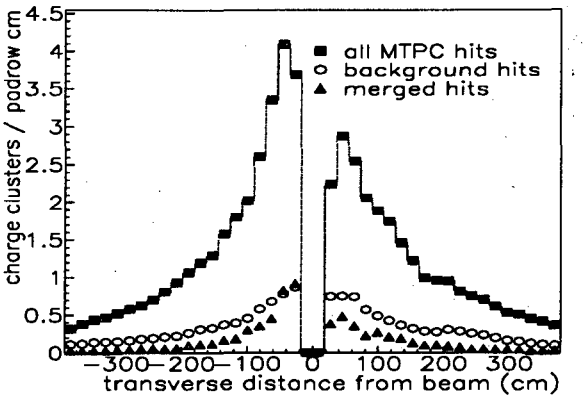

Figure 1: MTPC clusters per centimeter

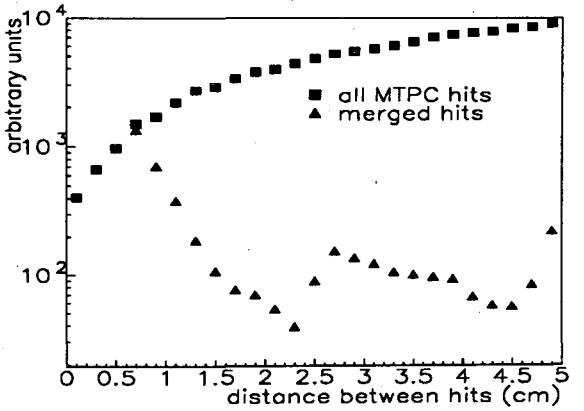

Figure 2: Distance between clusters

Footnotes and References

[1] R. Sauerwein, TPC-LBL-83-18, ALEPH Handbook, ALEPH 89-77

Integrated Preamplifier-Shaper for STAR and NA49

P.J. Barale, F. Bieser, W.E. Hearn, E.L. Hjort, P. Jacobs, S.A. Kleinfelder, M.A. Lisa, T.L. Noggle, A.M. Poskanzer, H.G. Ritter, C.Q. Vu, H.H. Wieman, M.E. Wright

The STAR central TPC and the NA49 TPCs need low noise, low power consumption, compact front-end electronics for readout of the pad signals. Following the example of the EOS TPC[1] all signal processing devices (preamplifier, shaper, analog store, and ADC) are mounted on the pad-plane and digitized and highly multiplexed signals are shipped off the detector with optical fibers. The essential components of the front-end electronics are two custom designed integrated circuits, a preamplifier/shaping amplifier and an analog-store/ADC[2] circuit. Both ICs have 16 channels. A front-end electronics card services 32 pads and thus consists of 2 shaper ICs and two analog store/ADC ICs.

The shaping amplifier consists of several stages: an integrating preamplifier, that is reset for each event, two two-pole integrators, a differentiator, and a fast operational amplifier.[3] The integrated circuit is fabricated in the Orbit CMOS p-well, 2 micron, 2 poly, 2 metal process.

Uniformity of time constants for all channels is an important requirement for TPC electronics. A variation of less than 5% over all channels is required for our application. Because of the tolerance of on-chip capacitors and resistors, provision is made for fine-tuning the peaking time by means of a three-bit binary code. All RC networks have identical values for R and for C and are tuned by switching in padding capacitors. The tuning range is about ±20% and tuning is accomplished during chip test by the burning of on-chip fuses.

The anode pad response is dominated by the slow drift of positive ions. Integration leads to a monotonically increasing pulse shape that makes a gaussian-like output pulse shape difficult to achieve. Great care has been taken to compensate for this long time constant tail in order to avoid pile-up effects for pulses that are later in time.

Several prototype versions have been produced and tested. The parameters of the integrated circuit are listed in Table 1. About 150,000 channels of preamplifier-shaper ICs have been produced and packaged for NA49. The version that will be used in STAR is undergoing an additional round of modifications.

References

1. G. Rai, A.A. Arthur, F. Bieser, C.W. Harnden, R. Jones, S.A. Kleinfelder, K. Lee, H.S. Matis, M. Nakamura, C. McParland, D. Nesbitt, G. Odyniec, D. Olson, H.G. Pugh, H.G. Ritter, T.J.M. Symons, H. Wieman, M. Wright, and R. Wright, IEEE Trans. Nucl. Sci. 37, 56 (1990).

2. S.A. Kleinfelder, IEEE Trans. Nucl. Sci. 37, 1230-1236 (1990); O.B. Milgrome and S.A. Kleinfelder, IEEE Trans. Nucl. Sci. 40, 721 (1993).

3. W.E. Hearn and M.E. Wright, LBL-33594.

Tables

Channels	16
Noise	800electrons rms @ 20pf
Gain	50mV/fC
Gain variation	±3%
Output level	-2V
Peaking time	180ns
Variation of time constants	±5%
Non-linearity	<2%
Cross talk	<1 part in 250
Tail correction	<0.5% @ 1 μs
Power consumption	<100mW per channel

Tab. 1. Performance parameters for the preamplifier-shaper.

Charged Particle Tracking in the STAR TPC

I. M. Sakrejda, J. T. Mitchell, and the STAR Collaboration

The Relativistic Heavy Ion Collider environment presents a unique challenge for charged particle tracking in the STAR TPC. These collisions will produce high charged particle densities (several thousand tracks per event), a large number being low momentum particles. This problem is being tackled with a tracking algorithm that is based on that used by the ALEPH TPC and subsequently refined for heavy ion collisions with the CERN NA36 TPC. A description of the algorithm currently used for the STAR TPC tracking follows.

Tracks are recognized in the TPC using what can best be described as a follow-your-nose method. The tracks are first constructed as 3-point links starting from the outside of the chamber, where the track density is the lowest. These base 3-point links are next extended inwards towards the center of the TPC. This extension is facilitated by a conformal map transformation that converts the helical particle trajectories into a space where the trajectories are linear, and a linear extrapolation can be used. If a point lies within tolerances of the extrapolation, it is added to the growing track segment.

Once a set of segments is found, a helix is fit to each segment in two components. One component is a circle fit of the helix projection to the bend plane, the other is a linear fit in the s-z plane, where s is the track length and z is the coordinate along the beam. With the resulting helix fit parameters, an attempt is made to improve or extend the track segments by associating points that lie within tolerances of the helix that were not attached using the linear extrapolation. This procedure begins with the longest segment and works down to the shortest segment. When a point is assigned to a segment, it is removed from the set of points considered for track association and the segments helix parameters are redetermined.

In some cases, the procedure outlined above produces more than one segment belonging to the same particle track. This is a problem particularly for low momentum tracks, which tend to spiral through the TPC. Therefore, track segments are further merged by comparing the helix parameters of the segment list as a final step.

The STAR TPC tracking is currently 87% efficient in tracking simulated central Au+Au events generated using the HIJING model. This value is valid in the range p_t>200 MeV/c and $|\eta|<1$. As an illustration, Figure 1 shows a sample set of hit points (top) along with a subset of associated points and their helix fits determined by the tracking program (bottom).

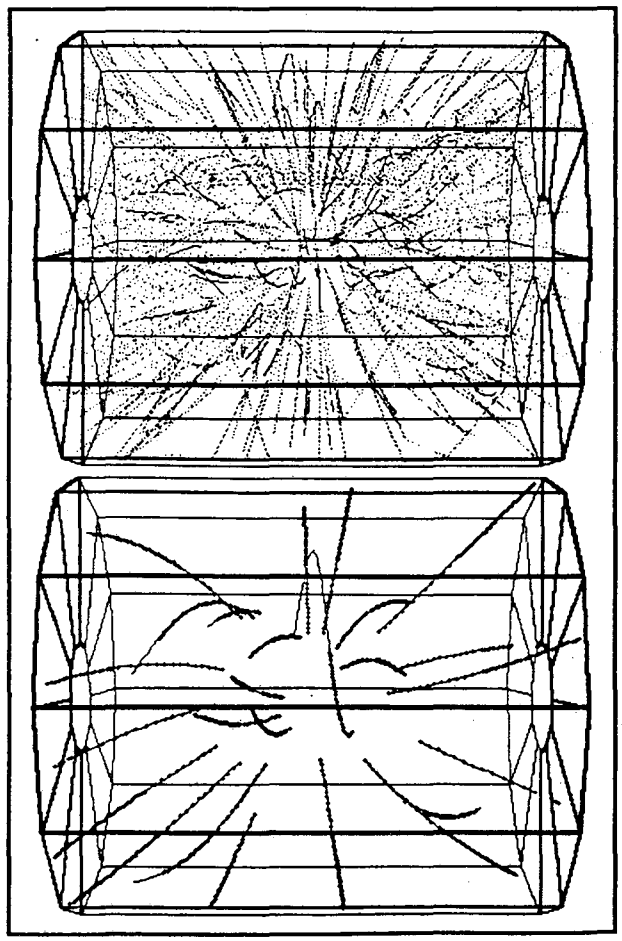

STAR TPC Tracking Capability in High Multiplicity Events

P.G. Jones and the STAR Collaboration

Considerable uncertainty prevails in the estimates of the charge particle multiplicity that will be encountered in central Au+Au collisions at RHIC. The main issue, as it pertains to STAR, is whether the TPC is able to cope with charge particle densities that exceed $dN/d\eta = 1000$ charged tracks. A simulation was carried out to determine the TPC track reconstruction efficiency and momentum resolution for events of very high multiplicity, assuming two different TPC gas options (P-10 and He-Ethane(50:50)).

In this study, events up to approximately $dN/d\eta = 4000$ have been generated by overlapping multiple central HIJING[1] events. These events have been filtered by the STAR GEANT program and the TPC Fast Simulator (TFS), with full accounting for secondary interactions and particle decays. Single events, corresponding to x1, x2 and x4 pseudorapidity density HIJING central Au+Au, have been tracked using the TPT track–following algorithm. When calculating the efficiency, it was required that there be at least 5 space points available for reconstruction, that the track be primary, and that a given Monte Carlo track is a dominant contributor to one and only one reconstructed track. Due to the number of merged hits it was decided to ignore the inner sector completely in the tracking procedure for the x4 event.

The results of this study[2] are collected in Tables 1 and 2. A reasonable track reconstruction efficiency is found even for x4 events, though at the expense of a considerable degradation in momentum resolution. It was found that as the track density increases the number of available unmerged hits decreases significantly. However, the distribution in the number of hits on reconstructed tracks follows this distribution quite closely. It would appear that only the unmerged hits close to the true track trajectory ultimately reside on reconstructed tracks. Merged hits will in general appear shifted from the track in the direction toward a neighboring track. Such hits often do not lie on either track (in the case of two-track merged clusters).

The He-Ethane gas does not appear to benefit track reconstruction considerably for high multiplicity events, compared to P-10. However, some attention should be given to the assumptions employed in TFS, especially those dealing with hit merging. Furthermore, even a slight improvement in cluster separation may yield significant improvements in the speed of track reconstruction, since the rejection of merged hits from track refitting accounts for most of the increase in CPU time spent in track reconstruction for the highest multiplicity events.

	x1	x2	x4
P-10	87	82	74
He-Ethane	91	84	81

Table 1: Track reconstruction efficiency (%) for primary tracks weighted by the transverse momentum distribution in the range $p_T > 200$ MeV/c and pseudorapidity $|\eta| < 1$.

	x1	x2	x4
P-10	1.5	1.6	4.0
He-Ethane	1.0	1.0	3.4

Table 2: Sigma of the momentum resolution (%) for primary tracks within the same p_T and pseudorapidity range.

Footnotes and References

[1] X.N. Wang and M. Gyulassy, Phys. Rev. **D44**, (1991) 3501.

[2] P.G. Jones, *STAR note #163.*

Charged Particle Identification in the STAR TPC

J. T. Mitchell and the STAR Collaboration

Charged particle identification in the STAR TPC will be accomplished by examining the energy deposited by the track as it traverses the gas in the TPC. The particle identification feasibility has been simulated using central Au+Au events generated with the HIJING model. The HIJING output is fed into GEANT to produce a set of hit points within the detector. GEANT uses the Urbán model [1] to assign an energy loss value to each point, thus producing a Landau distribution of energy loss values for the samples along the track. The GEANT information is subsequently input to the STAR TPC Fast Simulator (FST) [2], which simulates the TPC response and the hit reconstruction algorithm performance. The FST output then serves as the input for the pattern recognition program, which assigns each hit point to a track and determines the track momentum.

The dE/dx value for a track is calculated by first determining its track length over each pad that it traverses using the helix parameters of the track fit returned from the tracking algorithm. The dE/dx value for each point on the track is calculated using this information. Next, the points with the top 30% dE/dx values are eliminated from consideration. This effectively truncates the tail of the Landau distribution, leaving an approximate Gaussian distribution whose mean determines the dE/dx value of the track.

Particle identification can be realized by plotting the dE/dx value versus the momentum for each track. This plot is shown in Figure 1 for one central Au+Au HIJING event. This figure shows a clean separation of protons (*) from kaons (o) and pions (+) for momenta below 1.1 GeV/c. Kaons can be separated from pions below momenta of 0.6 GeV/c. Electron contamination is on the order of a few percent. The dE/dx resolution improves slightly when a 50:50 He-ethane gas mixture replaces P10 gas in the TPC.

Footnotes and References

1. GEANT, CERN Program Library W5013, p. 270.
2. STAR Conceptual Design Report, PUB-5347.

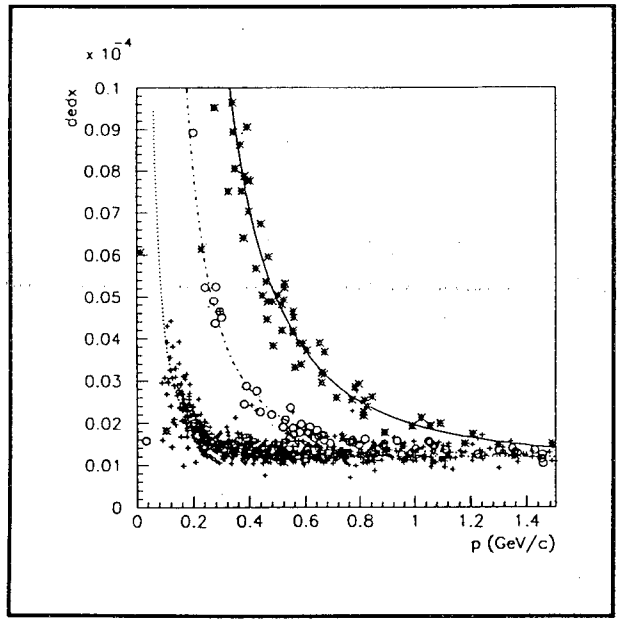

Fig. 1. Track dE/dx [GeV/cm] versus track momentum [GeV/c] for one central HIJING Au+Au event. * represents protons, o represents kaons, and + represents pions. The lines show the Bethe-Bloch curves for each particle species.

TSS: The STAR TPC Slow Simulator

R. J. Morse and The Star Collaboration

To date, all studies of the problems of pattern recognition/tracking, and spatial and momentum resolution in the high track density environment of the STAR TPC at the Relativistic Heavy Ion Collider (RHIC) have employed a parameterisation of the expected tpc pad response and cluster-finding/hit-recognition behaviour. Thus, the flow of these studies proceeds directly from Monte Carlo charged particle track crossings through tpc pad row volumes to reconstructed tpc hits.[1] In order to achieve a more realistic simulation of the response of the device and its event reconstruction software for alternative configurations of readout electronics (i.e. changing differentiation and integration constants, sampling frequency, and noise) and drift gases (i.e. changing drift velocity and transverse and longitudinal diffusion constants), it is necessary to perform a pixel data-level simulation; this must incorporate the geometry of the tpc pad plane in addition to the above parameters in order to yield pixel data which can be subjected to cluster-finding and hit-reconstruction analyses. This will permit realistic studies of the issues of two-track resolving-capability and dE/dx resolution as a function of fill gas properties and electronics characteristics which are necessary in order to fully optimize the design of the STAR TPC in order to achieve its physics goals. Hence, building upon earlier work[2], a so-called *slow simulator* for the STAR TPC has been implemented. As an example of the pixel data which has been simulated for the STAR TPC, we show the data from a $\sqrt{s}$/A=200 GeV Au + Au collision on a pad row approximately 60 cm from the interaction point. In Fig. 1, we see the plot of occupied pixels in the space of time bucket versus pad number while in Fig. 2 we see a the ADC spectrum on a single pad of the same row.

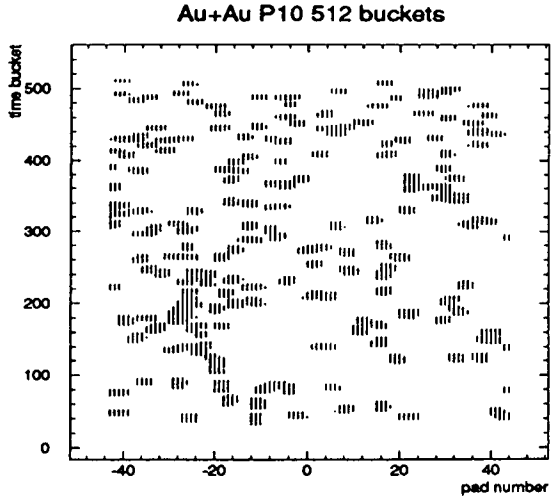

Fig. 1: This figure shows occupied pixels in time bucket versus pad number space for a pad row approximately 60 cm from the interaction point in a $\sqrt{s}$/A=200 GeV Au + Au collision.

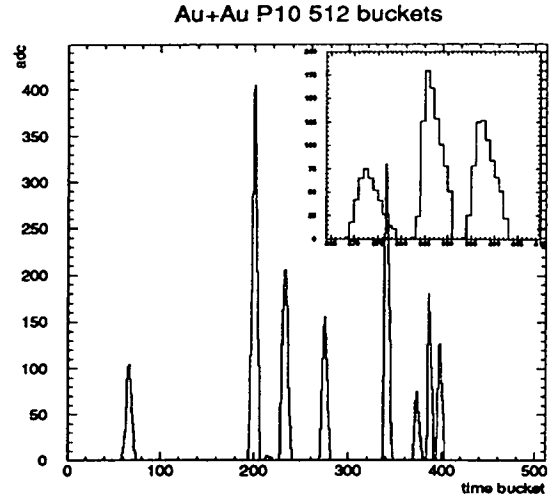

Fig. 2: This figure shows the ADC spectrum on a single pad from the preceeding figure.

Footnotes and References

[1] P. G. Jones, Star Note #163 (1994) and references therein.

[2] M. J. LeVine and D. Röhrich, proceedings of the STAR collaboration meeting (January 1992); Fancher and Schaffer, IEEE Trans. Nucl. Sci. NS26, 150 (1979).

TCL/TPH: The STAR TPC Cluster-Finding/Hit-Reconstruction

R. J. Morse and The Star Collaboration

At the front end of the analysis of the STAR TPC data stream it is necessary to have software which reduces the *event image*, in the form of charge deposited into pixels in the three dimensional pad, pad-row, and time bucket space, into reconstructed three dimensional space points or *hits*. The resulting space points can then be subjected to pattern recognition and track-fitting analyses in order to reconstruct the event kinematics. As an outgrowth of the design and evaluation of a pixel data-level simulation for the STAR TPC, simple prototype cluster reconstruction and hit reconstruction packages have been assembled. The algorithm of the cluster-finder, tcl, temporally sorts the pad *sequences* of occupied pixels presented by the data acquisition and then proceeds to assemble pad-contiguous sequences into *clusters*; the algorithm flags clusters containing sequences with multiple adc peaks for subsequent deconvolution of putative overlapping hits. The hit-reconstruction, tph, finds the center of gravity and longitudinal and transverse response of each cluster, and then improves upon the initial pad-dimension centroid and response width estimate using (for three pad hits) a three point-Gaussian hypothesis[1]; it then uses the appropriate TPC geometrical, drift gas, and electronics constants in order to convert these coordinates into space points. In the low multiplicity environment of $\sqrt{s}$/A=200 GeV p + p collisions, the cluster reconstruction efficiency of these simple algorithms is approximately 96%. In Fig. 1, we see the projection onto the TPC pad plane of the reconstructed hit coordinates for such an event. In Fig. 2 we see the reconstructed transverse and longitudinal pad response functions. Note the difference in the transverse response for the inner and outer pad rows reflecting the differing pad sizes, and that the transverse response from the slow simulator is consistent with earlier estimates of the transverse response expected from the STAR TPC[2].

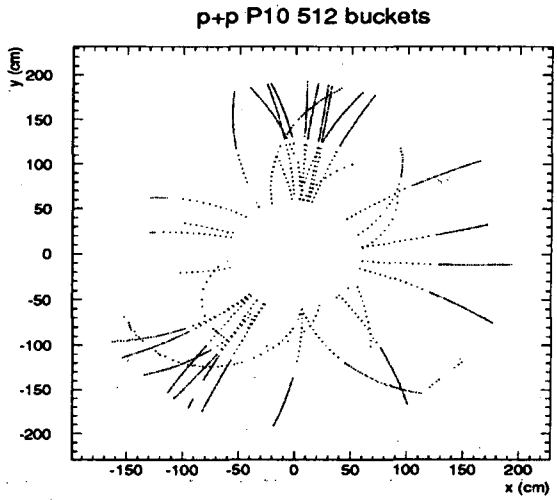

Fig. 1: This figure shows reconstructed hit coordinates from a simulated $\sqrt{s}$/A=200 GeV p + p collision.

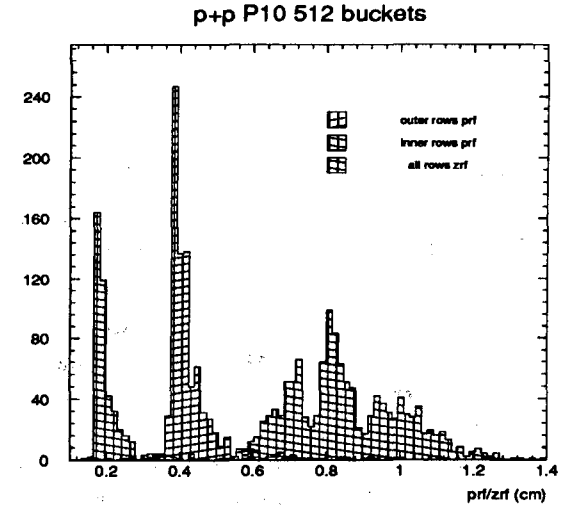

Fig. 2: This figure shows reconstructed transverse and longitudinal pad response functions from a simulated $\sqrt{s}$/A=200 GeV p + p collision.

Footnotes and References

[1]T. Pun and D. Schlatter, ALEPH-TPC-86-68 (1986); G. Lynch, TPC-LBL-78-17, (1978).

Footnotes and References

[2]P. G. Jones, STAR Note #33 (1992)

A Data Base for Tracking File Processing History

P. S. Gee, M. A. Bloomer, D. L. Olson and the STAR Collaboration

A Data File Manager is being developed for tracking all data files and their processing history for the STAR experiment at RHIC. It records the program and inputs used to generate each file, and has utilities to manage the possibly multiple file storage locations such as on disk and on tape.

The processing history of a data file helps to identify the initial conditions and program name and versions used to create the file. The initial conditions can include input files and job invocation script files. This information classifies the data files for retrieval purposes. For example, when new versions of software or new calibrations become available, the processing history helps to identify the data files that need to be reprocessed.

The information on the locations of a file facilitates efficient file retrieval. Possible locations for a file may include multiple locations on the same file system or different file systems. Other locations may include various kinds of near-line storage such as automatic tape libraries, or off-line storage such as removable tapes or disks. Knowing the location of the nearest copy of the file makes file retrieval faster and reduces load on the overall system.

The Data File Manager (DFM) tracks data files which result from simulation, detector calibration, data acquisition, and off-line event reconstruction. The simulation and run configurations, along with other parameters associated with the production of a data file, are also recorded.

The design goal of the Data File Manager is to maintain adequate information to answer the following types of questions:

1. What data files were generated based on a certain run configuration?
2. What was the run configuration used to generate a certain data file?
3. What are the possible calibration files to use for analysis of a group of events, using a given processing module?
4. What are all the ancestor files of a given file?
5. What are the locations of a file on disk and on tape?

The data base design must be consistent with the information being recorded. The DFM must provide interactive interfaces to query the data base. There must be a convenient way to populate the data base with accurate information.

A prototype of the DFM has been implemented using relational data base tables in an Informix database. A schematic of the core tables is shown in figure 1. In the diagram, the rectangular boxes represent relational data base tables. Arrows between boxes indicate references from one table to another. Fields of the table are written in the boxes. The '*' symbol after a field name indicates a primary key. The '#' symbol after a field name indicates a foreign key.

Two types of interfaces are provided for effective usage of DFM. The first is an interactive interface to allow query and modification of the data base by an interactive user. The second is DFM commands that can be included in job invocation scripts to take the relevant information to generate an SQL script. The SQL script can then be used to update the DFM data base.

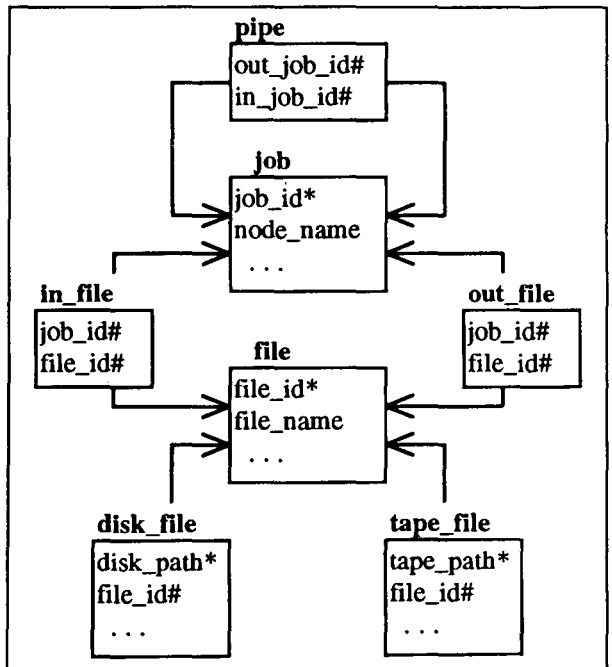

Figure 1: File Processing History

STAR TPC Sector Performance Testing

Eric Hjortt , B. Stringfellowt , Howard Wieman and the STAR Collaboration

The STAR TPC sectors are multiwire proportional chambers with pad readout. There are 24 sectors on each endcap of the TPC. Production of 24 inner and 24 outer sectors, along with spares, will begin in mid-1994. Using an outer sector production prototype and a partial inner sector we have studied sector performance.

A system for analyzing the performance of each sector has been developed at Purdue University using the outer sector production prototype. The system features 32 channels of readout electronics which use an integrated preamp/shaper chip similar to what will be used in the actual STAR front end electronics. A Macintosh computer running Labview software is used for data acquisition through a CAMAC crate. The system is capable of reading out the wire signals to measure gain as well as reading out the pad signals, and will be used to test each sector as it comes off the production line.

Long and short term tests of high voltage stability on the prototype resulted in some design changes in the production version of the sectors. However, we are confident that these problems, associated with anode voltage distribution circuits and not the wires themselves, have been solved. In addition, we will simulate the radiation levels expected at RHIC with a ^{90}Sr source. We have estimated the charge collection on the anode wires in the RHIC environment and found that our source can provide over 100 times that level. Each sector will be required to withstand this level without sparks or glow discharges.

Tests are in progress to determine whether or not the TPC performance may be improved by substituting a 50/50 mixture of He and Ethane for P10. The He/Ethane mixture requires that the anode voltage be about 200 Volts higher to achieve the same gain as P10. Our tests have shown that voltage stability scales with the gain, not the voltage, so we expect equivalent high voltage stability with He/Ethane. We have also studied the signal shapes produced by each of the gas mixtures. Preliminary results suggest that the difference is small enough that the same preamp/shaper electronics would suffice for either gas. Tests are in progress at Purdue to measure the longitudinal and transvers diffusion of the He/Ethane, and we are studying electron attenuation in He/Ethane here at LBL.

Due to size constraints at the edge of sectors the wires are held in place by a narrow (≈2mm) bead of epoxy. Slipping of the wires, which would reduce their tension cannot be tolerated. We have developed a method for measuring the tension of the wires in an assembled sector. The system uses a small jet of nitrogen to vibrate a wire. A laser focussed on the wire is reflected into a photodiode, and the resulting signal is Fourier transformed using a digital oscilloscope. The tension of the wire is found from the frequency of the first harmonic. This system can look through the upper planes of wires and measure the tension of the anode wires without making any physical contact with the wires themselves. We have not observed any decrease in tension in the 6 months since the outer sector prototype was built.

All materials exposed to the gas volume of the TPC are being tested for any outgassing which contaminates the TPC gas and results in a loss of electrons as they drift to the endcaps. The results of these tests are the flowrate of gas needed to maintain a given signal attenuation. By eliminating any materials which contaminate the gas we plan to be able to flow the gas through the TPC at a rate of one TPC volume every 10 days (≈3.5 l/m) while maintaining an attenuation of electrons over the 2 meter drift of less than 1%.

† Purdue University

Spatial Calibration of the STAR TPC with Photo-electric Wires

W.G. Gong, H. Wieman, G. Rai, M. Justice[1], D. Cebra[2], I. Huang[2], L. Wood[2], X.M. Chen[3], R. Dass[3], G.W. Hoffman[3], F. Moore[3], R. McGrath[4]

The traditional method for the spatial calibration of a TPC uses multiple laser beams to generate ionized tracks in the gas volume through two photon ionization. Past experience has shown difficulty in maintaining the stability of an optic path within 200 microns. For the STAR TPC, we has begun to explore a new approach which uses photo-electric wire arrays aligned along potential surfaces in the drift volume. Flushed with a diffused pulsed UV laser beam, photo-electrons are emitted from the wire surface. This approach will provide more stable, better positioned electron tracks. It may also be more economical and more effective than the traditional method.

To verify this approach, we have investigated the following issues: (1) what material can give high photo-electric efficiency and operational stability in the TPC gas environment, (2) how to position wires mechanically with precision and ease, and without undue complication, (3) how to deliver laser light uniformly into the TPC volume, (4) what can we learn from a test using the EOS TPC.

An ion chamber was built to measure photo-efficiencies with a Nd:YAG laser (λ= 266nm). Fig.1 shows measured photo-efficiencies for four representative materials in P-10 gas. Aluminum in a variety of forms (plate, wire, and aluminized-mylar foil) has the highest photo-efficiency measured in the gas. It shows stability against time and laser intensity. A conceptual design has been developed for the wire support system. A white plastic material, spectralon, has Lambertian reflectivity of 95% at λ = 266nm. It can be used for diffusing the laser beam inside the TPC volume. A special quartz fiber can be suitable for distributing the UV light from the laser to the TPC volume.

A test of photo-electric wires has been conducted in the EOS TPC recently. A few aluminum-alloy wires and aluminum-coated nylon line were strung in the equipotential plane of the field cage. A Cu sheet patterned with aluminized-mylar strip was used as the top drift plane. A spectralon reflector was placed inside the EOS TPC to diffuse the laser beam. Fig.2 shows a surface plot of electrons emitted from the top drift plane. The aluminized-mylar strip patterns were clearly visible although the light uniformity and delivery optics can be further improved. Since wires were initially placed at the same plane as the laser beam, electron signals from the wires were overshadowed by interferences arising from laser beam. Another test run is in progress after relocating the wires.

Footnotes and References

[1] Kent State Univ., [2] UC Davis, [3] Univ. of Texas, Austin, [4] SUNY Stony Brook.

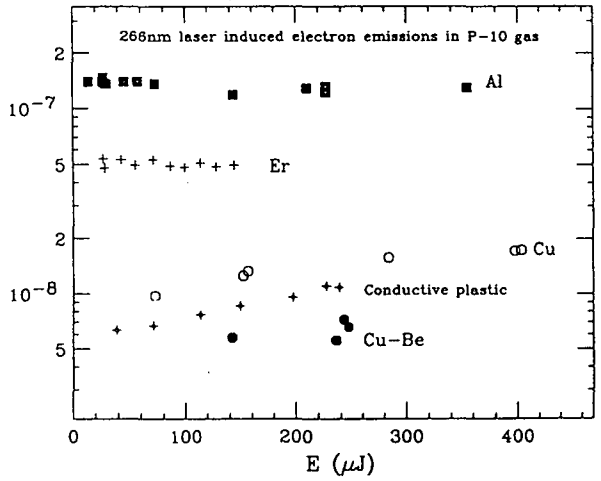

Fig.1: Measured photo-efficiencies of various materials in P-10 gas at λ= 266 nm as a function of the laser intensity.

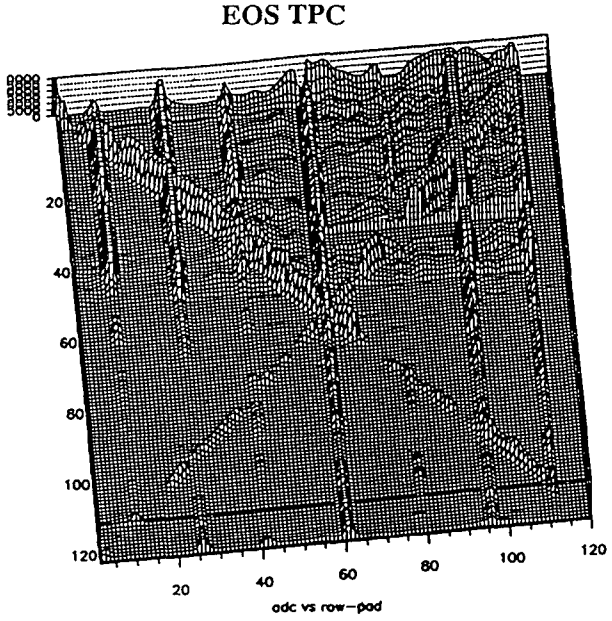

Fig.2: A surface plot of electrons emitted from a patterned plane inside the EOS TPC.

dE/dx information with the SVT in STAR

E. Paganis, S. Margetis and the STAR Collaboration

We present the first results of a feasibility study concerning the dE/dx capabilities of the Silicon Vertex Tracker (SVT) in the $1/\beta^2$ region. Only the SVT information is considered in this report, i.e. we did not use the TPC dE/dx information at all. Only tracks which crossed an active area in each layer were considered and a simple truncated mean result was extracted.

A knowledge of the mean energy deposited in the SVT could provide particle identification and assist tracking in the SVT (for low momentum tracks). Also during track matching between the SVT and TPC one could use the SVT together with the TPC dE/dx information to form an extra constraint.

We used a simple truncated mean method, which in this case is to take the average of the two (out of three) lower samples, although a more sophisticated maximum likelihood technique has been shown to give slightly better results[1]

We ran three central Fritiof RHIC Au+Au events to test the real performance of the dE/dx module. The particle separation is shown in figs. 1 and 2. In fig. 2 the particle population is shown for two different momentum ranges. The qualitative features of the previous figures are also seen here. As expected the number of pions is much higher than the other species. Given the anticipated momentum distribution of the different particle species (from Fritiof), the π/p separation is good over the whole pion momentum range (up to about 1 GeV). A very good mass separation is obtained for π/K up to about 450 MeV/c (fig.1), and p/K up to about 1 GeV/c. We also calculated the anticipated dE/dx resolution by taking a slice in momentum ($350 < p < 450$ MeV/c) and evaluate the ratio RMS/< dE/dx >. It is 14% which is in very good agreement with the calculations done in [1]. Further analysis is in progress.

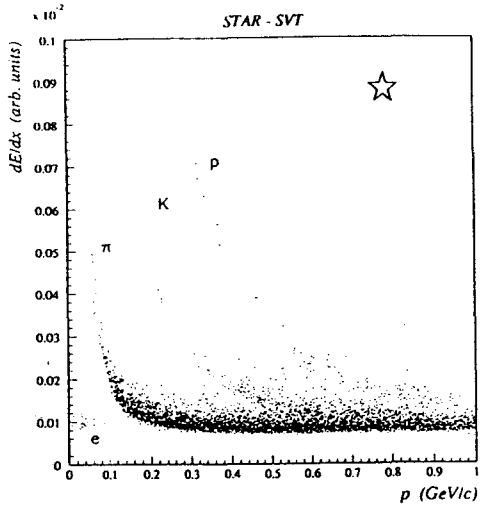

Figure 1. Energy loss spectrum for three Fritiof Au+Au events. Despite the very limited statistics, one can distinguish the dE/dx bands for the different particles. The particles at the lower left corner of the plot are δ–electrons.

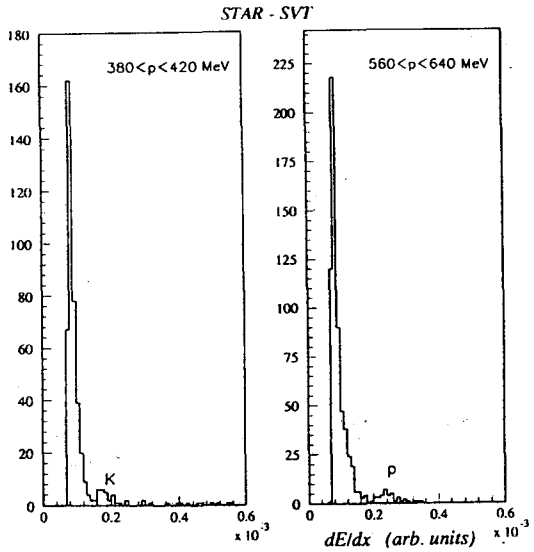

Figure 2. Energy loss spectrum for two slices in momentum taken from the previous figure.

Footnotes and References

[1] J. Cramer, SVT note and STAR CDR

P-type Silicon Drift Detectors for Tracking in High Energy and Nuclear Physics Experiments.

G.Odyniec, D.Lewak, C.J.Naudet, R.O'Donnell †, H.W.Rudolph, J.T.Walton †, N.W.Wang, and W.K.Wilson ††*

Silicon drift detectors (SiDD) were recently used in high energy fixed target experiments with excellent results. They provide both outstanding energy resolution and two-dimensional position measurements. So far, all SiDD's have been fabricated in national labs, using planar silicon micro fabrication technology on n-type high resistivity silicon substrates. Uniformity problems with high purity n-type silicon material have recently prompted our interest in SiDD's based on p-type substrates. A diagram of the cross-section of the p-SiDD that the LBL group has been working on is shown in Fig. 1. The device consists of parallel p-n^+ junctions (the cathodes) formed on both sides of a substrate of lightly doped (10^{12} cm^{-3}), ultra-high purity, p-type silicon. The cathodes are reverse biased to deplete the entire bulk of the detector and to create a uniform electric field in the direction parallel to the surface of the silicon. When electron-hole pairs are created by a particle passing through the detector, the electrons are swept out by the reverse biased cathodes, and the holes are focused down the midplane of the detector and drift toward the collecting electrodes (the anodes). The transit time of the holes allows the distance of the incident particle from the anode to be calculated. In a drift detector such as ours, which gives two-dimensional position information, the second position coordinate is obtained from charge division over the segmented anodes. The area of an individual anode is very small (250 μm pitch) to keep the output capacitance low. The charge pulses arriving at the anodes are amplified and sent to the readout system, then analyzed to calculate the position of the incident particle.

During the last ten months we fabricated and tested the first p-SiDD prototypes. Preliminary results show that the drift detectors are functioning; at this time, however, the drift distance is limited to a few millimeters. The goal is to extend the drift distance to 4 cm in the next 9-12 months.

Footnotes and References

* presently at JPL, Pasadena, CA

† Engineering Division, LBL

‡ presently at Wayne State University, Detroit

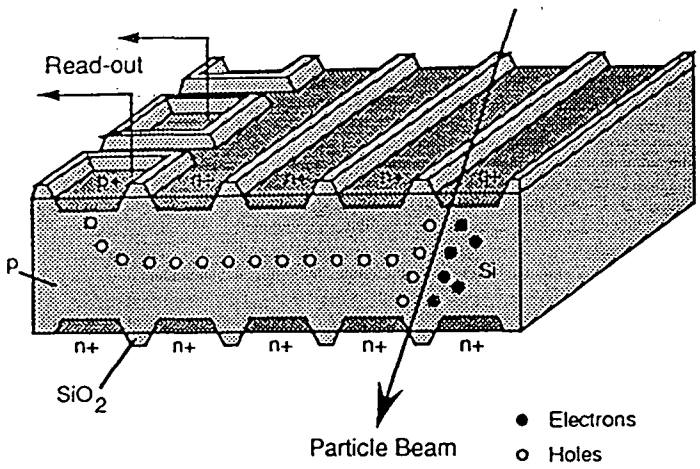

Fig. 1. Cross section of position sensitive p-SiDD. The holes and electrons created by the particle beam drift to the anodes, where they are collected.

Fabrication of P-type Silicon Drift Detectors.

N.W.Wang, D.Lewak, C.J.Naudet, R.O'Donnell †, G.Odyniec, J.T.Walton †, and W.K.Wilson ††*

Silicon Drift Detectors (SiDD's) are known for their excellent energy resolution and two-dimensional position measurement. Until now, all SiDD's have been fabricated on neutron transmutation doped, n-type silicon substrates. However, uniformity problems with high purity n-type silicon prompted our interest in SiDD's based on p-type silicon, and recently we fabricated and tested the first p-type silicon drift detectors. We have designed a set of masks for a p-SiDD using as a template the n-type SiDD masks developed by P.Rehak at Brookhaven National Laboratory (Fig.1). Our design retains the same number of cathodes and guard strips as the original Rehak design (333 cathodes and 83 guard strips). Cathodes are arranged in the active area with a pitch of 120 μm. The total length of the active area is 39.8 mm. In order to accommodate the guard structure, the length of the cathodes decreases towards the high voltage end. There are two lines of injector ports on our p-SiDD's. These injector lines contain sixteen 5x5 μm contacts to the p-SiDD substrate for calibration and electric testing of the detector. The p-SiDD has 178 anodes arranged with pitch of 250 μm (see Fig.1 from "P-type Silicon Drift Detectors for Tracking in High Energy and Nuclear Physics Experiments" in this report).

We have designed a process to fabricate SiDD's on p-type silicon that uses a simple double-sided alignment technique and a minimum number of mask layers (5, in our present design). Our fabrication procedure includes standard microfabrication processing steps (oxidation, ion implantation, photolithography, etching, diffusion, etc.). All these steps were performed in the new LBL Instrumentation Support Laboratory of the Engineering Division. The process is optimized to minimize leakage currents. One of the challenges of implementing SiDD's on p-type silicon is that the surface carrier population may be inverted by the presence of positive charge at the silicon/silicon dioxide interface, which results in large leakage currents. We developed a fabrication technique to prevent surface inversion: we have found that increasing the boron concentration at the surface above the boron concentration in the bulk effectively suppresses surface carrier inversion. However, the added surface layer of boron decreases junction breakdown voltages. Therefore, to reduce leakage currents, we have addressed both the problems of surface inversion and junction breakdown by testing different processing steps during fabrication and with numerical modeling.

Footnotes and References

* presently at JPL, Pasadena, CA

† Engineering Division, LBL

‡ presently at Wayne State University, Detroit

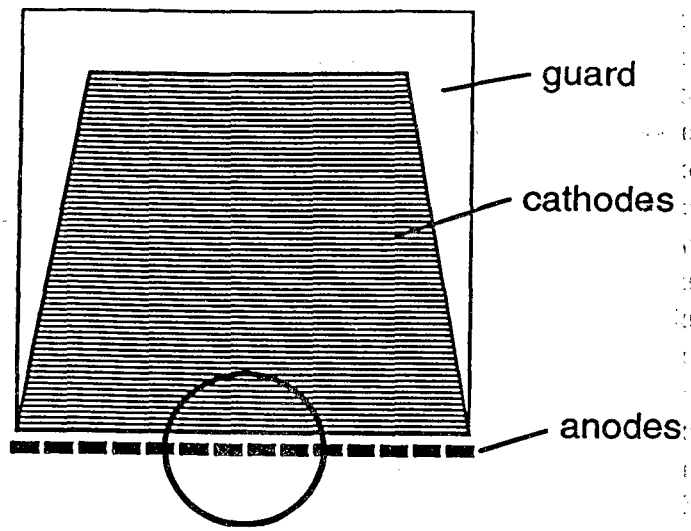

Fig. 1. Schematic of the top view of the p-SiDD. A magnified view (circled area) is shown in our other contribution to this report.

Studies of the Microstrip Gas Chambers*

W.G. Gong, H. Wieman, J.W. Harris, J. Mitchell

The Microstrip Gas Chamber (MSGC) has become an attractive choice for tracking applications which require high spatial resolution and high rate capability. Coupled to a Time Projection Chamber (TPC) as the readout device, the MSGCs can improve the spatial resolution when the transverse diffusion is not the dominant factor. The purpose of this project is to develop MSGCs suitable for a practical TPC readout.

The Microstrip Gas Chamber is built by using microelectronics technology. A typical structure of the MSGC is shown in Fig.1. Considerable efforts were made to master the microfabrication technique at the Berkeley Microfabrication Laboratory so that we can facilitate our R&D study and explore new fabrication approach.

MSGCs were constructed on a variety of substrates in order to address issues related to gain stability and packaging. Two types of glass were used, Corning C7740 and Schott S8900. Both the C7740 and S8900 glass have low resistivity which is necessary to reduces surface charge buildup that can affect the gas gain. An alumina substrates (Kyocera A201) was also investigated because ceramic packaging is widely used in the electronics industry, and construction of MSGCs on ceramics is a potential solution to the challenging problem of connecting high-density chambers to electronics.

A test facility was built for operating the MSGCs in Ar(90%)-CH_4(10%) gas with an ^{55}Fe x-ray source. MSGCs constructed on C7740 and S8900 glasses, and on ion-implanted A201 alumina substrate have been successfully tested. A pulse height spectrum taken with a ^{55}Fe x-ray source is shown in Fig.2 for a MSGC on S8900 glass. The energy resolution is 15% (FWHM) at the 6keV photo-peak. The gas gain ranged from 20 to 1000 when anode voltages varied from 360V to 530V. Exposed to a rate of 50000 x-ray photons/sec/mm^2, MSGCs constructed on C7740 and S8900 glasses were stable within 5% for several hours. The MSGC on A201 ceramics was less stable due to insufficient ion-implantations.

A new technique has been developed to control the resistivity of a substrate without using ion implantation. It is to coat a substrate with a thin film of S8900 glass by sputtering. We have obtained very good results on energy resolution and gain stability from a MSGC on quartz substrate coated with a thin film of S8900 glass.

Footnotes and References

* W.G. Gong, H. Wieman, J.W. Harris, J.T. Mitchell, W.S.Hong, V. Perez-Mendez, "Microstrip Gas Chambers on Glass and Ceramic Substrates", *IEEE Trans. on Nucl. Sci.*, Aug. 1994 (in print).

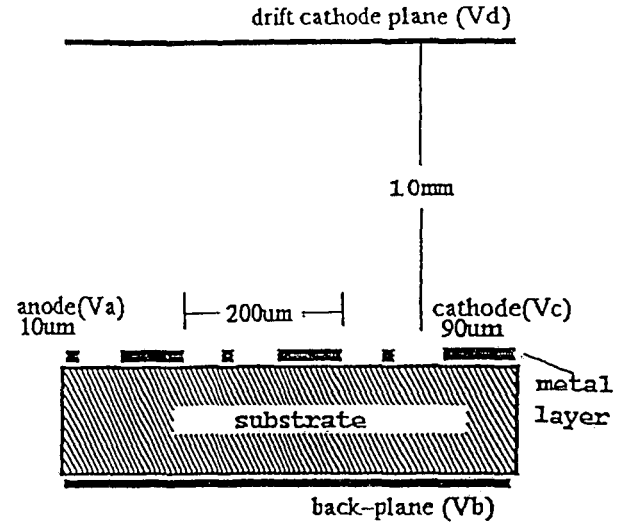

Fig.1: The structure of a MSGC.

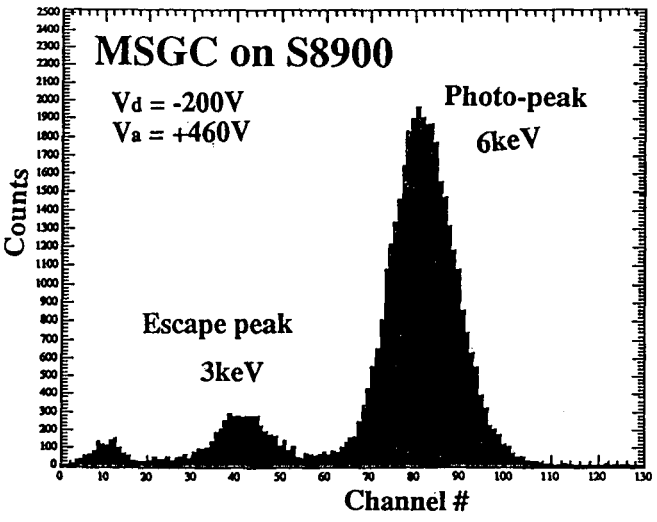

Fig.2: Pulse height spectrum for ^{55}Fe x-rays measured with a MSGC on S8900 glass.

The Micro Gap Chamber

W.G. Gong, H. Wieman, J.W. Harris

The microfabrication technology can bring in new ways to instrument gas counters. The Microstrip Gas Chamber(MSGC) has set an example in improving the spatial resolution and rate capability with respect to the conventional Multiwire Proportional Counter(MWPC). The Micro Gap Chamber[1] proposed recently by Bellazzini et al. shows that even better performance could be achieved by using the state-of-the-art fabrication technique. With our previous experiences gained in studying the Microstrip Gas Chamber, we set out to develop the Micro Gap Chamber.

The Micro Gap Chamber (MGC) is a miniaturized type of the Multi-Wire Proportional Chamber with the wires being replaced by thin-film strips (anode) and one cathode plane being replaced by a conducting layer (cathode) on a substrate. The anode and cathode are separated by a gap of 10 microns using high-quality insulator thin film. Fig. 1 shows a cross-sectional view of the Micro Gap Chamber we built at the Berkeley Microfabrication Laboratory. The Al anode strip has a width of 10μm, a thickness of 0.5μm, and a length of 2cm. The cathode layer is the low-resistivity Si wafer. The insulator strip has a width of 30μm, and a thickness of 2.5μm. It was prepared by the Chemical Vapor Deposition(CVD) and annealed at 850° to enhance its dielectric strength.

Because of the small gap between the anode and cathode, the electrical field strength is as high as a few million V/cm. To suppress the UV-photons generated during the avalanche process, a high proportion of quenching gas is called for. We could not operate our MGC in a gas mixture of Ar(90%)- CH_4(10%). We tried another gas mixture of Ar(60%)-DME(40%) which was used by Bellazzini. Though the DME gas is good quencher, it appeared that our premixed gas was not pure. No photo-peak for the 6keV x-ray from an ^{55}Fe source was observed. We finally used the Ethane gas as the quencher in both Ar(50%)-Ethane(50%) and He(50%)-Ethane(50%) mixtures and obtained good results.

Fig.2 shows the pulse height spectrum for ^{55}Fe x-rays measured in a gas mixture of Ar(50%)-Ethane(50%). The photo-peak and the escape peak were clearly resolved. The energy resolution is about 20% (FWHM) at 6kev.

The gas gain of our MGC is limited to about 1000. The energy resolution can still be improved. There is no segmentation in our cathode yet. Work to address these issues is in progress.

Footnotes and References

[1] F. Angelini, R. Bellazzini, A. Brez, M.M. Massai, R. Raffo, G. Spandre, and M.A. Spezziga, Nucl. Instru. Methods **A335**, 69(1993).

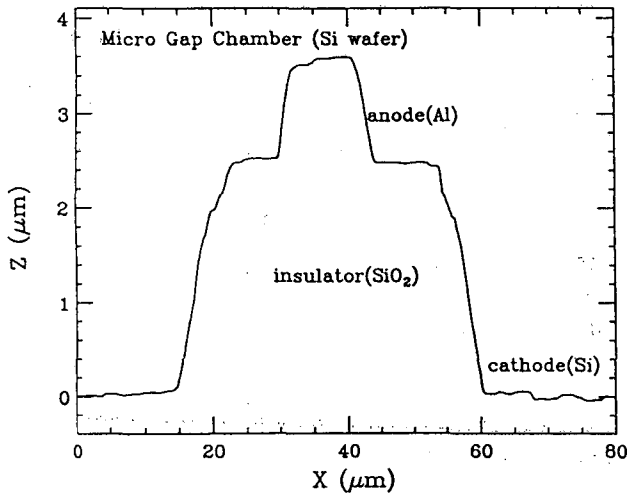

Fig.1: The cross-sectional view of a MGC.

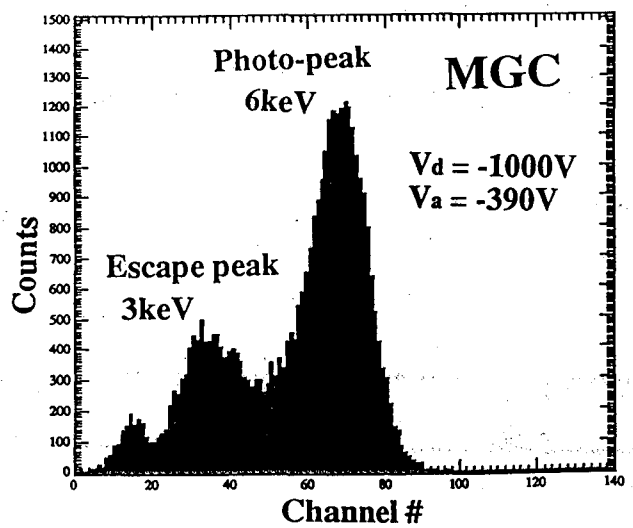

Fig.2: Pulse height spectrum for ^{55}Fe x-rays measured with a MGC in a gas mixture of Ar(50%)-Ethane(50%).

Nuclear and Electromagnetic Fragmentation of 2.25-TeV ^{197}Au Nuclei*

Y. D. He and P. B. Price

Until recently the heaviest projectile available at multi-TeV energies was ^{32}S at CERN. The present study of fragmentation of 2.25-TeV ^{197}Au ions was made possible both by the development of a Au beam at the Brookhaven AGS and by the development of BP-1 barium phosphate glass track-recording detectors with charge resolution $\sigma_Z \sim 0.1$ for nuclei with $Z > 60$.

In such an ultrarelativistic heavy ion collision, we focus on the problem of disentangling two modes of high-energy nucleus-nucleus interactions – a nuclear mode which takes place when a relativistic projectile and a target nucleus pass each other within the range of the strong force and an electromagnetic mode which occurs at larger impact parameters such that only the virtual photons from either the target or the projectile can interact with the other.

We report the first measurement of the total charge-loss cross section $\sigma_{tot} = \sigma_{em} + \sigma_{nuc}$ and partial cross sections (for $\Delta Z = 1, 2, ..., 9$) of 2.25-TeV ^{197}Au nuclei in various targets. The large Coulomb barrier for Au reduces the electromagnetic contribution σ_{em} in a Pb target to only 18% of σ_{nuc}, compared with $\sim$ 70% for 14.5 A GeV ^{28}Si and 120% for 200 A GeV ^{32}S.

With σ_{em} taken to be $\propto Z_T^{1.8}$, σ_{nuc} can be fitted with $\sigma_{nuc} = \alpha(A_P^{1/3} + A_T^{1/3} - b)^2$, with b = 0.83 and $\alpha = 59$ mb, essentially the same as found at energies of 1 to 2 A GeV. Electromagnetic partial cross sections for $\Delta Z = 1$ exceed $\sim$ 40 mb in the Pb, Sn, Cu, and Fe targets and are substantial for larger values of ΔZ in the heavier targets.

Our data show no evidence for a steeper dependence of charge-loss cross section than Z_T^2. This is not surprising. Because of the high Coulomb barrier of Au nuclei, we expect that neither double nor single electromagnetic excitation of the giant dipole resonance contribute to charged particle emission in Au.

*Condensed from a paper in *Z. Phys. A* **348** (1994) 105.

Observation of a New $I^G(J^{PC}) = 1^-(0^{++})$ Resonance at 1450 MeV*

K.M. Crowe, D.S. Armstrong, R. Bossingham, T. Case, F.H. Heinsius and the Crystal Barrel Collaboration

At present, it is far from clear whether or not the members of the lightest scalar meson nonet have been identified and understood. The two lowest-mass candidate states, the $f_0(975)$ and the $a_0(980)$, are well established from many experiments, but their properties are not easily reconciled with what is expected for conventional $q\bar{q}$ mesons. There has been much speculation that these particles, which have masses very near the $K\overline{K}$ threshold, are actually kaonic "molecules", *i.e.* $K\overline{K}$ bound states, or four-quark states, or other exotic states. Elsewhere in this annual report we discuss the identification of two isoscalar ($I = 0$) $J^{PC} = 0^{++}$ resonances with masses of 1365 MeV and 1520 MeV, which are also candidates for the scalar meson nonet. Here we present evidence for another new scalar meson, which along with these two isoscalar sates and the well-established $K_0^*(1430)$, could fill the scalar nonet, leaving the $f_0(975)$ and the $a_0(980)$ to be explained as exotics of some kind.

The data were obtained from a sample of proton-antiproton annihilations at rest leading to 6-photon final states. Kinematical fits were done to select the final state $\pi^0\pi^0\eta$, resulting in a sample of 2.80×10^5 good events, with a background estimated at less than 1%. The acceptance was flat over the Dalitz plot, except for a small ($\sim$ 2.5%) drop at the edges, and an acceptance-correction function, derived from Monte Carlo, was applied to the data to correct for this.

Two independent partial-wave analyses of these data were performed. The analyses differed primarily in the formalism used to treat the production amplitudes, however the resulting fits were of similar quality and the properties (masses, widths, amplitudes) of the resonances required to fit the data in both analyses were very similar, lending confidence in the rather model-independent nature of the results. One of the two formalisms was identical to the approach that we also used to fit the $\pi^0\pi^0\pi^0$ and $\pi^0\eta\eta$ final states, and here the parameters for the $\pi^0\pi^0$ and $\pi^0\eta$ S-wave were constrained to those extracted from that analysis.

The well-established resonances $a_0(980)$, $f_0(975)$, and $a_2(1320)$ were clearly identified in the Dalitz plot and required in the partial-wave analysis. The $f_0(1365)$ that we identified elsewhere was also required. In addition, a new isovector-scalar resonance, $a_0(1450)$, with a mass of (1450 ± 40) MeV and a width (270 ± 40) MeV, decaying to $\eta\pi^0$ was required to describe the data, contributing about 5% of the total strength in the $\pi^0\pi^0\eta$ final state.

In addition, some $\eta\pi$ P-wave is required in the fit. A resonance with these quantum numbers, *i.e.* 1^{-+}, could not be an ordinary meson. Such a state has been claimed at 1405 MeV and with a width of 180 MeV by the GAMS collaboration[1], however our data require a rather featureless, non-resonant $\eta\pi$ P-wave, and the data cannot be fitted with the GAMS parameters. A contribution to the $\pi\pi$ D-wave from the $f_2(1270)$ was allowed by the fit, but was not large enough to be considered as significant ($\sim$ 0.1% of the total strength). Finally, the fit was improved by adding a small higher-mass contribution to the $\eta\pi$ D-wave, at between 1600-1700 MeV and with a width between 180 and 250 MeV. However, this contribution was small ($\sim$ 1%) and the effect localized near the edges of the Dalitz plot, so we do not claim a new resonance there.

Footnotes and References

*C. Amsler *et al.*, accepted in Phys. Lett. B, May 1994.

Footnotes and References

[1] D. Alde *et al.*, Phys. Lett. B **205**(1988)397.

Observation of Two $J^{PC} = 0^{++}$ Isoscalar Resonances at 1365 and 1520 MeV*

K.M. Crowe, D.S. Armstrong, R. Bossingham, T. Case, F.H. Heinsius and the Crystal Barrel Collaboration

The Crystal Barrel Collaboration has undertaken a systematic study of proton-antiproton annihilations at rest using an external 200 MeV/c antiproton beam from the CERN Low Energy Antiproton Ring (LEAR). The main topic is the search for new resonances, especially non-mesonic states such as glueballs and quark-gluon hybrids. We have performed a coupled-channel analysis of $p\bar{p}$ annihilation into $\pi^0\pi^0\pi^0$ and $\eta\eta\pi^0$, where two $I = 0$ $J^{PC} = 0^{++}$ resonances with masses of 1365 MeV and 1520 MeV respectively are identified.

Previously we analyzed the two channels separately. In the reaction[1] $p\bar{p} \to 3\pi^0$, a $J^{PC} = 2^{++}$ state at 1515 MeV (width = 120 MeV), decaying to $\pi^0\pi^0$, was introduced in order to describe the experimental Dalitz plot. This resonance was identified as the AX particle previously discovered by the ASTERIX collaboration at LEAR. A surprisingly large fraction of P-wave initial states (60%) was required to achieve the fit.

In the reaction[2] $p\bar{p} \to \eta\eta\pi^0$ we found that the channel was dominated by an isoscalar 0^{++} resonance decaying into $\eta\eta$ with mass 1560 ± 25 MeV/c^2 and width 245 ± 50 MeV/c^2. Significant P-wave annihilation (12%) was required to achieve this fit.

In the new coupled-channels approach, we have fit the two Dalitz plots simultaneously without the assumption of any P-wave annihilation. The $\pi\pi$ S-wave was also required to fit the available low-energy phase shifts for $\pi\pi \to \pi\pi$. The resulting fits describe all the data with good χ^2, the parameters are consistent for all the resonances required, and the quality of the fits to $3\pi^0$ and $\eta\eta\pi^0$ are comparable to our earlier published individual fits to these Dalitz plots.

The significant differences with the earlier analyses are as follows: The $f_2(1515) \to 2\pi^0$ claimed in $p\bar{p} \to 3\pi^0$ is replaced by an $f_0(1520) \to 2\pi^0$ (width = 148^{+20}_{-25} MeV) which is also seen in its $\eta\eta$ decay mode in $p\bar{p} \to \eta\eta\pi^0$. This coupled-channel analysis modifies the $f_0(1520)$ mass and width somewhat from the values found earlier (mass = 1560 ± 25 MeV, width = 250 ± 50 MeV) from the individual fit to the $\eta\eta\pi^0$ data. It is now apparent that this resonance is not the same as the $f_0(1590)$ claimed by the GAMS collaboration (which has no significant $2\pi^0$ decay). Also, an $f_0(1365)$ (width = 268 ± 70 MeV) is required in both Dalitz plots, decaying to $\pi^0\pi^0$ and $\eta\eta$. This resonance is similar in mass and width to the $f_0(1400)$ listed by the Particle Data Group, however its large $\eta\eta$ decay is in contradiction to the PDG decay branching ratios.

A natural interpretation of $f_0(1365)$ would associate it with a $(u\bar{u}+d\bar{d})$ state in the same nonet as $K_0^*(1430)$. The $f_0(1520)$ could be assigned to the ninth member of the 0^{++} nonet. The observation of $f_0(1525) \to K_S^0 K_S^0$ with $\Gamma = 90$ MeV by the LASS group[3] would favor a mostly $s\bar{s}$ content. However, the branching ratios we obtain for $\pi\pi$ and $\eta\eta$ are close to those expected for $(u\bar{u} + d\bar{d})$. Another interpretation would be that the $f_0(1520)$ is a molecule associated to $\omega\omega$ and/or $\rho\rho$ thresholds, but the data rejects fitting the $f_0(1520)$ with a width for coupling to $\omega\omega$. The most interesting interpretation is that the $f_0(1520)$ is a glueball strongly mixed with $q\bar{q}$.

Footnotes and References

*V.V. Anisovich *et al.*, Phys. Lett. B323 (1994) 233.

[1]E. Aker *et al.*, Phys. Lett. B260 (1991) 249.

[2]C. Amsler *et al.*, Phys. Lett. B291(1992)347.

Footnotes and References

[3]D. Aston *et al.*,, Nucl.Phys. B296 (1988) 493; M. Baubillier *et al.*, Z.Phys. C17 (1983) 309.

Atomic-Force-Microscopic Study of Etched Nuclear Tracks at Extremely Short Distance Scale*

M. Drndic† Y. D. He, P. B. Price, D. P. Snowden-Ifft, and A. J. Westphal

We demonstrate that with an atomic force microscope it is now possible to scan and measure etched nuclear tracks due to highly charged ionizing particles for a sampling distance as short as ~ 0.5 μm at a density as high as $\sim 10^9$ cm^{-2}. Features of track cone measurements made with an atomic force microscope are presented in Table I in comparison with those made with an optical microscope. We listed the amount of material removed, G; attainable track density, ρ; parameters of etch pits measured; formula for detector signal, s; formula for detector sampling distance, L_s; and typical achievable charge resolution from one single measurement, σ_Z. Combining the data obtained with an optical microscope, we establish that charge resolution σ_Z varies with the sampling distance L_s as $\sigma_Z \propto 1/\sqrt{L_s}$ over more than two orders of magnitude in L_s, suggesting that the charge resolution is governed by intrinsic fluctuations in energy deposition. We found that at $L_s = 5$ μm, particles can be identified with $\sigma_Z = 0.3 - 0.4$. The results obtained in this work encourage us to believe that this novel technique will open a new regime for track-etch detectors with which a number of interesting topics can be explored. We point out four applications. The first would be its applicability to the study of heavy ion collisions where scans of high track densities are required. The second would be to measure etch cones due to low energy ions of few hundreds of keV in CR-39 plastic in order to study its response to ions in the low velocity ($\beta \leq 10^{-2}$) regime. The third would be the possible "dynamic" observation of the track-etch process in sequences of extremely short etches for different track-etch detectors. The fourth would be to observe fine-scale profiles of the walls of etch cones with the high spatial resolution of AFM.

Table 1: Characteristics of the optical microscopic and atomic force microscopic measurements of etch cones due to relativistic heavy ions.

features	optical microscope
G (μm)	$10 - 100$
ρ (cm^{-2})	$10^3 - 10^4$
parameter	semi-minor-axis, b
s	$\frac{(1+b^2/G^2)}{(1-b^2/G^2)}\frac{1}{\cos\theta}$
L_s	$\frac{s}{1+s\cos\theta}G$
σ_Z	$0.08 - 0.2$

features	atomic-force-microscope
G (μm)	$0.5 - 5$
ρ (cm^{-2})	$10^8 - 10^9$
parameter	depth, d
s	$(1 + d/G)\frac{1}{\cos\theta}$
L_s	sG
σ_Z	$0.3 - 0.8$

*Condensed from a paper in *Nucl. Instr. Meth. B* (1994) in press.

†On leave from Department of Physics, Harvard University, Cambridge, MA 02138.

Interactions of 11.4 A GeV ^{197}Au in Various Targets*

P. B. Price and Y. D. He

In experiment E882 at the Brookhaven AGS we studied projectile fragmentation of projectiles and their fragments with charge $68 \leq Z \leq 80$ with a resolution $\sigma_Z \leq 0.08$ charge unit. Using BP-1 phosphate glass track detectors interleaved with various targets, we have measured, for the first time, cross sections for interactions of 11.4 A GeV Au ions. These include: (1) nuclear and electromagnetic contributions to total and partial charge-changing cross sections; (2) nuclear charge pickup; and (3) total and partial charge-changing cross sections for interactions of secondary beams created in an initial target and studied in downstream targets. Perhaps the most surprising result is the very large cross section for fragmentation of secondary Hg nuclei created in charge pickup interactions of Au.

*Abstract of a paper in *23rd Intern. Conf. on Cosmic. Rays*, Calgary, Canada **2** (1993) 199.

First Measurement of Charge-Changing Cross Sections for 11.4 A GeV ^{197}Au in Various Targets *

Y. D. He and P. B. Price

Using a new type of phosphate glass detector with a remarkable charge resolution, we measured the cross sections for several interesting charge-changing interactions in peripheral collisions of 11.4 A GeV ^{197}Au nuclei with various targets, including nuclear charge pickup, nuclear spallation, and electromagnetic dissociation. We also measured the cross sections for fragmentation of secondary beams with $68 \leq Z \leq 80$.

*Abstract of a paper in *Nucl. Phys. A* **566** (1994) 363c.

Decreasing Inelasticity with Energy in pp Collisions*

Y. D. He

The energy dependence of inelasticity in the multiparticle production of high-energy hadronic interactions is studied. The similarity between multiparticle production in pp ($p\bar{p}$) and e^+e^- collisions leads to a complete picture of a universal hadronization process. Within this framework, the data of charged multiplicity at various collider energies are used to infer average inelasticity. The result shows that inelasticity in pp collisions decreases with increasing energy in the range of $\sqrt{s} = 5 - 900$ GeV. Consequences of the extrapolation of such a decreasing inelasticity to energies $10^{14} - 10^{18}$ eV as well as other model predictions in a series of cosmic ray experiments are also discussed.

*Abstract of a paper in *J. Phys. G* **19** (1994) 1953.

Apparent Binary Microscopic Response to Relativistic Ions of A Large Class of Track-Etch Detectors*

A. J. Westphal, Y. D. He, and P. S. Wojdowski

We find that a large class of glass track-etch detectors seems to behave in an extraordinarily simple way on microscopic scales in response to relativistic ions. The behavior of these detectors is consistent with binary, on-off behavior in response to restricted energy loss on microscopic scales, with the shape of the response curve as a function of Z/β on macroscopic scales determined solely by statistical fluctuations in energy loss. This model naturally reproduces the shapes of the response curves for a variety of detectors and etchants; it also correctly predicts the charge resolution of BP-1 glass and, with an additional hypothesis, the sign and magnitude of the registration temperature effect of BP-1. Several other materials, including at least two plastics, seem to exhibit binary or nearly binary behavior.

*Abstract of a paper in Nucl. Instr. Meth. B **86** (1994) 317.

Sensitivity of BP-1 glass detectors etched in methanesulfonic acid*

Y. D. He and M. Solarz

We recently discovered that methanesulfonic acid is a suitable etchant for BP-1 barium phosphate glass detectors. This paper reports on the sensitivity and charge resolution of BP-1 detectors etched in methanesulfonic acid in comparison with those etched in commonly used etchants such as hydrofluoric acid and fluoboric acid using 11 A GeV ^{197}Au ions at the Brookhaven Alternating Gradient Synchrotron. This new etchant, as a replacement for hydrofluoric acid, is environmentally easy to handle and would have applications to relativistic heavy-ion studies. We also tested ethanesulfonic acid and found it has no practical use due to its extremely slow general etch rate.

*Abstract of a paper in *Nucl. Instr. Meth. B* (1994) in press.

Response of the BP-1 Phosphate Glass Detector to Relativistic Heavy Ions*

Y. D. He, A. J. Westphal, and P. B. Price

We report on a systematic study of the response of the novel phosphate glass track-etch detector BP-1 to relativistic heavy ions. Using ^{197}Au beam with energies of 0.5, 0.7, and 11.4 A GeV, we demonstrate that the BP-1 detector can measure ionic charge with an unprecedented resolution above a threshold that can be set by proper choice of the chemical etchant after irradiation. These remarkable advantages have made it possible to use BP-1 to explore a number of interesting topics in high-energy heavy-ion physics and cosmic-ray astrophysics.

*Abstract of a paper in *Nucl. Instr. Meth. B* **84** (1994) 67.

NUCLEAR THEORY

Parton Equilibration in Relativistic Heavy Ion Collisions *

T. S. Biró†, E. van Doorn‡, B. Müller‡, M. H. Thoma†, and X. N. Wang

In high energy nucleon-nucleon collisions the production of minijets with p_T about a few GeV becomes increasingly important at colliding energies beyond the CERN ISR energy range. One would certainly expect that there could be a fairly large number of minijets produced in ultrarelativistic heavy ion collisions. From pQCD calculations, we can estimate the initial parton density, mostly gluons at high energies. We then investigate how this system approaches to equilibrium by solving a set of rate equations.

We can apply rate equations and particle distribution functions to describe the system only, when approximate local isotropy in momentum space is achieved. We assume a factorized Bose (Fermi) distributions for gluons (quarks)

$$f(k;T,\lambda_i) = \lambda_i \left(e^{\beta u\cdot k} \pm 1\right)^{-1}, \qquad (1)$$

where λ_g and λ_q are gluon and quark fugacities.

The most important reactions for establishing chemical equiulibrium are $gg \leftrightarrow ggg$ and $gg \leftrightarrow q\bar{q}$. Elastic scattering processes, on the other hand, are crucial for maintaining local thermal equilibrium.

The evolution of the parton densities $n_{q,g}$ according to both reactions mentioned above can be described by a coupled set of rate equations. Adding the equation for energy conservation assuming only longitudinal expansion we end up with a closed set of equations determining the temperature $T(\tau)$ and the quark and gluon fugacities $\lambda_{q,g}(\tau)$ as a function of the proper time τ

$$\begin{aligned}
\frac{\dot{\lambda}_g}{\lambda_g} + 3\frac{\dot{T}}{T} + \frac{1}{\tau} &\approx R_3\,(1-\lambda_g)\,, \\
\frac{\dot{\lambda}_q}{\lambda_q} + 3\frac{\dot{T}}{T} + \frac{1}{\tau} &\approx a\,R_2\left(\frac{\lambda_g}{\lambda_q} - \frac{\lambda_q}{\lambda_g}\right), \\
(\lambda_g \;+\; b\,\lambda_q)^{3/4}\,T^3\,\tau &= const\,. \qquad (2)
\end{aligned}$$

Here $a = 32/9N_f$, $b = 21N_f/64$ ($N_f \simeq 2.5$) and the equilibration rates are given by $R_2 = \sigma_2\, n_g/2$ and $R_3 = \sigma_3\, n_g/2$, where σ_2 and σ_3 are the thermally averaged, velocity weighted cross sections: $\sigma_2 = \langle\sigma(gg \to q\bar{q})\,v\rangle$ and $\sigma_3 = \langle(gg \to ggg)\,v\rangle$. In calculating these rates we have consider the Landau-Pomeranchuk effect and color screening which in turn also depend both on T and λ_g.

In the figure, we show our result with initial condition at LHC energy. We see that the system approaches to equilibrium though slowed down by the inclusion of Landau-Pomeranchuk effect.

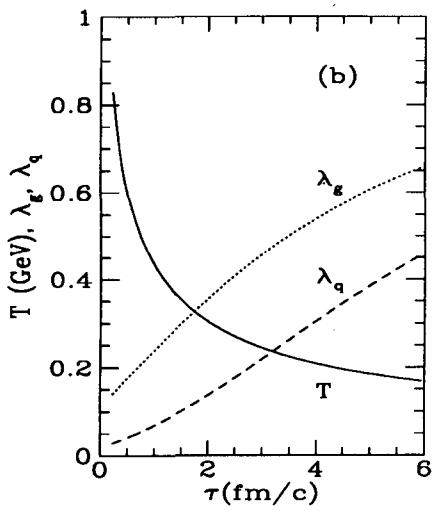

Time evolution of T and $\lambda_{q,g}$ at LHC.

*LBL-34164: published in Phys. Rev. C **48**, 1275(1993).

†Institut für Theoretische Physik, Universität Giessen, D-6300 Giessen, Germany

‡Department of Physics, Duke University, Durham, NC 27708-0305

Multiple Collisions and Induced Gluon Bremsstrahlung in QCD*

M. Gyulassy† and X.-N. Wang

In this paper, we initiated a study of multiple collision theory in pQCD concentrating on the eikonal limit. We calculated elastic and inelastic multiple collision amplitudes for a high energy parton propagating though a "plasma" of static target partons. We showed that the assumption of color neutrality was vital to recover the classical parton cascade picture in both large and small angle scattering. Our main simplifying assumption was that the mean free path ($\lambda \sim 1/g^2T$) in the target was large compared to the range of the interactions ($\mu^{-1} \sim 1/gT$). In particular, we showed how the classical Glauber scattering cross section emerges after ensemble averaging.

The main focus of the paper was to derive the total radiation amplitute, which can be expressed as a convolution of elastic multiple scattering amplitudes and an effective color current. This result was derived for the soft radiation ($x \ll 1$ and $k_\perp \ll \mu$) regime. The limitations of the approximations leading to that result were also carefully analyzed. We showed that the triple gluon diagrams can be neglected in the soft limit but are important to cut off the $k_\perp$ distributions on the scale μ. Only when $k_\perp \to 0$ can the effective current be pulled out of the multiple collision integral, and the radiation amplitude factored in momentum space. There is never a factorization of amplitudes in color space. However, the color neutrality condition, greatly simplifies the ensemble average of the squared amplitude. In addition, the off diagonal contributions in momentum space from $\vec{J}^c_{a_1\cdots a_m}(k;\{\mathbf{q}_{\perp i}\})\vec{J}^c_{a_1\cdots a_m}(k;\{\mathbf{q}'_{\perp i}\})$ drop out, if the transverse width of the target is large compared to the interaction range. Under these conditions, it was possible to calculate the induced radiation spectrum.

We defined the radiation formation factor, as the ratio of the induced radiation spectrum to the spectrum from an isolated collision. That factor measures the suppression of induced radiation with formation length, $\tau(k) > \lambda$, and reveals the non-abelian analog of the LPM effect. We showed how this factor interpolates between the saturated Factorization limit and the additive Bethe-Heitler limit. A compact "pocket" formula for the formation factor was derived illustrating the essential features of that interpolation.

Finally, we applied the formation factor to estimate the contribution of soft induced gluon radiation to the energy loss per unit length. The result in the Factorization limit, was shown to be consistent with the uncertainty principle bound of [1] with a numerical coefficient, $C_2\alpha_s$, that had a simple physical interpretation as the number of induced gluons radiated in the limited phase space with rapidity between zero and $\log(\mu\lambda/r_2)$ and with $k_\perp < \mu$. Up to un-calculated logarithmic factors the radiative energy loss was found to be comparable to the elastic energy loss [2]. We also showed how the linear energy dependence of dE/dz is recovered in the opposite (Bethe-Heitler) limit when $\lambda \gg E/\mu^2$.

*LBL-32682: Nucl. Phys. B in press.

†Physics Department, Columbia University, New York, NY 10027

[1] S. J. Brodsky and P. Hoyer, Phys. Lett. **B298**, 165 (1993)

[2] M. H. Thoma and M. Gyualssy, Nucl. Phys. **B351**, 491 (1991)

Perturbative Gluon Shadowing in Heavy Nuclei*

K.J. Eskola, J. Qiu† and X.-N. Wang

For sufficiently small values of x and/or of Q^2, gluon recombination results in a modification of the QCD evolution equations. In the limit of small-x the modified QCD evolution equation can be cast in the form

$$\partial_y \partial_t G(y,t) = cG(y,t) - \lambda \exp(-t - \mathrm{e}^t)[G(y,t)]^2, \tag{1}$$

where $y = \ln(1/x)$, $t = \ln[\ln(Q^2/\Lambda^2_{\rm QCD})]$, $G(y,t) = xg(x,Q^2)$ and $c = 12/(11 - 2N_f/3)$ with N_f the number of quark flavors.

Strength of the gluon recombination is controlled by the factor λ, originating from two possible sources. The two fusing gluon ladders, which couple 4 gluons to 2 gluons, can arise either from independent constituents of proton/nucleus or from the same one, as discussed in. We will refer to the former case as "independent" and to the latter as "non-independent" fusion. Since recombinations from both sources happen simultaneously, we divide the parameter λ into two parts:

$$\lambda = \lambda_{\rm I} + \lambda_{\rm II}, \tag{2}$$

where $\lambda_{\rm I}$ corresponds to the independent recombination and $\lambda_{\rm II}$ to the non-independent one.

In a proton, the strength of the independent fusion then takes the form

$$\lambda_{\rm I} = \frac{2}{3}\frac{1}{\pi R_p^2} \cdot \frac{\pi^3 c^2}{2\Lambda^2_{\rm QCD}}, \tag{3}$$

where $R_p \sim 1$ fm is the radius of a proton.

The magnitude of the non-independent fusion of the gluon ladders can be estimated as[1],

$$\lambda_{\rm II} \approx \frac{16}{81}\frac{1}{\pi(2/Q_i)^2} \cdot \frac{\pi^3 c^2}{2\Lambda^2_{\rm QCD}}, \tag{4}$$

where we have made a simplification by fixing the initial x of the valence quark to $x_i \sim 1$. We also approximate the scale of the initial valence quark by $Q_i \sim 2$ GeV.

Let us then consider a large loosely bound nucleus. Naturally, both types of fusions are still there but only for the independent one an $A^{1/3}$-scaling arises. In this case

$$\lambda^A_{\rm I} = \frac{9}{8}\frac{A}{\pi R_A^2} \cdot \frac{\pi^3 c^2}{2\Lambda^2_{\rm QCD}}, \tag{5}$$

where the nucleus is taken to be a sphere with a sharp surface at $R_A = 1.12A^{1/3}$ fm. The strength of the non-independent fusion remains the same as in the case of a free proton: $\lambda^A_{\rm II} = \lambda_{\rm II}$.

For a proton, we assume that the recombinations start to be effective at $x \sim x_0 \sim 0.01$. The gluon recombination is strongly enhanced in heavy nuclei and it starts at somewhat larger values of x than in protons. The corresponding boundary line x_0^A for a nucleus is approximately determined by the relative magnitude of the evolution terms in Eq. 1: $G_A(x_0^A) \sim G(x_0)\lambda_A/\lambda$, so that the relative contribution from the gluon fusion in a nucleus is about the same as in a nucleon. This gives $x_0^A \sim 0.05$–0.1.

We solve Eq. 1 using the method of characteristics. The results show a strong nuclear shadowing generated through the modified QCD evolution, and it may well be the dominant mechanism for the small-x modifications. We feel we now have more quantitative control over the nuclear gluon distribution at small x, based on perturbative QCD. We believe this study could serve as an interesting starting point for more detailed calculations of nuclear gluon shadowing and its consequences in ultra-relativistic heavy ion collisions.

---

*LBL-34163: published in Phys. Rev. Lett. **72**, 36 (1994).

†Dept. of Physics and Astronomy, Iowa State Univ., Ames, Iowa 50011.

[1] A. H. Mueller and Jianwei Qiu, Nucl. Phys. **B268**, 427

Space-time Structure of Initial Parton Production in Ultrarelativistic Heavy Ion Collisions*

K. J. Eskola and X.-N. Wang

In this paper, we use HIJING Monte Carlo model [1], which was developed for simulating parton and particle production in heavy ion collisions, to study the space-time evolution of the initial parton production. In HIJING, each hard parton scattering in hadronic reactions is simulated by using QCD cascading in which one can trace back the whole history of initial and final state radiation associated with that hard scattering. The life time of an intermediate off-shell parton is estimated via the uncertainty principle $t_q \sim E/q^2$ for given energy E and virtuality q. We then obtain the space and time vertices of all the produced partons. Given a space cell, we then calculate the time evolution of the momentum distribution of the produced partons by assuming classical trajectories without rescatterings. We will verify that after some time most of the partons will leave the space cell except those whose rapidities are close to the spatial rapidity of the cell, thus achieving local isotropy in momentum distribution which happens to look like thermal. This will provide a good starting point for treating equilibration via a set of rate equations for the number and energy densities

To estimate the parton production time, we plot in the Fig. 1 the total number of produced partons, on-shell as well as off-shell, as a function of time at the highest RHIC energy, $\sqrt{s}$ = 200 GeV/n. We see that long before the two nuclei overlap and hard scatterings take place, partons have already been produced via initial state bremsstrahlung. Some of the initially radiated partons will also initiate time-like branching trees. Note that, if the coherence is not broken by the hard scattering, partons which would have been emitted from the initial state radiation will not emerge as produced partons. Here we have also included the initiators of the space-like branching as produced partons. Therefore, if a parton does not have initial state radiation, it will only become a produced parton after the hard scattering, whereas, a parton is defined to be produced before the hard scattering if it has initial state radiation. From this figure, we can see that about 2/3 of the total number of partons are produced between $t = -0.5$ and 0.5 fm/c while about 200 semihard scatterings happen between $t = -0.1$ and 0.1 fm/c as indicated by dashed lines. We find also that about 2/3 of the total number of partons are produced in initial and final state radiations. The fraction of partons from branching should increase with the colliding energy and with smaller choices for μ_0.

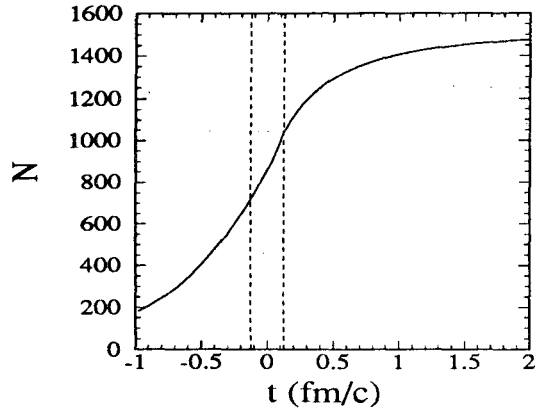

The total number of produced partons N as a function of time t, with $t = 0$ defined as when the two nuclei have complete overlap.

The initially produced partons are however far away from chemical balance due to small quark production cross sections.

*LBL-34156: published in Phys. Rev. D49, 1284 (1994).

[1] X.-N. Wang and M. Gyulassy, Phys. Rev. D 44, 3501 (1991); Phys. Rev. D 45, 844 (1992).

Minijet-associated Dilepton Production in Ultrarelativistic Heavy Ion Collisions*

K. J. Eskola and X.-N. Wang

In this paper, we investigate dilepton production associated with minijet final state radiation in heavy ion collisions at collider energies. It is expected that at energies $\sqrt{s} \gtrsim 200$ AGeV, minijets [(anti)quarks and gluons with $p_T \sim$ few GeV/c] are produced abundantly via multiple semihard scatterings. These minijets have important contributions to particle production, transverse energy and overall evolution of the formed quark-gluon system. Therefore, it would be interesting to study dilepton bremsstrahlung from the initially produced minijets. Especially, it is important to know whether the dileptons associated with minijets could compete with the lower order DY processes at midrapidity and small invariant dilepton masses $M \sim 1 - 3$ GeV/c^2, where a window for observing the thermal dileptons is expected. We take an approach by calculating the dilepton fragmentation functions of the final state minijets.

Unlike in the real photon fragmentation functions, the relatively large invariant masses $M \gg \Lambda$ of the dileptons fix the lower limit of the momentum scale of the QCD radiation processes. This makes the problem calculable in pQCD. In the leading logarithm approximation and in an axial gauge, the dilepton fragmentation functions can be calculated up to all orders in pQCD. Using the obtained fragmentation functions to convolute with minijet cross sections, we then compute the contribution to the dilepton production from the final state radiation of minijets.

As shown in the figure, dileptons from the fragmentation of minijets are found to be comparable to direct Drell-Yan at RHIC energy for small invariant mass $M \sim$ 1–2 GeV/c^2. At LHC energy, the associated dilepton production becomes dominant over a relative large range of the invariant mass.

The largest uncertainty in our calculation is the choice of the momentum scale $Q_{\max}$ used in the dilepton fragmentation functions. Since the correct scale in a matrix element calculation is channel-dependent, we used only an effective scale choice in the fragmentation functions to convolute with the minijet cross sections. We evaluated the dilepton spectrum for two choices of the scale, $Q_{\max} = p_T$, $2p_T$. However, the results with $Q_{\max} = p_T$ should give us the lower bound of the associated dilepton production. Another notorious uncertainty of the p_T cutoff p_0 in minijet-related problems is greatly reduced here due to the kinematic restriction $M \leq Q_{\max}$. For $Q_{\max} = p_T$, the p_T cutoff is replaced by M whenever M is larger than p_0.

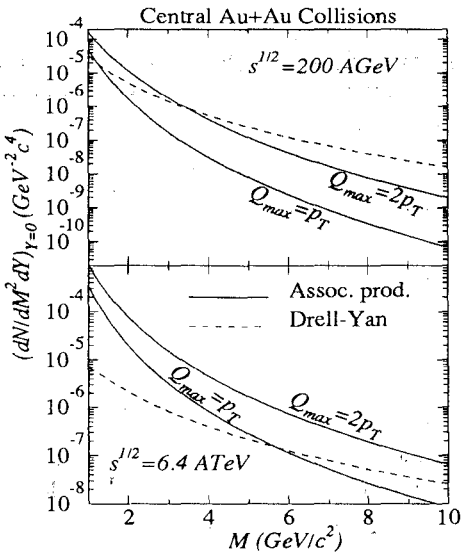

Mass spectra of minijet-associated and Drell-Yan dileptons.

*LBL-34409: published in Phys. Rev. **D49**, 4532 (1994).

Calculating Dilepton Rates from Monte Carlo Simulations of Parton Production*

K. J. Eskola and X.-N. Wang

Due to the relatively large invariant dilepton mass, $M \gg \Lambda$, the radiative corrections are calculable in pQCD up to all orders in the leading logarithm approximation. Collinear approximation is also used in convoluting the obtained dilepton fragmentation functions with minijet cross sections to compute the radiative contributions to dilepton production. Since there exist Monte Carlo simulations of QCD cascading which can take into account many other effects, like multiple ladder structure, it is important to check our semi-analytical approach with realistic Monte Carlo simulations.

To directly simulate dilepton production in a Monte Carlo event generator is rather difficult due to the small QED coupling constant as compared to that of QCD. To overcome this difficulty, one can multiply the number of specific QCD processes, which resemble those of dilepton production by an appropriate ratio of the corresponding differential probabilities. However, the problem is more complicated than one might first think. For radiative dilepton production, one has to take into account the fact that the corresponding radiated quarks and gluons in QCD can have further bremsstrahlung which is different from the QED case. The additional bremsstrahlung gives rise to an extra Sudakov form factor and one must include it in the differential ratio to give the correct dilepton emission. Given the differential branching probability for a quark to radiate a dilepton $d\mathcal{P}_{q\to \mathrm{DL}}/dM^2$ and to all possible partons $d\mathcal{P}_{q\to \mathrm{all}}/dM^2$, which all include the appropriate Sudakov form factors, the ratio should be

$$\mathcal{R}(M^2, Q^2_{\max}) \equiv \frac{d\mathcal{P}_{q\to \mathrm{DL}}}{dM^2} \Big/ \frac{d\mathcal{P}_{q\to \mathrm{all}}}{dM^2}, \qquad (1)$$

Using this ratio we then can calculated the radiative dilepton production from our Monte Carlo simulations and the result is consistent with our previous semi-analytical calculation[1] as shown in the figure.

We found that Sudakov form factors are essential for us to give the right results. If neglected, the resultant dilepton rate from final state radiation would differ from our early semi-analytical calculation by orders of magnitude. Due to the same reason, the differential ratio is quite sensitive to the maximum virtuality $Q_{\max}$ of the branching processes, similar to the fragmentation function approach. One therefore has to choose its value to be consistent with what is used in the Monte Carlo simulation of QCD cascading.

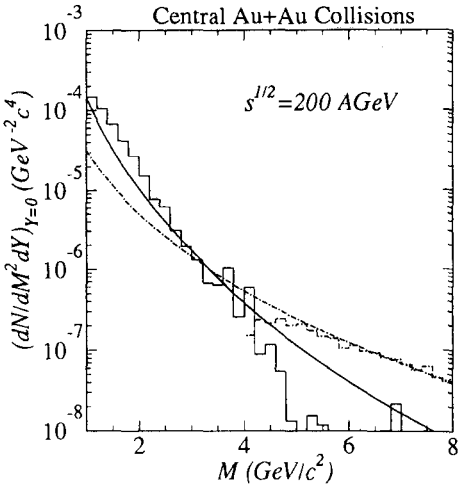

Mass spectrum of the minijet-associated (solid histogram) and direct DY (dashed histogram) dileptons from the Monte Carlo simulation and our direct calculation (solid and dashed curves, respectively) (with $Q_{\max} = 2p_T$, $\Lambda = 0.4$ GeV and $\mu_0 = 0.5$ GeV) in central $Au + Au$ collisions at $\sqrt{s} = 200$ AGeV.

*LBL-34664: published in Phys. Rev. **D49**, 4542 (1994).

[1] K. J. Eskola and X.-N. Wang,Phys. Rev. D.

Cluster Structure of Disoriented Chiral Condensates in Rapidity Distribution*

Z. Huang†*and X.-N. Wang*

It has been proposed that a disoriented chiral condensate (DCC) can lead to the so-called Centauro events in cosmic ray reactions. In this paper, we study the creation of the disoriented chiral condensate with a more realistic initial condition that may be expected in the high energy collisions. We re-examine the idea of a quench based on a linear σ-model and suggest that indeed, following a quench, correlated pion fields will populate near the light cone where the leading collision particles are expanding at speed of light. The pion condensates will have distinct cluster structures which may be reflected in the final pion production.

We assume that following a quench the possible DCC is to be described by classical low energy effective interactions of pions at zero temperature

$$\mathcal{L} = \int d^4x \left\{ \frac{1}{2}\partial_\mu\phi_i\partial^\mu\phi_i - \frac{\lambda}{4}\left(\phi_i\phi_i - v^2\right)^2 + H\sigma \right\}$$

where $\phi_i \equiv (\sigma, \pi)$ stands for a vector in internal space. $H\sigma$ is an explicit chiral symmetry-breaking term which is responsible for the mass of the pseudo-goldstone bosons, the pions.

We assume an approximate $1+1$ Lorentz invariant initial condition. The equations of motion then read

$$\left[\frac{1}{\tau}\frac{\partial}{\partial\tau}\left(\tau\frac{\partial}{\partial\tau}\right) - \frac{1}{\tau^2}\frac{\partial^2}{\partial\eta^2}\right]\sigma = - \lambda\,\sigma\left(\sigma^2+\pi^2-v^2\right) + H \;; \quad (1)$$

$$\left[\frac{1}{\tau}\frac{\partial}{\partial\tau}\left(\tau\frac{\partial}{\partial\tau}\right) - \frac{1}{\tau^2}\frac{\partial^2}{\partial\eta^2}\right]\pi = - \lambda\,\pi\left(\sigma^2+\pi^2-v^2\right) . \quad (2)$$

We assume that shortly after the collision, the typical configuration is that of a thermal random fluctuation at high temperature. The fluctuation is governed by the temperature. We choose $\phi(\tau_0)$ and $\partial\phi(\tau_0)/\partial\tau$ randomly according to gaussian distributions so that

$$\langle\phi(\tau_0,\eta)\rangle_\eta = \langle\frac{\partial}{\partial\tau}\phi(\tau_0,\eta)\rangle_\eta = 0 \quad (3)$$

but $\langle\phi^2(\tau_0,\eta)\rangle_\eta = v^2/4$ and $\langle(\frac{\partial}{\partial\tau}\phi(\tau_0,\eta))^2\rangle_\eta = v^2\ /\mathrm{fm}^2$.

Solving Eqs.(1) and (2), we find there are indeed π correlations as σ approaches to its vaccum expectation value as show in the figure, where the correlation function is defined as

$$C(\tau,\eta-\eta') = \frac{\boldsymbol{\pi}(\tau,\eta)\cdot\boldsymbol{\pi}(\tau,\eta')}{2[\pi^2(\tau,\eta)+\pi^2(\tau,\eta')]} . \quad (4)$$

We also see that the correlation lenght becomes smaller at later time.

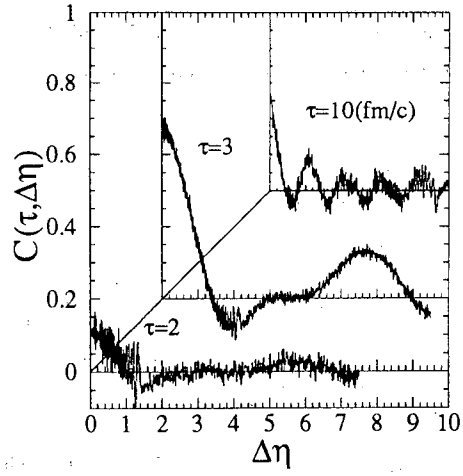

The correlation function $C(\tau,\Delta\eta)$ of DCC. The initial configuration is that of a thermal fluctuation at $\tau_0 = 1$ fm/c

*LBL-34931: published in Phys. Rev. **D49** R4335 (1994).

†Physics Division, LBL

D-meson as a Probe of Early Parton Rescattering*

X.-N. Wang and B. Müller†

The question of thermalization and equilibration depends crucially on the initial condition of the produced minijets. It also depends on the dynamics of the parton rescattering inside a dense medium. Therefore, it is of interest to have some observables which can probe the parton dynamics during equilibration process. In this paper, we present arguments indicating that the total charmed quark production may be used for this purpose.

In general, we can divide the charm production into three stages: (1) initial production similar to minijets; (2) pre-equilibrium production from secondary parton cascade; (3) and thermal production. For a reasonable range of temperatures (T ~200–400 MeV), the thermal production is far below the initial one due to the heavy quark mass $M_c \approx 1.5$ GeV/c^2. On the other hand, secondary parton scatterings in the initially produced dense, though not thermalized, partonic system could lead to significant charmed quark production.

Shown in the figure is our estimate of the secondary charm production[1]. In our calculation of the minijet and initial charm production, we have assumed that gluons and quarks are shadowed by the same amount at small x. This shadowing essentially suppresses low p_T minijet and charm production. Therefore, the ratio $R_{AB}^{\rm charm} = \sigma^{AB}/AB\sigma^{pp}$ for the initial charm production at low $p_T = 1$ GeV/c as shown in the figure(dashed line) is only about 0.5 for central $Au+Au$ collisions at $\sqrt{s} = 200$ AGeV. However, if the pre-equilibrium contribution with $\tau_0 = 1$ fm/c and $\tau_i = 0.1$ fm/c is included (solid line) the ratio becomes about 1 in the central rapidity region. At $\sqrt{s} = 6000$ AGeV, the shadowing suppresses the initial production by 2/3 (dotted line) and the pre-equilibrium production is so abundant that it increases the ratio $R_{AB}^{\rm charm}$ to 1.7 even though we have chosen a short thermalization time of $\tau_0 = 0.3$ fm/c.

The pre-equilibrium enhancement over the initial charm production depends sensitively on the value of thermalization time τ_0. This demonstrates that the total charm production can be used as a measure of the thermalization time scale. We also note that the pre-equilibrium enhancement is only relative to the suppression by gluon shadowing. Since gluon shadowing is also a fundamental issue in its own right, it is therefore essential to study the charm production systematically in $p+p$ and $p+A$ collisions at the same energy where the only nuclear effect comes from gluon shadowing.

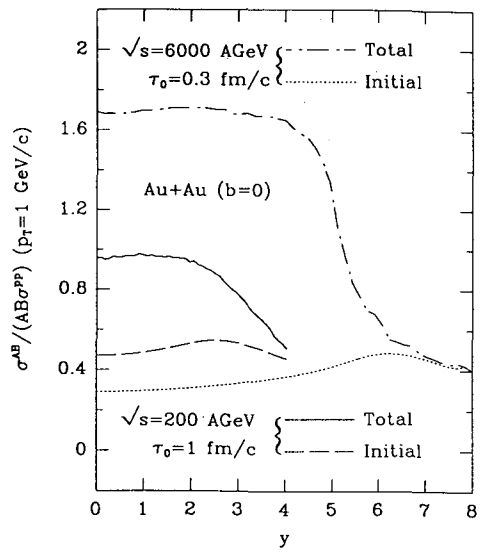

The ratio $R_{AB}^{\rm charm} = \sigma^{AB}/AB\sigma^{pp}$ for charm production at $p_T = 1$ GeV/c as functions of rapidity in central $Au+Au$ collisions at $\sqrt{s} = 200$ (6000) GeV. The solid (dotdashed) line is for the total charm with thermalization time $\tau_0 = 1$ (0.3) fm/c while the dashed (dotted) line is only for the initial production.

*LBL-34485: published in Nucl. Phys.**A566**, 555c (1994).

†Physics Department, Duke University, Durham, NC 27706

[1]B. Müller and X.-N. Wang, Phys. Rev. Lett. **68**, 2437 (1992)

Pre-Equilibrium Parton Dynamics*

edited by *X.-N. Wang*

Since the beginning of the search for a quark gluon plasma and the emergence of high energy nuclear collisions, the issues related to thermal and chemical equilibration have always been a focal point of many theoretical investigations. These issues are critical for experimental detection of a quark gluon plasma in high energy nuclear collisions, because most of our knowledge of the plasma and its signals has been based on the assumption that it is in both thermal and chemical equilibrium. In the last few years, it was realized that hard or semihard processes will dominate the collision dynamics and constitute most of the initial energy deposition in the central region of ultrarelativistic nuclear collisions. Several Monte Carlo models have been developed to study the production and evolution of a dense partonic system. However, there is still not a consensus on issues related to parton equilibration. As a first attempt to bring together experts in the field to address these issues, a workshop on Pre-Equilibrium Parton Dynamics in Ultrarelativistic Heavy Ion Collisions was held at Lawrence Berkeley Laboratory from August 23 to September 3, 1993. The following are the titles of papers which are collected in this proceedings.

Relativistic Heavy Ion Collisions: "Recreating" the Early Universe in the Laboratory (*B. Müller*); Minijets in the Two-component Dual Parton Model in Hadronic and Heavy Ion Collisions (*F. W. Bopp, R. Engel, I. Kawrakow, D. Petermann, and J. Ranft*); Space-time Evolution of Production of Semihard QCD-quanta in Ultrarelativistic Heavy Ion Collisions (*K. J. Eskola and X.-N. Wang*); QCD-based Space-time Description of High Energy Nuclear Collisions (*K. Geiger*); QCD Cascading (*I. Sarcevic*); Gluon Multiplication in High Energy Heavy Ion Collisions (*L. Xiong and E. Shuryak*); Time Evolution of the Quark-Gluon Plasma (*F. Cooper, J. Dawson, Y. Kluger, and H. Shepard*); Transport Equations Embodying Particle Production and Back-reaction (*J. M. Eisenberg*); Color Collective Effects at the Early Stage of Ultrarelativistic Heavy Ion Collisions (*S. Mrówczyński*); Collective Nonabelian Phenomena in Quark Gluon Plasma (*J. C. Parikh*); Color Diffusion in QCD Transport Theory (*A. V. Selikhov and M. Gyulassy*); Influence of the Landau-Pomeranchuk Effect on Lepton Pair Production (*J. Cleymans, V. V. Goloviznin, and K. Redlich*); Classical and Quantum Coherence in Bremsstrahlung (*J. Knoll*); Medium Effects on Heavy Ion Dynamics (*C. M. Ko*); Landau-Pomeranchuk Effect in QCD and Radiative Energy Loss (*X.-N. Wang and M. Gyulassy*); Signatures for QGP in Dilepton Spectrum (*M. Asakawa*); Quark-Gluon Plasma Freeze-out from a Supercooled State? (*T. Csörgő and L. P. Csernai*); Effective Action of a QCD Chiral Order Parameter (*H.-T. Elze*); Soft Interaction, Intermittency and Phase Transition (*R. C. Hwa*); Nonperturbative Effects in the SU(3) Gluon Plasma (*D. H. Rischke, M. I. Gorenstein, A. Schäfer, and W. Greiner*); Colour Confinement in Hadron-Nucleus Collisions (*D. Kharzeev and H. Satz*); Modelling Coherence and Chaos in High-Energy Collisions (*G. Wilk, Z. Włodarczyk, and R. M. Weiner); Exotic Charmed Baryon Production in Ultrarelativistic Heavy Ion Collisions* (J. Zimànyi, T. S. Birò, and P. Lèvai*); Bose-Condensates in High Energy Nucleus-nucleus Collisions* (U. Ornik, M. Plümer and D. Strottman*); Relativistic Heavy Ion Physics at CERN* (H. H. Gutbrod*); The PHENIX Experiment at RHIC* (S. R. Tonse and J. H. Thomas*); The STAR Experiment at RHIC* (J. W. Harris).

*LBL-34831: Proceedings of the workshop on Pre-Equilibrium Parton Dynamics in Ultrarelativistic Heavy Ion Collisions, Lawrence Berkeley Laboratory, August 23 to September 3, 1993.

Higher-Twist Effects in the Drell-Yan Angular Distribution*

K.J. Eskola†, P. Hoyer†, M. Vänttinen‡, and R. Vogt

The Drell-Yan process of inclusive muon pair production in hadronic collisions is the most important means of determining the valence parton content of hadrons other than the nucleon. The reaction is described as the annihilation of a massless quark and an antiquark into a virtual photon which decays into a muon pair. Because of rotational invariance and parity conservation, the polar angle distribution of massless muons in the muon pair rest frame must be of the form $1 + \lambda \cos^2\theta$, where $\lambda = 1$, since the annihilation of on-shell spin-1/2 particles produces a transversely polarized virtual photon. Experimentally, this is observed in most of the kinematic region. At large x_F, however, the photon appears to become longitudinally polarized. We studied a higher-twist mechanism leading to longitudinal polarization, within a model suggested by Berger and Brodsky (BB)[1].

To produce a large x_F muon pair, x_a, the momentum fraction of the projectile parton, is near 1. Fock states of the projectile where one parton carries most of the momentum have large energy, $\Delta E \simeq -\frac{\mathbf{k}_{\perp a}^2}{2p(1-x_a)}$ where $-\mathbf{k}_{\perp a}$ and $(1-x_a)p$ are the transverse and longitudinal momenta of the soft parton(s). When $x_a \to 1$, the lifetime of the Fock state is short and perturbation theory is applicable. In the BB model, the spectator valence quark transfers its momentum to the active quark via single gluon exchange. Thus the whole pion state participates in the scattering, implying longitudinal polarization due to helicity conservation in the pion-virtual photon interaction.

As a first approximation, BB took the nonperturbative wave function of the pion to be $\delta(z - 1/2)$. In the limit $x_a \to 1$, $\mathbf{k}_{\perp a}^2/Q^2 \to 0$ with $Q^2 \sim (1-x_a)^2$, they found $\lambda = ((1-x_a)^2 - 4\mathbf{k}_{\perp a}^2/9Q^2)/((1-x_a)^2 + 4\mathbf{k}_{\perp a}^2/9Q^2)$. It is clear that if $(1-x_a)^2$ vanishes faster than $\mathbf{k}_{\perp a}^2/Q^2$, $\lambda \to -1$. Experimentally, a drop in λ at large x_F is observed, but the data lie well above the asymptotic result. We show that there are important nonasymptotic corrections to the limiting expression at present energies. The BB model evaluated with exact kinematics is, in fact, in rather good agreement with the data.

At present fixed target energies, $|\mathbf{p}| = \mathcal{O}(10\text{ GeV})$, hence $(1-x_F)|\mathbf{p}| = \mathcal{O}(1\text{ GeV}) \simeq \langle|\mathbf{Q}_\perp|\rangle$ for $x_F = 0.9$. Thus it is not surprising to find large deviations due to finite energy effects. The improved agreement with data when such effects are taken into account is encouraging. However, it is also an indication that one should carefully reconsider the applicability of the twist expansion of QCD on which the BB model is based.

In the leading twist QCD approach, the time scale τ_I of the hard interaction is much shorter than the lifetime of the Fock state, τ_F. In the BB model, the limit was taken such that $\tau_I/\tau_F = \mathcal{O}(1-x_a)$ is vanishing so that factorization is still valid. On the other hand, in the limit [2] $x_a \to 1$, $Q^2 \to \infty$ with $\mathbf{k}_{\perp a}^2/Q^2 \sim (1-x_a)$, we have $\tau_I \sim \tau_F$. In this limit the twist expansion breaks down and two new diagrams contribute at leading order.

At finite energies, it is not obvious which of the asymptotic limits is more appropriate. Applications of perturbative QCD depend on an idealized high energy limit. The effects of finite energy corrections should be studied since they reflect the inherent uncertainties of the approach.

---

*LBL-35430: Submitted to *Phys. Lett. B.*

†Laboratory of High Energy Physics, University of Helsinki

‡Research Institute for Theoretical Physics, University of Helsinki

[1] E.L. Berger and S.J. Brodsky, *Phys. Rev. Lett.* **42**, 940, (1979)

[2] S.J. Brodsky, P. Hoyer, A.H. Mueller and W.-K. Tang, *Nucl. Phys.* **B369** 519, (1992)

QCD and Intrinsic Heavy Quark Predictions for Leading Charm and Beauty Hadroproduction*

R. Vogt and S.J. Brodsky†

Flavor correlations between the produced particle and the projectile have been reported in charm production. For example, in $\pi^-(\bar{u}d)p$ and π^-A interactions, the "leading" $D^-(\bar{c}d)$ x_f distribution is harder than the "nonleading" $D^+(c\bar{d})$ distribution, suggesting that hadronization at large x_F involves the coalescence of the charm quarks with projectile spectator quarks.

The asymmetry between leading and nonleading charm,

$$\mathcal{A} = \frac{\sigma(\text{leading}) - \sigma(\text{nonleading})}{\sigma(\text{leading}) + \sigma(\text{nonleading})} , \qquad (1)$$

has been recently measured[1]. The p_T-integrated asymmetry, $\mathcal{A}(x_f)$, increases from ~ 0 for $x_f \sim 0$ to ~ 0.5 around $x_f = 0.65$ while the x_f-integrated asymmetry is consistent with zero.

Leading order QCD predicts that c and $\bar{c}$ quarks are produced with identical distributions. Next-to-leading order calculations produce a small charge asymmetry due to qg and $q\bar{q}$ interference, unrelated to flavor correlations. Final-state coalescence may occur when the heavy quarks and spectator valence quarks have the same velocity. String fragmentation models can produce large x_f charmed hadrons because the D^- inherits all the remaining projectile momentum when the string invariant mass is small. However, these models overestimate the asymmetry at low x_f.

We assume that this coalescence occurs in the initial state. In the intrinsic charm model, the π^- can fluctuate into a $|\bar{u}dc\bar{c}\rangle$ Fock state. At minimum invariant mass $\mathcal{M}$ where all the partons have approximately the same velocity, it is easy for them to coalesce into charmed hadrons and produce leading particles at large x_f.

We calculate the asymmetry within a two-component model: parton fusion with coalescence, and intrinsic charm with valence-quark recombination[2]. The x_f distribution is the sum of these two components, $d\sigma/dx_f = d\sigma_{\rm pf}/dx_f + d\sigma_{\rm ic}/dx_f$. Hadronization of intrinsic charm model can occur in two ways: through standard fragmentation and coalescence of the intrinsic c with spectator valence quarks. Nonleading charmed is only produced by fragmentation while leading charm is produced by both fragmentation and coalescence.

The normalization of the intrinsic charm cross section is determined from the probability $P_{\rm ic}$. The cross section is proportional to the total inelastic cross section since a soft interaction brings the particles on shell, introducing a resolving factor $\mu^2/4\widehat{m}_c^2$, so that $\sigma_{\rm ic} = P_{\rm ic}\sigma_{\pi p}^{\rm in}\frac{\mu^2}{4\widehat{m}_c^2}$ and $\sigma_{\rm ic} \sim 1$ μb for a single charmed hadron with $x_f > 0$. The intrinsic charm cross section is proportional to α_s^4 because gluon vertices with the pion valence quarks and the intrinsic $c\bar{c}$ pair must be included in the amplitude. In the parton fusion model, the structure functions include the coupling of gluons and quarks to hadrons, making the rate proportional to α_s^2.

Our model reproduces the general trend of the data both as a function of x_f and p_T^2. The asymmetry should decrease with increasing energy since the fusion cross section grows faster than the inelastic cross section. We extended our model to $b\bar{b}$ production. The asymmetry is expected to have the same characteristics for charm and beauty, having important consequences for CP violation studies.

---

*LBL-35380: Submitted to *Nucl. Phys. B.*

†SLAC, Stanford University

[1] M. Adamovich *et al., Phys. Lett.* **B305**, 402, (1993); G. A. Alves *et al., Phys. Rev. Lett.* **72**, 812, (1994)

[2] R. Vogt, S. J. Brodsky, and P. Hoyer, *Nucl. Phys.* **B383**, 643, (1992)

Transport Phenomena in QCD

H. Heiselberg

The kinetic properties of relativistic quark-gluon and electron-photon plasmas are described in the weak coupling limit. The troublesome Rutherford divergence at small scattering angles is screened by Debye screening for the longitudinal or electric part of the interactions. The transverse or magnetic part of the interactions is effectively screened by Landau damping of the virtual photons and gluons transferred in the QED and QCD interactions respectively. Including screening a number of transport coefficients for QCD and QED plasmas can be calculated to leading order in the interaction strength, including rates of momentum and thermal relaxation (stopping and thermalisation), electrical conductivity, viscosities, flavor and spin diffusion of both high temperature[1] and degenerate plasmas[2].

The viscosities have been calculated for QGP to higher orders as well[3]. For strongly interacting plasmas other screening mechanisms taken from lattice calculations are employed. By solving the Boltzmann equation for quarks and gluons including screening, the viscosity is calculated to leading orders in the coupling constant. The leading logarithmic order is calculated exactly by a full variational treatment. The next to leading orders are found to be important for the transport properties of quark-gluon plasmas created in relativistic heavy ion collisions and the early universe, where the coupling constant is large. The resulting viscosities at RHIC and LHC energies are so large that Bjorken hydrodynamic expansion models cannot be applied to the early stages of heavy-ion collisions. Rather the plasmas expand like free streaming initially.

Color diffusion[4] as well as damping[5] of quarks and gluons in quark-gluon plasmas is, however, shown not to be sufficiently screened and the rates depends on an infrared cut-off of order the "magnetic mass". The diffusion of color is found to be much slower than the diffusion of spin and flavor because color is easily exchanged by the gluons in the very singular forward scattering processes. If the infrared divergence is cut off by a magnetic mass, $m_{mag} \sim \alpha_s T$, the color diffusion is $D_{color} \sim (\alpha_s \ln(1/\alpha_s) T)^{-1}$, a factor α_s smaller than spin and flavor diffusion. A similar effect is expected in electroweak plasmas at temperatures above M_W due to $W^{\pm}$ exchanges. The color conductivity in quark-gluon plasmas and the electrical conductivity in electroweak plasmas are correspondingly small in relativistic heavy ion collisions and the very early universe.

---

[1] H.Heiselberg: "Transport in Quark and Gluon Plasmas", LBL-34911, Proceedings of Workshop on "Parton Cascade", aug. 23-sept. 3, 1993, LBL-34831 p. 125, Ed. X.-N. Wang

[2] H.Heiselberg, C.J.Pethick: "Transport and Relaxation in Degenerate Quark Matter", *Phys. Rev.* **D48**, 2916 (1993)

[3] H.Heiselberg: "Viscosities in Quark-gluon Plasmas", LBL-34929, *Phys. Rev.* **D49**, (1994) in press

[4] H.Heiselberg: "Color, Spin and Flavor Diffusion in Quark-gluon Plasmas", LBL-35097, *Phys. Rev. Lett.* **72** (1994)

[5] H.Heiselberg, C.J.Pethick: "Quark and Gluon Relaxation Times in Quark-gluon Plasmas", *Phys. Rev.* **D47**, R769 (1993)

Quark Matter Structure in Neutron Stars

H. Heiselberg

For physically reasonable bulk and surface properties, the lowest energy state of dense matter has been shown to consists of quark matter coexisting with nuclear matter in the presence of an essentially uniform background of electrons[1]. We estimate the size and nature of spatial structure in this phase, and show that at the lowest densities the quark matter forms droplets embedded in nuclear matter, whereas at higher densities it can exhibit a variety of different topologies as rods, plates and bubbles. The typical length scale of these structures are very sensitive to the surface tension of quark matter - a quantity that can only be estimated with some uncertainty. Typically, the droplet sizes are larger than $\sim$ 5 fm. The mixed phase appear already around twice nuclear matter densities and a major fraction of the interior of neutron stars could consist of matter in this new phase according to detailed O-V calculations[2]. The solid core provides new mechanisms for glitches and cooling of neutron stars that can be compared to observations. The mixed phase will also soften the equation of state which affects core collapse in supernovae.

The properties of strange quark matter droplets (strangelets) have charge densities varying spatially on length scales of order the Debye screening length $\sim$ 5 fm. Describing the quark matter by a simple bag model the charge densities and electrostatic potentials are calculated in the Thomas-Fermi approximation[3]. The resulting relation between the total charge, Z, and the mass number, A, differs from previous work. Whereas small droplets of quark matter are almost uniformly charged, large droplets of quark matter act like a conductor and are only charged within a screening length from the surface. Including surface energies in addition to Coulomb energies, the binding energies of quark matter droplets are calculated and fission is found to be unlikely.

---

[1] H.Heiselberg, C.J.Pethick, E.Staubo, "Quark Matter Droplets in Neutron Stars", *Phys. Rev. Lett.* **70**, 1355 (1993)

[2] E.Staubo, H.Heiselberg, C.J.Pethick, "Quark Matter Structure of Neutron Stars", *Nucl. Phys.* **A566**, 577c (1994)

[3] H.Heiselberg: "Screening in Quark Matter Droplets", *Phys. Rev.* **D48**, 1418 (1993)

Simplified nuclear Boltzmann-Langevin simulation*

Jørgen Randrup and Sakir Ayik[a]

[a]) *Department of Physics, Tennessee Technological University, Cookeville, Tennessee 38505*

Within the framework of the Fokker-Planck formulation[1] of the nuclear Boltzmann-Langevin theory[2], we have derived simple analytical expressions for the transport coefficients that are accurate for small temperatures and near equilibrium. The drift and diffusion coefficients are then given by

$$V_1 \approx W_0 \,[f_1^0 - f_1 - f_1^0 \bar{f}_1^0 \textstyle\sum_2 C_{12}(f_2^0 - f_2)] \,,$$

$$D_{12} \approx W_0 \,[f_1^0 \bar{f}_1^0 \delta_{12} - f_1^0 \bar{f}_1^0 C_{12} f_2^0 \bar{f}_2^0] \,.$$

Here f_1^0 denotes the Fermi-Dirac equilibrium phase-space occupancy for states having the momentum $\mathbf{p_1}$ and $\bar{f}_1^0 = 1 - f_1^0$ is the associated vacancy factor.

The overall rate of the transport process is governed by the relaxation time t_0, where

$$t_0^{-1} = W_0 \approx \pi^2 \frac{\tau^2}{\epsilon_F^2}[1 - \pi^2 \frac{\tau^2}{\epsilon_F^2}] \rho \sigma_0 V_F \,,$$

in agreement with expressions derived for Fermi liquids. The coefficient C_{12} expresses the correlation induced between the occupancies at the two momenta $\mathbf{p_1}$ and $\mathbf{p_2}$ and is given by

$$\rho \phi_0 C_{12} = \frac{3}{\pi^2} \frac{\epsilon_1 - \epsilon_0}{T} \frac{\epsilon_2 - \epsilon_0}{T} + \sum_{\ell \geq 0} \frac{\phi_0}{\phi_\ell} (\frac{p_1 p_2}{2m})^\ell [2 - (-1)^\ell] P_\ell(\cos\theta_{12}) \,.$$

For the Fermi surface moments we have $\phi_\ell \approx \phi_0 \epsilon_0^\ell$ to leading order in the small quantity τ/ϵ_F.

The diffusion coefficient exhibits the general decomposition into diagonal and off-diagonal parts[3], and the form of the monopole and dipole terms are dictated by the demand that particle number, energy, and momentum be strictly conserved throughout each separate history. It is also possible to show that the resulting transport process leads towards the correct quantum-statistical equilibrium distribution, not only for the average phase-space density but also for its correlated fluctuations.

The numerical effort associated with solving the *BL* equation for the nucleon phase-space density f can then be reduced by several orders of magnitude, by picking the stochastic changes in f on the basis of the transport coefficients, rather than by simulating the basic two-particle-two-hole processes as previously done. This novel method was illustrated for a maximally simple *BL* model applied to the equilibration in a Fermi-Dirac gas.

The approximate expressions offer a welcome opportunity for making significant savings in the computational effort and they are expected to be of great practical value in this regard. This is especially true for the maximally simple *BL* model that retains only the key complexities arising from conservation laws and quantum statistics; the emerging simplicity makes the numerical simulation especially fast and the model may form the basis for practically useful calculations. Of course, being only approximate in nature, the method needs to be further studied in order to assess its quantitative utility; our preliminary studies give cause for optimism in this regard.

In addition to their computational utility, the formulas derived are obviously also very useful for analytical studies, both within nuclear physics and beyond, and there are presently a number of efforts underway to exploit this fact.

*LBL-34484: Nuclear Physics A572 (1994) 489

[1] J. Randrup and B. Remaud, Nuclear Physics A514 (1990) 339

[2] S. Ayik and C. Gregoire, Physics Letters B212 (1988) 269; Nuclear Physics A513 (1990) 187

[3] G.F. Burgio, Ph. Chomaz, and J. Randrup, Physics Letters B254 (1991) 340; Nucl. Phys. A529 (1991) 157

Statistical Properties of Anti-Symmetrized Molecular Dynamics*

Akira Ohnishi[a] *and Jørgen Randrup*

[a]) *Research Center for Nuclear Physics, Osaka University, Ibaraki, Osaka 567, Japan*

There is currently significant effort devoted to the exploration of nuclear collisions at medium energies which create transient physical environments that have fairly unique characteristics and may provide experimental information on general nuclear properties, such as the equation of state. This undertaking poses significant theoretical challenges, since the absence of equilibrium makes it difficult to develop quantitatively reliable models. Moreover, the high complexity of the reactions requires the use of microscopic simulation models, which makes considerable demands on computational resources.

It is important to ascertain the statistical properties of such dynamical models, especially in connection with the simulation of fragment production processes, because the relative fragment yields will to a large extent be governed by the corresponding statistical weights, due to the complexity of the dynamics.

In order to elucidate this essential feature, we have examined the statistical limit of the microscopic Anti-symmetrized Molecular Dynamics simulation model[1], which is a simplied version of the Fermionic Molecular Dynamics model[2]. It provides a quantum-mechanical description of the nuclear A-body system (for example, the shell effects are automatically included) and has been successful for understanding and reproducing various heavy-ion data.

By statistical sampling of the appropriate canonical distribution, we have calculated some of the key thermodynamic properties, such as the dependence of the average energy on temperature, whose derivative is the specific heat and which is closely related to the partition function.

It has been found that with regard to these properties, the equilibrium behaves in a classical manner, when we adopt the mean field approximation for the canonical weight, $\mathcal{W}_{\rm mf} = \exp(-\beta < \hat{H} >)$, even though the underlying many-body states used to calculate $< \mathcal{H} >$ are described by anti-symmetric wave functions of *AMD*. We have discussed the origin of this shortcoming, and have found that inaccurate estimates of the mean excitation energy arise from the energy dispersion of each wave packet, or in other words, the time-dependence of the wave function itself. This key point is brought out by the difference between the quantal canonical weight $\mathcal{W}_Q =< \exp(-\beta\hat{H}) >$ and its mean field approximation $\mathcal{W}_{\rm mf} = \exp(-\beta\mathcal{H})$. These weights grow more similar to one another the smaller the dispersion of the Hamiltonian operator is. However, a small dispersion of the Hamiltonian corresponds to a quasi-static situation, and thus it is does not occur in actual time-dependent processes. This feature is quite general and applies to any time-dependent mean field theory, such as the time-dependent Hartree-Fock theory and Fermionic Molecular Dynamics.

We have also discussed a method by which this problem can be largely remedied, in the context of statistical equilibrium: For each wave packet, a corrected canonical weight $\mathcal{W}_{QC}$ is obtained by use of the quantal dispersion of the Hamiltonian, σ_H^2. The mean excitation energy and specific heat calculated in this manner exhibit a remarkably improved statistical behavior. However, it still needs to be studied how to treat this problem in a time-dependent context.

*LBL-33703: Nuclear Physics A565 (1994) 474

[1] A. Ono, H. Horiuchi, T. Maruyama, and A. Ohnishi, Prog. Theo. Phys. 87 (1992) 1185; Phys. Rev. Lett. 68 (1992) 2898

[2] H. Feldmeier, Nucl. Phys. A515 (1990) 147

Statistical nuclear multifragmentation with collective expansion and Coulomb forces*

Jørgen Randrup

A conceptually simple explosion-evaporation model of nuclear disassembly was developed about a decade ago[1], and it was subsequently turned into a means for generating complete multifragment events[2]. A standard version of the associated simulation code, *FREESCO*, was made available to the community[3], and it has been employed by numerous groups as an aid in the analysis and interpretation of the data.

Recently, in connection with the analysis of data on central collisions of heavy nuclei, a need has arisen for reference simulations based on more complicated physical scenarios than those considered in the standard *FREESCO* code. In response, we have developed a simulation code *WIX* with which it is possible to explore a larger variety of scenarios for the disassembly of a single specified nuclear source. The basic multifragmentation mechanism is the same as that of the explosion-evaporation model, namely an explosive transformation of the source into an assembly of prefragments based on the appropriate statistical weight, and in fact the new code can be regarded as merely as a number of additional features grafted onto the standard *FREESCO*. The most important new features are 1) the consistent incorporation of the *Coulomb interaction* between the prefragments (both in the partition function and during the separation stage), 2) the incorporation of a *collective expansion* of the source, 3) the explicit construction of the *freeze-out configuration*, and 4) the possibility for the source to be both *deformed* and *hollow*. This new code is already being employed by several groups, and may be of broader interest, so it is worthwhile to make a standard version and present a description of its physical contents.

This work first gives a condensed review of the underlying statistical multifragmentation model; then the various new features are described, relative to the standard *FREESCO* treatment, and subsequently the most significant effects are illustrated. In the appendix it is briefly described how to run the code. We hope that this exposition will be an aid to those who wish to employ the code in their particular studies and that it may stimulate corresponding refinements in other models, so that more informative confrontations with the data can be made.

As has been the case with *FREESCO*, the code *WIX* is freely available upon request (and is already in use around the world). It is primarily to assist actual and potential users that this presentation has been made, and in order to enable the general readership to better judge the physical basis for simulations made with the code.

It should finally be emphasized that *WIX* (as well as *FREESCO*) should be regarded as a tool, rather than a specific model. It presents a convenient framework for addressing many questions related to nuclear multifragmentation processes, by showing what the statistical disassembly of a nuclear source would produce under well-defined idealized circumstances. Accordingly, the code may be used to provide a meaningful reference against which actual data, or more complicated model calculations, can be judged. Of course, should the data show evidence of actual explosive disassembly, then *WIX* may offer a suitable means for extracting the characteristic quantities of interest, such as the source temperature and the degree of collectivity.

*LBL-33865: Computer Physics Communications 77 (1993) 153; supported in part by Gesellschaft für Schwerioneneforschung mbH D-6100 Darmstadt 11, Germany

[1] S.E. Koonin and J. Randrup, Nucl Phys A356 (1981) 223; G. Fai and J. Randrup, Nucl Phys A381 (1982) 557

[2] G. Fai and J. Randrup, Nucl. Phys. A404 (1983) 551

[3] G. Fai & J. Randrup, Comp Phys Comm 42 (1986) 385

Energy Dependence of Massive-Fragment Multiplicity*

Raul Donangelo[a], *Jorge A. López*[b], *and Jørgen Randrup*
[a]) *Instituto de Fisica da Universidade Federal, RJ-21945 Rio de Janeiro, Brazil*
[b]) *Department of Physics, University of Texas, El Paso, Texas 79968-0515*

The mechanism for producing massive fragments ($Z > 5$) in the collision between two heavy nuclei at intermediate beam energies remains uncertain in spite of considerable experimental and theoretical efforts, and many different models have been formulated to study the nuclear disassembly process. In the present work we explore the potential of the exclusive measurement of the massive-fragment multiplicity as a test to distinguish between two extreme reaction mechanisms, and use multifragmentation, sequential-binary and fission-evaporation models to simulate the decay of an excited nucleus for the purpose of comparing the different outcomes.

For the multifragmentation mechanism we use the model of Ref. [1], whose main ingredients are as follows: For a given mass and charge partition, it is assumed that the fragments and nucleons coexist in a thermalized mixture within a prescribed volume. The excitation energies and entropies of the hot fragments are calculated with a liquid-drop model extended to finite temperatures. In forming the ensemble, all possible fragmentation channels are taken into account and their relative statistical weights are calculated from the total channel entropy. These initially hot primary fragments are then allowed to de-excite via light-particle evaporation.

For the opposite extreme, sequential production of fragments, we consider two alternative approaches. One is the sequential-binary model of Ref. [2], in which the source is taken as a compound nucleus and is assumed to disassemble by sequential binary decay. Thus, the initial binary split produces two new sources which may subsequently undergo further binary decay, provided that their excitation energy is high enough. Nucleon emission emerges as the most extreme mass-asymmetric split. This binary decay procedure is iterated until stability is reached. The resulting multifragment final state consists of individual nucleons and nuclear fragments. The fission widths for each of the possible splits are obtained on the basis of the simple Bohr-Wheeler transition-state treatment.

An alternative model for sequential production of fragments is given in Ref. [3], in which a sequential-fission chain produces excited fragments that subsequently cool down by light-particle evaporation (*i.e.* first fission, then evaporation). While the fission widths are still given by the Bohr-Wheeler formula, the conditional barriers are obtained differently, and the light-particle evaporation is treated by the Hauser-Feshbach theory. In order to achieve an informative comparison between the models, we assume that the angular momentum of the original compound nucleus vanishes and that the charge of the fragments corresponds to β stability.

Our studies have shown that two opposite disassembly scenarios, simultaneous multifragmentation and sequential binary division, produce no significant differences for the energy dependence of the multiplicity of fragments with $Z > 5$. On the other hand, both of these differ from the fission-evaporation model which yields a very small number of massive fragments, and consequently this scenario can probably be ruled out as the dominant decay mechanism responsible for events with high massive-fragment multiplicity. This suggests that the massive-fragment multiplicity does not provide a stringent test of the theoretical models of nuclear fragmentation.

*LBL-32844: Physical Review C48 (1993) 465
[1] J.P. Bondorf *et al.*, Nucl. Phys. A444 (1985) 460
[2] J.A. López & J. Randrup, Nucl. Phys A491 (1989) 477
[3] R.J. Charity *et al.*, Nucl. Phys. A483 (1988) 371

Theory of Nuclear Multifragmentation III. Pre-transition nucleon radiation*

Jorge A. López[a] *and Jørgen Randrup*
[a]) *Department of Physics, University of Texas, El Paso, Texas 79968-0515*

The term "multifragmentation" has been employed to denote a variety of different physical processes leading to several or many complex fragments. In the present study we picture multifragmentation as a specific decay mode of a highly excited compound nucleus. Thus, in analogy with the Bohr-Wheeler description of nuclear fission[1] the shape of the compound nucleus performs a brownian-like motion as the system explores its available phase-space and the partial width for passing across the conditional barrier for a specific multifragmentation channel can then be calculated by statistical means. Such a transition-state treatment of nuclear multifragmentation was developed in ref. [2]. After the system has passed over the conditional barrier, a complicated further dynamical evolution occurs, during which some of the prefragments may recombine or otherwise react, but eventually a number of distinct nuclear fragments emerge. This post-transition dynamics was subsequently studied in ref. [3] by treating the evolution of the interacting prefragments as a generalized damped nuclear reaction.

In the present study we focus on the dynamics of the system *prior* to the crossing of the conditional multifragmentation barrier. This pretransition stage of the multifragmentation process is important, because the system may radiate a considerable number of nucleons during the relatively slow shape evolution. As a consequence, the system typically suffers a significant loss of mass and energy before arriving at the conditional barrier, so the potential-energy surface is continually being modified and the breakup widths are correspondingly affected. In other words, at the time when the irreversible transition into an assembly of interacting prefragments occurs, the total system is smaller and colder than the original one and the statistical weights governing the branching ratios between the various multifragment channels must be modified accordingly.

Within the transition-state formalism, we have developed a set of coupled equations for the mass and energy loss from an evolving source. Invoking two alternative radiation mechanisms, thermionic emission and Weisskopf evaporation, the loss of matter and energy was calculated. Mass losses ranging from 10 to 30 per cent were found, and typical temperature drops of 20 per cent were obtained. The main modification of the multifragmentation barrier was found to be a reduction of the *rms* size of the transition configuration. These effects of the radiation combine to produce a net reduction of the decay widths that varied in magnitude from a factor of 10 to 10^6 for the combination of system, channels, and energies considered.

Two factors were found to have a large effect on the reduction of the multifragmentation widths, namely the loss of excitation energy and the contraction of the transition configuration.

We expect that the present type of treatment is likely to provide an upper bound on the effect of pretransition nucleon radiation, because a typical source formed in a central nuclear collision may possess a certain amount of ordered outwards motion, as a result of the initial compression, and so there will be less time for the pretransition radiation to occur.

*LBL-33938: Nuclear Physics A571 (1994) 379
[1] N. Bohr and J.A. Wheeler, Phys. Rev. 56 (1939) 426
[2] J.A. López & J. Randrup, Nucl. Phys. A503 (1989) 183
[3] J.A. López & J. Randrup, Nucl. Phys. A512 (1990) 345

Maximum Entropy Distribution and Closure for Bose-Einstein and Fermi-Dirac Radiation Transport*

J. Cernohorsky and S.A. Bludman†

In many radiation hydrodynamical problems it is not efficient to treat the radiation transport by solving the Boltzmann equation. Instead, its first two angular moments, involving three angular (Eddington) moments e, f and p, of the distribution function are considered and a closure of the form $p(e, f)$ is required.

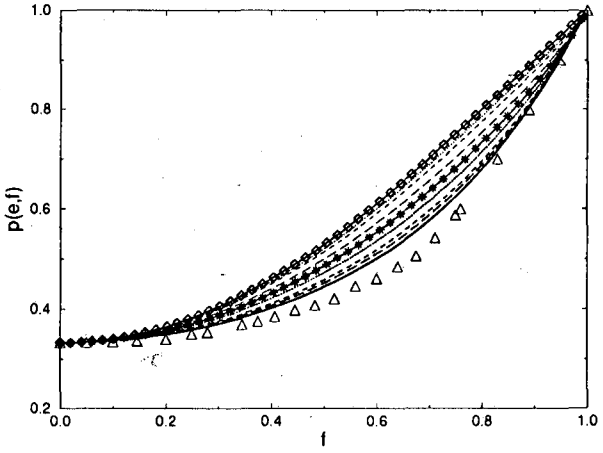

MEC-BE. (top ◇):LP-closure[3],(bottom−): classical limit (Minerbo closure[1]),bottom-to-top e =0, 0.1, 0.2, 0.5, 1.(∗), 2., 5., 10, ∞(◇), △: MC-data(FD)

With the maximum entropy (ME) formalism[1], we derive the ME distribution function for arbitrary quantum statistics. This procedure naturally contains a relation between e, f and p. However, because it involves non-analytical angular integrals, without simplification of the distribution function it is only readily implemented numerically. We develop a unified formalism for classical, Bose-Einstein, and Fermi-Dirac radiation and study the relation between the Eddington factors for all cases, without introducing any approximations.

Their properties are primarily determined by the quantum statistics, e.g. in the FD case the exclusion principle imposes a maximal angular packing[2], limiting the flux $f \leq 1-e$ and pressure $p \leq 1-2e+(4/3)e^2$ for a given occupation density e. The ME closure (MEC) contains previously known closures that depend only on f as limiting cases in occupancy[1,3]. For intermediate e, MEC depends on both e and f.

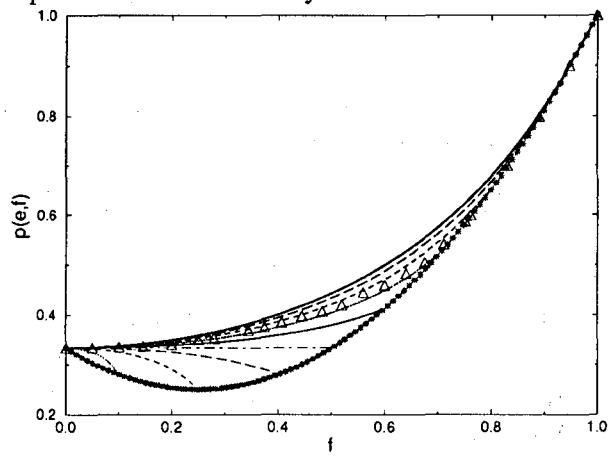

MEC-FD. top: classical limit ($e \to 0$). ∗···∗: maximal packing envelope. Top to bottom e = 0.1, 0.2, 0.3, 0.4, 0.5, 0.6, 0.75, 0.9 ; △: MC-data.

The Fermi-Dirac variable Eddington factor (MEC-FD) exhibits scale invariance, which allows its analytical formulation

$$p(e,f) = \frac{2(1-e)(1-2e)}{3}\chi\left(\frac{f}{1-e}\right) + \frac{1}{3} \quad ,$$

with $\chi(x) = 1 - 3\,x/q(x) \approx x^2(3 - x + 3x^2)/5$, where $q(x)$ is the inverse of the Langevin function

$$x = \coth q - 1/q \; .$$

MEC-FD agrees well with exact Monte Carlo neutrino transport closures during early stages of neutron star formation, and is expected to accurately approximate the exact solution of the Boltzmann equation.

*LBL-34920: Accepted for *ApJ.*, in press.

†Dept. of Physics, University of Pennsylvania

[1]G.N. Minerbo, *JQSRT* **20**, 541, (1987) ; G.C. Pomraning, *JQSRT* **26**, 385, (1981)

[2]H.-T. Janka *et al.*, *Astr.Ap.* **265**, 345, (1992)

[3]C.D. Levermore and G.C. Pomraning, *ApJ* **248**, 321, (1981)

Symmetries in Neutrino-Electron Scattering*

J. Cernohorsky

The symmetries of the neutrino-electron scattering (NES) kernel as it appears in the collision integral of the Boltzmann transport equation are exposed and discussed with particular attention to their consequences.

The kernel must explicitly conserve particle number at each vertex and vanish in local thermodynamic equilibrium (lte). I have demonstrated that this latter requirement must be met by the combination of detailed balance between in and out beams and the "transpositional symmetry" of the kernel, a property that had gone unnoticed previously.

In contrast, the prescription given in the literature[1] and hitherto used in neutrino transport codes in supernova collapse simulations imposes the lte-symmetry directly, thereby violating lepton number conservation.

Because the kernel has a higher symmetry than previously implied, exploitation of this extra symmetry approximately doubles the computational efficiency of the algorithm that calculates the neutrino-electron scattering opacity in practical applications.

In the appendix a practitioner's quide to implementing the NES opacity, and its structure in Eddington moment transport schemes is given and discussed.

*LBL-34921: Accepted for *ApJ*, Sep. 20 1994 issue.

[1] S.W. Bruenn, *ApJS* **58**, (1985), W.R. Yueh and J.R. Buchler, *ApJ* **217**, (1977)

Frame Dragging of Relativisitic Rotating Stars*

N. K. Glendenning and F. Weber

Dynamical effects of rotation in gravitational fields in some cases seem strange, and none more strange than the reversal of the centrifugal force in the vicinity of a Schwarzschild black hole demonstrated by Abramowicz. In this paper we discuss another but unrelated phenomenon associated with the rotation of a star which, though less spectacular, runs counter to classical expectation and accounts in part for a numerical observation concerning the Kepler frequency. Two groups, Haensel et al. and Friedman et al, independently made the usefull observation, based on *numerical* solutions of Einstein's equations, that the the Kepler frequency of a *rotating* neutron star at the mass limit of a sequence can be approximated to an accuracy of better than ten percent by a factor, less than unity, times the *classical* expression for the Kepler frequency of a satellite in circular orbit around the corresponding *spherical non-rotating* star No hint was provided as to how this result could emerge from the GR expression of the Kepler frequency of a rotating star. The result, however, has been utilized in papers too numerous to cite, and provides an enormous simplification of the problem because the solution of the numerically intensive and complicated general relativistic equations for a rotating star can be replaced by the solution of the much simpler Oppenheimer-Volkoff (OV) equations.

Mach's critical attention to the concept of inertial forces no doubt played an important role in focussing attention on the effects of rotating matter on inertial frames. Thirring appears to have been the first to realize that in Einstein's theory, a rotating mass shell drags the local inertial frames [1]. Hartle incorporated the effect into his calculation of the equilibrium configurations of rotating stars [2]. He notes that the centrifugal force acting on a fluid element of the star is governed by the rate of rotation of the star, assumed to be uniform, *relative* to the *local* inertial frames, which are dragged by the star's rotation, in the same direction.

The above statement by Hartle is correct, but the words by themselves imply that inasmuch as the centrifugal effects are governed by the *difference* of two frequencies of the same sign, that the effects should be smaller, that is to say, the Kepler frequency is correspondingly increased, and larger than the value given by the expression for a satellite at the equator of a non-rotating star (for which no frame dragging occurs). This turns out to be incorrect. The reason that the quoted words of a quarter century ago do not convey the correct implication is discussed by analyzing the GR self-consistency condition on the Kepler frequency. We show how the very usefull empirical formula can be understood as a counterintuitive result of the effects of frame dragging on the star's structure,

$$\Omega_K = \omega + \frac{\omega'}{2\psi'} + e^{\nu-\psi}\left[\frac{\nu'}{\psi'} + \left(\frac{\omega'}{2\psi'}e^{\psi-\nu}\right)^2\right]^{1/2}. \quad (1)$$

After some derivation we arrive at the result

$$\Omega_K = \left(1 + \frac{\omega}{\Omega_K} - \left(\frac{\omega}{\Omega_K}\right)^2\right)^{-1/2}\sqrt{\frac{M}{R^3}}, \quad (2)$$

where ω is the frame dragging frequency of the local inertial frames at the equator. Because $\omega(r) < \Omega_K$ always holds, our result exhibits the prefactor, always less than unity, times the classical expression, as in the empirical formula referred to above.

*Submitted for publication; LBL-33401

[1] H. Thirring, Phys. Zs. **19** (1918) 33

[2] J. B. Hartle, Ap. J. **150** (1967) 1005

Solid Quark-Hadron Phase Transition in Neutron Stars*

N. K. Glendenning

We have shown recently that in all earlier work of the last two decades on the quark/hadron phase transition in neutron stars, a degree of freedom was unintentionally frozen out which yielded a description of the transition as a *constant* pressure one[1] This had the explicit consequence of excluding the coexistence phase of hadrons and quarks from the star. The degree of freedom is the possibility of reaching the lowest energy state by rearranging electric charge between the regions of hadronic matter and quark matter in phase equilibrium. Because of this freedom, the pressure in the mixed phase varies as the proportions of the phases and is not a constant in the coexistence phase. It can therefore occupy a finite radial region in the interior of the star. The microphysics behind this preference for charge rearrangement is the charge-symmetric nuclear force which acts to relieve the high isospin asymmetry of neutron star matter as soon as it is in equilibrium with quark matter. This introduces a positive charge on the hadronic regions and a compensating negative charge on the quark matter. There is little need of leptons because charge neutrality can be achieved with lower energy among the *conserved* baryon number carrying baryons and quarks. Fig. 1 shows the charge *densities* on quark and hadronic regions, and this figure emphasises how the two phases in equilibrium are actually in interaction with each other, the charge density exchanged between them varying with the proportion of the phases (as metered by the depth in the star). The competition of the Coulomb and surface energies then establishes the shapes, sizes and spacings of the rarer phase in the background of the other so as to minimize the lattice energy. A Coulomb lattice structure of varying geometry is thus introduced to the interior of neutron stars. Many observable phenomena are likely to be associated with the presence of this solid, including all transport properties as well as pulsar glitches. Since the thickness, some kilometers, of mixed phase is a sensitive function of neutron star mass, or more particularly to its pressure profile, pulsars having such a region will be highly individualistic in their behavior according to fairly small variations in their mass. The early estimates that suggest that the phase transition occurs at a high density in neutron star matter are flawed by the fact that a very beta unstable description of the quark phase was used, $N_d = 2N_u$, which shifts the transition to a high density. We find both from qualitative arguments based on the finite size of nucleons and also from detailed models of hadronic and quark matter in beta equilibrium that the mixed phase is expected to begin at densities of about 3 times nuclear.

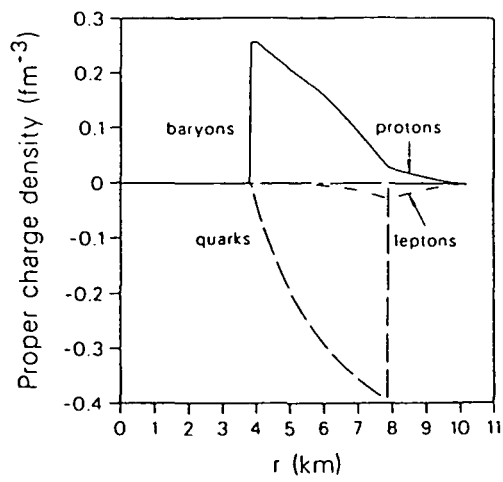

Figure 1: Charge densities in baryon regions and quark regions of coexistence phase region of star between 4 and 8 km, and small uniform lepton charge density.

*Invited paper, Bergen, Norway, 1993: LBL-34783

[1] N. K. Glendenning, Phys. Rev. D 46 (1992) 4161.

Fast Pulsars, Compact Stars, and the Strange Matter Hypothesis*

F. Weber and N. K. Glendenning

The typical mass-radius relationship for strange stars with a nuclear crust, whose maximum density is the neutron drip density, is shown in Fig. 1. Since the crust is bound by

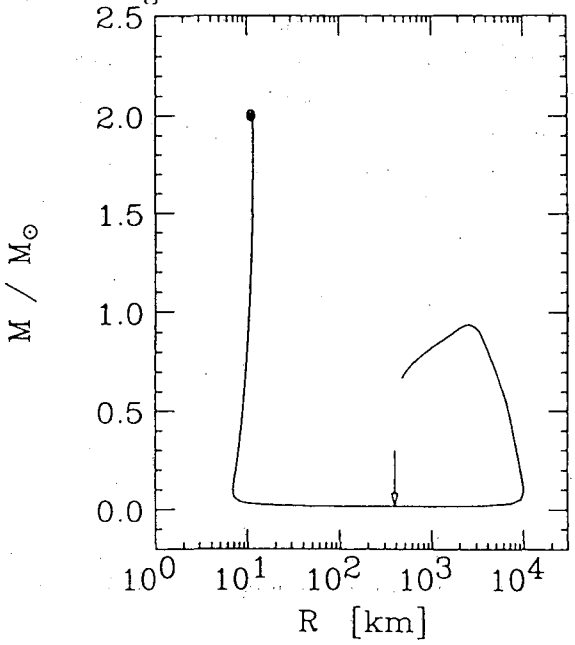

Figure 1: Radius as a function of mass of a strange compact stars and strange dwarfs.

the gravitational interaction (and not by confinement, which is the case for the strange matter core), stars possessing masses that are larger than the minimum mass of the sequence have a mass-radius relation that is qualitatively similar to the one for neutron stars. The sequence of strange stars has a minimum-mass of $\sim 0.015\,M_\odot$ or about 15 Jupiter masses, which is smaller than that of neutron star sequences, about $0.1\,M_\odot$ (radius $\sim$ 200 km). The low-mass strange stars may be of considerable importance since they may be difficult to detect and therefore may effectively *hide baryonic matter*. Furthermore, of interest to the subject of cooling of strange stars is the crust thickness of strange stars. It ranges from $\sim$ 400 km for stars at the lower mass limit and is a fraction of a kilometer for the star at the maximum mass[1]. The endpoint refers to that star whose strange-matter core radius has shrunken to zero, thus possessing mass and radius values of a white dwarf star. Finally we note the dependence of the minimum-mass of a strange star on its inner crust density, ϵ_{cr}. As an example, for $\epsilon_{cr} = 10^{-4}\,\epsilon_{drip}$ one obtains a minimum-mass star of $4 \times 10^{-4}\,M_\odot$ (0.4 Jupiter masses) and radius $\sim$ 820 km.

At the present time there appears to be only one crucial *astrophysical test* of the strange-quark-matter hypothesis, and that is whether strange quark stars can give rise to the observed phenomena of pulsar glitches. In the crust quake model an oblate solid nuclear crust in its present shape slowly comes out of equilibrium with the forces acting on it as the rotational period changes, and fractures when the built up stress exceeds the sheer strength of the crust material. The only existing investigation which deals with the calculation of the thickness, mass and moment of inertia of the nuclear crust that can exist on the surface of a rotating, general relativistic strange quark star has only recently been performed[1]. It was found that the data on relative frequency changes $\Delta\Omega/\Omega$ of observed glitches (Ω denotes the star's rotational frequency) and the measured values of the ratio $(\Delta\Omega/\Omega)/(\Delta\dot{\Omega}/\dot{\Omega})$ for the Crab and Vela pulsars can be understood from the computed crustal moment of inertia of strange stars.

*Invited paper; Astrophysics of Quark-Gluon Plasma, Calcutta, 1993: LBL-33771

[1]N. K. Glendenning and F. Weber, Ap. J. **400** (1992) 647.

Survey of Properties of Rotating Stars and Implications*

F. Weber and N. K. Glendenning

We report investigations of a number of properties of neutron stars based on a large representative sample of equations of state. Properties include the transition in the core to quark matter, gravitational radiation reaction instabilities that limit the rate of rotation, hadronic crusts on strange stars, and the glitching of strange stars with crusts.

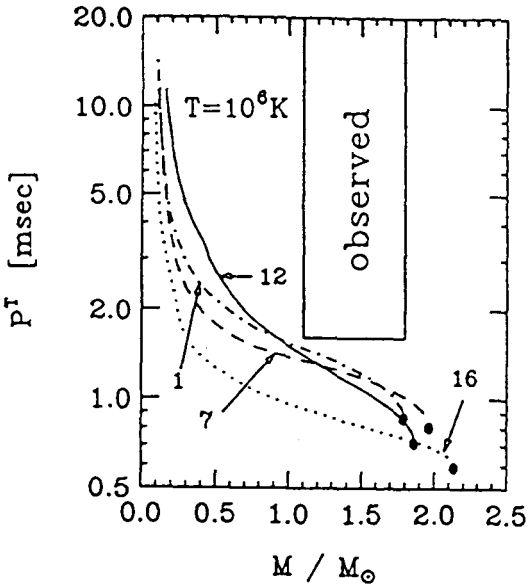

Figure 1: Rotational periods at which gravity wave instabillities limit rotation. So far observed stars lie in the marked region.

The recent finding of the possible existence of a mixed solid phase of baryon matter and quark matter in dense neutron star matter is stressed. The equations of state are then used to construct models of rapidly rotating neutron stars, whose masses and rotational periods are compared with observational data on pulsars. The indication of this work is that the gravitational radiation-reaction instability sets a lower limit on stable rotation for massive *neutron stars* of $P \sim 0.8$ msec. Lighter ones having typical pulsar masses of $\sim 1.45\, M_\odot$ are predicted to have mimimum rotational periods of ~ 1 msec. This finding may have very important implications for the nature of any pulsar that is found to have a shorter period, say below ~ 0.5 msec. At least for the studied broad collection of nuclear equations of state, rotation at such small periods is not allowed, and thus the interpretation of such objects as rapidly rotating neutron stars fails. Such objects, however, can be understood as rapidly rotating self-bound *strange stars*. The plausible ground-state state in that event is the deconfined phase of (3-flavor) strange-quark-matter. From the QCD energy scale this is as likely a ground-state as the confined phase. At the present time there appears to be only one crucial astrophysical test of the strange-quark-matter hypothesis, and that is whether strange quark stars can give rise to the observed phenomena of pulsar glitches. We demonstrate that the nuclear solid crust that can exist on the surface of a strange star can have a moment of inertia sufficiently large that a fractional change can account for the magnitude of pulsar glitches. Furthermore low-mass strange stars can have enormously large nuclear crusts (up to $\sim$ 400 km) which might considerably alter the cooling rate of strange stars and enables such objects to be possible hiding places of baryonic matter.

If strange-quark-matter is the ground-state of baryonic matter at zero pressure then the conclusion that the confined hadronic phase of nucleons and nuclei is only metastable would be almost inescapable, which would have far-reaching consequences for laboratory nuclear physics, the early universe, and astrophysical compact objects.

*Invited paper, Bodram Turkey, 1993: LBL-34783

Excitation of a quantal gas in a time-dependent potential

J. Blocki[a], *F. Brut*[b], *and W.J. Swiatecki*
[a]) *Institute for Nuclear Studies, PL-05-400 Swierk, Poland*
[b]) *Institut des Sciences Nucleaires, F-38026 Grenoble-Cedex, France*

Numerical studies of the excitation of 112 fermions in oscillating nucleus-like Woods-Saxon potentials are compared with analogous classical calculations in infinitely deep cavities. For oscillation frequencies such that $\hbar\omega$ is large compared to the level spacings, and for excitations small compared to the separation energy, a close correspondence is observed. For small frequencies a suppression of the excitation (relative to the classical result) is found.

Acta Physics Polonica B25 (1994) 637

Nuclear Physics: Macroscopic Aspects

W.J. Swiatecki

A systematic macroscopic, leptodermous approach to nuclear statics and dynamics is described, based formally on the two assumptions $\hbar \to 0$ and $b/R \ll 1$, where b is the surface diffuseness and R the nuclear radius. The resulting static model of shell-corrected nuclear binding energies and deformabilities is accurate to better than 1 part in a thousand and yields a firm determination of the principal properties of the nuclear fluid. As regards dynamics, the above approach suggests that nuclear shape evolutions will often be dominated by dissipation, but quantitative comparisons with experimental data are more difficult than in the case of statics. In its simplest liquid drop version the model exhibits interesting formal connections to the classic astronomical problem of rotating gravitating masses.

Presented at *Perspectives in Nuclear Structure*, Copenhagen, Denmark, June 14-18, 1993, Nuclear Physics A (in press); LBL-34928.

SEMINARS

Nuclear Science Division

E.F. Barasch Touro College	Gas-MicroStrip Detector, A Good Candidate for the All-Purpose High-Rate Proportional Chamber	January 8, 1993
M.M. Hindi U. of Tennessee	Double K-Shell Ionization in the Electron Capture Decays of ^{125}I and ^{139}Ce	January 8, 1993
Rudi Hwa U. of Oregon	Multiplicity Fluctuations, Intermittency, and Phase Transitions	January 11, 1993
A. Belkacem LBL	First Measurement of Electron Capture from e^+,e^- Production in Relativistic Heavy Ion Collisions at the Bevalac	January 25, 1993
A. Schlachter LBL	The Advanced Light Source: Photon Beams of Unprecedented Brightness	February 1, 1993
S. Perlmutter LBL	Discovery of the Farthest Known Supernova, and the Cosmological Implications	February 8, 1993
G. Pielert LLNL	QMD—Quantum Molecular Dynamics: the Model and its Numerical Realization	February 26, 1993
D. Greiner LBL	Recent Results from NA36: Is it (plasma) soup yet?	March 1, 1993
K. Aleklett Uppsala	PIAFE, a European Reactor-Based Radioactive Beams Project	March 5, 1993
L. Schroeder LBL	Making Science Policy at the White House	March 8, 1993
J. Rafelski U. of Arizona	Search for the Quark-Gluon Plasma: Evidence for Formation of a High Specific Entropy State	March 15, 1993
G. Bertsch U. of Washington	Single-Particle and Collective Motion in Buckyballs	March 22, 1993
D. Geesaman Argonne	Deep Inelastic Muon Scattering from Nucleons and Nuclei: Who knows what Evil Lurks	March 29, 1993
E. Wasserman Los Alamos	Search for Time Reversal Invariance Violation in Polarized Neutron Decay	March 30, 1993
C. Beausang U. of Liverpool	Eurogam and the Next Revolution in Superdeformed γ-ray Spectroscopy	April 5, 1993

Z. Fraenkel Weizmann Inst.	The CERES Dilepton Spectrometer at the CERN SPS	April 12, 1993
J. Thomas LLNL	The PHENIX Detector at RHIC	April 19, 1993
G. Greene Inst. Standards & Technology	Nuclear and Particle Physics with Low-Energy Neutrons	April 20, 1993
C. Hyde-Wright U. of Washington	Looking for Protons in the Nucleus: Quasi-elastic Electron Scattering	May 3, 1993
A. Rosenfeld LBL	Energy Efficiency in CA, the US, and the Second and Third Worlds	May 10, 1993
C. Moisan U. of Montreal	The Production of Heavy Quarks at the Z^0 Resonance	May 14, 1993
B. Blank Gradignan	Spectroscopy at the Proton Drip Line, a New Detection Set-Up—New Results	May 17, 1993
J.D. Walecka CEBAF	Overview of the CEBAF Scientific Program	May 24, 1993
P. Seidl LBL	Inertial Confinement Fusion with Heavy Ion Accelerators	June 7, 1993
K. Van Bibber LLNL	A Large-Scale Dark Matter Axion Search	June 14, 1993
A. Stuchberry Australian Natl. University	Physics of Transient Hyperfine Magnetic Fields and Measurements of Nuclear Magnetic Moments	June 28, 1993
B. Frois Saclay	New Frontiers of Nuclear Physics Explored by Electron Accelerators	August 2, 1993
B. Balanetkin U. of Wisconsin	Solar Neutrinos: Data Confront Theory	August 6, 1993
E. Friedlander LBL	Universality, Fine Structure, and Scaling of Multiplicity Distributions	August 9, 1993
D. Dong LBL	Mystery Spot, Entropy of Biological Vision, and Recognizing Cerenkov Pattern	August 10, 1993
P. Doll U. of Karlsruhe	Status of the Air Shower Experiment KASCADE at Karlsruhe	August 11, 1993
F. Weber U. of Munich	Rapidly Rotating Neutron Stars, Fast Pulsars, and the Strange Matter Hypothesis	August 16, 1993

B. Mueller Duke	Relativistic Heavy Ion Collisions: Probing the Early Universe in the Lab	August 23, 1993
S. Bludman U. of Pennsylvania	The Two Solar Neutrino Problems	August 27, 1993
U. Heinz U. of Regensberg	QCD Transport Theory	August 30, 1993
R. Weiner U. of Marburg	Superstitions and Prejudices in the Study of Bose-Einstein Correlation	September 8, 1993
Y. Lazarev JINR	New Findings in Heavy Element Research at Dubna	September 9, 1993
H. Maier HMI	Experimental Determination of Wave Functions for States in ^{208}Pb	September 20, 1993
G. Igo UCLA	Measurement of the Spin Structure of the Deuteron and the Bjorken Sum Rule—CERN Experiment NA47	September 27, 1993
R. Tighe LBL	Evidence for the Ground-State Proton Decay of ^{105}Sb	October 11, 1993
W. Greiner Frankfurt	Cluster Radioactivity	October 18, 1993
T. O'Donnel U. of Michigan	Heavy Ion Physics with the University of Michigan 7–Tesla Solenoid	October 19, 1993
R. Novotny Giessen	Multifragment Events in the Reaction $^{58}Ni + ^{27}Al$ at 15.8 MeV/nucleon	November 5, 1993
L. deBraeckeler U. of Washington	Measurement of the Weak Induced Current in Mass 8 Nuclei	November 8, 1993
F. Sakata U. of Tokyo	Gauge Structure of the TDHF-Manifold	November 12, 1993
E. Shuryak SUNY	Why Is a Nucleon Bound?	November 17, 1993
N. Glendenning LBL	Why the Quark-Hadron Coexistence Phase in Neutron Stars is a Solid	November 22, 1993
I. Dremin Lebedev Inst.	Multiplicity Distributions and Fractality in QCD	November 29, 1993
W. Stoeffl LLNL	New Results from the LLNL Neutrino Mass Experiment	December 6, 1993
S. Kumar Yale	In Search of Strange Quark Matter	December 20, 1993

Nuclear Theory Group

A. Ohnishi RCNP, Osaka Univ.	Antisymmetric Molecular Dynamics	January 11, 1993
R. Hwa U. of Oregon	Multiplicity Fluctuations, Intermittency, and Phase Transitions	January 11, 1993
J. Blocki Warsaw, Poland	Order vs. Chaos in Nuclear Physics	January 25, 1993
J. Skalski Warsaw, Poland	Nuclear Dipole Transitions Induced by Reflection Asymmetry	February 1, 1993
J. Skalski Warsaw, Poland	Quantum Particles in a Cavity	February 8, 1993
V. Flambaum U. of New South Wales, Australia	Enhancement of Weak Interactions and Quantum Chaos	February 12, 1993
K. Eskola LBL and Helsinki	Highlights of CERN Workshop on LHC	March 1, 1993
J-W. Qiu Iowa State U.	Cronin Effect and Multiple Scattering in QCD	March 10, 1993
J. Cernohorsky LBL	Report on the Brightest Pulsar	March 15, 1993
J. Cernohorsky LBL	Neutrino Transport in Supernovae	April 6, 1993
H. Weigert U. of Regensberg	Kinetic Theory of QCD	April 13, 1993
N. Glendenning LBL	Solid Structure of the Hadron/Quark Mixed Phase in Neutron Stars	June 1, 1993
J. Lopez UT–El Paso	Similarity Approach to Fragmentation	July 13, 1993
S. Ayik U. of Tennessee	Damping of Collective Vibrations in a Memory-Dependent Transport Model	July 15, 1993
H. Heiselberg LBL	Color Transparency and Cross-Section Fluctuations in Relativistic Heavy Ion Collisions	August 2, 1993
S. Frauendorf IHK	Shapes of Liquid Sodium Clusters	August 9, 1993

B. Banerjee Tata Inst. Fund. Resch.	Supercooling, Nucleation, and Quark-Hadron Phase Transition in the Early Universe	August 11, 1993
H. Heiselberg LBL	Pasta in Pulsars: Structure of Quark Matter in Neutron Stars	September 13 1993
M. Herrmann INT, Seattle	HBT Analysis in a Solvable Model	October 18, 1993
C. Jarzynski LBL	Thermalization of Noninteracting Particles by Collisions with a Massive Scatterer: From an Exponential to a Gaussian Velocity Distribution	November 10, 1993
B. Kolpeliovich Dubna, Russia	Hadronization of Quarks in Nuclear Matter	November 15, 1993
S. Drozdz Krakow, Poland	Quantal Description of Nuclear Dissipation: Regularity Versus Chaos	November 18, 1993
Y. Zhuo Beijing, China	Equilibration in Relativistic Heavy-Ion Collisions Around 1 GeV/A	November 22, 1993
M. Lua Iowa State Univ.	Cronin Effects in Photo-Nuclear Jet Production	November 29, 1993
R. Mehren LLNL	Superdeformation in the Mass Region $A \approx 150$	December 16, 1993

Author Index

Author Index

D

E

F

G

H

I

J

K

L

M

N

O

P

Q

R

S

T

V

W

X

Y

Z

Lawrence Berkeley Laboratory
Technical and Electronic Information Department
University of California
Berkeley, California 94720